Table 7.71. Average Annual Building Loss Normalized by Building Value – Two-Story Engineered Building

Building Characteristics				Residential Buildings(8 Units per Floor)				Commercial Buildings(1 Unit per Floor)			
Roof Deck	Missile Environ.	Glazing Coverage	Roof Cover	Terrain Roughness (m)				Terrain Roughness (m)			
				0.03	0.35	0.70	1.0	0.03	0.35	0.70	1.00
Metal	A	20%	BUR	0.0088	0.0084	0.0057	0.0045	0.0125	0.0114	0.0078	0.0060
			EPDM	0.0101	0.0092	0.0064	0.0051	0.0136	0.0120	0.0083	0.0066
		33%	BUR	0.0109	0.0100	0.0068	0.0054	0.0151	0.0138	0.0094	0.0074
			EPDM	0.0120	0.0107	0.0075	0.0059	0.0159	0.0142	0.0099	0.0078
		50%	BUR	0.0138	0.0124	0.0085	0.0068	0.0181	0.0159	0.0110	0.0087
			EPDM	0.0147	0.0130	0.0091	0.0073	0.0187	0.0163	0.0114	0.0091
	B	20%	BUR	0.0074	0.0071	0.0048	0.0038	0.0100	0.0086	0.0058	0.0045
			EPDM	0.0087	0.0078	0.0055	0.0044	0.0112	0.0094	0.0065	0.0051
		33%	BUR	0.0090	0.0083	0.0056	0.0044	0.0119	0.0103	0.0070	0.0054
			EPDM	0.0101	0.0090	0.0063	0.0050	0.0130	0.0109	0.0076	0.0060
		50%	BUR	0.0113	0.0099	0.0068	0.0054	0.0144	0.0121	0.0083	0.0065
			EPDM	0.0122	0.0105	0.0074	0.0060	0.0153	0.0126	0.0088	0.0070
	C	20%	BUR	0.0063	0.0055	0.0038	0.0030	0.0084	0.0069	0.0046	0.0035
			EPDM	0.0076	0.0064	0.0045	0.0037	0.0097	0.0077	0.0054	0.0043
		33%	BUR	0.0072	0.0062	0.0042	0.0033	0.0098	0.0081	0.0054	0.0042
			EPDM	0.0084	0.0071	0.0050	0.0041	0.0109	0.0088	0.0061	0.0049
		50%	BUR	0.0090	0.0076	0.0052	0.0042	0.0119	0.0095	0.0064	0.0050
			EPDM	0.0101	0.0084	0.0060	0.0049	0.0129	0.0102	0.0070	0.0057
	D	20%	BUR	0.0045	0.0025	0.0020	0.0017	0.0051	0.0026	0.0020	0.0018
			EPDM	0.0059	0.0034	0.0028	0.0025	0.0065	0.0036	0.0029	0.0026
		33%	BUR	0.0047	0.0025	0.0020	0.0018	0.0054	0.0027	0.0021	0.0018
			EPDM	0.0061	0.0035	0.0028	0.0026	0.0067	0.0037	0.0029	0.0026
		50%	BUR	0.0058	0.0033	0.0027	0.0023	0.0078	0.0044	0.0034	0.0030
			EPDM	0.0072	0.0042	0.0034	0.0030	0.0090	0.0053	0.0042	0.0037
Concrete	A	20%	BUR	0.0064	0.0074	0.0048	0.0036	0.0110	0.0108	0.0071	0.0054
			EPDM	0.0067	0.0075	0.0049	0.0036	0.0112	0.0110	0.0072	0.0055
		33%	BUR	0.0090	0.0093	0.0061	0.0046	0.0140	0.0134	0.0090	0.0070
			EPDM	0.0092	0.0094	0.0062	0.0047	0.0142	0.0135	0.0091	0.0070
		50%	BUR	0.0126	0.0119	0.0081	0.0063	0.0174	0.0157	0.0107	0.0084
			EPDM	0.0128	0.0121	0.0082	0.0064	0.0176	0.0158	0.0109	0.0085
	B	20%	BUR	0.0049	0.0058	0.0037	0.0027	0.0082	0.0077	0.0049	0.0036
			EPDM	0.0050	0.0059	0.0038	0.0028	0.0084	0.0078	0.0050	0.0037
		33%	BUR	0.0069	0.0072	0.0046	0.0035	0.0105	0.0097	0.0063	0.0047
			EPDM	0.0070	0.0073	0.0047	0.0035	0.0107	0.0098	0.0064	0.0048
		50%	BUR	0.0098	0.0092	0.0061	0.0047	0.0135	0.0117	0.0078	0.0060
			EPDM	0.0099	0.0093	0.0062	0.0049	0.0137	0.0118	0.0079	0.0061
	C	20%	BUR	0.0035	0.0040	0.0024	0.0017	0.0064	0.0058	0.0035	0.0025
			EPDM	0.0037	0.0041	0.0025	0.0018	0.0066	0.0059	0.0037	0.0026
		33%	BUR	0.0048	0.0050	0.0031	0.0022	0.0082	0.0073	0.0045	0.0033
			EPDM	0.0049	0.0051	0.0032	0.0023	0.0084	0.0074	0.0047	0.0034
		50%	BUR	0.0073	0.0068	0.0044	0.0034	0.0109	0.0089	0.0058	0.0044
			EPDM	0.0074	0.0069	0.0046	0.0035	0.0110	0.0090	0.0059	0.0045
	D	20%	BUR	0.0016	0.0006	0.0005	0.0004	0.0027	0.0008	0.0006	0.0005
			EPDM	0.0018	0.0007	0.0006	0.0005	0.0029	0.0010	0.0007	0.0006
		33%	BUR	0.0019	0.0007	0.0005	0.0004	0.0032	0.0010	0.0006	0.0005
			EPDM	0.0021	0.0008	0.0006	0.0005	0.0034	0.0011	0.0008	0.0006
		50%	BUR	0.0038	0.0018	0.0015	0.0012	0.0063	0.0033	0.0025	0.0022
			EPDM	0.0039	0.0020	0.0016	0.0013	0.0065	0.0035	0.0026	0.0022

Table 7.72. Average Annual Building Loss Normalized by Building Value – Five-Story Engineered Building

Building Characteristics				Residential Buildings(8 Units per Floor)				Commercial Buildings(1 Unit per Floor)			
Roof Deck	Missile Environ.	Glazing Coverage	Roof Cover	Terrain Roughness (m)				Terrain Roughness (m)			
				0.03	0.35	0.70	1.0	0.03	0.35	0.70	1.00
Metal	A	20%	BUR	0.0078	0.0069	0.0052	0.0044	0.0104	0.0094	0.0068	0.0056
			EPDM	0.0091	0.0080	0.0062	0.0054	0.0115	0.0103	0.0077	0.0064
		33%	BUR	0.0090	0.0080	0.0059	0.0050	0.0124	0.0109	0.0079	0.0065
			EPDM	0.0103	0.0090	0.0069	0.0059	0.0133	0.0117	0.0087	0.0073
		50%	BUR	0.0116	0.0101	0.0077	0.0067	0.0155	0.0130	0.0098	0.0083
			EPDM	0.0128	0.0111	0.0087	0.0076	0.0165	0.0138	0.0106	0.0091
	B	20%	BUR	0.0076	0.0067	0.0050	0.0043	0.0097	0.0084	0.0061	0.0050
			EPDM	0.0089	0.0077	0.0060	0.0052	0.0107	0.0093	0.0070	0.0058
		33%	BUR	0.0087	0.0076	0.0057	0.0048	0.0114	0.0096	0.0070	0.0058
			EPDM	0.0099	0.0086	0.0067	0.0057	0.0124	0.0104	0.0078	0.0065
		50%	BUR	0.0112	0.0095	0.0074	0.0064	0.0145	0.0117	0.0090	0.0077
			EPDM	0.0124	0.0105	0.0083	0.0073	0.0154	0.0125	0.0097	0.0084
	C	20%	BUR	0.0075	0.0067	0.0050	0.0043	0.0094	0.0080	0.0059	0.0048
			EPDM	0.0088	0.0078	0.0060	0.0052	0.0103	0.0089	0.0067	0.0056
		33%	BUR	0.0086	0.0076	0.0057	0.0047	0.0110	0.0092	0.0067	0.0055
			EPDM	0.0099	0.0086	0.0066	0.0057	0.0120	0.0099	0.0074	0.0063
		50%	BUR	0.0110	0.0094	0.0073	0.0063	0.0139	0.0110	0.0085	0.0073
			EPDM	0.0121	0.0104	0.0082	0.0072	0.0150	0.0118	0.0093	0.0080
	D	20%	BUR	0.0063	0.0039	0.0033	0.0030	0.0067	0.0038	0.0031	0.0027
			EPDM	0.0076	0.0050	0.0043	0.0039	0.0078	0.0047	0.0039	0.0035
		33%	BUR	0.0067	0.0041	0.0034	0.0031	0.0074	0.0041	0.0033	0.0029
			EPDM	0.0080	0.0052	0.0044	0.0040	0.0084	0.0050	0.0042	0.0037
		50%	BUR	0.0088	0.0061	0.0053	0.0049	0.0113	0.0080	0.0068	0.0063
			EPDM	0.0101	0.0071	0.0062	0.0057	0.0123	0.0088	0.0076	0.0070
Concrete	A	20%	BUR	0.0044	0.0044	0.0029	0.0022	0.0085	0.0078	0.0053	0.0041
			EPDM	0.0045	0.0045	0.0030	0.0023	0.0086	0.0079	0.0054	0.0042
		33%	BUR	0.0059	0.0058	0.0039	0.0030	0.0107	0.0096	0.0066	0.0052
			EPDM	0.0060	0.0059	0.0039	0.0031	0.0108	0.0097	0.0067	0.0053
		50%	BUR	0.0093	0.0083	0.0061	0.0051	0.0144	0.0120	0.0088	0.0073
			EPDM	0.0093	0.0085	0.0062	0.0051	0.0144	0.0121	0.0089	0.0075
	B	20%	BUR	0.0042	0.0042	0.0027	0.0021	0.0077	0.0068	0.0045	0.0035
			EPDM	0.0043	0.0043	0.0028	0.0021	0.0078	0.0069	0.0046	0.0036
		33%	BUR	0.0056	0.0054	0.0036	0.0028	0.0097	0.0083	0.0057	0.0045
			EPDM	0.0056	0.0054	0.0037	0.0028	0.0099	0.0084	0.0058	0.0045
		50%	BUR	0.0088	0.0078	0.0058	0.0048	0.0134	0.0108	0.0080	0.0067
			EPDM	0.0089	0.0079	0.0058	0.0049	0.0135	0.0109	0.0081	0.0068
	C	20%	BUR	0.0041	0.0042	0.0027	0.0021	0.0074	0.0064	0.0043	0.0033
			EPDM	0.0042	0.0043	0.0028	0.0022	0.0074	0.0065	0.0044	0.0034
		33%	BUR	0.0055	0.0054	0.0036	0.0027	0.0094	0.0079	0.0054	0.0042
			EPDM	0.0057	0.0055	0.0037	0.0028	0.0095	0.0080	0.0054	0.0043
		50%	BUR	0.0086	0.0078	0.0058	0.0047	0.0128	0.0101	0.0076	0.0064
			EPDM	0.0087	0.0079	0.0058	0.0048	0.0130	0.0102	0.0077	0.0065
	D	20%	BUR	0.0026	0.0011	0.0008	0.0007	0.0045	0.0019	0.0013	0.0011
			EPDM	0.0028	0.0012	0.0009	0.0008	0.0046	0.0020	0.0014	0.0012
		33%	BUR	0.0033	0.0014	0.0010	0.0009	0.0054	0.0024	0.0017	0.0013
			EPDM	0.0035	0.0015	0.0011	0.0009	0.0056	0.0025	0.0018	0.0014
		50%	BUR	0.0062	0.0040	0.0035	0.0031	0.0099	0.0068	0.0058	0.0053
			EPDM	0.0063	0.0041	0.0035	0.0031	0.0100	0.0069	0.0059	0.0053

Table 7.73. Average Annual Building Loss Normalized by Building Value – Eight-Story Engineered Building

Building Characteristics				Residential Buildings(8 Units per Floor)				Commercial Buildings(1 Unit per Floor)			
Roof Deck	Missile Environ.	Glazing Coverage	Roof Cover	Terrain Roughness (m)				Terrain Roughness (m)			
				0.03	0.35	0.70	1.0	0.03	0.35	0.70	1.00
Metal	A	20%	BUR	0.0106	0.0088	0.0074	0.0067	0.0113	0.0095	0.0076	0.0066
			EPDM	0.0118	0.0099	0.0085	0.0078	0.0122	0.0103	0.0084	0.0074
		33%	BUR	0.0116	0.0096	0.0079	0.0071	0.0128	0.0106	0.0084	0.0073
			EPDM	0.0128	0.0106	0.0090	0.0081	0.0138	0.0114	0.0092	0.0081
		50%	BUR	0.0148	0.0124	0.0106	0.0097	0.0170	0.0141	0.0119	0.0108
			EPDM	0.0161	0.0135	0.0117	0.0107	0.0179	0.0149	0.0127	0.0116
	B	20%	BUR	0.0103	0.0085	0.0071	0.0065	0.0108	0.0088	0.0071	0.0063
			EPDM	0.0115	0.0096	0.0082	0.0075	0.0117	0.0097	0.0079	0.0070
		33%	BUR	0.0112	0.0091	0.0076	0.0069	0.0122	0.0098	0.0078	0.0069
			EPDM	0.0124	0.0102	0.0086	0.0078	0.0130	0.0106	0.0086	0.0076
		50%	BUR	0.0143	0.0118	0.0102	0.0094	0.0163	0.0134	0.0114	0.0105
			EPDM	0.0155	0.0130	0.0112	0.0104	0.0173	0.0142	0.0122	0.0113
	C	20%	BUR	0.0102	0.0083	0.0070	0.0064	0.0105	0.0085	0.0069	0.0060
			EPDM	0.0114	0.0094	0.0081	0.0074	0.0114	0.0093	0.0077	0.0068
		33%	BUR	0.0110	0.0089	0.0074	0.0067	0.0117	0.0094	0.0075	0.0066
			EPDM	0.0123	0.0100	0.0085	0.0077	0.0126	0.0102	0.0083	0.0074
		50%	BUR	0.0140	0.0116	0.0101	0.0093	0.0161	0.0130	0.0112	0.0104
			EPDM	0.0153	0.0127	0.0111	0.0104	0.0169	0.0138	0.0120	0.0111
	D	20%	BUR	0.0096	0.0070	0.0062	0.0058	0.0094	0.0065	0.0056	0.0052
			EPDM	0.0108	0.0081	0.0073	0.0069	0.0103	0.0073	0.0064	0.0060
		33%	BUR	0.0102	0.0074	0.0065	0.0061	0.0103	0.0069	0.0060	0.0055
			EPDM	0.0115	0.0085	0.0076	0.0071	0.0112	0.0078	0.0068	0.0062
		50%	BUR	0.0134	0.0104	0.0093	0.0089	0.0150	0.0118	0.0108	0.0101
			EPDM	0.0146	0.0114	0.0104	0.0099	0.0160	0.0126	0.0115	0.0109
Concrete	A	20%	BUR	0.0051	0.0040	0.0028	0.0023	0.0080	0.0063	0.0045	0.0037
			EPDM	0.0051	0.0040	0.0029	0.0024	0.0080	0.0064	0.0046	0.0037
		33%	BUR	0.0064	0.0049	0.0036	0.0029	0.0098	0.0076	0.0056	0.0045
			EPDM	0.0065	0.0050	0.0036	0.0030	0.0098	0.0077	0.0056	0.0046
		50%	BUR	0.0105	0.0086	0.0070	0.0063	0.0146	0.0119	0.0098	0.0087
			EPDM	0.0106	0.0086	0.0071	0.0063	0.0147	0.0119	0.0098	0.0088
	B	20%	BUR	0.0048	0.0036	0.0025	0.0021	0.0075	0.0057	0.0041	0.0033
			EPDM	0.0049	0.0037	0.0026	0.0021	0.0075	0.0058	0.0041	0.0033
		33%	BUR	0.0060	0.0045	0.0032	0.0027	0.0091	0.0068	0.0050	0.0041
			EPDM	0.0060	0.0046	0.0033	0.0027	0.0091	0.0069	0.0050	0.0041
		50%	BUR	0.0100	0.0080	0.0066	0.0060	0.0139	0.0112	0.0093	0.0084
			EPDM	0.0100	0.0081	0.0067	0.0060	0.0140	0.0112	0.0094	0.0085
	C	20%	BUR	0.0047	0.0035	0.0025	0.0020	0.0072	0.0054	0.0038	0.0030
			EPDM	0.0047	0.0035	0.0025	0.0020	0.0072	0.0054	0.0039	0.0032
		33%	BUR	0.0058	0.0043	0.0031	0.0025	0.0087	0.0065	0.0046	0.0038
			EPDM	0.0059	0.0043	0.0032	0.0026	0.0087	0.0065	0.0047	0.0039
		50%	BUR	0.0096	0.0078	0.0065	0.0058	0.0136	0.0108	0.0091	0.0084
			EPDM	0.0098	0.0078	0.0065	0.0060	0.0136	0.0109	0.0092	0.0083
	D	20%	BUR	0.0040	0.0021	0.0016	0.0014	0.0060	0.0032	0.0025	0.0021
			EPDM	0.0041	0.0022	0.0017	0.0014	0.0061	0.0033	0.0025	0.0022
		33%	BUR	0.0049	0.0027	0.0021	0.0018	0.0072	0.0039	0.0031	0.0027
			EPDM	0.0052	0.0027	0.0022	0.0019	0.0072	0.0040	0.0031	0.0027
		50%	BUR	0.0090	0.0066	0.0057	0.0055	0.0126	0.0096	0.0086	0.0080
			EPDM	0.0091	0.0066	0.0059	0.0054	0.0127	0.0096	0.0086	0.0081

Table 7.74. Average Annual Content Loss Normalized by Building Value – Two-Story Engineered Building

Building Characteristics				Residential Buildings (8 Units per Floor)				Commercial Buildings(1 Unit per Floor)			
Roof Deck	Missile Environ.	Glazing Coverage	Roof Cover	Terrain Roughness (m)				Terrain Roughness (m)			
				0.03	0.35	0.70	1.0	0.03	0.35	0.70	1.00
Metal	A	20%	BUR	0.0037	0.0034	0.0022	0.0016	0.0052	0.0048	0.0030	0.0022
			EPDM	0.0039	0.0035	0.0022	0.0017	0.0053	0.0048	0.0031	0.0022
		33%	BUR	0.0049	0.0044	0.0028	0.0021	0.0068	0.0064	0.0042	0.0032
			EPDM	0.0050	0.0044	0.0029	0.0021	0.0068	0.0064	0.0042	0.0032
		50%	BUR	0.0068	0.0059	0.0039	0.0030	0.0086	0.0078	0.0052	0.0040
			EPDM	0.0069	0.0060	0.0040	0.0031	0.0086	0.0078	0.0052	0.0040
	B	20%	BUR	0.0029	0.0027	0.0017	0.0012	0.0040	0.0032	0.0019	0.0013
			EPDM	0.0031	0.0028	0.0018	0.0013	0.0041	0.0032	0.0020	0.0014
		33%	BUR	0.0039	0.0035	0.0022	0.0016	0.0051	0.0044	0.0027	0.0020
			EPDM	0.0040	0.0035	0.0023	0.0017	0.0051	0.0044	0.0028	0.0020
		50%	BUR	0.0054	0.0046	0.0030	0.0023	0.0066	0.0055	0.0036	0.0026
			EPDM	0.0055	0.0047	0.0031	0.0024	0.0066	0.0055	0.0036	0.0027
	C	20%	BUR	0.0022	0.0018	0.0011	0.0008	0.0032	0.0023	0.0013	0.0009
			EPDM	0.0024	0.0019	0.0011	0.0008	0.0033	0.0023	0.0014	0.0009
		33%	BUR	0.0028	0.0022	0.0014	0.0010	0.0040	0.0031	0.0018	0.0013
			EPDM	0.0030	0.0023	0.0014	0.0011	0.0041	0.0031	0.0019	0.0013
		50%	BUR	0.0041	0.0033	0.0021	0.0016	0.0053	0.0040	0.0025	0.0018
			EPDM	0.0042	0.0033	0.0022	0.0017	0.0053	0.0040	0.0025	0.0019
	D	20%	BUR	0.0013	0.0005	0.0003	0.0003	0.0016	0.0005	0.0003	0.0002
			EPDM	0.0015	0.0006	0.0005	0.0004	0.0018	0.0006	0.0004	0.0003
		33%	BUR	0.0014	0.0005	0.0003	0.0003	0.0018	0.0005	0.0003	0.0003
			EPDM	0.0016	0.0006	0.0005	0.0004	0.0020	0.0006	0.0004	0.0004
		50%	BUR	0.0023	0.0011	0.0008	0.0007	0.0034	0.0017	0.0013	0.0011
			EPDM	0.0025	0.0012	0.0009	0.0008	0.0036	0.0018	0.0014	0.0012
Concrete	A	20%	BUR	0.0030	0.0032	0.0020	0.0014	0.0049	0.0048	0.0030	0.0022
			EPDM	0.0030	0.0032	0.0020	0.0014	0.0049	0.0048	0.0030	0.0021
		33%	BUR	0.0044	0.0042	0.0027	0.0020	0.0066	0.0064	0.0042	0.0032
			EPDM	0.0044	0.0043	0.0027	0.0020	0.0066	0.0064	0.0042	0.0031
		50%	BUR	0.0065	0.0059	0.0039	0.0030	0.0085	0.0078	0.0052	0.0040
			EPDM	0.0065	0.0059	0.0039	0.0030	0.0085	0.0078	0.0052	0.0040
	B	20%	BUR	0.0022	0.0025	0.0015	0.0010	0.0036	0.0030	0.0018	0.0012
			EPDM	0.0021	0.0024	0.0015	0.0010	0.0036	0.0031	0.0018	0.0012
		33%	BUR	0.0033	0.0033	0.0020	0.0015	0.0048	0.0043	0.0027	0.0019
			EPDM	0.0032	0.0032	0.0020	0.0014	0.0048	0.0043	0.0027	0.0019
		50%	BUR	0.0050	0.0045	0.0029	0.0022	0.0065	0.0055	0.0036	0.0026
			EPDM	0.0050	0.0045	0.0029	0.0022	0.0065	0.0055	0.0036	0.0026
	C	20%	BUR	0.0014	0.0014	0.0008	0.0005	0.0027	0.0021	0.0011	0.0007
			EPDM	0.0014	0.0014	0.0007	0.0005	0.0027	0.0020	0.0011	0.0007
		33%	BUR	0.0021	0.0019	0.0011	0.0007	0.0037	0.0030	0.0017	0.0012
			EPDM	0.0021	0.0019	0.0011	0.0008	0.0037	0.0030	0.0017	0.0012
		50%	BUR	0.0037	0.0031	0.0019	0.0015	0.0052	0.0040	0.0025	0.0018
			EPDM	0.0036	0.0031	0.0020	0.0015	0.0051	0.0040	0.0025	0.0018
	D	20%	BUR	0.0005	0.0001	0.0000	0.0000	0.0011	0.0002	0.0001	0.0000
			EPDM	0.0005	0.0001	0.0000	0.0000	0.0011	0.0002	0.0001	0.0000
		33%	BUR	0.0007	0.0001	0.0000	0.0000	0.0014	0.0002	0.0001	0.0001
			EPDM	0.0007	0.0001	0.0000	0.0000	0.0014	0.0002	0.0001	0.0001
		50%	BUR	0.0018	0.0008	0.0006	0.0005	0.0032	0.0016	0.0012	0.0010
			EPDM	0.0018	0.0008	0.0006	0.0005	0.0032	0.0016	0.0012	0.0010

Table 7.75. Average Annual Content Loss Normalized by Building Value – Five-Story Engineered Building

Building Characteristics				Residential Buildings(8 Units per Floor)				Commercial Buildings(1 Unit per Floor)			
Roof Deck	Missile Environ.	Glazing Coverage	Roof Cover	Terrain Roughness (m)				Terrain Roughness (m)			
				0.03	0.35	0.70	1.0	0.03	0.35	0.70	1.00
Metal	A	20%	BUR	0.0031	0.0025	0.0017	0.0013	0.0050	0.0042	0.0029	0.0022
			EPDM	0.0032	0.0026	0.0018	0.0015	0.0051	0.0043	0.0030	0.0024
		33%	BUR	0.0038	0.0031	0.0022	0.0017	0.0062	0.0052	0.0036	0.0028
			EPDM	0.0040	0.0033	0.0023	0.0018	0.0063	0.0054	0.0037	0.0030
		50%	BUR	0.0055	0.0046	0.0034	0.0029	0.0083	0.0067	0.0050	0.0041
			EPDM	0.0056	0.0047	0.0035	0.0030	0.0085	0.0069	0.0051	0.0043
	B	20%	BUR	0.0029	0.0024	0.0016	0.0013	0.0045	0.0035	0.0024	0.0018
			EPDM	0.0032	0.0025	0.0018	0.0014	0.0047	0.0036	0.0025	0.0020
		33%	BUR	0.0037	0.0030	0.0020	0.0016	0.0056	0.0044	0.0030	0.0024
			EPDM	0.0038	0.0031	0.0022	0.0017	0.0058	0.0045	0.0031	0.0025
		50%	BUR	0.0053	0.0043	0.0032	0.0027	0.0078	0.0059	0.0044	0.0037
			EPDM	0.0054	0.0044	0.0034	0.0028	0.0079	0.0060	0.0045	0.0038
	C	20%	BUR	0.0029	0.0023	0.0016	0.0013	0.0044	0.0032	0.0022	0.0017
			EPDM	0.0031	0.0025	0.0017	0.0014	0.0045	0.0033	0.0023	0.0018
		33%	BUR	0.0036	0.0029	0.0021	0.0016	0.0054	0.0041	0.0028	0.0022
			EPDM	0.0038	0.0031	0.0022	0.0017	0.0056	0.0042	0.0029	0.0023
		50%	BUR	0.0052	0.0043	0.0032	0.0027	0.0074	0.0054	0.0041	0.0035
			EPDM	0.0053	0.0044	0.0033	0.0028	0.0076	0.0055	0.0042	0.0036
	D	20%	BUR	0.0023	0.0011	0.0008	0.0007	0.0031	0.0013	0.0010	0.0008
			EPDM	0.0025	0.0012	0.0010	0.0008	0.0033	0.0015	0.0011	0.0009
		33%	BUR	0.0026	0.0012	0.0009	0.0008	0.0036	0.0016	0.0012	0.0009
			EPDM	0.0028	0.0014	0.0010	0.0009	0.0038	0.0018	0.0013	0.0011
		50%	BUR	0.0040	0.0026	0.0022	0.0020	0.0061	0.0042	0.0035	0.0032
			EPDM	0.0042	0.0027	0.0023	0.0021	0.0063	0.0043	0.0036	0.0032
Concrete	A	20%	BUR	0.0021	0.0019	0.0012	0.0009	0.0045	0.0038	0.0025	0.0019
			EPDM	0.0021	0.0019	0.0012	0.0009	0.0045	0.0038	0.0025	0.0019
		33%	BUR	0.0030	0.0027	0.0017	0.0013	0.0058	0.0050	0.0033	0.0026
			EPDM	0.0030	0.0027	0.0017	0.0013	0.0058	0.0050	0.0033	0.0026
		50%	BUR	0.0050	0.0043	0.0031	0.0026	0.0081	0.0066	0.0048	0.0040
			EPDM	0.0050	0.0043	0.0031	0.0026	0.0081	0.0066	0.0048	0.0040
	B	20%	BUR	0.0020	0.0018	0.0011	0.0008	0.0040	0.0031	0.0020	0.0015
			EPDM	0.0020	0.0017	0.0011	0.0008	0.0040	0.0031	0.0020	0.0015
		33%	BUR	0.0029	0.0025	0.0016	0.0012	0.0053	0.0041	0.0028	0.0021
			EPDM	0.0028	0.0024	0.0016	0.0012	0.0053	0.0041	0.0028	0.0021
		50%	BUR	0.0048	0.0040	0.0029	0.0025	0.0076	0.0057	0.0043	0.0036
			EPDM	0.0048	0.0040	0.0029	0.0024	0.0075	0.0057	0.0043	0.0036
	C	20%	BUR	0.0019	0.0017	0.0011	0.0008	0.0038	0.0028	0.0018	0.0013
			EPDM	0.0019	0.0017	0.0011	0.0008	0.0038	0.0028	0.0018	0.0013
		33%	BUR	0.0028	0.0025	0.0016	0.0012	0.0051	0.0038	0.0025	0.0019
			EPDM	0.0028	0.0025	0.0016	0.0012	0.0051	0.0038	0.0025	0.0019
		50%	BUR	0.0047	0.0040	0.0029	0.0024	0.0072	0.0053	0.0040	0.0033
			EPDM	0.0047	0.0040	0.0029	0.0024	0.0073	0.0053	0.0040	0.0033
	D	20%	BUR	0.0013	0.0004	0.0002	0.0002	0.0026	0.0009	0.0006	0.0004
			EPDM	0.0013	0.0004	0.0003	0.0002	0.0026	0.0009	0.0006	0.0004
		33%	BUR	0.0017	0.0006	0.0004	0.0003	0.0032	0.0012	0.0008	0.0006
			EPDM	0.0017	0.0006	0.0004	0.0003	0.0032	0.0012	0.0008	0.0006
		50%	BUR	0.0034	0.0022	0.0019	0.0017	0.0058	0.0039	0.0033	0.0030
			EPDM	0.0034	0.0022	0.0018	0.0016	0.0059	0.0039	0.0033	0.0030

Table 7.76. Average Annual Content Loss Normalized by Building Value – Eight-Story Engineered Building

Building Characteristics				Residential Buildings(8 Units per Floor)				Commercial Buildings(1 Unit per Floor)			
Roof Deck	Missile Environ.	Glazing Coverage	Roof Cover	Terrain Roughness (m)				Terrain Roughness (m)			
				0.03	0.35	0.70	1.0	0.03	0.35	0.70	1.00
Metal	A	20%	BUR	0.0038	0.0028	0.0022	0.0019	0.0054	0.0041	0.0031	0.0026
			EPDM	0.0040	0.0029	0.0023	0.0021	0.0055	0.0042	0.0033	0.0027
		33%	BUR	0.0044	0.0032	0.0025	0.0022	0.0064	0.0049	0.0037	0.0031
			EPDM	0.0045	0.0033	0.0027	0.0023	0.0066	0.0051	0.0038	0.0032
		50%	BUR	0.0063	0.0050	0.0042	0.0038	0.0093	0.0074	0.0062	0.0056
			EPDM	0.0065	0.0051	0.0043	0.0039	0.0095	0.0076	0.0064	0.0057
	B	20%	BUR	0.0037	0.0026	0.0021	0.0019	0.0051	0.0037	0.0028	0.0024
			EPDM	0.0038	0.0027	0.0022	0.0019	0.0052	0.0038	0.0029	0.0025
		33%	BUR	0.0042	0.0030	0.0024	0.0021	0.0061	0.0043	0.0033	0.0028
			EPDM	0.0044	0.0031	0.0025	0.0022	0.0062	0.0045	0.0034	0.0029
		50%	BUR	0.0060	0.0047	0.0040	0.0036	0.0089	0.0070	0.0059	0.0054
			EPDM	0.0062	0.0049	0.0041	0.0037	0.0091	0.0072	0.0060	0.0055
	C	20%	BUR	0.0036	0.0025	0.0020	0.0018	0.0049	0.0034	0.0026	0.0022
			EPDM	0.0038	0.0026	0.0021	0.0019	0.0051	0.0035	0.0027	0.0023
		33%	BUR	0.0041	0.0029	0.0023	0.0020	0.0058	0.0041	0.0031	0.0026
			EPDM	0.0043	0.0030	0.0024	0.0021	0.0059	0.0042	0.0032	0.0027
		50%	BUR	0.0058	0.0046	0.0039	0.0036	0.0088	0.0067	0.0057	0.0053
			EPDM	0.0061	0.0047	0.0040	0.0037	0.0089	0.0069	0.0059	0.0054
	D	20%	BUR	0.0034	0.0021	0.0018	0.0016	0.0045	0.0026	0.0021	0.0019
			EPDM	0.0036	0.0023	0.0019	0.0018	0.0047	0.0028	0.0023	0.0020
		33%	BUR	0.0038	0.0024	0.0020	0.0018	0.0051	0.0030	0.0024	0.0022
			EPDM	0.0040	0.0025	0.0021	0.0019	0.0053	0.0032	0.0026	0.0023
		50%	BUR	0.0057	0.0042	0.0037	0.0035	0.0083	0.0063	0.0056	0.0052
			EPDM	0.0058	0.0043	0.0038	0.0036	0.0085	0.0064	0.0057	0.0054
Concrete	A	20%	BUR	0.0024	0.0016	0.0011	0.0008	0.0046	0.0033	0.0023	0.0018
			EPDM	0.0024	0.0015	0.0011	0.0009	0.0046	0.0033	0.0023	0.0018
		33%	BUR	0.0031	0.0021	0.0015	0.0012	0.0057	0.0042	0.0030	0.0024
			EPDM	0.0031	0.0021	0.0015	0.0012	0.0058	0.0042	0.0030	0.0024
		50%	BUR	0.0053	0.0042	0.0034	0.0031	0.0089	0.0070	0.0058	0.0052
			EPDM	0.0054	0.0042	0.0035	0.0031	0.0089	0.0071	0.0058	0.0052
	B	20%	BUR	0.0022	0.0014	0.0009	0.0008	0.0043	0.0029	0.0020	0.0016
			EPDM	0.0023	0.0014	0.0009	0.0007	0.0043	0.0028	0.0020	0.0016
		33%	BUR	0.0029	0.0019	0.0013	0.0011	0.0054	0.0036	0.0026	0.0021
			EPDM	0.0029	0.0019	0.0013	0.0010	0.0053	0.0036	0.0026	0.0021
		50%	BUR	0.0051	0.0039	0.0033	0.0029	0.0084	0.0066	0.0055	0.0050
			EPDM	0.0051	0.0039	0.0033	0.0029	0.0085	0.0066	0.0055	0.0050
	C	20%	BUR	0.0022	0.0013	0.0009	0.0007	0.0041	0.0026	0.0018	0.0014
			EPDM	0.0021	0.0013	0.0009	0.0007	0.0041	0.0026	0.0018	0.0014
		33%	BUR	0.0028	0.0017	0.0012	0.0010	0.0051	0.0034	0.0024	0.0019
			EPDM	0.0028	0.0017	0.0012	0.0010	0.0051	0.0034	0.0024	0.0019
		50%	BUR	0.0049	0.0038	0.0032	0.0029	0.0083	0.0063	0.0053	0.0050
			EPDM	0.0050	0.0038	0.0032	0.0029	0.0083	0.0063	0.0054	0.0049
	D	20%	BUR	0.0020	0.0009	0.0006	0.0005	0.0037	0.0018	0.0013	0.0011
			EPDM	0.0020	0.0009	0.0007	0.0005	0.0037	0.0018	0.0013	0.0011
		33%	BUR	0.0025	0.0013	0.0009	0.0008	0.0044	0.0023	0.0017	0.0015
			EPDM	0.0026	0.0012	0.0009	0.0008	0.0044	0.0023	0.0017	0.0014
		50%	BUR	0.0047	0.0034	0.0029	0.0028	0.0078	0.0058	0.0052	0.0048
			EPDM	0.0047	0.0034	0.0030	0.0027	0.0079	0.0058	0.0052	0.0048

Table 7.77. Percent Increases in the Average Annual Total Loss due to Changes in Building Parameters (Minimum/Average/Maximum) – Engineered Residential and Commercial Buildings

Two-Story Engineered Buildings		
Building Parameter	Metal Roof Deck	Concrete Roof Deck
Residential to Commercial Building Class	0% / 24% / 42%	23% / 46% / 87%
Built-up to Single Ply Membrane Roof Cover	2% / 14% / 46%	-1% / 4% / 25%
20% to 33% Glazing Coverage	0% / 16% / 28%	5% / 28% / 44%
33% to 50% Glazing Coverage	17% / 32% / 99%	18% / 90% / 435%
Missile Environment D to C	37% / 103% / 253%	66% / 368% / 808%
Missile Environment C to B	18% / 29% / 42%	25% / 44% / 72%
Missile Environment B to A	18% / 28% / 44%	28% / 37% / 58%
Concrete to Metal Roof Deck	1% / 66% / 458%	
Five-Story Engineered Buildings		
Building Parameter	Metal Roof Deck	Concrete Roof Deck
Residential to Commercial Building Class	-6% / 25% / 45%	30% / 65% / 98%
Built-up to Single Ply Membrane Roof Cover	4% / 12% / 29%	-1% / 2% / 13%
20% to 33% Glazing Coverage	3% / 14% / 21%	21% / 32% / 40%
33% to 50% Glazing Coverage	21% / 43% / 145%	28% / 92% / 321%
Missile Environment D to C	14% / 56% / 130%	18% / 142% / 294%
Missile Environment C to B	0% / 3% / 7%	-2% / 4% / 9%
Missile Environment B to A	2% / 8% / 15%	4% / 10% / 21%
Concrete to Metal Roof Deck	6% / 58% / 395%	
Eight-Story Engineered Buildings		
Building Parameter	Metal Roof Deck	Concrete Roof Deck
Residential to Commercial Building Class	-7% / 12% / 26%	47% / 61% / 76%
Built-up to Single Ply Membrane Roof Cover	4% / 9% / 16%	-3% / 1% / 6%
20% to 33% Glazing Coverage	5% / 10% / 15%	19% / 27% / 37%
33% to 50% Glazing Coverage	29% / 48% / 100%	51% / 109% / 221%
Missile Environment D to C	2% / 13% / 35%	2% / 29% / 61%
Missile Environment C to B	1% / 3% / 6%	1% / 5% / 10%
Missile Environment B to A	3% / 5% / 10%	3% / 9% / 14%
Concrete to Metal Roof Deck	12% / 82% / 334%	
All Engineered Buildings		
Building Parameter	Metal Roof Deck	Concrete Roof Deck
Two to Five Stories	-23% / 25% / 130%	-40% / 32% / 242%
Five to Eight Stories	-4% / 33% / 105%	-25% / 18% / 122%

decks, and thus losses are primarily driven by glazing damage, which is influenced by both usage, since internal pressure is confined to smaller internal areas when there are multiple units, and missile environment.

The number of stories also has a significant impact on the normalized average annual total losses (see last two rows of Table 7.77). For example, with all else being the same, the predicted average annual losses for the five-story engineered buildings are up to 242% higher than those for the two-story buildings engineered buildings.

7.14 Loss Model Results for Industrial Buildings

Loss functions for industrial buildings have been developed following the same procedure as the other model building classes (based on 20,000 years of hurricane

simulation). The model buildings are assumed to be used as factories. The assumed subassembly cost distributions are listed in Table 7.78.

Example building and content loss functions are given in Appendix N. The average annual building and content losses (both normalized by the total building value) for all industrial buildings examined are presented in Tables 7.79 and 7.80, respectively. The average annual loss is obtained by summing all losses produced during the 20,000-year hurricane simulation period and then dividing by 20,000 years. The values given in Tables 7.79 and 7.80 reflect the average annual losses for industrial buildings located in the South Florida area.

Table 7.81 presents a summary of the effects of the various building parameters on normalized average annual total loss. The wall construction has the largest impact on average annual loss with an increase of 34% on average for unreinforced masonry walls versus reinforced masonry walls. This is due to the weaker resistance of the joist/wall connections for unreinforced masonry versus reinforced masonry walls since unreinforced masonry walls do not contain bond beams or tie beams with reinforcement to which the anchorage can be welded to or wrapped around (NRC, 1991). Average annual total losses are shown to increase by 16% on average when the metal roof deck has aged and fatigued, which has been modeled with a 50% reduction in the base uplift resistance. The effect of the surrounding missile environment on building losses is small since the modeled industrial building does not comprise glazing. However, small increases were observed (up to 3%) when the missile environment changed from the no-missile environment (D) to the environment associated with a mixture of commercial and residential type missiles (A) since costs are associated with re-finishing wall surfaces and replacing entry and/or overhead doors that have been impacted by windborne debris.

Table 7.78. Subassembly Cost Distributions for Industrial Buildings

Subassemblies	Cost Ratios	
Foundations		
Footings & Foundations	4.8%	7.0%
Piles & Caissons	0.0%	
Excavation & Backfill	2.2%	
Substructures		
Slab on Grade	6.8%	6.8%
Special Substructures	0.0%	
Superstructure		
Columns and Beams	0.0%	10.5%
Structural Walls	0.0%	
Elevated Floors/Diaphragms	0.0%	
Roof Decking/Framing	10.5%	
Stairs	0.0%	
Exterior Closure		
Walls	4.7%	6.1%
Exterior Wall Finishes	0.0%	
Doors	1.4%	
Windows & Glazed Walls	0.0%	
Roofing		
Roof Covering	4.5%	7.9%
Insulation	2.7%	
Openings & Specialties	0.7%	
Interior Construction		
Partitions	4.0%	9.8%
Interior Doors	1.9%	
Wall Finishes	1.0%	
Floor Finishes	0.6%	
Ceiling Finishes	0.7%	
Interior Surface of Exterior Walls	1.6%	
Conveying		
Elevators	0.0%	0.0%
Special Conveyors	0.0%	
Mechanical		
Plumbing	6.2%	37.2%
Fire Protection	4.4%	
Heating	11.8%	
Cooling	14.8%	
Special Systems	0.0%	
Electrical		
Service & Distribution	1.7%	14.8%
Lighting & Power	12.5%	
Special Electrical	0.6%	
Special Construction		
Specialties (& Additives)	0.0%	0.0%
Total	100%	100%

Table 7.79. Average Annual Building Loss Normalized by Building Value – Industrial Building

Building Characteristics		100% Roof Deck Capacity				50% Roof Deck Capacity			
		Terrain Surface Roughness (m)				Terrain Surface Roughness (m)			
Wall Construction	Missile Environment	0.03	0.35	0.70	1.0	0.03	0.35	0.70	1.0
Unreinforced Masonry	A	0.0286	0.0147	0.0107	0.0088	0.0297	0.0155	0.0115	0.0096
	B	0.0286	0.0147	0.0107	0.0088	0.0296	0.0155	0.0116	0.0097
	C	0.0286	0.0148	0.0107	0.0089	0.0297	0.0157	0.0117	0.0098
	D	0.0285	0.0145	0.0106	0.0087	0.0295	0.0153	0.0114	0.0096
Reinforced Masonry	A	0.0200	0.0108	0.0081	0.0067	0.0231	0.0130	0.0100	0.0084
	B	0.0201	0.0109	0.0081	0.0068	0.0231	0.0131	0.0099	0.0085
	C	0.0201	0.0110	0.0081	0.0068	0.0231	0.0132	0.0100	0.0086
	D	0.0200	0.0106	0.0079	0.0066	0.0230	0.0128	0.0098	0.0084

Table 7.80. Average Annual Content Loss Normalized by Building Value – Industrial Building

Building Characteristics		100% Roof Deck Capacity				50% Roof Deck Capacity			
		Terrain Surface Roughness (m)				Terrain Surface Roughness (m)			
Wall Construction	Missile Environment	0.03	0.35	0.70	1.0	0.03	0.35	0.70	1.0
Unreinforced Masonry	A	0.0126	0.0057	0.0038	0.0029	0.0128	0.0059	0.0041	0.0032
	B	0.0126	0.0057	0.0038	0.0029	0.0128	0.0059	0.0041	0.0033
	C	0.0126	0.0057	0.0038	0.0030	0.0128	0.0060	0.0041	0.0033
	D	0.0126	0.0057	0.0038	0.0029	0.0128	0.0059	0.0041	0.0033
Reinforced Masonry	A	0.0069	0.0031	0.0021	0.0016	0.0085	0.0044	0.0032	0.0026
	B	0.0069	0.0031	0.0021	0.0016	0.0086	0.0044	0.0031	0.0026
	C	0.0069	0.0031	0.0021	0.0016	0.0086	0.0044	0.0032	0.0027
	D	0.0069	0.0031	0.0021	0.0016	0.0086	0.0044	0.0032	0.0027

Table 7.81. Percent Increase in Average Annual Total Loss Due to Changes in Building Parameters (Minimum/Average/Maximum) – Industrial Buildings

Parameter	Increase in Building Loss
Reinforced Masonry to Unreinforced Masonry Walls	16% / 34% / 53%
Missile Environment D to A	0% / 1% / 3%
0% to 50% Reduction in Roof Deck Resistance	3% / 16% / 34%

Chapter 8. Building Stock Classification Methods

8.1 Introduction

In this section, two case studies are provided to demonstrate methods used to characterize the building stock in Southeast Florida. In Section 8.2, we show how aerial photography can be used to classify building geometries. In Section 8.3, we illustrate the use of a contractor survey to gather data on roof cover types.

8.2 Aerial Photography Samples

Commercial Building Stock. The classification of commercial buildings in Dade, Broward and Palm Beach counties is achieved by inspection of aerial photographs showing samples of the building stock within the three counties. Twenty-five aerial photographs were sampled from the three counties. The twenty-five photographs include ten random samples from areas classified as "Commercial and Services," ten random samples from areas classified as "Industrial," and five random samples from areas classified as "Institutional." The types of facilities included in these three land use categories are listed in Table 8. 1. Table 8.2 shows the photograph coverage area and the number of buildings shown within each of the randomly selected areas. Figure 8.1 shows the locations of the selected areas on a map of South Florida.

Table 8.1. Number of Aerial Photographs and Facility Type Examples by Land Use Category

Land Use Category	Number of Aerial Photographs	Facility Type Examples
Commercial and Services	10	Retail Sales and Services, Wholesale Sales and Services, Professional Services, Cultural and Entertainment, Tourist Services, and Oil and Gas Storage
Industrial	10	Food Processing, Timber Processing, Mineral Processing, and Oil and Gas Processing.
Institutional	5	Educational, Religious, Military, Medical and Health Care, Governmental, Correctional, and Commercial Child Care.

The South Florida Water Management District Land Use/Land Cover data set is used to generate the random sample. The data is in the form of a GIS polygon data layer. For example, there are 1148 polygons associated with the "Commercial and Services" category. Each of these polygons are assigned an integer number identifier from 1 to 1148. A random number generator was then used to select ten distinct integer numbers between 1 and 1148 (each number having an equal probability of being chosen) and the ten polygons associated with the randomly selected integer numbers were used.

Table 8.2. Coverage Area and Number of Buildings Within Each Photograph

Land Use Category	Photograph ID	Area(*1000 sq. ft.)	Number of Buildings
Commercialand Services	COMM01	5800	3
	COMM02	4400	18
	COMM03	9000	28
	COMM04	6600	27
	COMM05	4400	24
	COMM06	4400	15
	COMM07	4400	5
	COMM08	4600	27
	COMM09	18480	51
	COMM10	5000	14
Industrial	INDU01	9600	42
	INDU02	9800	10
	INDU03	6800	12
	INDU04	4800	33
	INDU05	22680	90
	INDU06	9900	62
	INDU07	5400	32
	INDU08	6800	25
	INDU09	8200	43
	INDU10	12600	38
Institutional	INST01	4600	53
	INST02	5000	23
	INST03	4800	14
	INST04	4600	11
	INST05	5600	23
Total		188260	723

Table 8.3 presents a breakdown of the percentage of buildings having shapes defined as L, T, C, Rectangular, Circular, Z, H, X and Triangular. Overall, the rectangular shape accounts for over three quarters of the building shapes. The rectangular shape, combined with the relatively simple L shape account for over 80% of the building shapes. The observation that the vast majority of the buildings can be described by these simple shapes indicates that modeling the overall building stock in a damage simulation can be adequately accomplished using the simple rectangular-shaped building models described in Chapters 6 and 7.

Residential Building Stock. Using the aerial photographs used to estimate roof cover damage in the Miami area, we estimated the fraction of one and two story houses, and the fraction of homes with either hip or gable roofs. We did not attempt to characterize the plan shapes of the residential buildings.

From these photographs a total of 1633 homes could be seen. Two story homes comprised 21% of the population, all of which were observed to have gable roofs. In the case of the one story homes, 23% had hip roofs, with the remainder having gable roofs. No flat-roofed homes were observed in these photographs. In cases where the homes had a roof which was a combination of a hip section and a flat section it was classified as a hip roof building. The same classification scheme was used for homes with combined flat and gable roofs. In cases where the roof was a hip/gable combination, the building was classified by the roof style that was dominant.

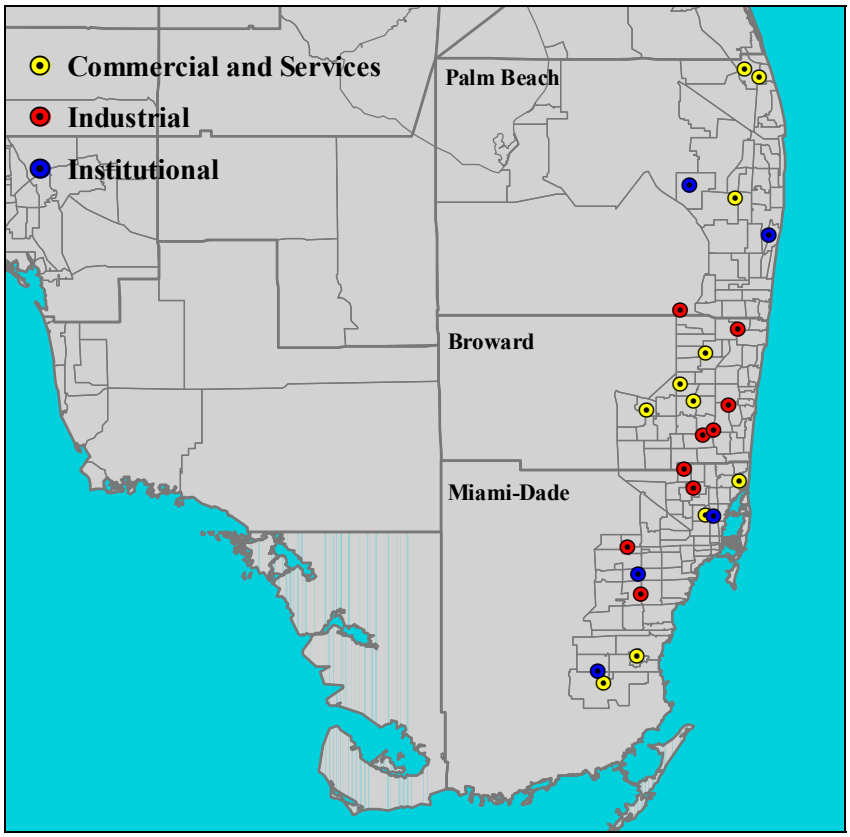

Figure 8.1. Commercial Building Stock Aerial Photograph Locations.

Table 8.3. Shapes of Institutional, Commercial and Industrial Buildings

	% of Buildings Associated with Each Building Shape			
Building Shape	Institutional	Commercial	Industrial	All
C	2.4	7.5	1.5	2.5
L	10.5	7.5	9.3	8.8
T	1.6	2.1	1.4	1.5
Complex	4.0	7.1	4.3	7.9
Rectangular	81.4	68.4	78.3	75.8
Circular	-	0.5	0.9	0.6
Z	-	-	3.5	1.8
H	-	-	0.9	0.6
X	-	0.6	-	0.1
Triangular		0.6	-	0.1

The building shape data base developed by ARA during the Florida Residential Construction Mitigation Program (RCMP) is comprised of 1103 homes. The roof shapes of these homes consists of 29% hip roof, 56% gable, 10% combination (e.g., hip/gable, hip/flat, etc.) and 5% other (e.g., flat, mansard). Single story homes comprised 85% of the total population of buildings in the RCMP building characteristics database. These proportions are comparable to the aerial photography results.

The HUD post-Andrew damage survey of 466 homes indicates that 80% are single story, and gable roofs comprise 80% of the population of one story homes. Of the two story homes, in excess of 95% had gable roofs.

The suggested simplified default building stock geometry for single family residential construction in Southeast Florida is:

Single Story Gable	60%
Single Story Hip	20%
Two Story Gable	20%

8.3 Contractor Survey

In order to estimate the distribution of roof cover types expected in the Southeast Florida area, a survey form was developed by Mr. Tom Smith, and sent to over twenty roofing contractors who do business in Palm Beach, Broward and Dade Counties. The survey form sent to the roofing contractors is shown in Figure 8.2. A total of eleven responses were received from the roofing contractors. In the brief discussion of the survey results, commercial/ industrial/institutional roof covers and residential roof cover responses are treated separately.

Commercial/Industrial/Institutional Roof Covers. The results of the survey with respect to existing roof covers and newly installed roof covers are given in Tables 8.4 and 8.5, respectively. For the existing population of buildings, the survey results clearly indicate that built-up and modified bitumen roof covers are the most commonly applied roof cover for non-residential buildings in Southeast Florida. These roof covers are expected to constitute approximately 85% of the existing population of non-residential buildings. As discussed earlier, the roof cover modeling methodology treats the failure of modified bitumen and built up roofs in the same manner.

The results of the survey with respect to new roof cover installations indicates the total combined population of built-up and modified bitumen roofs is about the same as for the existing population of roof covers, but there is a trend towards using more modified bitumen roofs than built-up with aggregate surface.

As seen in Table 8.6, the results of the survey show that existing roof covers were not typically installed such the resistance of the roofs would be higher in the more highly loaded corner regions.

The uplift capacity of the roof covers on commercial/industrial/and institutional buildings is implied by the results given in Table 8.7. Only two of the eleven respondents indicated that they felt roof covers were installed such that they met the Factory Mutual FM 1-90 standards.

Quality of installation is addressed in Table 8.8, where it is suggested that on average, prior to 1993, only 50% of the roofs were well installed. The contractors indicate that the quality of installation has improved beginning in about 1993-1994, about the time the newest edition of the South Florida Building Code was issued.

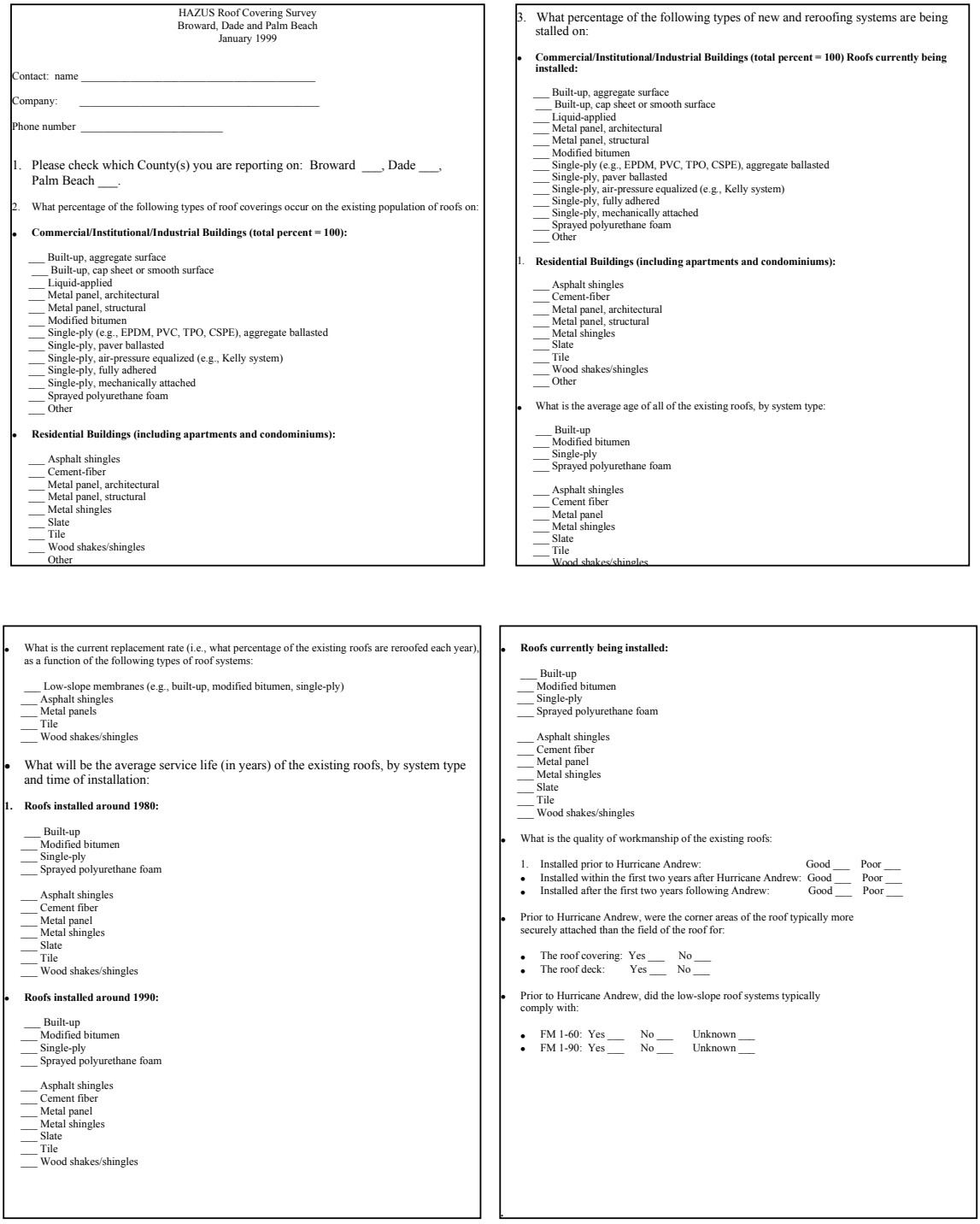

HAZUS Roof Covering Survey
Broward, Dade and Palm Beach
January 1999

Contact: name _____

Company: _____

Phone number _____

1. Please check which County(s) you are reporting on: Broward ___, Dade ___, Palm Beach ___.

2. What percentage of the following types of roof coverings occur on the existing population of roofs on:

- **Commercial/Institutional/Industrial Buildings (total percent = 100):**

___ Built-up, aggregate surface
___ Built-up, cap sheet or smooth surface
___ Liquid-applied
___ Metal panel, architectural
___ Metal panel, structural
___ Modified bitumen
___ Single-ply (e.g., EPDM, PVC, TPO, CSPE), aggregate ballasted
___ Single-ply, paver ballasted
___ Single-ply, air-pressure equalized (e.g., Kelly system)
___ Single-ply, fully adhered
___ Single-ply, mechanically attached
___ Sprayed polyurethane foam
___ Other

- **Residential Buildings (including apartments and condominiums):**

___ Asphalt shingles
___ Cement-fiber
___ Metal panel, architectural
___ Metal panel, structural
___ Metal shingles
___ Slate
___ Tile
___ Wood shakes/shingles
___ Other

3. What percentage of the following types of new and reroofing systems are being stalled on:

- **Commercial/Institutional/Industrial Buildings (total percent = 100) Roofs currently being installed:**

___ Built-up, aggregate surface
___ Built-up, cap sheet or smooth surface
___ Liquid-applied
___ Metal panel, architectural
___ Metal panel, structural
___ Modified bitumen
___ Single-ply (e.g., EPDM, PVC, TPO, CSPE), aggregate ballasted
___ Single-ply, paver ballasted
___ Single-ply, air-pressure equalized (e.g., Kelly system)
___ Single-ply, fully adhered
___ Single-ply, mechanically attached
___ Sprayed polyurethane foam
___ Other

1. **Residential Buildings (including apartments and condominiums):**

___ Asphalt shingles
___ Cement-fiber
___ Metal panel, architectural
___ Metal panel, structural
___ Metal shingles
___ Slate
___ Tile
___ Wood shakes/shingles
___ Other

- What is the average age of all of the existing roofs, by system type:

___ Built-up
___ Modified bitumen
___ Single-ply
___ Sprayed polyurethane foam

___ Asphalt shingles
___ Cement fiber
___ Metal panel
___ Metal shingles
___ Slate
___ Tile
___ Wood shakes/shingles

- What is the current replacement rate (i.e., what percentage of the existing roofs are reroofed each year), as a function of the following types of roof systems:

___ Low-slope membranes (e.g., built-up, modified bitumen, single-ply)
___ Asphalt shingles
___ Metal panels
___ Tile
___ Wood shakes/shingles

- What will be the average service life (in years) of the existing roofs, by system type and time of installation:

1. **Roofs installed around 1980:**

___ Built-up
___ Modified bitumen
___ Single-ply
___ Sprayed polyurethane foam

___ Asphalt shingles
___ Cement fiber
___ Metal panel
___ Metal shingles
___ Slate
___ Tile
___ Wood shakes/shingles

- **Roofs installed around 1990:**

___ Built-up
___ Modified bitumen
___ Single-ply
___ Sprayed polyurethane foam

___ Asphalt shingles
___ Cement fiber
___ Metal panel
___ Metal shingles
___ Slate
___ Tile
___ Wood shakes/shingles

- **Roofs currently being installed:**

___ Built-up
___ Modified bitumen
___ Single-ply
___ Sprayed polyurethane foam

___ Asphalt shingles
___ Cement fiber
___ Metal panel
___ Metal shingles
___ Slate
___ Tile
___ Wood shakes/shingles

- What is the quality of workmanship of the existing roofs:

1. Installed prior to Hurricane Andrew: Good ___ Poor ___
- Installed within the first two years after Hurricane Andrew: Good ___ Poor ___
- Installed after the first two years following Andrew: Good ___ Poor ___

- Prior to Hurricane Andrew, were the corner areas of the roof typically more securely attached than the field of the roof for:

- The roof covering: Yes ___ No ___
- The roof deck: Yes ___ No ___

- Prior to Hurricane Andrew, did the low-slope roof systems typically comply with:

- FM 1-60: Yes ___ No ___ Unknown ___
- FM 1-90: Yes ___ No ___ Unknown ___

Figure 8.2. Survey Form Sent to Roof Contractors to Ascertain Relative Frequency of Roof Cover Types.

Table 8.4. Responses to the Question: "What Percentage of the Following Types of Roof Coverings Occur on the Existing Populations of Commercial/Institutional/Industrial Buildings?"

Roof Cover Type	Response Number											
	1	2	3	4	5	6	7	8	9	10	11	AVE
Built-up, aggregate surface	20	30	50	60		60	40	30	30	55	30	41.8
Built-up, cap sheet or smooth surface	40	8	5	20		15	20	10	40	15	13	19.2
Liquid-applied	0	1	0	0		0	0	0	0	0	1	0.2
Metal panel, architectural	0	5	5	0.05		0	0	10	0	0	5	0.6
Metal panel, structural	0	3	0	0.05		0	0	0	0	0	5	0.8
Modified bitumen	40	25	30	15		25	20	18	30	25	25	26.1
Single-ply aggregate ballasted	0	10	0	0		0	5	0	0	0	2	1.8
Single-ply, paver ballasted	0	2	0	0		0	0	0	0	2	2	0.6
Single-ply, air-pressure equalized	0	1	0	0		0	0	0	0	0	1	0.2
Single-ply, fully adhered	0	5	5	0.05		0	0	10	0	0	2	2.3
Single-ply, mechanically attached	0	5	5	2		0	0	5	0	2	2	2.2
Sprayed polyurethane foam	0	5	0	0.05		0	5	2	0	1	1	1.5
Other	0	0	0	1		0	0	5	0	0	1	0.7
Total	100	100	100	98.2		100	90	90	100	100	90	100

Table 8.5. Responses to the Question: "What Percentage of the Following Types of New and Re-roofing Systems are Being Installed on Commercial/Institutional/Industrial Buildings?"

Roof Cover Type	Response Number											
	1	2	3	4	5	6	7	8	9	10	11	AVE
Built-up, aggregate surface	20	30	50	10		70	30	40	30	30	19	32.9
Built-up, cap sheet or smooth surface	40	5	0	30		4	15	20	40	10	19	18.3
Liquid-applied	0	2	0	0		0	0	0	0	0	0	0.2
Metal panel, architectural	0	7	10	5		0	0	5	0	3	1	3.1
Metal panel, structural	0	2	0	1		0	0	0	0	0	1	0.4
Modified bitumen	40	30	30	50		25	20	21	30	50	50	34.6
Single-ply aggregate ballasted	0	10	0	0		0	20	0	0	0	6	3.6
Single-ply, paver ballasted	0	3	0	0		0	0	0	0	0	1	0.4
Single-ply, air-pressure equalized	0	1	0	0		0	0	0	0	0	1	0.2
Single-ply, fully adhered	0	2	5	1		1	10	10	0	0	1	3.0
Single-ply, mechanically attached	0	3	5	2		0	0	2	0	2	1	1.5
Sprayed polyurethane foam	0	3	0	1		0	5	2	0	0	0	1.1
Other	0	2	0	0		0	0	0	0	5	0	0.7
Total	100	100	100	100		100	100	100	100	100	100	100

Table 8.6. Responses to the Question: "Prior to Hurricane Andrew, Were the Corner Areas of the Roof Typically More Securely Attached than the Field of the Roof?"

	Response Number										
	1	2	3	4	5	6	7	8	9	10	11
The roof covering	No	No	No	No	Yes	No	No	No	No	No	No
The roof deck	No	No	No	No	Yes	No	No	No	No	Yes	No

Table 8.7. Responses to the Question: "Prior to Hurricane Andrew, Did the Low Slope Roof Systems Typically Comply with FM I-60 or FM I-90?"

	Response Number										
	1	2	3	4	5	6	7	8	9	10	11
FM 1-60	Yes	Yes		No	Yes	U	No	Yes	U	U	Yes
FM 1-90	No	No	Yes	No	Yes	U	No	No	U	U	No

U = Unknown

Table 8.8. Responses to the Question: "What is the Quality of Workmanship of the Existing Roofs?"

Installation Time	Response Number											Summary
	1	2	3	4	5	6	7	8	9	10	11	
Prior to Hurricane Andrew	G	G	P	P	G	G	P	G	G	P	P	55% G, 45% P
Within first two years following Andrew	G	P	G/P	P	G	G	P	G	G	P	P	50% G, 50% P
After the first two years following Andrew	G	P	G	P	G	G	G	G	G	G	G	82% G, 18% P

Residential Roof Covers. Not surprisingly, the survey results indicate that 90% of the residential roof covers are either tile or shingle, with tile roofs being more common than shingle roofs (Table 8.9). Wood shakes and metal panels were felt to be the next most common roof cover type, representing 3.3% and 2.3% of the total roof covers in use in residential buildings.

In new construction and re-roofing (Table 8.10), shingle and tiles again are estimated to comprise about 90% of the roofs.

The RCMP data on 1100 homes in Dade, Broward, and Palm Beach counties indicates that about 47% have shingles, 45% tiles, 6% built-up, and the remaining 2% are wood shakes, slate and metal roof. These data will be used to develop the default inventory data for the South Florida regional study.

Table 8.9. Responses to the Question: "What Percentage of the Following Types of Roof Coverings Occur on the Existing Populations of Residential Buildings (Including Apartments and Condominiums)?"

Roof Cover Type	Response Number											
	1	2	3	4	5	6	7	8	9	10	11	AVE
Asphalt shingles	80	35	40	33	30	10	50		55	40	40	41.3
Cement-fiber	0	2	0	0	0	0	0		0	0	1	0.3
Metal panel, architectural	0	5	10	2	0	0	0		0	0	6	2.3
Metal panel, structural	0	1	0	1	0	0	0		0	0	1	0.3
Metal shingles	0	3	0	0	0	0	0		0	0	1	0.4
Slate	0	2	0	0	0	0	0		0	0	1	0.3
Tile	20	40	40	60	70	90	50		45	40	40	49.5
Wood shakes/shingles	0	10	10	3	0	0	0		0	0	10	3.3
Other	0	4	0	1	0	0	0		0	20	0	2.5
Total	100	102	100	100	100	100	100		100	100	100	100

Table 8.10. Responses to the Question: "What Percentage of the Following Types of New and Re-roofing Systems are Being Installed on Residential Buildings (Including Apartments and Condominiums)?"

Roof Cover Type	Response Number											
	1	2	3	4	5	6	7	8	9	10	11	AVE
Asphalt shingles	50	30	10	65	50	5	50		50	40	40	39
Cement-fiber	0	0	0	0	0	0	0		0	0	0	0
Metal panel, architectural	0	8	10	3	0	0	0		0	0	0	2.1
Metal panel, structural	0	1	0	0	0	0	0		0	0	0	0.1
Metal shingles	0	3	0	0	0	0	0		0	0	0	0.3
Slate	0	1	0	0	0	0	0		0	0	0	0.1
Tile	50	45	70	30	50	95	50		50	40	60	54
Wood shakes/shingles	0	5	10	1	0	0	0		0	0	0	1.6
Other	0	7	0	1	0	0	0		0	20	0	2.8
Total	100	100	100	100	100	100	100		100	100	100	0

Chapter 9. Loss Model Validation Studies for Hurricanes Andrew, Erin, Opal and Hugo

9.1 Introduction

The objective of the validation studies is to assess the performance of the hazard-load-resistance-damage-loss model through comparisons of simulated and observed loss statistics. The modeling approach entails selecting a population of buildings that are representative of those associated with the study regions (in these examples, South Florida, the Florida Panhandle, and South Carolina), locating these buildings within the study region, assigning the terrain values, performing the hurricane simulation, damaging the buildings during the passage of the hurricane and finally computing the losses. Each of the steps noted above requires some assumptions, particularly with respect to the building stock. The assumptions regarding the building stock are discussed on a case by case basis later in this section.

Loss model validation studies have been completed using the load, damage and loss models described in Chapters 4 through 7, coupled with the terrain modeling described in Chapter 3. The end-to-end loss validation studies are performed using ZIP Code averaged loss data for Hurricane Andrew obtained from two different sources, residential loss data provided by an insurance company for Hurricanes Erin and Opal, and residential loss data using ZIP Code averaged data for Hurricane Hugo in South Carolina.

The loss data provided for the Hurricanes Andrew and Hugo comparisons represents the total repair and replacement losses associated with the building and the contents. The ZIP Code averaged loss data are given in Bhinderwala (1995). A second set of Hurricane Andrew data is also ZIP Code averaged data for building and content losses. The loss data for Hurricanes Erin and Opal represents losses associated with damage to the building only.

Since both the actual and modeled losses are very sensitive to the wind speeds experienced at a given location, each set of loss comparisons is accompanied with a discussion of the modeled wind speeds, with comparisons of modeled and observed wind speeds presented where possible.

9.2 Example Results – Hurricane Andrew

For the Hurricane Andrew damage to loss simulation, the building stock is modeled assuming 80% of the homes were single story (25% hip, 75% gable). All two story homes are modeled as having gable roofs. 63% of the one story homes and 50% of the two story homes are assumed to have a garage. 40% of the homes use 6d roof sheathing nails spaced at 6″ on center at the edges and 12″ on center in the field, with the remaining 60% of the homes having sheathing nailed with 8d nails using the 6″/12″ spacing. All roof-wall connections are assumed to be strapped. The roof cover of the homes are modeled with 50% of the homes having a shingle roof cover and 50% of the homes

having tiles as the roof cover. All loss analyses for Hurricane Andrew are performed with the construction quality factor set equal to one. The average surface roughness at the ZIP Code level is estimated using both the FWMD data and the MRLC data. Therefore, two example sets of results are given, one using the FWMD terrain data base and the other using the MRLC terrain database. The hurricane simulation is performed with the wind speeds computed at the geographic centroid of each ZIP Code. The houses are assumed to be randomly oriented within a ZIP Code.

The loss ratios (total loss divided by the total coverage limits) are plotted vs. the maximum modeled peak gust wind speed (open terrain) computed at each ZIP Code centroid. The value of the contents in this example is taken as 70% of the value of the structure, and the losses are capped so that they cannot exceed the insured value of the structure and/or contents. It is worth noting that in many instances the cost of rebuilding a severely damaged house can exceed the replacement value of the house because it is more expensive to demolish and replace the building than it is to build a new building on a site which does not have an existing structure. Total losses exceeding the replacement value of a building occurred frequently in the heavily damaged areas associated with Hurricane Andrew.

Comparisons of the predicted and observed losses are plotted vs. the modeled peak gust wind speed at the centroid of the ZIP Code in Figure 9.1 for both terrain cases. The results indicate that using the Hazus loading, damage and loss models for residential buildings works reasonably well.

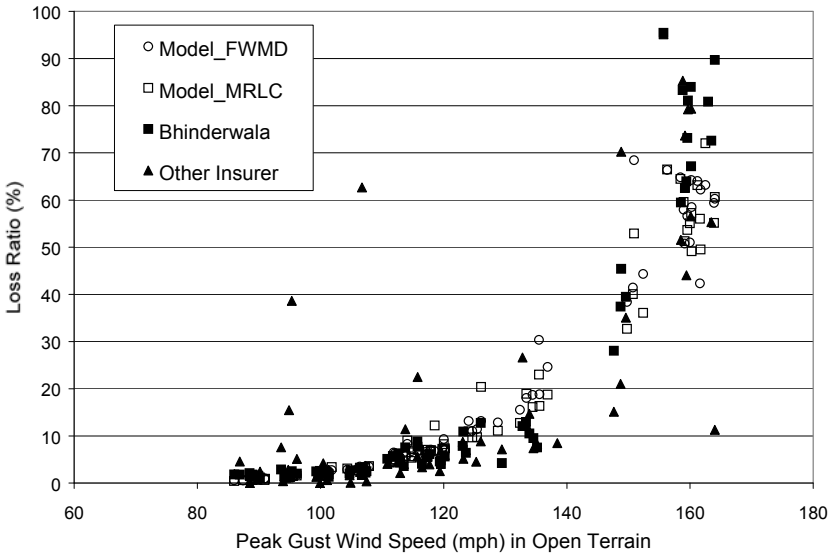

Figure 9.1. Comparison of Observed and Simulated ZIP Code Averaged Losses Produced by Hurricane Andrew in Dade County, Florida.

Figure 9.2 shows an *x-y* plot comparing modeled and observed losses for the two different terrain database cases. Results are given for losses in the range of 0 to 10%, 0 to 50% and 0 to 100%, to help visualize how the model performs for various loss ranges. To facilitate the assessment of the loss sensitivity to the assumed terrain, modeled loss ratios using the FWMD terrain data and the MRLC terrain data are compared in Figure 9.3. No significant bias is found using either of these two databases.

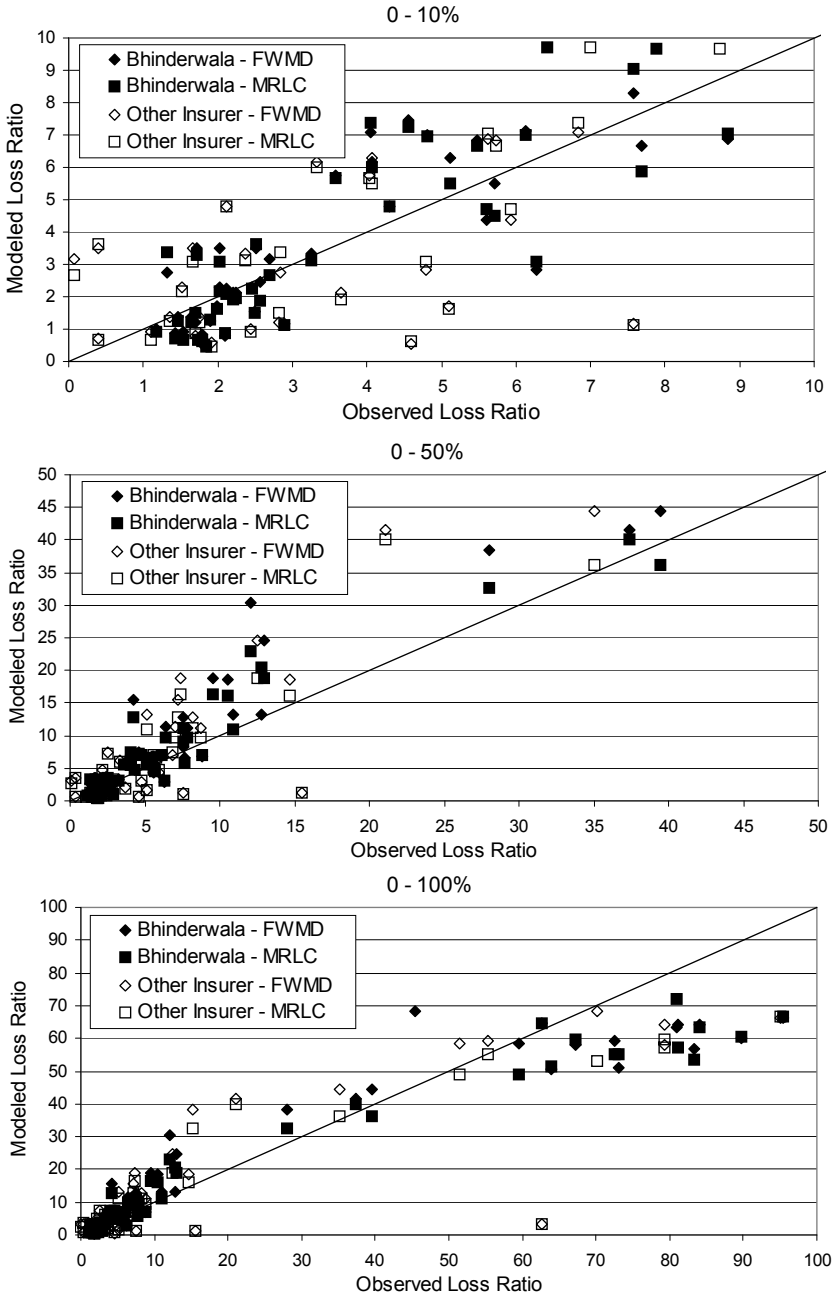

Figure 9.2. Comparison of Modeled vs. Observed Losses.

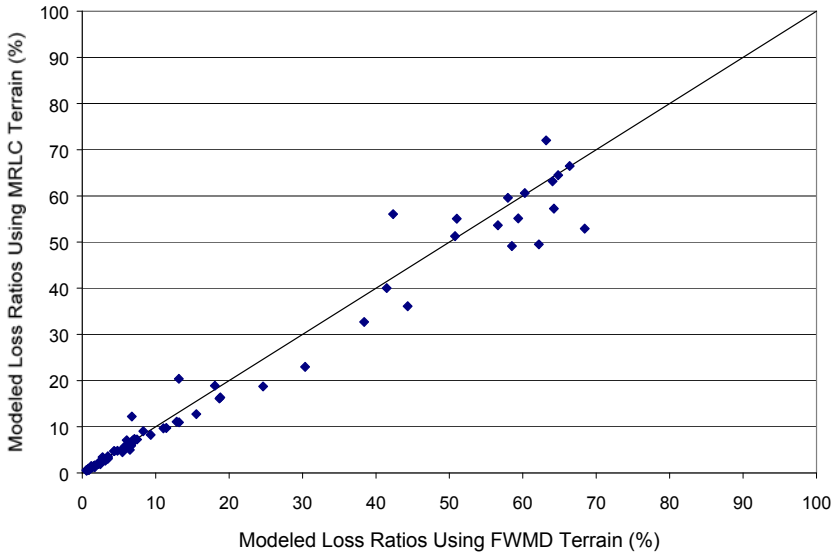

Figure 9.3. Comparison of Modeled Losses Using FWMD Terrain and MRLC Terrain.

The geographic variation of the observed and modeled losses is shown in Figures 9.4 through 9.7. Comparing the losses given in Figures 9.4 and 9.5 (both actual losses) provides an indication of the statistical variation that can be expected from the data alone, without taking into account errors introduced by wind speed modeling, terrain, etc.

Total Losses. The total loss (building plus content), summed over all of Dade County, is estimated assuming that both the number of policies and value of these policies in each ZIP Code are the same. In each case, a contribution to the estimated total loss was computed only if the insurer had policies in the given ZIP Code. This is clearly not the case in Dade County, but a comparison presented in this manner is valid, and helps mask the identity of a given insurer. The aggregate losses are given in Table 9.1. Note that the actual and modeled totals given in Table 9.1 differ between cases because the number of ZIP Codes having policies is different for the different insurers.

The results shown in Table 9.1 indicate that the modeled losses resulting from the two terrain models (FWMD and MRLC) are slightly lower than the observed losses, with the FWMD terrain model yielding the higher values of the estimated losses.

Modeled Wind Speeds in Dade County Produced by Hurricane Andrew. Figure 9.8 shows a contour representation of the maximum peak gust wind speeds produced by the hurricane model for the Hurricane Andrew simulation. The maximum wind speeds produced by the model are of the order of 165 mph, with the maximum wind speeds occurring in the same area as the maximum losses as shown in Figures 9.4 and 9.5. Figure 9.8 also shows the locations of three anemometers where wind speed and directions were recorded during the storm, as well as the location of the nine NAHB survey sites discussed in Chapter 4, for which wind speed estimates were provided by NOAA/HRD.

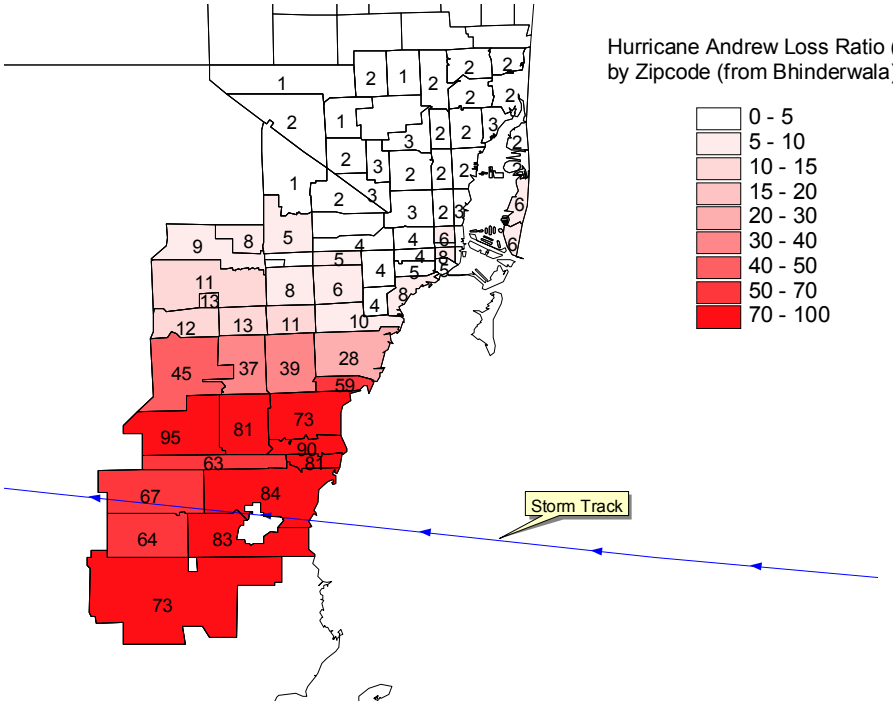

Figure 9.4. Loss Ratios by ZIP Code in Dade County (Bhinderwala Data).

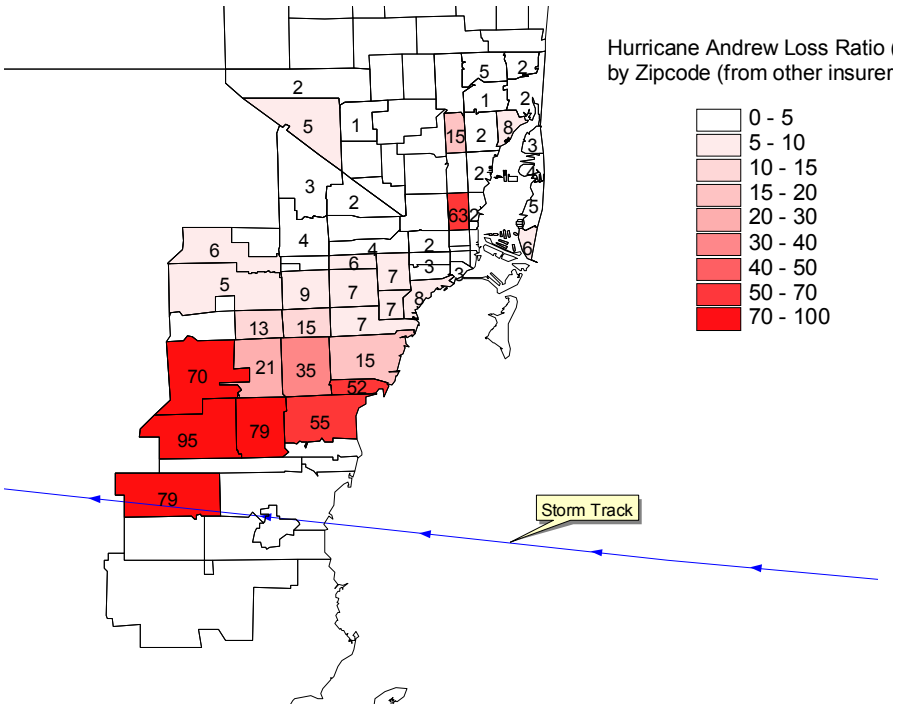

Figure 9.5. Loss Ratios by ZIP Code in Dade County (Other Insurer Data).

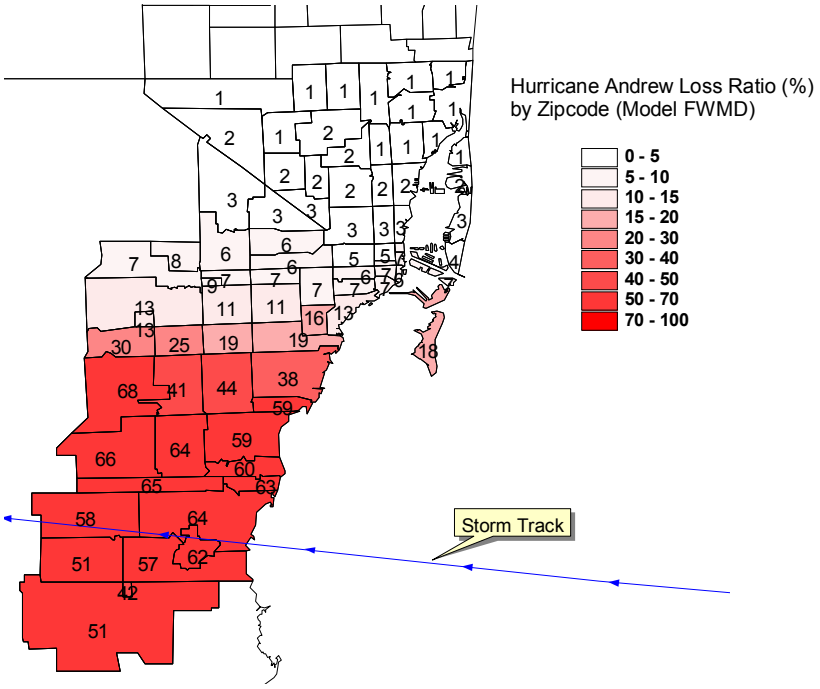

Figure 9.6. Modeled Loss Ratio (FWMD).

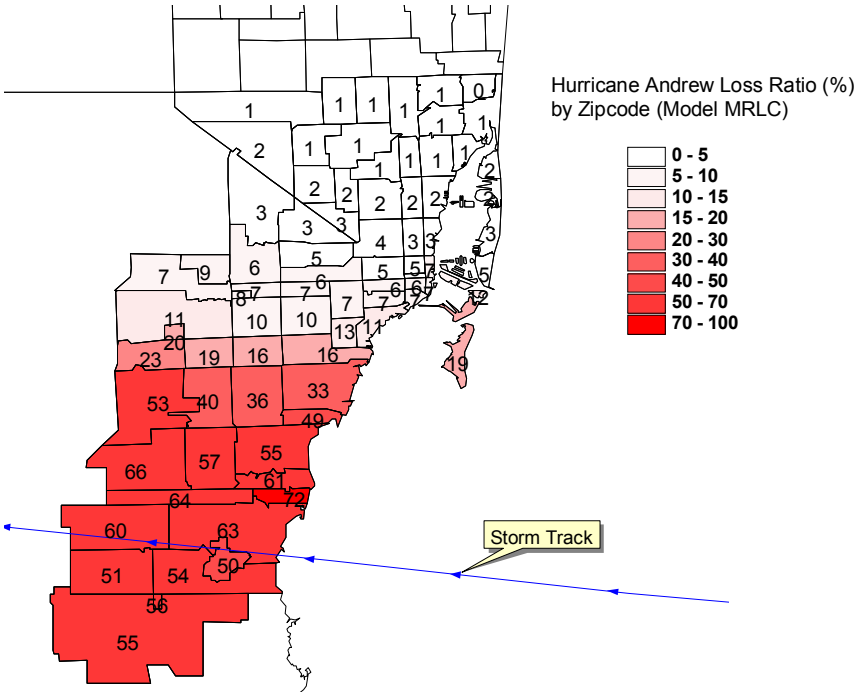

Figure 9.7. Modeled Loss Ratio (MRLC).

Table 9.1. Comparison of Modeled and Observed Losses from Hurricane Andrew

Case	Actual Loss Ratio(%)	Modeled Loss Ratio (%) (FWMD)	Modeled Loss Ratio (%) (MRLC)
Bhinderwala	19.1	18.0	17.0
Other Insurer	15.7	15.3	13.8

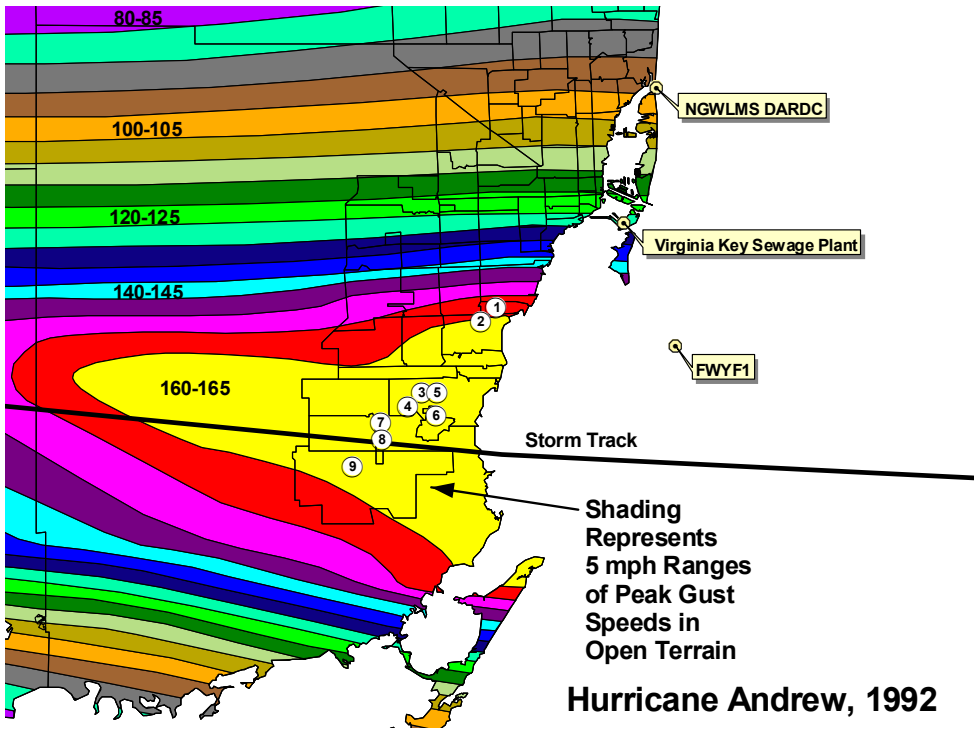

Figure 9.8. Swath of Modeled Peak Gust Wind Speeds Produced by Hurricane Andrew.

Figure 9.9 presents comparisons of the simulated and observed peak gust wind speeds and the mean wind directions at the three anemometer sites. The agreement between the observed and modeled wind speeds and directions is generally good. One major discrepancy in the comparison of the peak gust wind speed recorded at the Haulover site at 08:00 is associated with an anomalous gust. Note that the wind speeds recorded at the Virginia Key site are not from a continuous record and, thus, the peak values shown may not correspond to the maximum in the storm.

Figures 9.10 through 9.12 show comparisons of the model generated peak gust wind speeds at the locations of the nine NAHB damage surveys to the estimates of wind speeds and direction at these same sites derived by NOAA/HRD personnel. The comparisons of the wind speed traces suggest the NOAA/HRD representation of the wind field is somewhat broader than that produced by the wind field model. At the two northern locations (positions 1 and 2 as shown in Figure 9.8), the maximum values of the HRD estimated peak gust wind speeds are about 10 mph to 15 mph higher than those obtained from the wind field model.

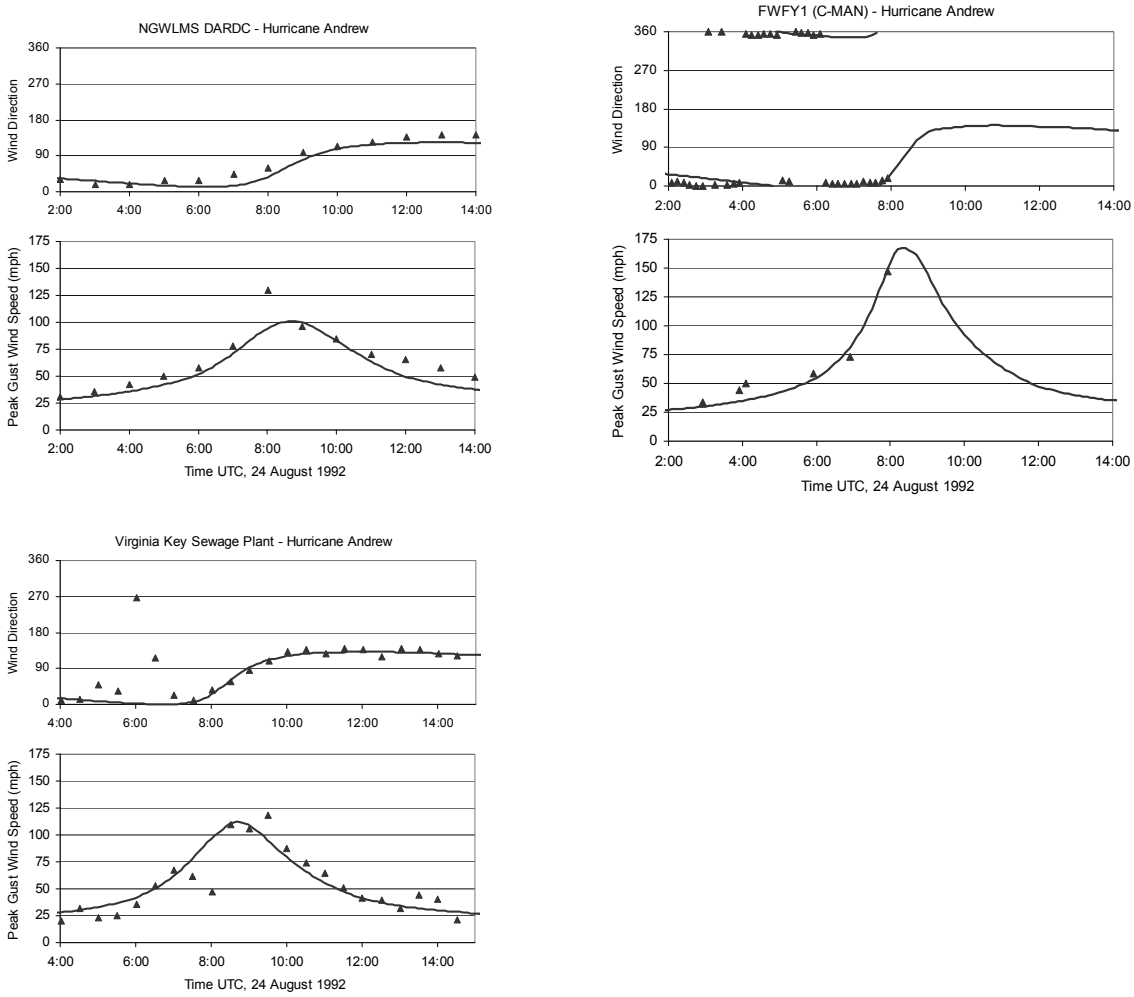

Figure 9.9. Comparison of Simulated and Observed Peak Gust Wind Speeds and Directions Produced by Hurricane Andrew. Gust Data at Virginia Key Location Derived from One Minute Mean Values. All Wind Speeds are Given for the Actual Terrain at a Height of 10 m Above Ground.

Moving towards the south, the differences in the magnitude of the HRD maximum wind speeds and the simulated wind speeds reduce, where at the southern most points, the modeled wind speeds are slightly higher (~10 mph) than the HRD values.

Overall, the differences between the modeled wind speeds and the HRD estimated wind speeds are typically less than 10%, a difference which is less than the uncertainty attributable to adjusting the aircraft measured wind speeds to surface level wind speeds as indicated in Powell and Houston (1996).

The wind speed and direction traces from the wind field model and those provided by HRD are used in the conjunction with the damage and loss models to determine the effect of these different wind speed estimates on predicted losses. The building stock used in this damage and loss analysis is the same as described earlier for the basic Hurricane

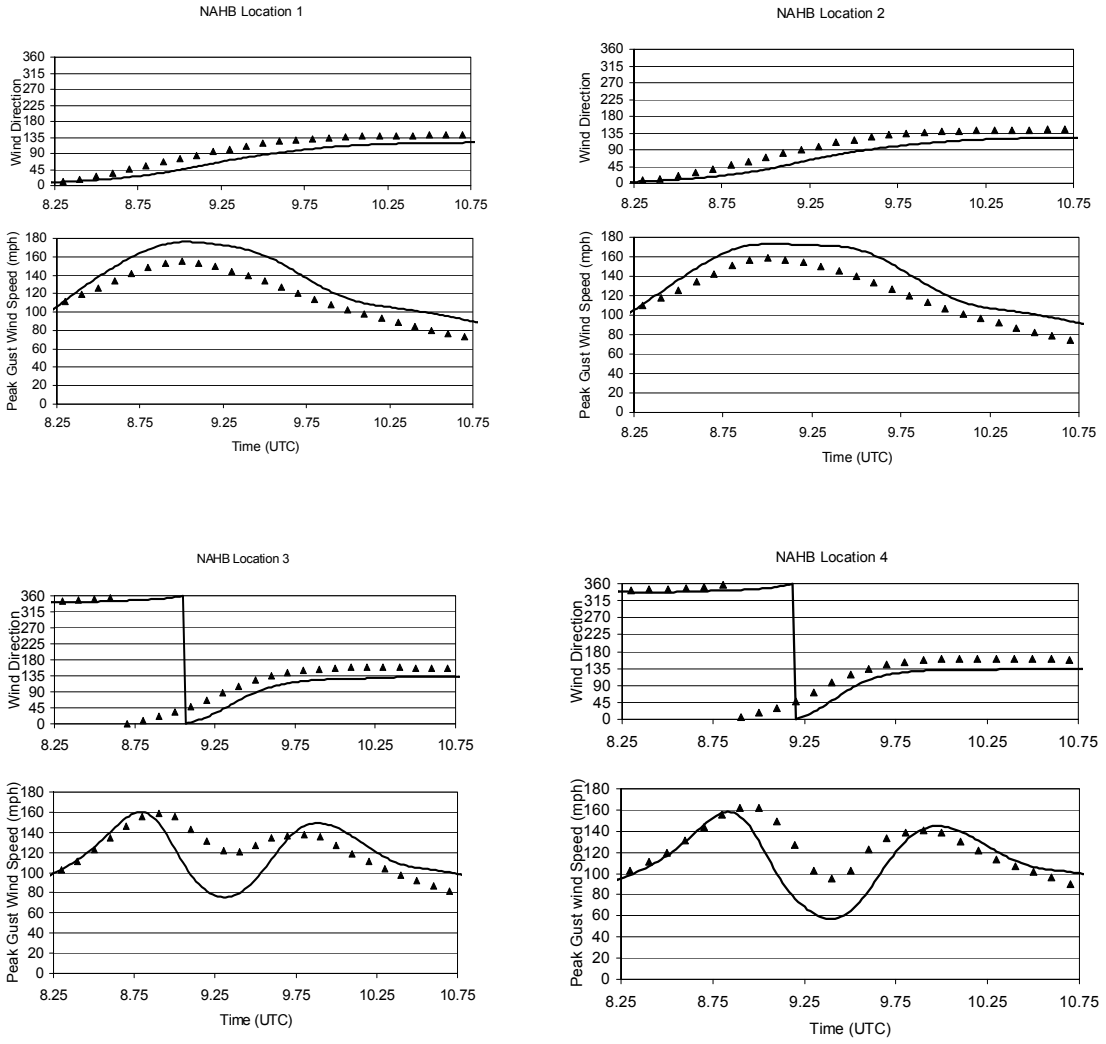

Figure 9.10. Comparison of Simulated Peak Gust Wind Speeds and Wind Direction Obtained Using the Hurricane Wind Field Model (shown as triangles) to Wind Speeds Estimated by the Hurricane Research Division (shown as continuous line) at NAHB Locations 1 through 4 as Indicated in Figure 9.8.

Andrew loss simulation example. The loss example is performed using two surface roughness (z_0 = 0.15 m and z_0 = 0.35 m). Results are given in Table 9.2, along with estimates of the observed losses near the locations of each of the nine wind speed traces (compare loss ratio data given in Figures 9.4 and 9.5 to locations 1 through 9 shown in Figure 9.8). The losses predicted using the HRD wind speeds are notably higher than those predicted using the wind speed trace produced by the wind field model at locations one and two, simply because the HRD wind speeds are consistently higher. At locations 3 through 9, the losses produced using the HRD wind speed trace are lower than those obtained using the wind field model generated wind speed trace. The high losses produced using the modeled wind speed trace are primarily a result of the high wind speeds occurring for longer periods of time and being associated with larger wind direction changes than those produced by the HRD trace.

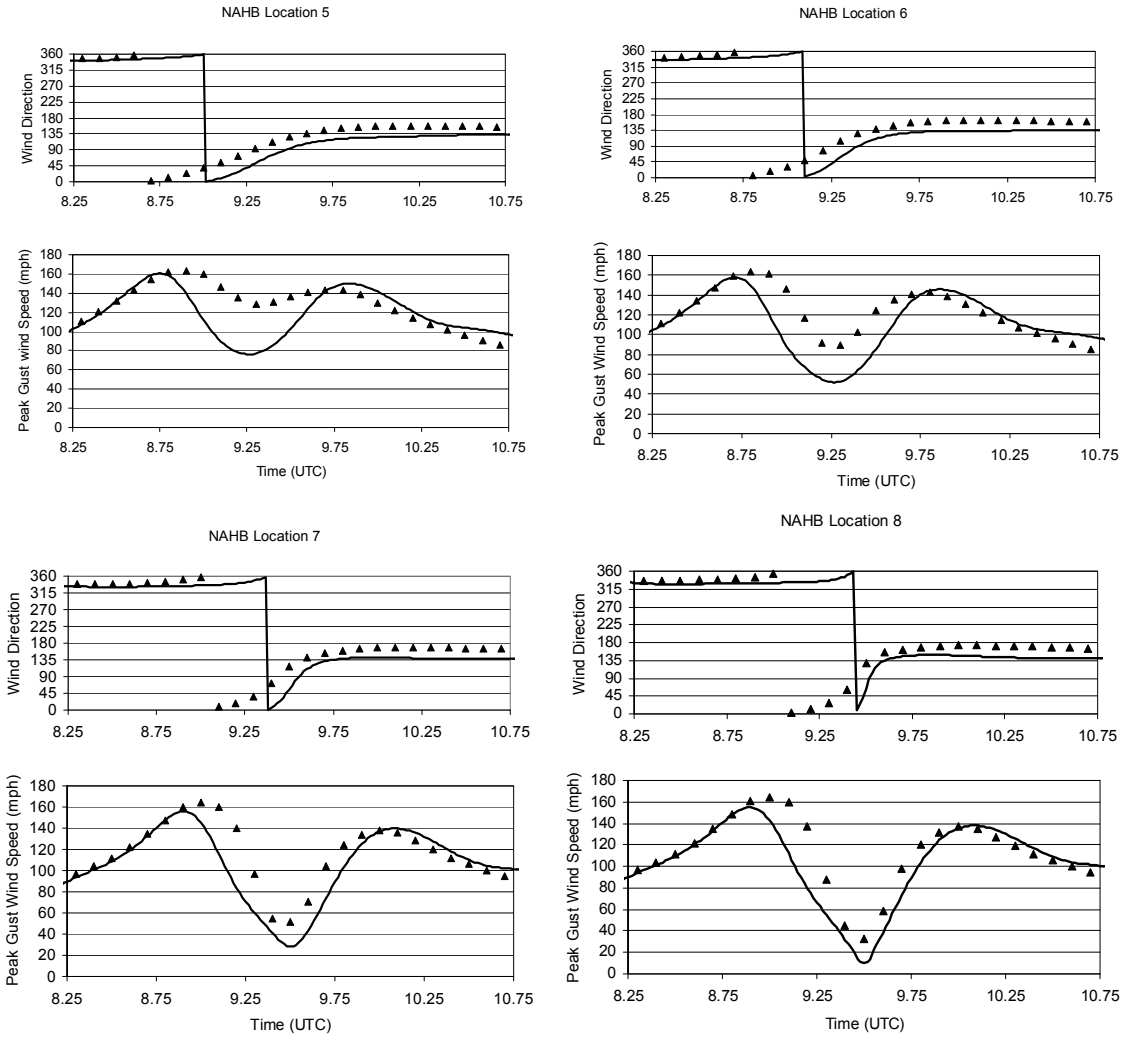

Figure 9.11. Comparison of Simulated Peak Gust Wind Speeds and Wind Direction Obtained Using the Hurricane Wind Field Model (shown as triangles) to Wind Speeds Estimated by the Hurricane Research Division (shown as continuous line) at NAHB Locations 5 through 8 as Indicated in Figure 9.8.

9.3 Example Results – Hurricanes Erin and Opal

Hurricane Erin and Opal Wind Speed Simulations. Figures 9.13 and 9.14 show contour plots of the foot print of maximum peak gust wind speeds swept out by Hurricanes Erin and Opal, as obtained from the hurricane wind field model. Figures 9.13 and 9.14 also show the locations of 4 anemometers used in the wind speed validation studies. Figures 9.15 and 9.16 show comparisons of the simulated and observed peak gust wind speeds of the four anemometer locations of both storms. In the wind speed validation examples given in Figures 9.15 and 9.16, note that the records from Eglin AFB and the Panama City Beach stations are not continuous records and, as a result, the maximum gust wind speeds produced at these sites may not have been recorded.

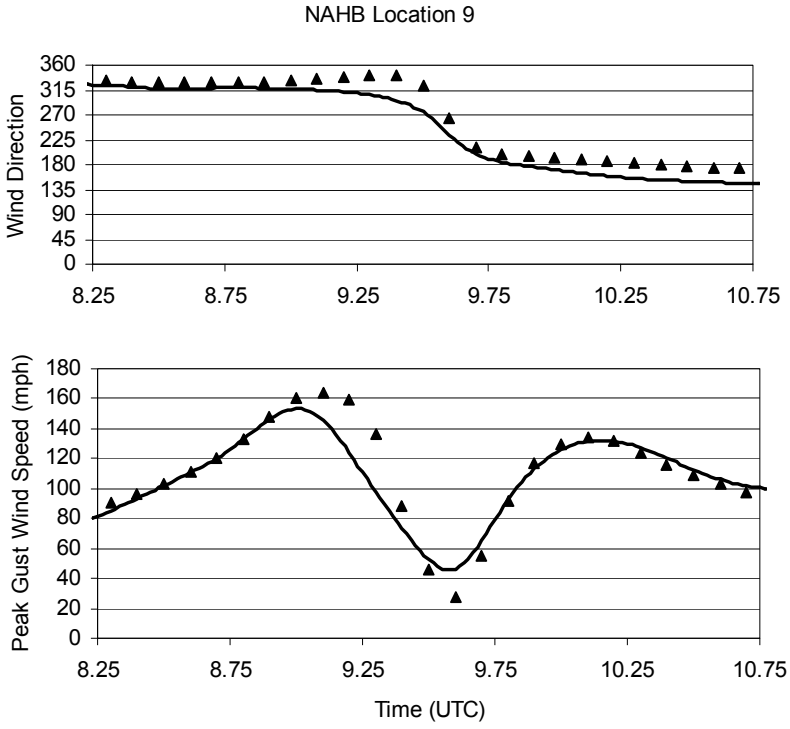

Figure 9.12. Comparison of Simulated Peak Gust Wind Speeds and Wind Direction Obtained Using the Hurricane Wind Field Model (shown as triangles) to Wind Speeds Estimated by the Hurricane Research Division (shown as continuous line) at NAHB Location 9 as Indicated in Figure 9.8.

Table 9.2. Comparisons of Loss Ratios Obtained Using the HRD Wind Speed Estimates to the Wind Field Model Wind Speed Estimates

Location	Wind Field Model Estimated Peak Gust Wind Speed (mph)	HRD Estimated Peak Gust Wind Speed (mph)	Loss Ratios Predicted Using Wind Field Model Wind Speeds (z_0=0.15 m)	Loss Ratios Predicted Using HRD Wind Speeds (z_0=0.15 m)	Actual Loss Ratios (%)	Loss Ratios Predicted Using Wind Field Model Wind Speeds (z_0=0.35 m)	Loss Ratios Predicted Using HRD Wind Speeds (z_0=0.35 m)
1	158.5	176.1	66%	85%	~50%-60%	51%	75%
2	161.4	173.2	71%	86%	~50%-60%	56%	74%
3	159.6	160.3	68%	61%	~80%	53%	44%
4	159.4	158.1	64%	55%	~80%	49%	38%
5	160.4	160.5	70%	61%	~80%	54%	44%
6	161.2	157.5	66%	54%	~80%	51%	39%
7	160	155.8	61%	49%	~60%-80%	45%	33%
8	160.6	154.9	62%	46%	~60%-80%	44%	30%
9	159.9	153.1	55%	44%	~70%	40%	30%

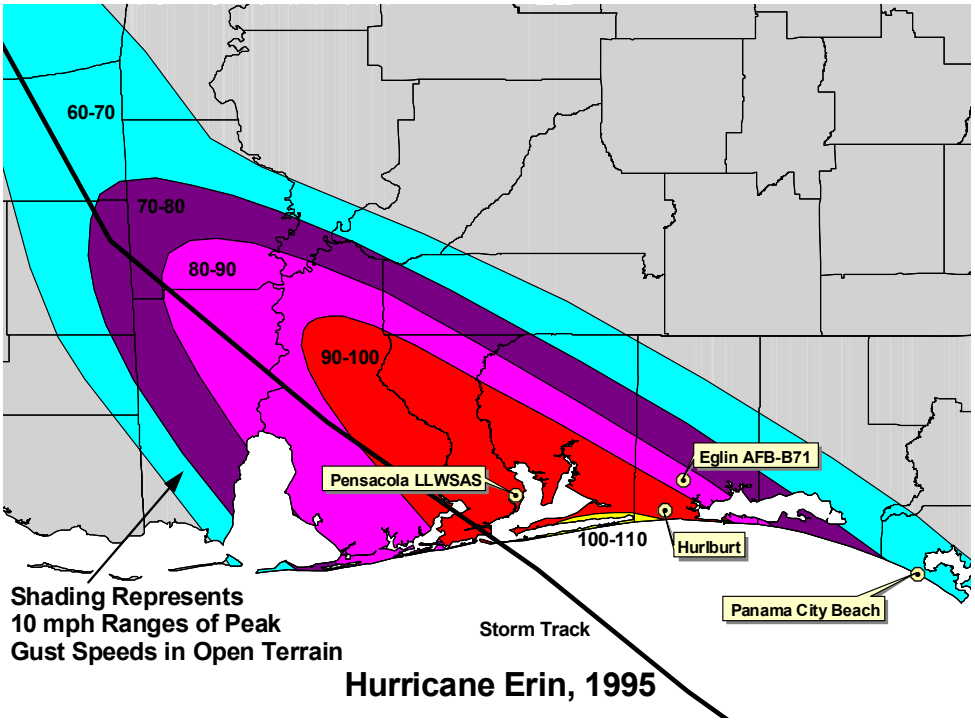

Figure 9.13. Swath of Simulated Peak Gust Wind Speeds (10 m in Open Terrain) Produced by Hurricane Erin.

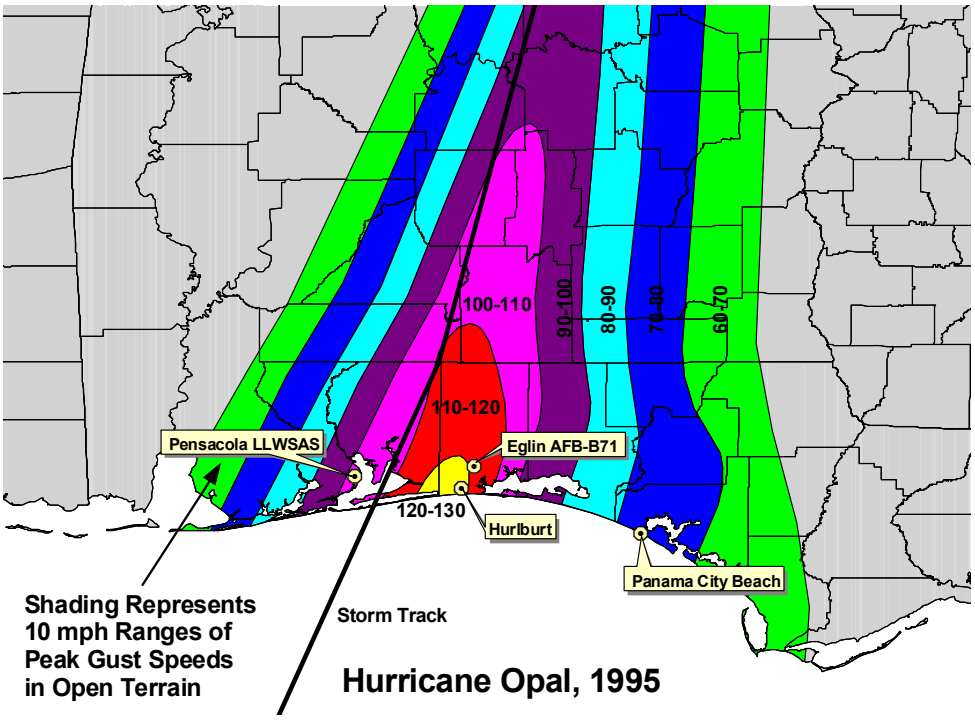

Figure 9.14. Swath of Simulated Peak Gust Wind Speeds (10 m in Open Terrain) Produced by Hurricane Opal.

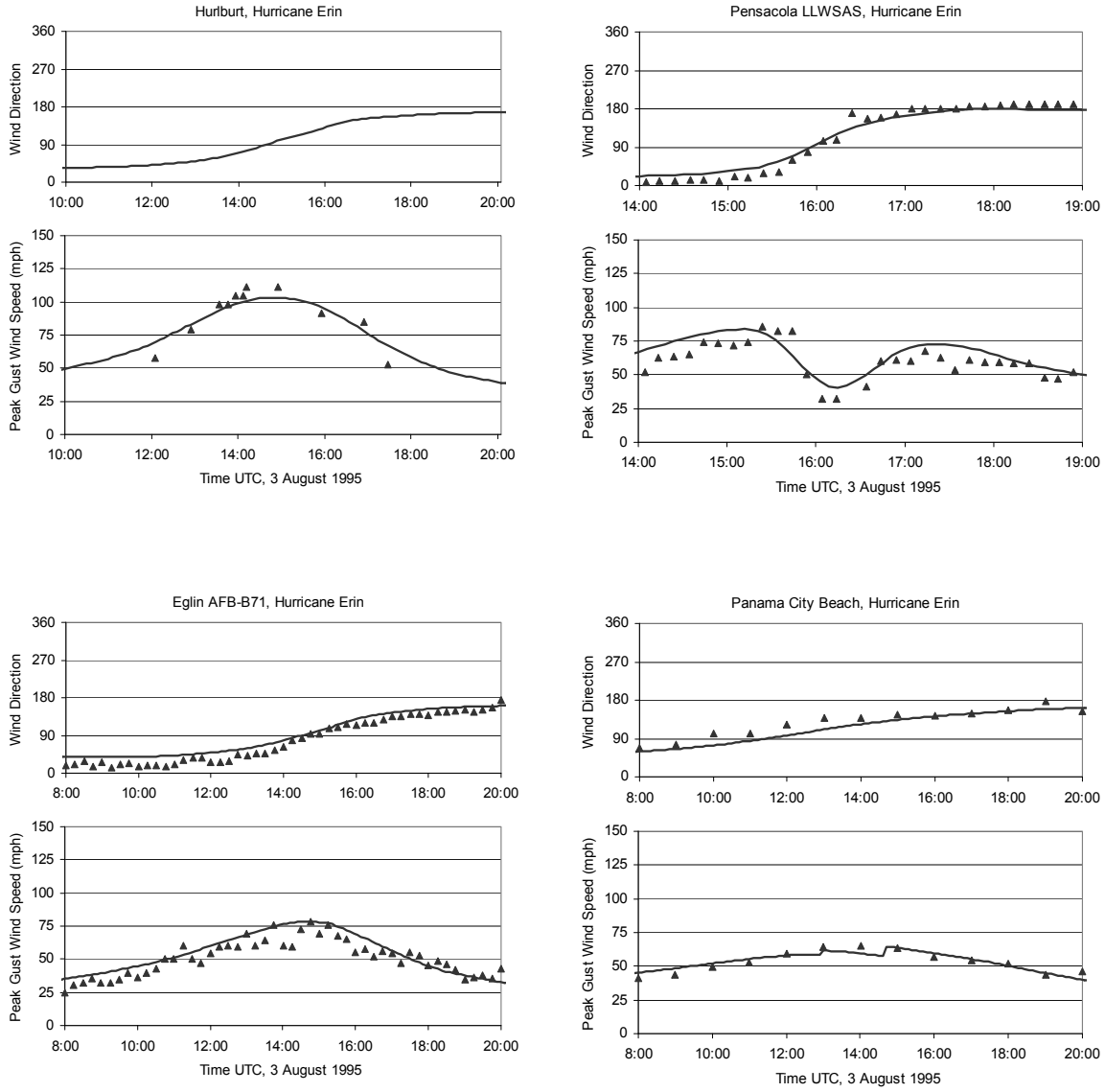

Figure 9.15. Comparison of Simulated and Observed Peak Gust Wind Speeds and Directions Produced by Hurricane Erin. Gust Data at Eglin AFB Location Derived from One Minute Mean Values. All Wind Speeds are Given for the Actual Terrain at a Height of 10 m Above Ground.

In the case of Hurricane Erin, the comparisons at the Hulburt Field station suggest that the model may be underestimating the peak gust wind speeds by about 5%, but is generally good elsewhere. In the case of Hurricane Opal, the agreement between modeled and observed wind speeds for locations on the right hand side of the storm is reasonable, but the model is overestimating the wind speeds on the left hand side of the storm as indicated by the comparison of wind speeds at the Pensacola station. The maximum simulated peak gust wind speeds are typically within about 5% to 10% of the observed values. The overall shapes of the simulated traces are similar to the observed traces indicating that the duration characteristics of the modeled and observed storms are similar.

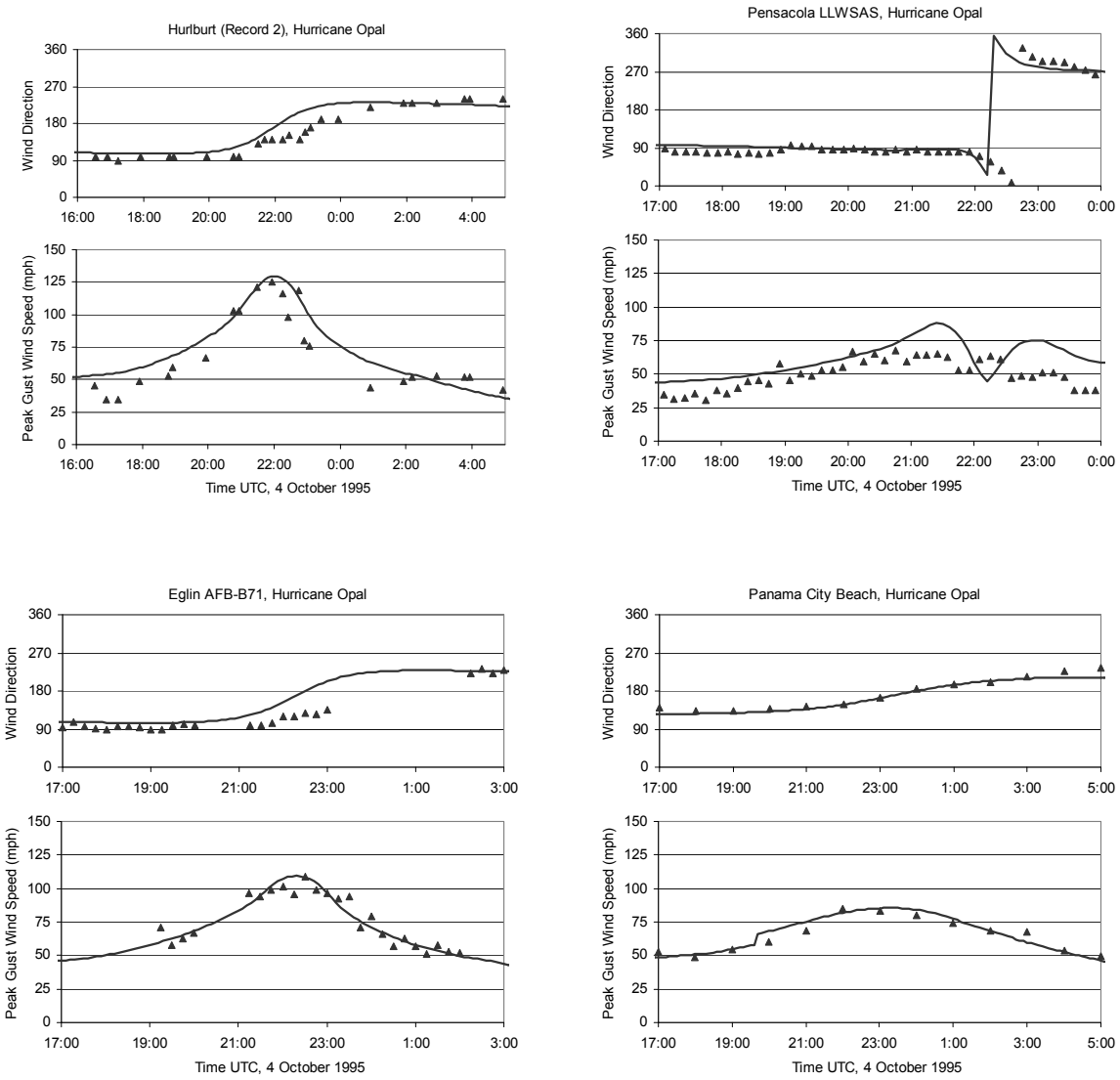

Figure 9.16. Comparison of Simulated and Observed Peak Gust Wind Speeds and Directions Produced by Hurricane Opal. All Wind Speeds are Given for the Actual Terrain at a Height of 10 m Above Ground.

Comparison of Modeled and Observed Loss Statistics. In the Erin and Opal loss validation studies, the building stock is modeled assuming 25% of the single story buildings have hip roofs and 75% have gable roofs. All two story homes are modeled as having gable roofs. 70% of the one story homes and 45% of the two story homes are assumed to have a garage. The roof deck is assumed to be attached to the roof trusses with 6d nails for 40% of the buildings and with 8d nails for 60% of the buildings. Roof-wall connections are assumed to be strapped in 80% of the cases and toe-nailed for the other 20%. The fraction of one and two story homes is estimated from statistical information provided by the insurer. All loss analyses for Hurricanes Erin and Opal are performed with the construction quality factor set equal to one. Approximately 40% of the homes were able to be geo-coded, and thus their "exact" location and hence terrain

environment could be established. Thus, for each house that could be geo-coded, the terrain is obtained by determining which land use category the house is located, and then assigning the appropriate surface roughness using the surface roughness tables given in Chapter 3. Each has been checked to determine if the unit is located on a barrier island or on the mainland. In the case of the homes that could not be geo-coded (approximately 50% of the units), the location and terrain characteristics for each house are estimated by assuming that for a given ZIP Code, the non geo-coded policies belong to the same population as the geo-coded policies.

Hurricane Erin and Opal simulations are performed with wind speed traces being recorded using grid points spaced at 0.10°. Since the wind speed grid used in the simulation of the storms does not correspond to the exact location of each home, the wind speed experienced by each house is obtained by using the wind speed and direction trace associated with the nearest grid point. Using this wind speed and direction trace, damage and ensuing losses are produced for all potential building types in the assumed building stock. The total loss ratio in each ZIP Code and county examined is estimated by summing the simulated losses weighted in proportion to the assumed number of units associated with each combination of deck thickness, roof shape, etc.

Figures 9.17 and 9.18 show the comparison of modeled and observed loss ratios at ZIP Code level for Hurricanes Erin and Opal, respectively. Only ZIP Codes with more than 10 policies are included in the comparison. The model is seen to provide reasonable agreement between modeled and actual loss ratios for Hurricane Erin. However, for Hurricane Opal, the model significantly underestimates the loss ratios of ZIP Codes with modeled peak gust wind speeds between 80 and 100 mph and overestimates the loss ratios of ZIP Codes with modeled peak gust wind speeds greater than 120 mph. In the comparison of observed and modeled losses averaged over the counties impacted by Hurricanes Erin and Opal given in Figures 9.19 through 9.22, it can be seen that near the point of landfall, the model tends to overestimate the losses in Santa Rosa County for Hurricane Opal and underestimate the losses in Santa Rosa County for Hurricane Erin, suggesting the wind field model maybe underestimating the Hurricane Erin wind speeds near the eyewall and overestimating the Hurricane Opal speeds. Besides the simulated wind speeds, a number of factors, including the assumed building stock, terrain, assumption of the non geo-coded policies belonging to the same population as geo-coded ones, can all contribute to the discrepancies between the modeled and actual loss ratios.

9.4 Example Results – Hurricane Hugo

Figure 9.23 shows the maximum peak gust wind speed contours of Hurricane Hugo produced by the hurricane model. The maximum wind speeds predicted by the model are between 130 mph and 140 mph. Figure 9.23 also shows the locations of ten anemometers and the actual and modeled maximum peak gust wind speeds at these locations where wind speeds and directions were recorded during the storm. The mean of the modeled-to-actual gust wind speed ratios is 1.02 and the COV is 0.08. Figures 9.24 through 9.26 show comparisons of the model generated peak gust wind speeds and directions to the estimates of wind speeds and directions at each of the ten locations. The overall performance of the hurricane model is, again, satisfactory.

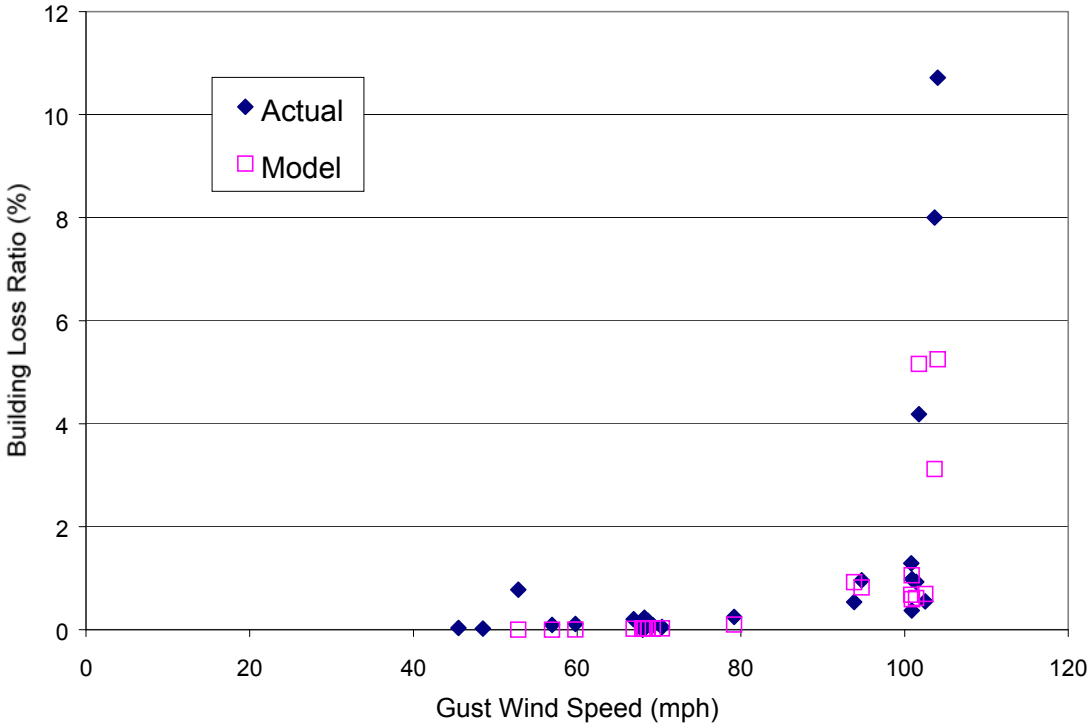

Figure 9.17. Hurricane Erin Building Loss Ratio Comparison.

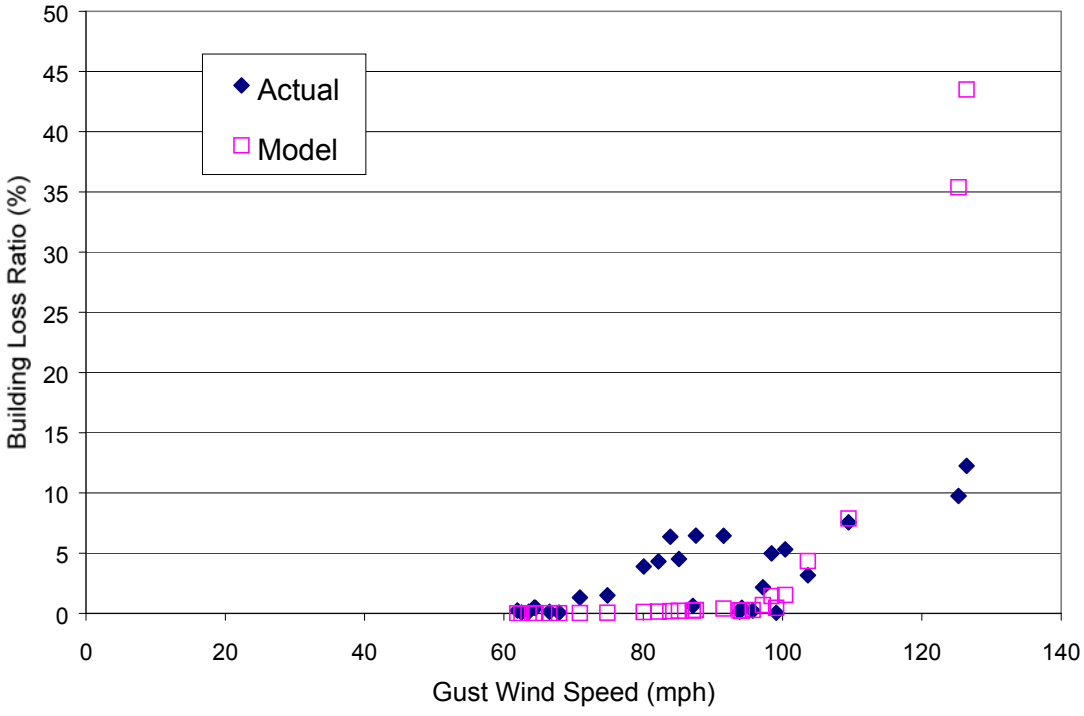

Figure 9.18. Hurricane Opal Building Loss Ratio Comparison.

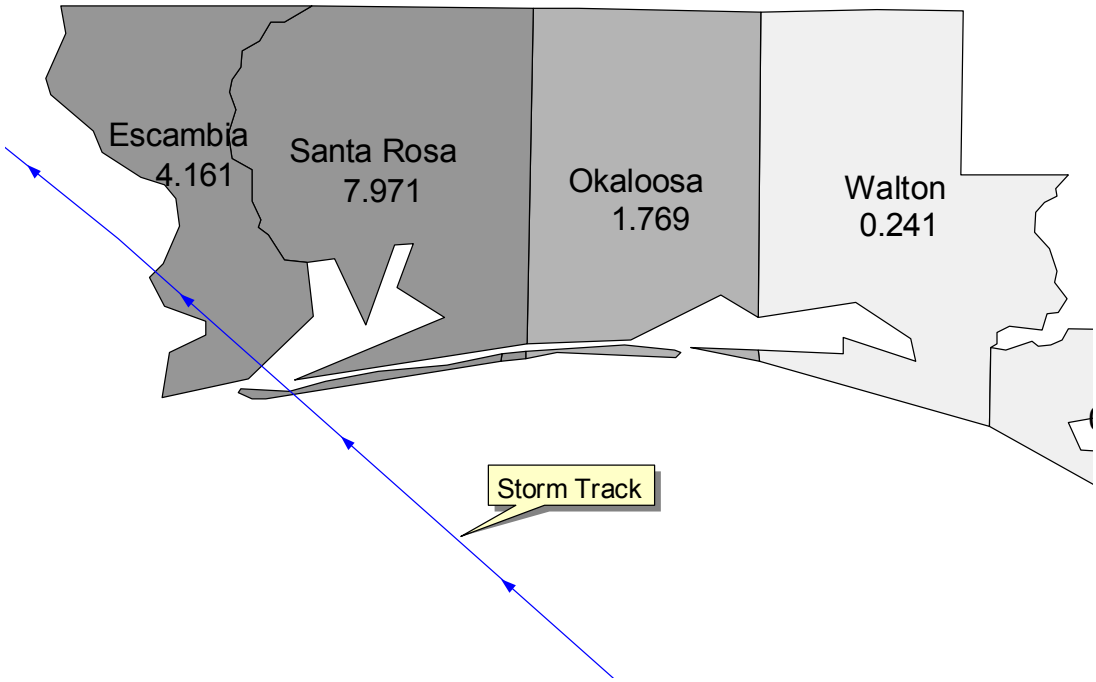

Figure 9.19. Actual Building Loss Ratios – Hurricane Erin.

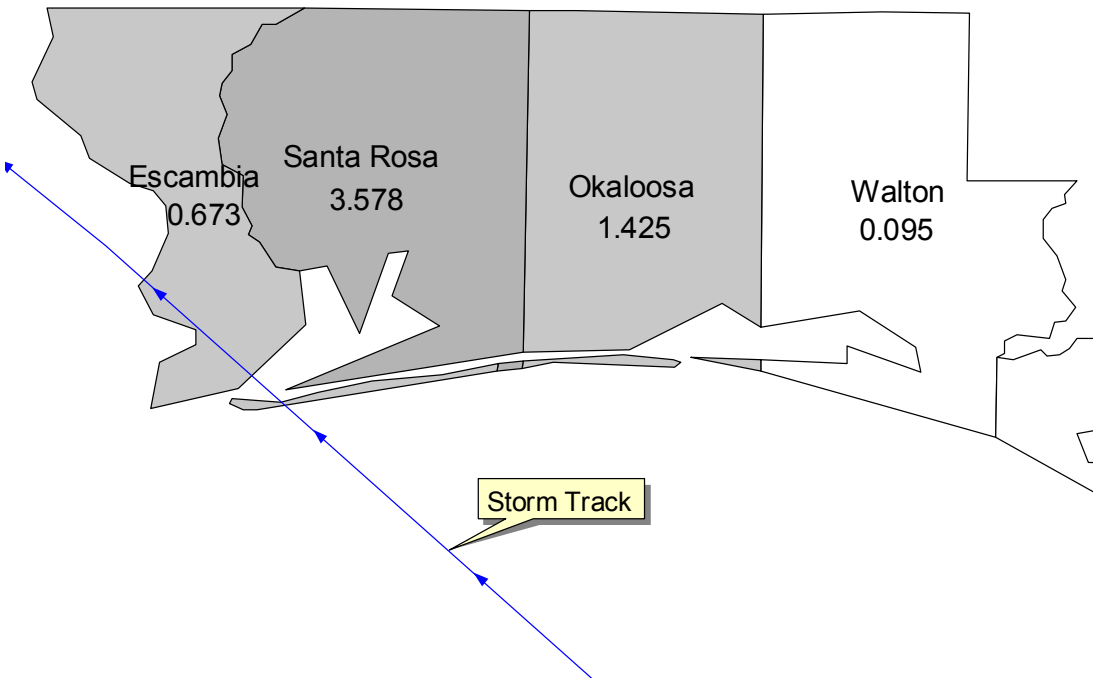

Figure 9.20. Modeled Building Loss Ratios – Hurricane Erin.

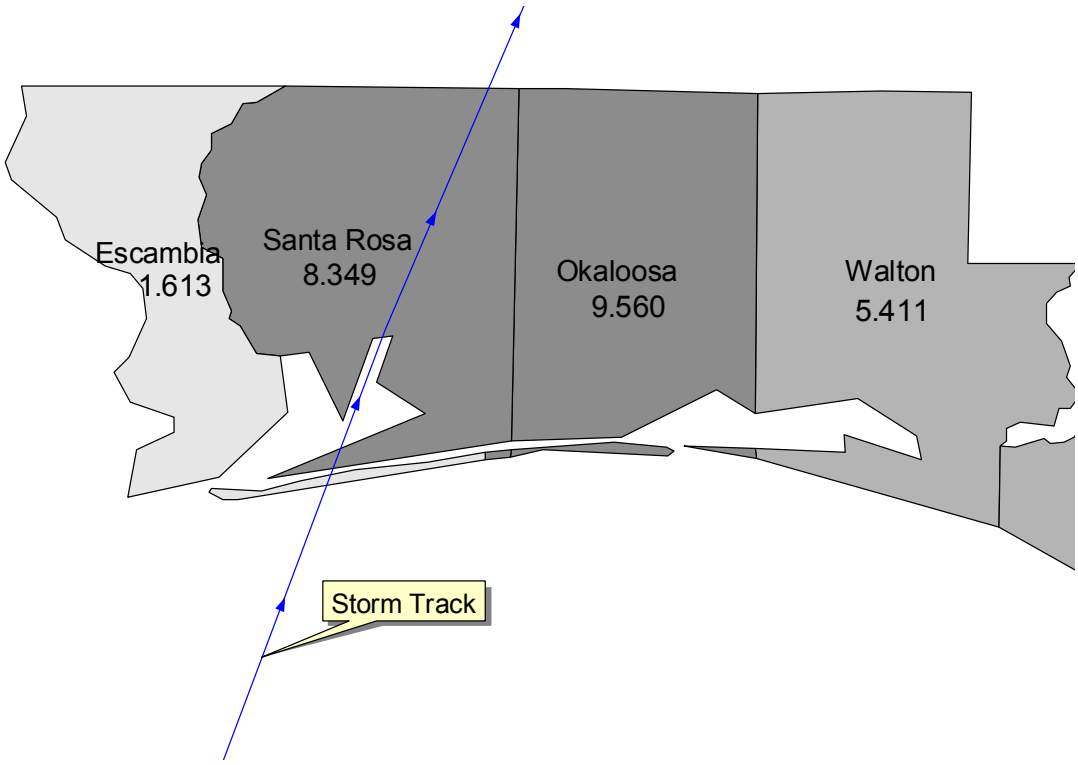

Figure 9.21. Actual Building Loss Ratios – Hurricane Opal.

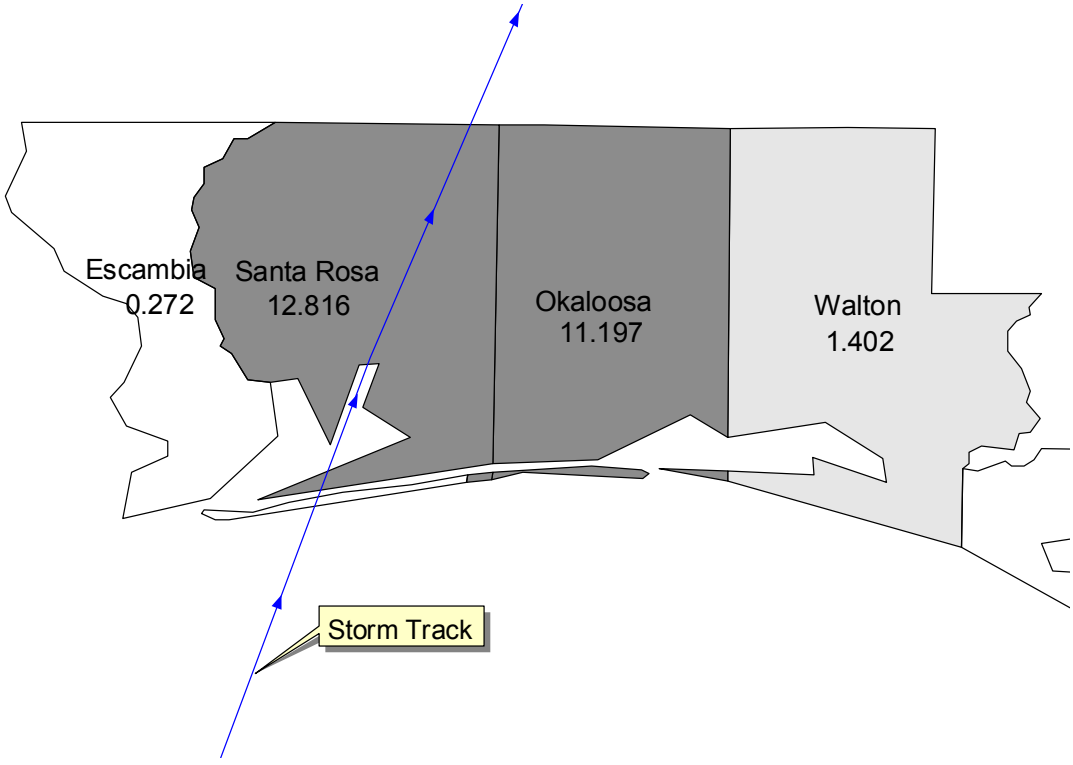

Figure 9.22. Modeled Building Loss Ratios – Hurricane Opal.

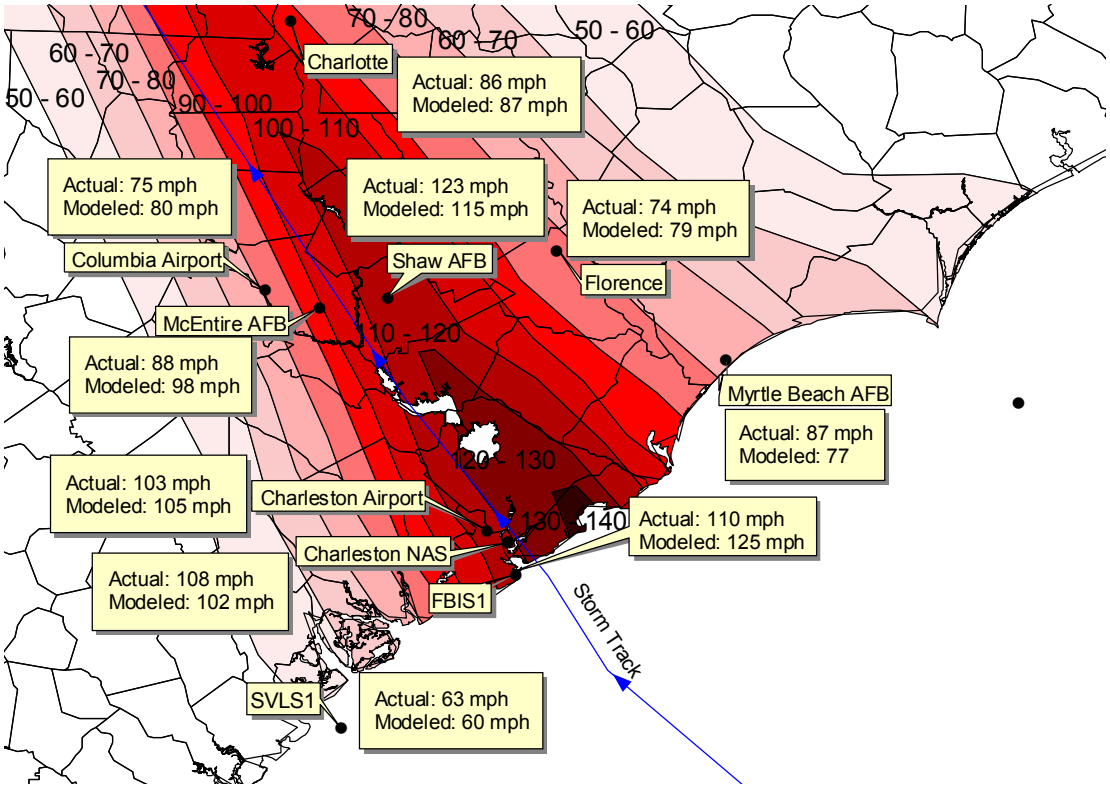

Figure 9.23. Swath of Simulated Peak Gust Wind Speeds (10 m in Open Terrain) Produced by Hurricane Hugo.

In the Hugo loss validation study, the building stock is modeled assuming 70% of the homes are single story and 30% of the homes are two stories. 71% of the one story homes and 50% of the two story homes are assumed to have a garage. 75% of the homes are assumed to have gable roofs and 25% of the homes are assumed to have hip roofs. All roof covers are assumed to be shingles. 30% of the homes are assumed to use 6d nails for roof-deck attachment, and 70% of the homes are assumed to use 8d nails. Roof-wall connections are assumed to be toe-nailed in 90% of the cases and strapped for the other 10%. The construction quality factor is set equal to one in the analysis. The average surface roughness at each ZIP Code is estimated using MRLC data. The model houses are assumed to be randomly oriented within a ZIP Codes. The insured value of the contents is taken as 70% of the insured building value.

For each ZIP Code and each building configuration, a number of simulations are performed and the average loss ratio is calculated. Then, by taking into account the assumed building stock distribution within each ZIP Code, a weighted average of the loss ratios (for all modeled building configurations) is obtained. Comparisons of the predicted and observed loss ratios are plotted vs. the modeled peak gust wind speed at the centroid of the ZIP Code in Figure 9.27, which shows reasonably good agreement between the two. The total losses (building plus contents) summed over the entire state of South Carolina was estimated assuming that both the number of policies and value of these

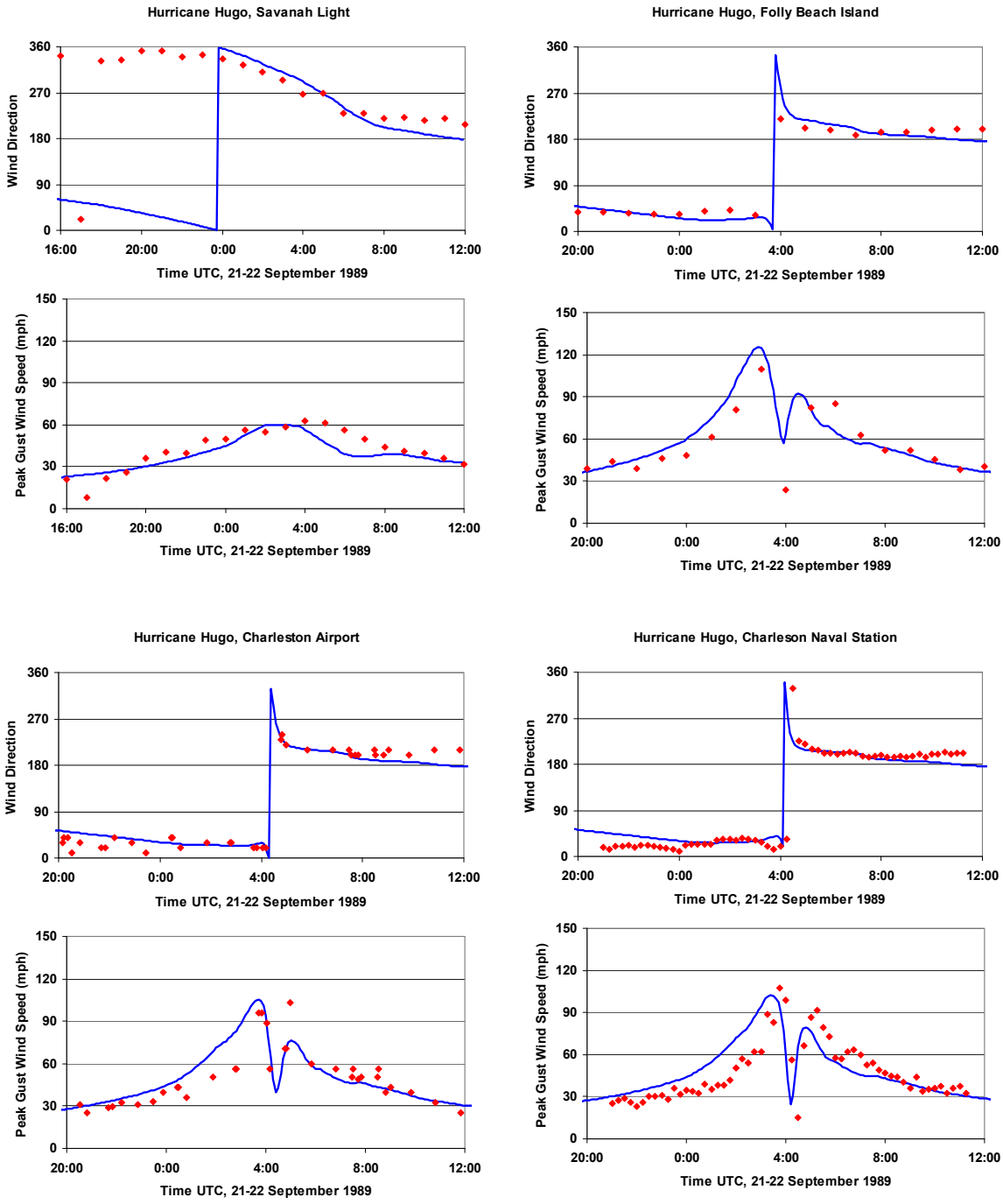

Figure 9.24. Comparison of Simulated and Observed Peak Gust Wind Speeds and Directions Produced by Hurricane Hugo. All Wind Speeds are Given for the Actual Terrain at a Height of 10 m Above Ground.

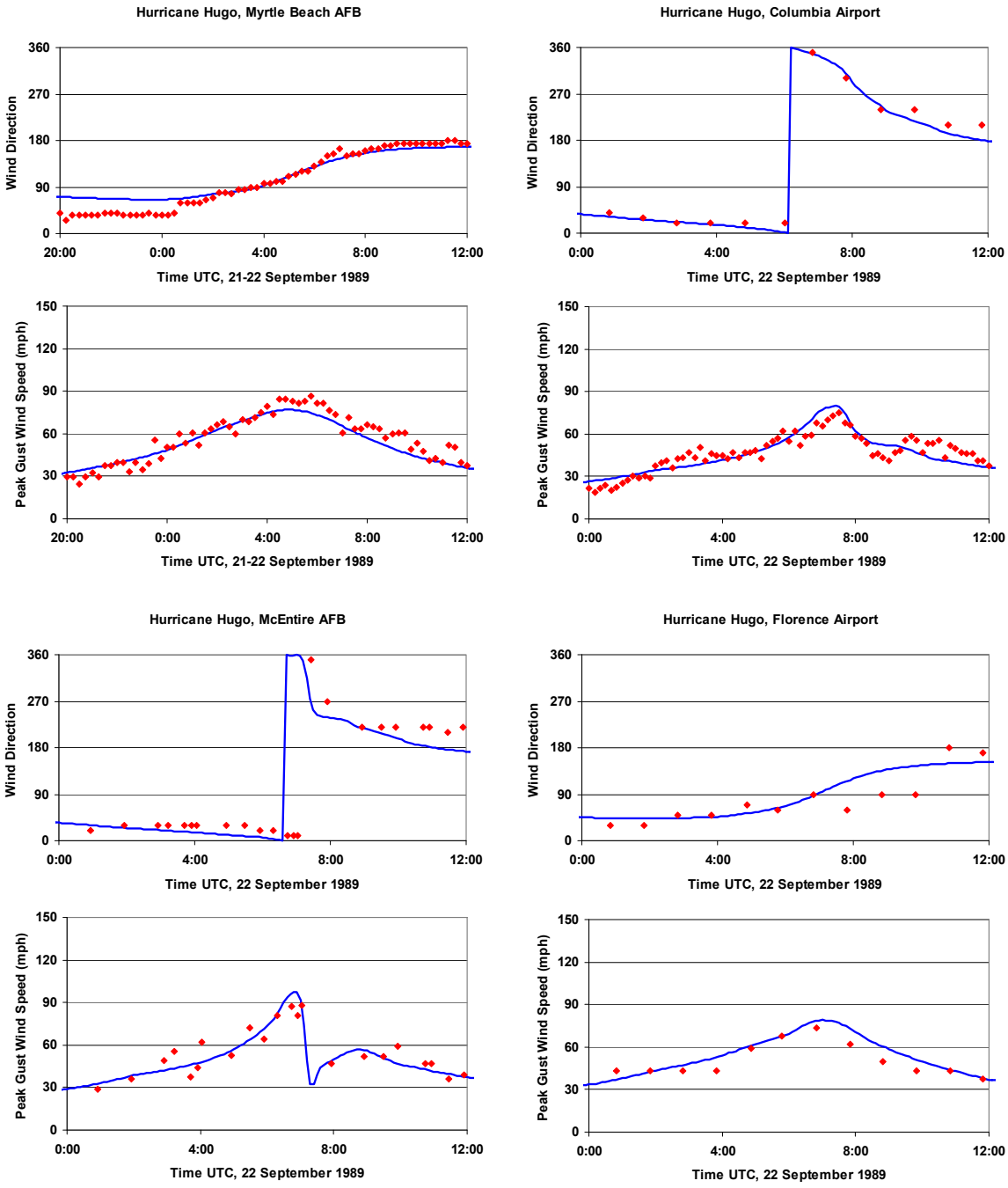

Figure 9.25. Comparison of Simulated and Observed Peak Gust Wind Speeds and Directions Produced by Hurricane Hugo. All Wind Speeds are Given for the Actual Terrain at a Height of 10 m Above Ground.

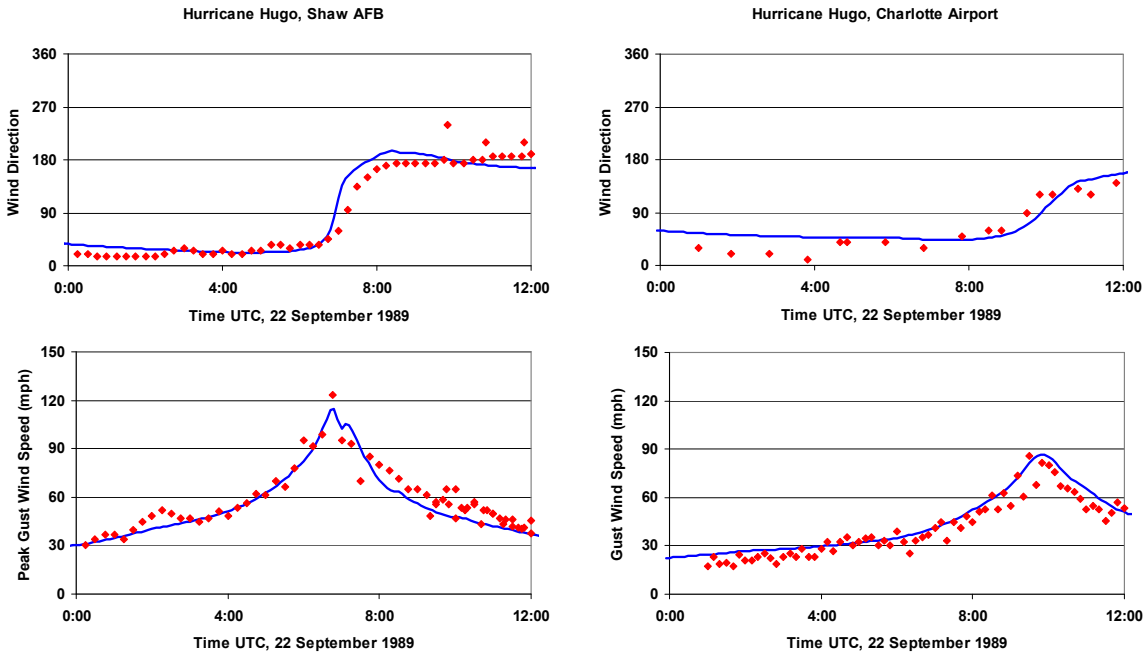

Figure 9.26. Comparison of Simulated and Observed Peak Gust Wind Speeds and Directions Produced by Hurricane Hugo. All Wind Speeds are Given for the Actual Terrain at a Height of 10 m Above Ground.

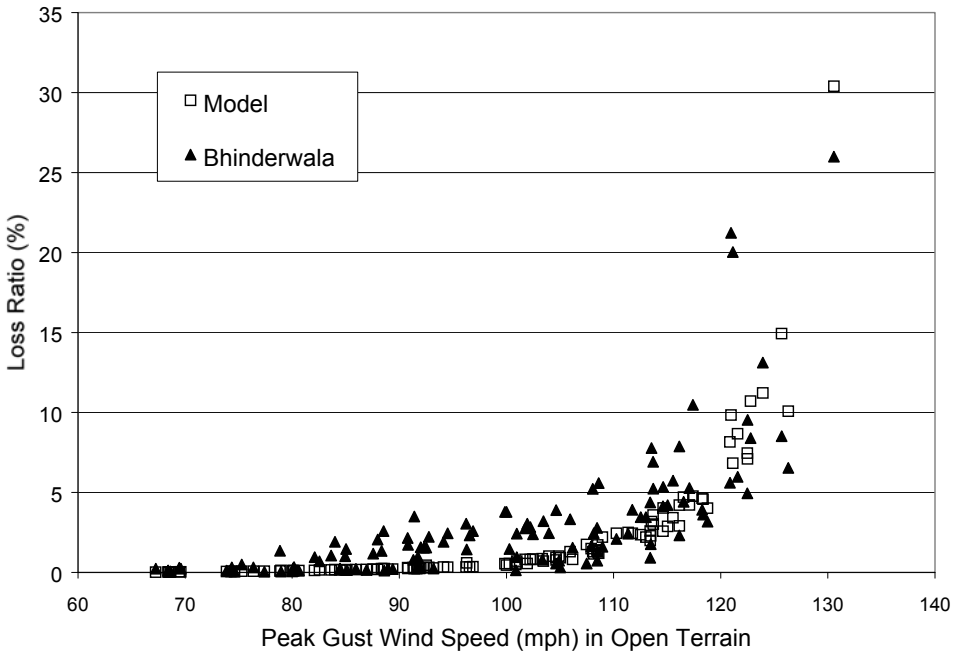

Figure 9.27. Comparison of Observed and Simulated ZIP Code Averaged Losses Produced by Hurricane Hugo in South Carolina.

policies in each ZIP Code are the same (for the same reason as in Andrew validation study). The results shown in Table 9.3 indicate that the modeled losses are slightly lower than the observed losses. The geographic variation of the observed and modeled losses are shown in Figures 9.28 and 9.29, respectively.

Table 9.3. Comparison of Modeled and Observed Aggregate Losses from Hurricane Hugo

Case	Actual Loss Ratio(%)	Modeled Loss Ratio (%)
Bhinderwala	2.96	2.32

9.5 Summary

End-to-end comparisons of modeled and observed insured losses have been presented using five different sets of insurance loss data, covering four hurricanes and three different insurers. The model validation study has been performed for residential buildings only. All modeled losses have been produced using the full load and resistance based damage and loss methodology described in Chapters 4 through 7 (as opposed to the fast-running loss curves used in the end product), and include only direct wind-induced damage to the model buildings, with no modeling of additional damage that some structures will have experienced due to falling trees, nor the inclusion of the effects of minor damage associated with wind driven rain entering a structure through non-breached windows, doors etc.

Figure 9.30 shows a comparison of the modeled and observed losses for the five data sets, plotted vs. the model estimated value of the maximum peak gust wind speed at the ZIP Code centroid. The modeled Hurricane Andrew data in Figure 9.30 are for the case with the terrain modeled using the FWMD LULC database. The losses are given as a percentage, defined as the total loss of the building and contents divided by the insured value of the building and contents. The loss ratios are plotted both on a linear scale (left plot) and on a logarithmic scale (right plot). The agreement between the modeled and the observed losses is generally good, particularly for wind speeds greater than about 100 mph. Figure 9.31 presents an *x-y* plot showing modeled losses plotted vs. the insurance loss data, where again, the agreement between the modeled and the observed losses is good. Overall, if one assumes that the value of the buildings (and contents, if applicable) in each ZIP Code plotted in Figure 9.30 is the same, the average model loss is 8.15%, compared to an observed average of 8.85%, a difference of less than 10%.

The comparisons given in Figure 9.30 and 9.31 overall show good agreement, but suggest that the damage and loss models may underestimate the small losses that occur at lower wind speeds (less than about 100 mph). This underestimate of the losses at these lower wind speeds is not unexpected since, as noted above, the damage and ensuing losses produced by tree blowdown is not modeled, nor are some other small losses associated with damage not explicitly modeled in the damage model, such as minor loss of some types of wall covering, leaking fenestrations, damage of soffits, chimneys, vents, etc.

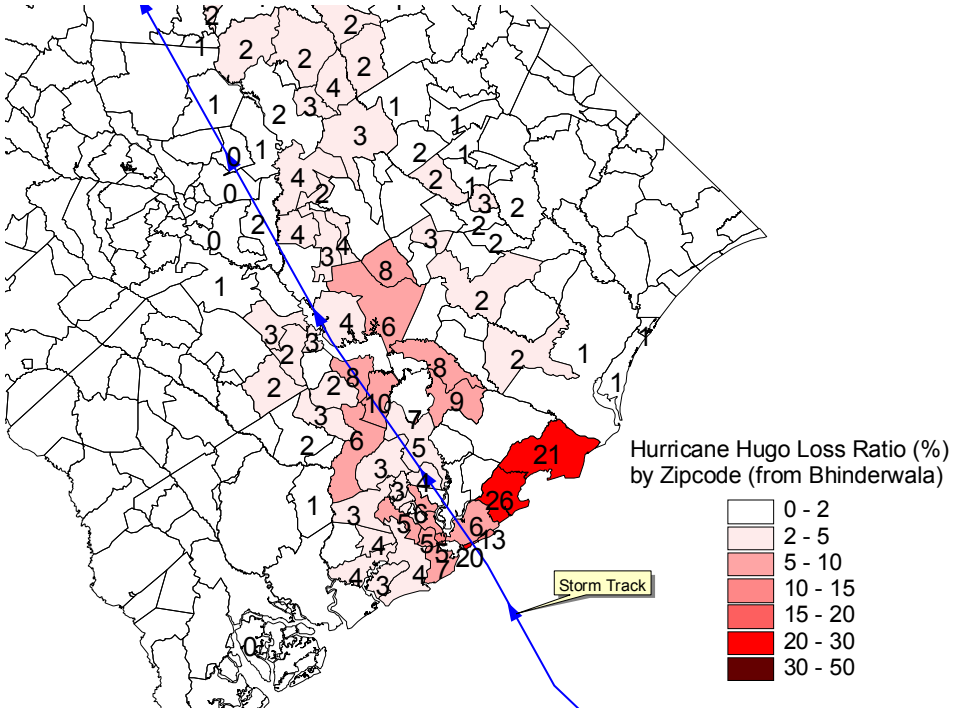

Figure 9.28. Loss Ratios by ZIP Code in South Carolina (Bhinderwala Data).

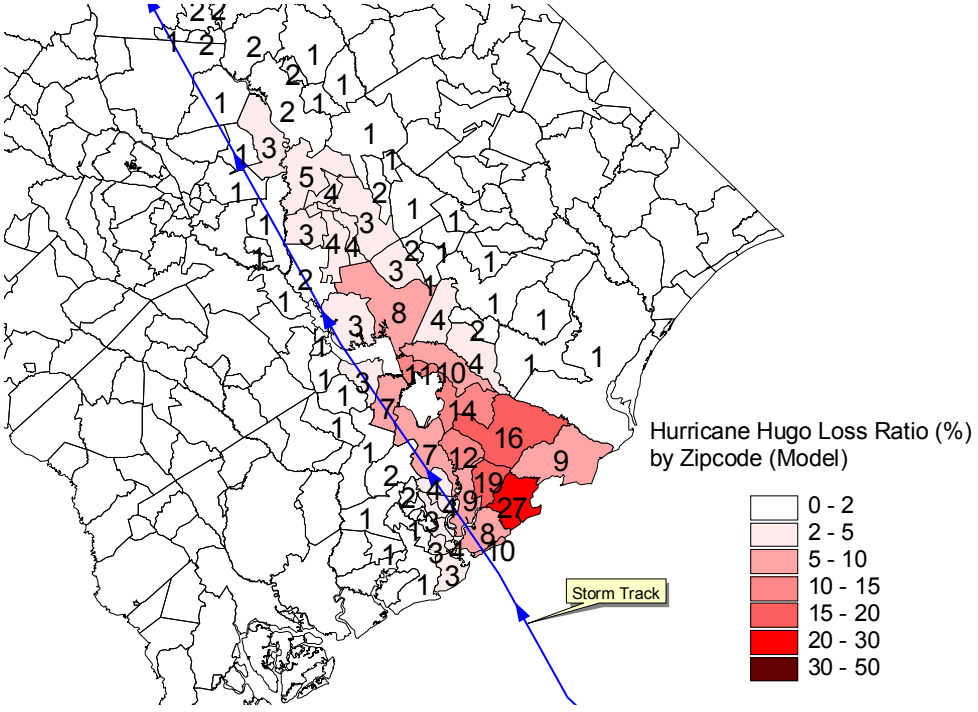

Figure 9.29. Modeled Loss Ratio (MRLC).

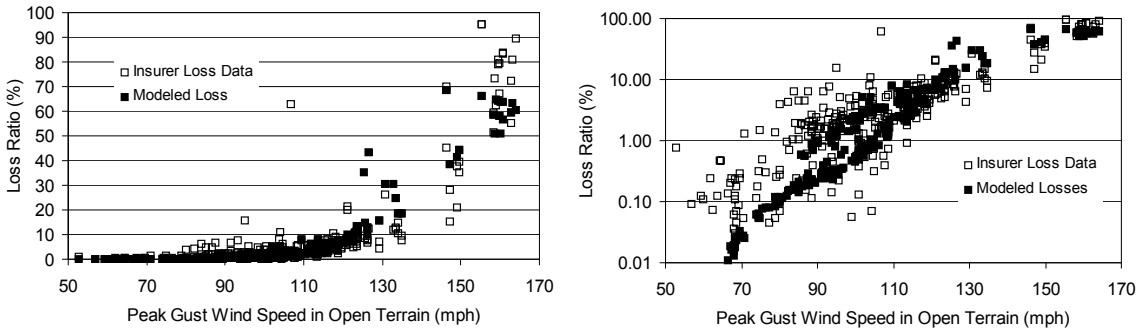

Figure 9.30. Comparison of Modeled and Observed Losses vs. Wind Speed.

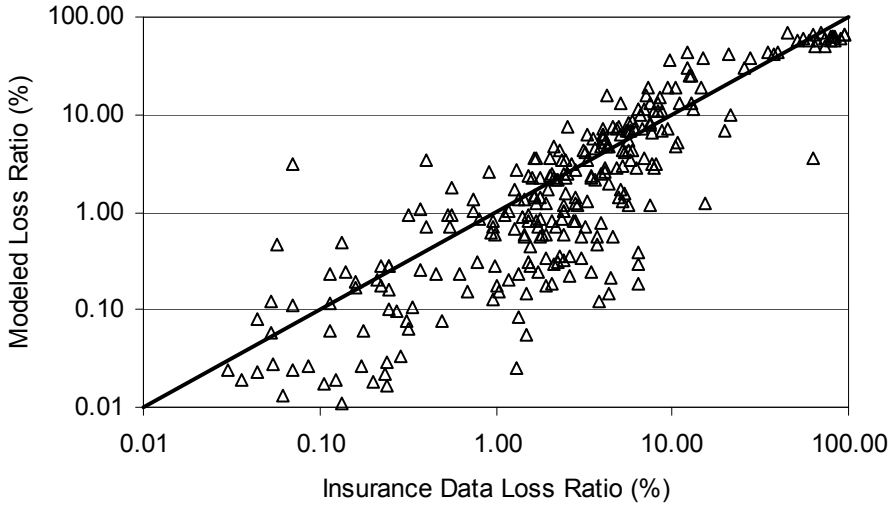

Figure 9.31. Comparison of Modeled and Observed Losses.

Furthermore, in the case of Hurricane Hugo, losses experienced by homeowners to appurtenant structures (fences, driveways, sheds, decks, etc.) were lumped into payments made for losses to the structure and cannot be separated. The loss estimation model does not account for the additional costs associated with these losses.

In summary, the loss validation studies run with the full development model have shown that the damage and loss models reproduce the observed losses reasonably well. Given the recent addition of the tree blowdown methodology (Chapter 12), an updated analysis is needed to determine whether the the losses predicted with the final version of the model are adequately estimated. The validation studies should also be re-run using the end user version of the Hazus Hurricane Model to assess whether the fast-running loss curves applied at the census tract level adequately encapsulate the details considered in the full development model (e.g., storm duration, changes in wind direction, etc.).

Chapter 10. Debris Generated from Damaged Buildings

10.1 Introduction

Debris generated by severe wind events can be categorized into five general types (Holmlin, 1993): medical (or bio-hazardous) wastes, hazardous or toxic wastes (HTW's), household garbage, burnable roadside debris, and construction and demolition debris. Burnable road side debris, which is primarily trees and other yard wastes, is often the largest among those five types of debris. Based on the scope of work specified by FEMA, only debris generated from damaged buildings (i.e., construction and demolition debris produced immediately after the event and during the rebuilding and repairing phases) and tree blow down are calculated in the current version of the model. This chapter presents the building debris model. The tree debris model is presented in Chapter 12.

Building debris consists of construction and demolition waste that is generally non-hazardous and not water soluble. Construction and demolition debris can be further categorized as wood (which is bio-degradable), masonry, metal (which is recyclable), and other (which includes gypsum board, carpet, asphalt roofing material, insulation, ceiling, pipe, etc.). Masonry and other debris are usually disposed of in authorized landfills. Debris removal is often one of the most costly and challenging operations following a natural disaster (Holmlin, 1993). Due to contamination with different types of waste materials, it is also difficult to recycle most of the structural waste (debris). Accurate and prompt estimating of the total debris generated and its distribution is vital to ensure the success of a debris removal operation after a hurricane.

A simple model for estimating the volume and type of debris has been developed by the U.S. Army Corp of Engineers (USACE) using historical data from hurricanes Frederic, Hugo, and Andrew. The USACE model was used to estimate debris produced in Escambia County for hurricanes Erin and Opal. This simple model is intended to be used for estimating debris produced by single-family residential buildings only. The model yields estimates of the expected volumes of burnable debris, landfill debris, soil debris, and metallic debris based on the category of hurricane winds occurring in a county combined with factors related to business use, number of households, vegetation density (light, medium or heavy) and a storm wet/dry multiplier. The model error is typically within ±30% (Moorse, 2001). Recent developments of this model have enabled the analysis to be done at a census track level, resulting in higher accuracy. The major limitation of this model is the inability to take into account various construction and usage classes. For example, the model significantly overestimated the building debris produced by Typhoon Paka in Guam because the model was not able to take into account the reduction in building losses associated with the large number of residential buildings having hardened concrete roofs.

To overcome the limitations of the USACE model, a new debris estimation model has been developed based on the damage states for structural and non-structural components of several model buildings. For each damaged component, the debris generated in each

category (wood, masonry, metal and other) is calculated based on the component's damage state and weight statistics. Then, by adding up the debris produced by all the damaged components, the total debris weight for that model building can be estimated. The debris volume is simply estimated by dividing the debris weight by its density. The accuracy of the new model depends heavily on the accuracy of underlying databases (which includes unit weights of the building components, debris distribution matrix, and detailed building configuration). Therefore, efforts have been devoted to the database development for the new debris model. Limited case studies have been conducted to test and calibrate the new model, and the results are summarized at the end of this section.

10.2 Description of Methodology

The form of the debris model is:

$$\mathrm{D} = \sum_{i=1}^{n} W_i f(d_i) \mathrm{D}_i \tag{10.1}$$

where D = debris distribution vector for the model building, which consists of debris from wood, masonry, metal and other, respectively; W_i = total weight of building component i; $f(\cdot)$ = damage intensity function, $0 \le f(\cdot) \le 1$; d_i = damage state of building component i, which is obtained from the physical damage model; D_i = debris distribution vector for building component i, which specifies the ffactions of total component weight in wood, masonry, metal and other. Since the building component weights and debris distribution vectors are available from a number of sources, the only new development needed is to define the damage intensity functions.

Similar to the economic loss model, the debris model has to produce debris estimation based on the damage states provided by the load-resistance physical damage model, which include number of damaged fenestrations, roof cover damage, roof sheathing damage, wall damage, and water damage (amount of water entering the building). The building components can be divided into two categories: those modeled explicitly by the damage model (primarily damage to the building envelope) and those modeled implicitly by the damage model (i.e., their damage states have to be estimated based on envelope damage). For components that are modeled explicitly in the damage model, it was assumed that $f(d_i) = d_i$. For components that are not modeled explicitly (e.g., building interior), the damage intensity functions were assumed to be similar in format to those used in the economic loss model, however with different parameters. For example, the interior damage due to water entering damaged fenestration was modeled as 1/4 of the rate defined by the damage intensity function in the economic loss model. Those parameters were developed using a combination of historical data and judgment. The interior damage intensity functions for roof cover, roof sheathing, and fenestration damages are defined as:

$$I_{cv} = f(d_{cv}) = \begin{cases} 0.5 d_{cv} & \text{without secondary water resistance} \\ 0.05 d_{cv} & \text{with secondary water resistance} \end{cases} \tag{10.2}$$

$$I_{sh} = f(d_{sh}) = 1.8 d_{sh} \tag{10.3}$$

$$I_{fen} = f(d_{fen}) = 1.0 d_{fen} \tag{10.4}$$

where I_{cv} = interior damage level due to roof cover damage; d_{cv} = percentage of roof cover damage; I_{sh} = interior damage level due to roof sheathing damage; d_{sh} = percentage of roof sheathing damage; I_{fen} = interior damage level due to fenestration damage; d_{fen} = the amount (in.) of wind driven rain in the interior due to fenestration damage. The final interior damage level (I) is calculated as the maximum of interior damage levels due to roof cover, roof sheathing, and fenestration damages, i.e., I = max(I_{cv}, I_{sh}, I_{fen}). The damage levels for all interior assemblies, such as partition wall, ceiling, floor finish, wall finish, content, etc., given an interior damage level, are assumed to be the same. Therefore, the total interior debris is estimated by (assuming m interior components):

$$\mathrm{D}_{int} = I \sum_{i=1}^{m} W_i \mathrm{D}_i \tag{10.5}$$

where D_{int} = interior debris distribution vector. It is further assumed that, for engineered buildings, non-modeled load-bearing structural components (such as columns and beams, concrete or metal deck floors, and load-bearing partition walls) will not be damaged and therefore no debris could be produced from those components. However, finishes on those components can be damaged by water entering the building.

For buildings that reach the destruction damage state (see definitions in Chapter 6), the entire building will be torn down and the debris produced by demolition will equal to the total building weight. In the present debris model, global damage indicators (such as total roof cover damage ratio, total roof deck damage ratio, roof frame failure, wall frame failure, etc.) are monitored and once the destruction state is reached, the total building weight will be used as the total debris weight. The total building weight is pre-calculated based on the specified construction for the model building (in the case when construction types for certain components are not given, default construction types are used in the analysis). Note that the weight of foundation is not included in the total building weight calculation. The default construction characteristics for economy, average, custom, and luxury residential buildings are defined in the residential economic loss model. The default construction characteristics for commercial buildings will be discussed later.

After total debris weight in each category (wood, masonry, metal and other) is determined, the total debris volume is estimated by dividing the total debris weight of each type by its density. However, since debris can't be fully packed, the debris density will be much less than its material's density. In the debris model, the debris density for masonry is assumed to be 2/3 of concrete masonry density (125 pcf) and the debris densities for the remaining types of debris are assumed to be 1/2 of their material densities. Due to mixture of different materials, the material density for *other* types of

debris is not readily available. It is assumed to be 70 pcf in the present debris model (between the densities of wood and masonry).

Component Unit Weight. Building component (or assembly) weights are closely related to building dead loads, while content weights are closely related to sustained live loads. Therefore, it is natural to refer to the current building code for this information. Specifically, the ASCE 7-98 Commentary (1999) is used to obtain the building component weights and live load statistics in this study. For items that are not included in the ASCE Commentary, references are made to the manufacturer's manuals. RSMeans (2001) is also used to obtain unit weights for a number of building assemblies. Table 10.1 lists the collected average building component weights. The COV for each item is assumed to be 20%. Table 10.2 lists the sustained live load statistics for residential buildings and several types of commercial buildings. For building usage types that are not listed in this table, a mean of 10 psf and standard deviation of 5 psf are assumed. Note that sustained live load statistics are based on specified areas of observation (see Table 10.2-2). The standard deviation of the average sustained load for an area greater than the observation area is:

$$\sigma_n = \sqrt{\frac{\sigma}{n}} \tag{10.6}$$

where σ_n = standard deviation of the sustained load for an area n times of the observation area and σ = observed standard deviation of the sustained load.

Debris Distribution Matrix. The debris distribution matrix defines how the debris is distributed among the four debris types (wood, masonry, metal, and other). As shown in Table 10.3, for each building component, four numbers are given, which represent the portion of debris in each debris type. For example, for combined wood and masonry exterior wall, 45% of the debris is wood, 45% of the debris is masonry, 5% of the debris is metal and the remaining 5% of the debris is other. Even though most of the time the debris distribution is intuitive and readily determined (such as metal shingle, plywood deck, and fibrous glass insulation), there are still cases that require engineering judgment. Further validation of those cases is desirable in the future.

Default Component Construction Types for Commercial Buildings. For components that are not specified in the model building, the default construction types are assumed to be the same as those specified in the RSMeans (2001). Table 10.4 lists the indices of the construction types for roof frame, insulation, partition construction, floor construction, floor finish, ceiling finish, and wall finish. The descriptions and weights for related indices are listed in Tables 10.5 through 10.11, respectively. The weights for floor finish and wall finish are calculated based on their finish composition.

Table 10.1. Component Unit Weight Used in the Debris Model

Category	Component	Unit Weight (psf)
Roof Cover	Slate, 1/4″	10
	26 gage metal shingle or metal panel	2
	Wood shingles	3
	Three-ply ready roofing	1
	Asbestos-cement shingles	4
	Slate, 3/16″	7
	Single-ply, sheet membranes	0.7
	Roman tile	12
	Ludowici tile	10
	Liquid applied membranes	1
	Five-ply felt and gravel	6
	Corrugated asbestos-cement roofing	4
	Copper or tin	1
	Cement tile	16
	Book tile, 3″	20
	Book tile, 2″	12
	Bituminous, smooth surface membranes	1.5
	Bituminous, gravel-covered membranes	5.5
	Asphalt shingles	2
	Four-ply felt and gravel	5.5
	Spanish	19
Roof Deck	Decking, 2″ wood	5
	Wood sheathing (per in. thickness)	3
	Decking, 3″ (Douglas fir)	8
	Deck, metal, 20 gage	2.5
	Deck, metal, 18 gage	3
	Plywood (per in. thickness)	3.2
Roof Frame	16″ deep @ 6' Bar Joist	17.5
	2×4 @24″ slope 4/12	2.0
	2×6 @ 48″ 2×3 batten@36″	1.2
	Metal truss	12
	Post and beam	8
Insulation	Rigid insulation, 1/2″	0.8
	Urethane foam with skin	0.5
	Polystyrene foam insulation	0.2
	Fibrous glass insulation (4″ thick)	4.4
	Fiberboard insulation	1.5
	Cellular glass insulation (4″ thick)	2.8
	Perlite insulation	0.8
Ceiling	Acoustical fiber board	1
	Gypsum Board (1/2″ thickness)	2
	Mechanical duct allowance	4
	Plaster on tile or concrete	5
	Plaster on wood lath	8
	Suspended metal lath and cement plaster	15
	Suspended metal lath and gypsum plaster	10
	Suspended steel channel system	2
	Wood furring suspension system	2.5
Coverings, Roof, and Wall	Fiberboard, 1/2″	0.8
	Gypsum sheathing, 1/2″	2
Exterior Wall	8″ medium weight hollow CMU, grout 40″ O.C.	45
	6″ normal weight solid CMU	64
	4″ normal weight solid CMU	41
	6″ light weight solid CMU	51

Table 10.1. Component Unit Weight Used in the Debris Model (continued)

Category	Component	Unit Weight (psf)
Exterior Wall	6″ medium weight hollow CMU, full grout	59
	6″ medium weight hollow CMU, grout 16″ O.C.	44
	6″ medium weight hollow CMU, grout 24″ O.C.	39
	6″ medium weight hollow CMU, grout 32″ O.C.	36
	6″ medium weight hollow CMU, grout 40″ O.C.	34
	6″. medium weight hollow CMU, grout 48″ O.C.	33
	6″. medium weight hollow CMU, no grout	28
	6″ medium weight solid CMU	60
	4″ medium weight solid CMU	38
	8″ clay brick wythes	79
	8″ light weight solid CMU	69
	8″ medium weight hollow CMU, full grout	81
	8″ medium weight hollow CMU, grout 16″ O.C.	59
	4″ medium weight hollow CMU, no grout	26
	8″ medium weight hollow CMU, grout 32″ O.C.	47
	2×6 @ 16″, 5/8″ gypsum, insulated, 3/8″ siding	12
	8″ medium weight hollow CMU, grout 48″ O.C.	44
	8″ medium weight hollow CMU, no grout	36
	8″ medium weight solid CMU	81
	8″ normal weight solid CMU	87
	Exterior stud walls with brick veneer	48
	8″ medium weight hollow CMU, grout 24″ O.C.	51
	10″ normal weight solid CMU	110
	10″ light weight solid CMU	87
	10″ medium weight hollow CMU, full grout	102
	10″ medium weight hollow CMU, grout 16″ O.C.	73
	10″ medium weight hollow CMU, grout 24″ O.C.	63
	10″ medium weight hollow CMU, grout 32″ O.C.	58
	10″ medium weight hollow CMU, grout 40″ O.C.	56
	10″ medium weight hollow CMU, grout 48″ O.C.	54
	4-″ light weight solid CMU	32
	10″ medium weight solid CMU	102
	12″ clay brick wythes	115
	12″ light weight solid CMU	105
	12″ medium weight hollow CMU, full grout	123
	2×4 @ 16″, 5/8″ gypsum, insulated, 3/8″ siding	11
	12″ medium weight hollow CMU, grout 24″ O.C.	75
	12″ medium weight hollow CMU, grout 32″ O.C.	68
	4″ clay brick wythes	39
	12″ medium weight hollow CMU, grout 40″ O.C.	65
	12″ medium weight hollow CMU, grout 48″ O.C.	62
	12″ medium weight hollow CMU, no grout	50
	12″ medium weight solid CMU	124
	12″ normal weight solid CMU	133
	16″ clay brick wythes	155
	12″ medium weight hollow CMU, grout 16″ O.C.	87
	10″ medium weight hollow CMU, no grout	44
Floors and Floor Finishes	Asphalt block (2″), 1/2″ mortar	30
	Cement finish (1″) on stone-concrete fill	32

Table 10.1. Component Unit Weight Used in the Debris Model (concluded)

Category	Component	Unit Weight (psf)
Floor and Floor Finishes	Ceramic or quarry tile (3/4″) on 1/2″ mortar bed	16
	Ceramic or quarry tile (3/4″) on 1″ mortar bed	23
	Hardwood flooring, 7/7″	4
	Linoleum or asphalt tile, 1/4″	1
	Terrazzo (1″) on stone-concrete fill	32
	Concrete floor on steel beam (Commercial)	38
	Steel deck on steel beam (Commercial)	30
	Concrete fill finish (per inch thickness)	12
	Carpet	2
	Wood block (3″) on 1/2″ mortar base	16
	Terrazzo (1″) on 2″ stone-concrete	32
	Terrazzo (1-1/2″) directly on slab	19
	Subflooring, 3/4″	3
	Solid flat tile on 1″ mortar base	23
	Slate (per mm thickness)	15
	Marble and mortar on stone-concrete file	33
	Wood block (3″ 0 on mastic, no fill	10
Floors, Wood-Joist	2×6 joists, 12″ spacing double wood floor	6
	2×8 joists, 12″ spacing double wood floor	6
	2×8 joists, 24″ spacing double wood floor	5
	2×8 joists, 16″ spacing double wood floor	8
	2×10 joists, 12″ spacing double wood floor	7
	2×10 joists, 16″ spacing double wood floor	6
	2×12 joists, 24″ spacing double wood floor	6
	2×12 joists, 16″ spacing double wood floor	7
	2×12 joists, 12″ spacing double wood floor	8
	2×10 joists, 24″ spacing double wood floor	6
	2×6 joists, 16″ spacing double wood floor	5
	2×6 joists, 24″ spacing double wood floor	5
Frame Partitions	Movable steel partitions	4
	Wood studs, 2×4, unplastered	4
	Wood studs, 2×4, plastered two sides	20
	Wood or steel studs, 1/2″ gypsum board each side	8
	Wood studs, 2×4, plastered one side	12
	Gypsum board and sound deadening board on wood or steel stud	15
Doors	Interior and Exterior	10
Garage Doors	Regular garage doors	1.6
Skylight	Skylight, metal frame, 3/8″ wire glass	8
Sliders	3/16″ tempered sliding glass door	4
Windows	Windows, glass, frame and sash	8

Table 10.2. Sustained Load Statistics

Usage Type	Occupancy	Mean (psf)	Std (psf)	Area (ft^2)
Office Building	Offices	10.9	5.9	200
Residential	Renter	6	2.6	200
Residential	Owner	6	2.6	200
Residential	Attic	2	0.87	200
Commercial	Default	10	5	200
Hotel	Guest room	4.5	1.2	200
School	Classrooms	12	2.7	1000

Table 10.3. Debris Distribution Matrix

Category	Type	Wood	Masonry	Metal	Other
Ceiling	Gypsum board (2 mm thickness)	0.00	0.00	0.00	1.00
	Gypsum board or plaster on wood furring	0.10	0.00	0.00	0.90
	Suspended metal lath and gypsum plaster	0.00	0.00	0.15	0.85
	Suspended steel channel system	0.00	0.00	1.00	0.00
Content	Commercial	0.30	0.00	0.20	0.50
	Residential	0.60	0.00	0.00	0.40
Exterior Wall	Combined wood and masonry	0.45	0.45	0.05	0.05
	Unreinforced and reinforced Masonry	0.00	0.90	0.05	0.05
	Wood	0.90	0.00	0.05	0.05
Exterior Wall Siding	Aluminum siding, metal panel	0.00	0.00	1.00	0.00
	Brick veneer, block	0.00	1.00	0.00	0.00
	NA	0.00	0.00	0.00	0.00
	Stone veneer, vinyl, stucco	0.00	0.00	0.00	1.00
	Wood	1.00	0.00	0.00	0.00
Floors	Commercial (concrete)	0.05	0.00	0.05	0.90
	Commercial (steel joist, flat form, concrete)	0.00	0.00	0.40	0.60
	Commercial (steel joist/truss)	0.00	0.00	0.80	0.20
	Residential	0.70	0.00	0.00	0.30
Garage Doors	All	0.00	0.00	1.00	0.00
Insulation	Fibrous glass, All other	0.00	0.00	0.00	1.00
Interior Partition	50% Concrete, 50% Wood Stud	0.10	0.00	0.00	0.90
	Concrete Block	0.00	0.00	0.00	1.00
	Movable Steel Partition	0.00	0.00	0.90	0.10
	Steel stud	0.00	0.00	0.20	0.80
	Wood stud	0.20	0.00	0.00	0.80
Regular Doors	All	0.90	0.00	0.00	0.10
Roof Cover	Asphalt shingle, asbestos shingle, flat tile, other tile, Slate, built-up roof, single-ply membrane, and Other	0.00	0.00	0.00	1.00
	Metal shingle, metal panel	0.00	0.00	1.00	0.00
	Wood shake	1.00	0.00	0.00	0.00
Roof Deck	Concrete	0.00	0.00	0.00	1.00
	Plywood, T&G, OSB, Dimensional lumber, Batten	1.00	0.00	0.00	0.00
Roof Frame	Metal truss	0.00	0.00	1.00	0.00
	Wood truss, wood joist, post and beam	1.00	0.00	0.00	0.00
Skylight	All	0.00	0.00	0.10	0.90
Sliders	All	0.00	0.00	0.10	0.90
Windows	All	0.20	0.00	0.10	0.70

10.3 Validation Studies

The US Army Corps of Engineers (USACE) is the principal organization responsible for debris clean-up and removal. Other local and state government agencies may also coordinate the debris clean-up efforts. USACE after action reports are the most readily available sources for model validation and testing. These reports contain information on the total amount (either by volume or by weight) of debris produced by hurricanes. However, since the after action reports don't differentiate burnable roadside debris from construction and demolition debris, assumptions have to be made to the ratio of these two types of debris (recall that only construction and demolition debris is estimated by the

Table 10.4. Default Building Component Construction Types

ID	Building Type	Roof Frame	Insul.	Partit. Const.	Floor Const.	Floor Finish	Ceiling Finish	Wall Finish
M010	Apartment, 1-3 Story	6	5	5	7	9	11	13
M020	Apartment, 4-7 Story	6	5	5	7	9	11	13
M030	Apartment, 8-24 Story	6	5	6	7	9	11	13
M040	Auditorium	9	5	4	7	23	14	14
M050	Bank	1	5	7	10	3	7	5
M060	Bowling Alley	6	5	3	10	34	14	21
M070	Bus Terminal	6	5	3	10	6	7	20
M080	Car Wash	6	5	3	10	36	17	21
M090	Church	5	7	10	10	33	17	21
M100	Club, Country	11	10	7	10	1	5	2
M110	Club, Social	6	5	3	10	10	7	10
M120	College, Classroom, 2-3 Story	6	5	3	7	22	7	19
M130	College, Dorm, 2-3 Story	2	5	6	2	24	1	19
M140	College, Dorm, 4-8 Story	3	5	3	3	24	7	19
M150	College, Laboratory	6	5	3	5	11	7	8
M160	College, Student Union	2	5	7	2	5	14	5
M170	Community Center	6	5	7	10	5	7	21
M180	Courthouse, 1 Story	1	5	10	10	12	4	12
M190	Courthouse, 2-3 Story	3	5	10	3	12	4	12
M200	Factory, 1 Story	6	5	4	10	34	2	21
M210	Factory, 3 Story	2	5	7	2	31	2	21
M220	Fire Station, 1 Story	6	5	4	10	8	2	21
M230	Fire Station, 2 Story	6	5	4	7	8	2	21
M240	Fraternity/Sorority House	10	3	7	6	16	3	21
M250	Funeral Home	11	6	5	10	18	2	7
M260	Garage, Auto Sales	6	5	7	10	8	2	21
M270	Garage, Parking	12	10	3	10	36	17	21
M280	Garage, Underground Parking	1	10	3	1	36	17	21
M290	Garage, Repair	6	5	4	10	31	3	21
M300	Garage, Service Station	11	5	4	10	34	10	21
M310	Gymnasium	5	6	4	10	30	7	4
M320	Hangar, Aircraft	6	2	4	10	36	17	21
M330	Hospital, 2-3 Story	1	5	6	1	13	15	1
M340	Hospital, 4-8 Story	6	5	5	3	13	15	1
M350	Hotel, 4-7 Story	6	5	5	3	24	7	17
M360	Hotel, 8-24 Story	6	5	5	7	24	11	17
M370	Jail	3	5	3	3	20	7	21
M380	Laundromat	6	5	7	10	34	2	21
M390	Library	4	5	7	4	4	7	21
M400	Medical Office, 1 Story	11	3	5	10	5	7	5
M410	Medical Office, 2 Story	6	5	5	7	5	7	6
M420	Motel, 1 Story	11	3	5	10	27	10	18
M430	Motel, 2-3 Story	7	5	3	28	8	18	8
M440	Movie Theatre	6	5	4	4	7	21	7
M450	Nursing Home	8	5	7	32	9	6	9
M460	Office, 2-4 Story	6	5	7	9	7	9	7
M470	Office, 5-10 Story	6	5	7	9	3	9	7
M480	Office, 11-20 Story	6	5	7	9	3	9	7
M490	Police Station	6	5	4	20	7	18	7
M500	Post Office	6	5	4	8	10	21	7
M510	Racquetball Court	6	5	6	25	7	21	7

Table 10.4. Default Building Component Construction Types (concluded)

ID	Building Type	Roof Frame	Insul.	Partit. Const.	Floor Const.	Floor Finish	Ceiling Finish	Wall Finish
M520	Religious Education	6	5	4	5	10	21	7
M530	Restaurant	11	3	7	14	10	16	7
M540	Restaurant, Fast Food	6	5	7	35	10	21	7
M550	Rink, Hockey/Indoor Soccer	6	5	3	26	10	21	7
M560	School, Elementary	6	5	4	15	10	15	7
M570	School, High, 2-3 Story	2	5	4	21	2	15	7
M580	School, Jr. High, 2-3 Story	6	5	4	7	7	3	7
M590	School, Vocational	6	5	4	21	7	3	7
M600	Store, Convenience	11	3	7	34	10	21	7
M610	Store, Department, 1 Story	7	5	7	4	10	21	7
M620	Store, Department, 3 Story	6	5	7	2	3	11	7
M630	Store, Retail	6	5	7	34	10	21	7
M640	Supermarket	6	5	2	34	10	21	7
M650	Swimming Pool, Enclosed	11	5	4	19	10	20	7
M660	Telephone Exchange	6	5	7	29	10	21	2
M670	Town hall, 1 Story	6	5	7	17	10	18	7
M680	Town Hall, 2-3 Story	6	5	7	17	7	18	7
M690	Warehouse	6	5	3	31	7	21	7
M700	Warehouse, Mini	6	5	6	36	10	21	17

Table 10.5. Roof Frame Construction Types and Unit Weights

ID	Construction Type	Weight (psf)
1	Cast-in-place concrete slab	48.0
2	Concrete flat plate (8″)	96.0
3	Concrete slab on metal deck and beam	34.0
4	Concrete waffle slab (10″)	120.0
5	Laminated wood arches	3.0
6	Open web steel joist	17.5
7	Pre-cast concrete beam and plank	80.0
8	Pre-cast double tees	42.0
9	Steel Truss	3.0
10	Wood Rafter	1.2
11	Wood Truss	2.0

Table 10.6. Insulation Types and Unit Weights

ID	Construction Type	Weight (psf)
1	Cellular glass insulation (4″ thick)	2.8
2	Fiberboard	1.5
3	Fiberglass sheets	1.5
4	Fibrous glass insulation (4″ thick)	4.4
5	Perlite/EPS composite	0.8
6	Polyisocyanurate sheets	0.4
7	Polystyrene (2″ thick)	0.4
8	Rigid insulation, 1/2″	0.8
9	Urethane foam with skin	0.5

Table 10.7. Partition Construction Types and Unit Weights

ID	Construction Type	Weight (psf)
1	2×4 unplastered wood or metal studs	4
2	50% concrete block, 505 gypsum board on metal studs	22
3	Concrete block	36
4	Concrete block and toilet partitions	26
5	Gypsum board and sound deadening board on wood or metal studs	15
6	Gypsum board on concrete block and metal studs	32
7	Gypsum board on wood or metal studs	8
8	Lightweight concrete block	24
9	Movable steel partitions	4
10	One side plaster on wood or metal studs	12
11	Two sides plaster on wood or metal studs	20

Table 10.8. Floor Finish Types and Unit Weights

ID	Finish Type	Weight (psf)
1	50% carpet, 30% hardwood, 20% ceramic tile	6.8
2	50% carpet, 40% marble tile, 10% terrazzo	17.4
3	50% carpet, 40% vinyl composition tile, 10% quarry tile	3.7
4	50% carpet, 50% ceramic tile	12.5
5	50% carpet, 50% vinyl composition tile	1.5
6	50% quarry tile, 50% vinyl composition tile	12.0
7	50% vinyl composition tile, 30% carpet, 20% terrazzo	7.5
8	50% vinyl composition tile, 50% paint	0.5
9	60% carpet, 30% vinyl composition tile, 10% ceramic tile	3.8
10	60% carpet, 35% hardwood, 5% ceramic tile	3.8
11	60% epoxy, 20% carpet, 20% vinyl composition tile	5.0
12	60% hardwood, 20% carpet, 20% terrazzo	9.2
13	60% vinyl composition tile, 20% ceramic tile, 20% terrazzo	11.6
14	65% carpet, 35% quarry tile	9.4
15	65% vinyl composition tile, 25% carpet, 10% terrazzo	4.4
16	70% carpet, 10% hardwood, 20% ceramic tile	6.4
17	70% carpet, 15% terrazzo, 15% vinyl composition tile	6.4
18	70% carpet, 30% ceramic tile	8.3
19	70% terrazzo, 30% ceramic tile	29.3
20	70% vinyl composition tile, 20% carpet, 10% ceramic tile	3.4
21	70% vinyl composition tile, 20% carpet, 10% terrazzo	4.3
22	70% vinyl composition tile, 25% carpet, 5% ceramic tile	2.4
23	70% vinyl composition tile, 30% carpet	1.3
24	80% carpet, 10% vinyl composition tile, 10% ceramic tile	4.0
25	80% carpet, 20% ceramic tile	6.2
26	80% rubber mat, 20% paint	1.6
27	85% carpet, 15% ceramic tile	5.2
28	85% carpet, 5% vinyl composition tile, 10% ceramic tile	4.1
29	90% carpet, 10% terrazzo	5.0
30	90% hardwood, 10% ceramic tile	5.9
31	90% metallic hardener, 10% vinyl composition tile	1.9
32	95% vinyl tile, 5% ceramic tile	2.1
33	Carpet	2.0
34	Vinyl composition tile	1.0
35	Quarry tile	23.0

Table 10.9. Floor Construction Types and Unit Weights

ID	Construction Type	Weight (psf)
1	Cast-in-place concrete beam and slab	120.0
2	Concrete flat plate	120.0
3	Concrete slab with metal deck and beams	38.0
4	Concrete waffle slab	120.0
5	Metal deck on open web steel joist	17.5
6	Wood joist	6.0
7	Open web steel joists, slab form, concrete	30.0
8	Pre-cast concrete beam and plank	80.0
9	Pre-cast double tees with concrete topping	58.0

Table 10.10. Wall Finish Types and Unit Weights

ID	Construction Type	Weight (psf)
1	40% vinyl wall covering, 35% ceramic tile, 25% epoxy coating	8.5
2	40% vinyl wall covering, 40% paint, 20% ceramic tile	5.0
3	50% paint, 40% glazed coating, 10% ceramic tile	2.3
4	50% paint, 50% ceramic tile	11.5
5	50% paint, 50% vinyl wall covering	0.5
6	50% vinyl wall covering, 45% paint, 5% ceramic tile	1.7
7	50% wallpaper, 25% wood paneling, 25% paint	1.1
8	60% paint, 40% epoxy coating	0.0
9	60% vinyl wall covering, 40% paint	0.6
10	65% paint, 25% vinyl wall covering, 10% ceramic tile	2.6
11	70% paint, 20% vinyl wall covering, 10% ceramic tile	2.5
12	70% paint, 20% wood paneling, 10% vinyl wall covering	0.9
13	70% paint, 25% vinyl wall covering, 5% ceramic tile	1.4
14	70% paint, 30% epoxy coating	0.0
15	75% paint, 15% glazed coating, 10% ceramic tile	2.3
16	75% paint, 25% ceramic tile	5.8
17	75% vinyl covering, 20% paint, 5% ceramic tile	1.9
18	90% paint, 10% ceramic tile	2.3
19	95% paint, 5% ceramic tile	1.2
20	Glazed coating	0.0
21	Paint	0.0

Table 10.11. Ceiling Finish Types and Unit Weights

ID	Finish Type	Weight (psf)
1	90% paint, 10% suspended fiberglass board	0.2
2	Fiberglass board on exposed grid system	3.0
3	Gypsum board on wood furring	4.5
4	Gypsum plaster on suspended metal lath	10.0
5	Gypsum plaster on wood furring	10.0
6	Mechanical duct allowance	4.0
7	Mineral fiber tile on concealed zee bars	2.0
8	Textured finish	0.2
9	Painted gypsum board	2.0
10	Painted gypsum board on furring	3.0
11	Painted gypsum board on resilient channels	2.0
12	Plaster on tile or concrete	5.0
13	Plaster on wood lath	8.0
14	Suspended fiberglass board	1.5
15	Suspended metal lath and cement plaster	15.0
16	Suspended steel channel system	2.0

present debris model), which is not ideal for a validation study. Therefore, references were made to a number of published papers on debris removal (Dowd, 1990; Tansel, 1993; Dewberry and Davis, 1993) to identify appropriate cases for model validation.

After Hurricane Andrew, Tansel (1993) carried out a detailed debris analysis for five zones with significant structural damage in Dade County. Table 10.12 lists the zone location, number of buildings, exterior wall construction distribution, average exterior damage ratio, and total structural debris for each of the five zones investigated. The amount of structural debris was estimated based on an average type of residence and structural damage states. The damage statistics in each zone were calculated using the data collected by the Metro-Dade County Building and Zoning Department. Structures with more than 50% damage were judged uninhabitable and assumed to be demolished. The debris simulation is performed using model buildings with different combinations of number of stories (1-story or 2-story), roof shape (hip or gable), wall construction (wood frame or masonry), nail size (6d or 8d), and roof cover type (shingle or tile). The total debris produced by each model building under the simulated wind speed in each zone is calculated and then aggregated within the zone to obtain the average amount of debris per building (weighted by the assumed building stock). The total amount of structural debris in each zone is calculated by multiplying the average amount of debris per building with the total number of buildings in that zone. For Dade County, the building stock is modeled assuming 80% of the homes are single story. 75% of the homes are assumed to have gable roofs and 25% of the homes are assumed to have hip roofs. The number of homes having shingle roof cover is assumed to be the same as that having tile roof cover. 40% of the homes are assumed to use 6d nails on roof deck and the remaining homes are assumed to use 8d nails. All the homes are assumed to have straps for roof-to-wall connection. The distribution of exterior wall construction types in each zone is assumed to be the same as that listed in Table 10.12. The exterior wall construction distribution for Zone 4, which is not given in the paper by Tansel (1993), is assumed to be the same as that of Zone 5 (in the same zip code). Table 10.12 also shows the simulated average debris weight per building, average debris volume per building, total structural debris weight in each zone, and the ratio between simulated and actual debris in each zone. The mean of the model-to-actual ratios is 1.05 and the standard deviation is 0.58. The result is very promising given that the debris model relies heavily on engineering judgment.

Table 10.13 shows debris comparisons for hurricanes Hugo and Andrew at a regional level. Dowd (1990) reported the debris removal and channel shoaling of USACE in hurricane Hugo. Political subdivisions made 359 requests to FEMA and an estimated 15,500,000 cubic yards of debris were removed by or for these subdivisions. USACE assisted and administrated the debris removal mission in seven counties (Berkeley, Charleston, Darlington, Dorchester, Lancaster, Orangeburg, and Sumter), with a total of 4,589,559 cubic yards of debris removed. Tansel (1993) estimated that 2.9 million tons of construction and demolition debris were generated by hurricane Andrew. The USACE after action report (USACE, 1993) gives an estimate of 40 million cubic yards of debris in Dade County. The debris simulation is performed at a zip code level. Similar to the first validation study, the average debris weight and volume per building in each zip code

Table 10.12. Structural Debris Comparison for Hurricane Andrew

Zone (zip code)	Actual Data				Simulation Results			Model / Actual
	Number of Buildings	Exterior Wall Construction Distribution	Average Exterior Damage Ratio	Structural Debris (tons)	Average Debris Weight per Building (lb)	Average Debris Volume per Building ($yard^3$)	Total Structural Debris (tons)	
Zone 1 (33186)	14,000	85% wood frame	63%	182,650	27,252	145	173,215	0.95
Zone 2 (33156)	18,000	75% concrete	24%	456,365	25,864	127	211,364	0.46
Zone 3 (33156)	604	50% wood frame; 50% concrete	53%	11,376	24,665	125	6,764	0.59
Zone 4 (33031)	2,500	-	48%	42,900	53,232	264	60,418	1.41
Zone 5 (33031)	1,100	85% wood frame	47%	14,390	53,232	264	26,584	1.85

Table 10.13. Debris Comparison for Hurricanes Hugo and Andrew

Storm	Region	Actual Weight (tons)	Actual Volume ($yard^3$)	Modeled Weight (tons)	Modeled Volume ($yard^3$)	Model/ Actual (weight)	Model/ Actual (volume)
Hugo	South Carolina	-	15,500,000	951,009	9,130,843	-	0.59
Hugo	USACE Admin. Region	-	4,589,559	782,480	7,366,394	-	1.61
Andrew	Dade County	2,900,000	40,000,000	3,396,991	35,323,080	1.17	0.88

are simulated first (using the assumed building stock). The total debris weight or volume in each zip code is then calculated by multiplying the total number of houses in each zip code with the average debris weight or volume per building. The total amount of debris in the study region is estimated by adding up the total debris in each zip code. The default building stock in Dade County is assumed to be the same as that in the first validation study and the default building stock for South Carolina is assumed to be: 70% one-story and 30% two-story; 75% gable and 25% hip; 30% using 6d nails and 70% using 8d nails; 10% using straps and 90% using toe-nails for roof-to-wall connection. The total number of houses in each zip code is estimated using 1990 census data. As shown in Table 10.13, the debris model underestimated the debris volume in South Carolina and overestimated debris volume in the regions administrated by USACE (seven counties).

For hurricane Andrew, both the modeled debris weight and debris volume are reasonably close to the actual values. It is not clear in the paper by Dowd (1990) whether all the political subdivisions that made requests to FEMA for debris removal assistance are within South Carolina. Therefore, the actual study region may cover a larger area than the state of South Carolina, which may help to explain the underestimation of debris volume by the model. The overestimation of the debris volume in the USACE administrated region may likely be to the opposite. The study region may only include portions (most likely just municipalities) of the seven counties that were mentioned in the paper.

10.4 Final Remarks

A building debris estimation model has been developed based on building component damage states and building component weight statistics. The model is capable of providing estimates of the amount (both weight and volume) of construction and demolition debris in each of the four debris types (wood, masonry, metal and other). Limited validation studies have shown that the model can produce reasonable estimates of the total building debris produced by a hurricane.

Chapter 11. Short Term Shelter Requirements

11.1 Introduction

The model for estimating the number displaced households and short term shelter needs follows that used for the Hazus Earthquake Model. The concept and formulation are described in the Hazus (Earthquake) Technical Manual (FEMA, 1999). The only modification for the Hurricane Model is that building loss ratios, instead of building damage states, are used to estimate the proportion of uninhabitable housing units.

The shelter model provides two estimates for each census tract:

1. The number of displaced households due to loss of habitability
2. The number of people requiring only short-term public shelter.

Loss of habitability is calculated from modeled damage to residential buildings, whose severity is expressed in terms of loss ratios due to physical damage, and from estimated loss of water or power supply to residential buildings or units.

11.2 Description of Methodology

The form of the displaced households model is:

$$D = \left(U_a + \beta U_b\right)\frac{H}{S+M}, \tag{11.1}$$

where

D - Number of displaced households,

U_a - Number of uninhabitable units due to damage (Equation 11.2),

U_b - Number of uninhabitable units due to loss of water or power (Equation 11.3),

H - Total number of households,

S - Total number of single-family dwelling units,

M - Total number of dwelling units in multi-family buildings,

β - Adjustment factor for household tolerance to loss of power or water (user input).

The ratio $H/(S+M)$ represents the occupancy rate averaged over the single-family and multi-family categories. U_a and U_b are estimated as follows, respectively,

$$U_a = S \cdot \int_0^1 f_s(x) \cdot w_s(x)\, dx + M \cdot \int_0^1 f_m(x) \cdot w_m(x)\, dx, \tag{11.2}$$

$$U_b = R_u\left[(S+M)-U_a\right]. \tag{11.3}$$

where,

$f_s(x)$ - Probability density function of loss ratio x for single-family buildings,

$f_m(x)$ - Probability density function of loss ratio x for multi-family buildings,

$w_s(x)$ - Un-inhabitability function in terms of loss ratio x, single-family buildings,

$w_m(x)$ - Un-inhabitability function in terms of loss ratio x, multi-family buildings,

R_u - Damage ratio to power and water facilities.

Examples of the modeled probability density function $f_s(x)$, for the case of single-family buildings for the building stock in North Florida, are shown in Figure 11.1 in the form of probability mass functions. As wind speed increases, the mass of the probability moves toward unity, indicating that all buildings experience a complete loss. Building stock data used for the loss ratio computations for Florida are presented in Figure 11.2.

Figure 11.3 shows an empirical un-inhabitability function for single-family buildings in terms of loss ratio x, where below 20% loss a building is considered still inhabitable and above 50% a building is assumed to be completely uninhabitable, while for buildings with a loss ratio between these two values a linear proportion is assumed to be uninhabitable. For multi-family buildings, as shown in Figure 11.4, the linear range is defined between 10% and 50% empirically, since some of the units in a building with relatively mild overall damage and loss may already have become uninhabitable.

Examples of computed percentage of household being displaced are shown in Figure 11.5.

Similar to the Hazus Earthquake Model, the number of people likely seeking public shelter is estimated based on the number of displaced households, D, recognizing that only a fraction of the displaced households will likely seek public shelter and this fraction is a function of several demographic variables such as income and ethnicity, as expressed below:

$$N = \frac{D \cdot P}{H} \sum_{i=1}^{5}\sum_{j=1}^{5}\sum_{k=1}^{2}\sum_{l=1}^{3}\left(\alpha_{ijkl} \cdot I_i E_j O_k A_l\right), \tag{11.4}$$

where

N - Number of people likely seeking public shelter,

D - Number of displaced households (Equation 11.1),

P - Population,

H - Total number of households,

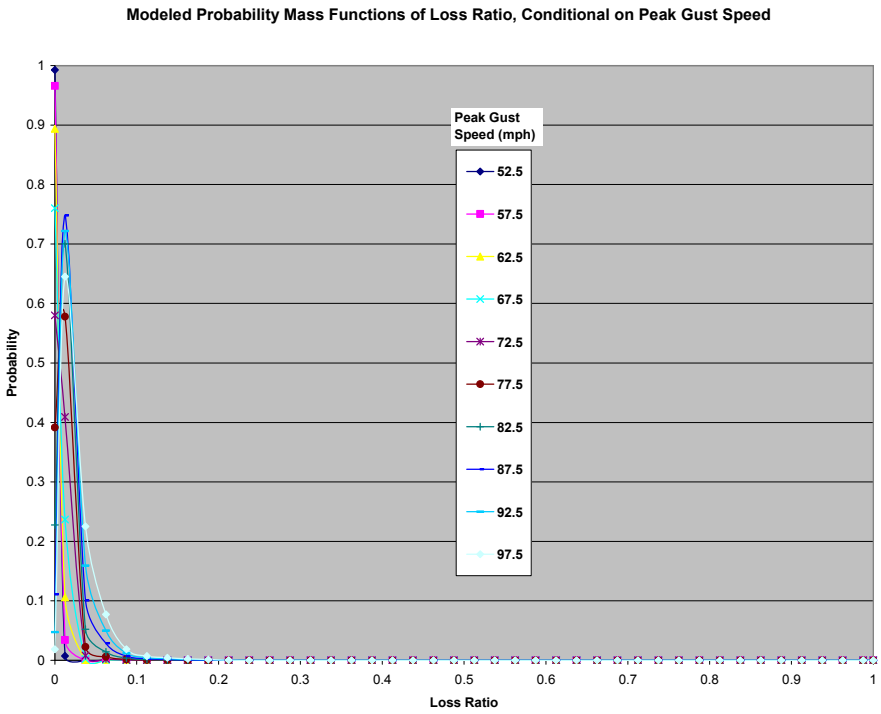

(a). Lower Peak Gust Wind Speeds (between 50 mph and 100 mph)

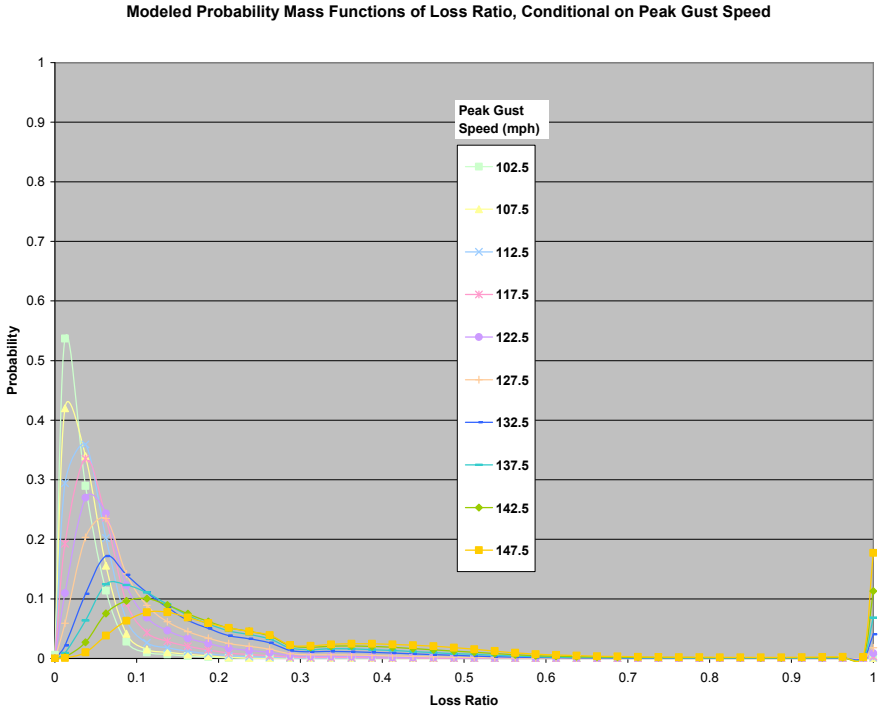

(b). Medium Peak Gust Wind Speeds (between 100 mph and 150 mph)

Figure 11.1. Modeled Probability Mass Function of Loss Ratios.

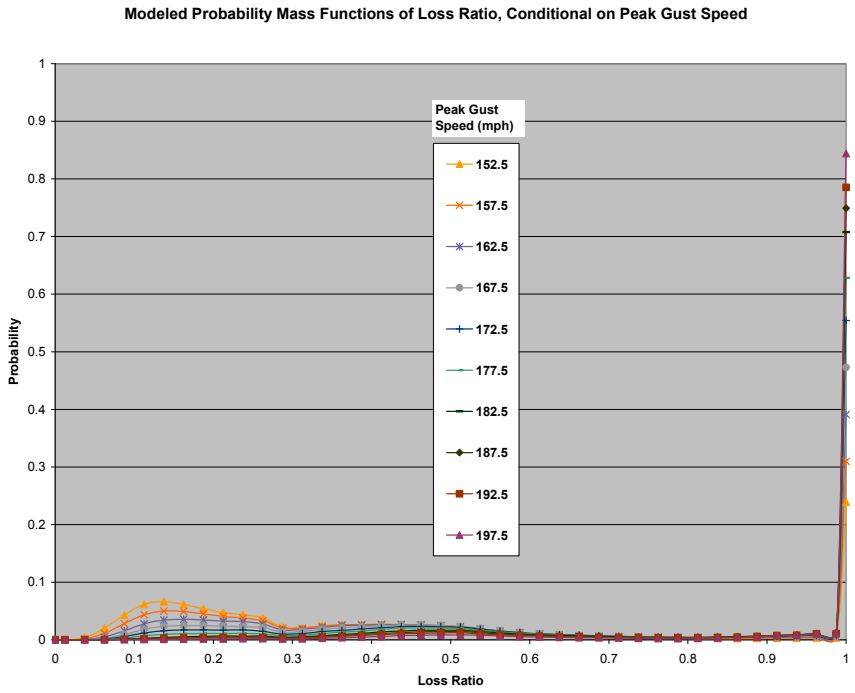

(c) High Peak Gust Wind Speeds (between 150 mph and 200 mph)

Figure 11.1. Modeled Probability Mass Function of Loss Ratios (concluded).

I_i - Percentage of population in the i^{th} income class,

E_j - Percentage of population in the j^{th} ethnic class,

O_k - Percentage of population in the k^{th} ownership class,

A_l - Percentage of population in the l^{th} age class,

α_{ijkl} - A fractional coefficient, which is a weighted average of empirical fractions of displaced households from various demographic classes who seek public shelter:

$$\alpha_{ijkl} = w_I\left(F_I\right)_i + w_E\left(F_E\right)_j + w_O\left(F_O\right)_k + w_A\left(F_A\right)_l \ , \tag{11.5}$$

where the weights and fractions are defined in Tables 11.1 and 11.2, respectively, with their default values. Note that Equations 11.4 and 11.5 are formulated assuming that the demographic variables are mutually independent and the displaced households are distributed among demographic classes in proportion to their number of households. An example of computed results is shown in Figure 11.6.

11.3 Simplified Methodology

The methodology represented by Equation 11.2 requires the full probability density function of building loss as a function of peak gust wind speed. In an effort to reduce the data storage requirements and computational requirements imposed by Equation 11.2, a

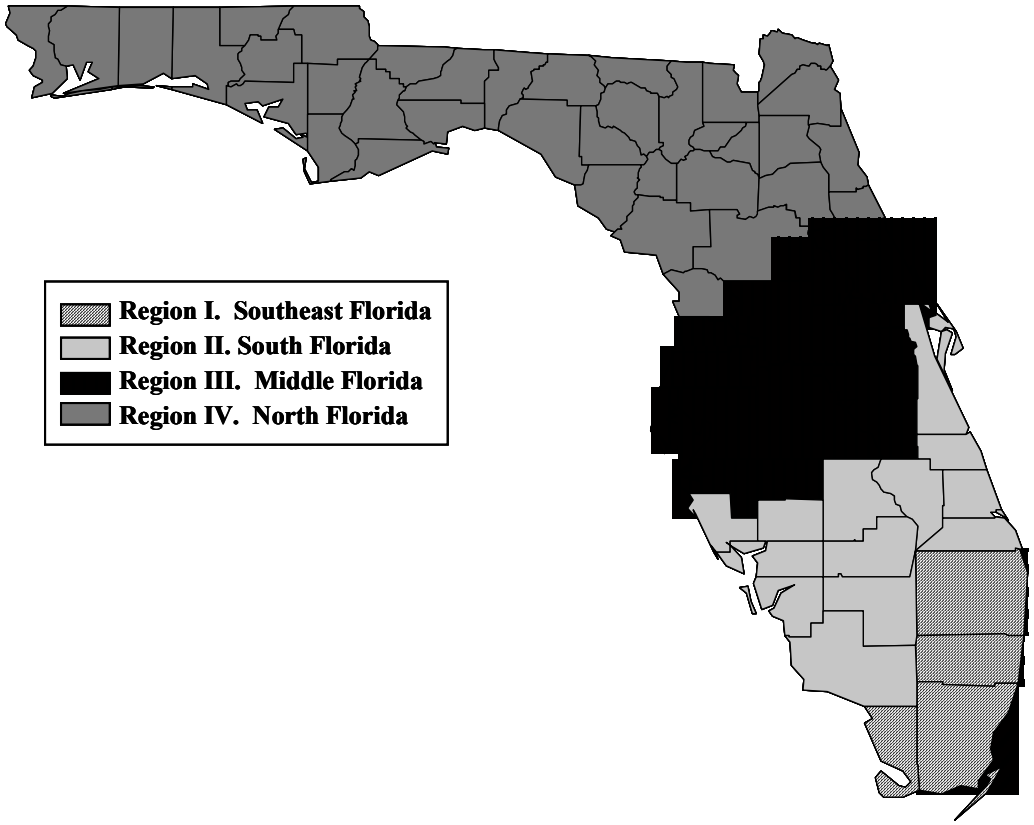

	Region I	Region II	Region III	Region IV
Roof Shape				
Gable	0.62	0.61	0.75	0.73
Hip	0.38	0.39	0.25	0.27
Roof Cover				
Regular Shingle	0.70	1.00	1.00	1.00
Hurricane Shingle	0.30	0.00	0.00	0.00
Roof-Wall Connection				
Toe Nail	0.10	0.09	0.25	0.15
Strap	0.90	0.91	0.75	0.85
Roof Deck Fastening				
6d@6/12	0.25	0.46	0.29	0.40
8d@6/12	0.32	0.32	0.29	0.35
8d@6/6	0.43	0.22	0.41	0.26
Opening Protection				
No Protection	0.70	0.85	0.95	0.92
Dade Shutter	0.30	0.15	0.05	0.08

Figure 11.2. Building Stock Data Used for the Loss Ratio Computation.

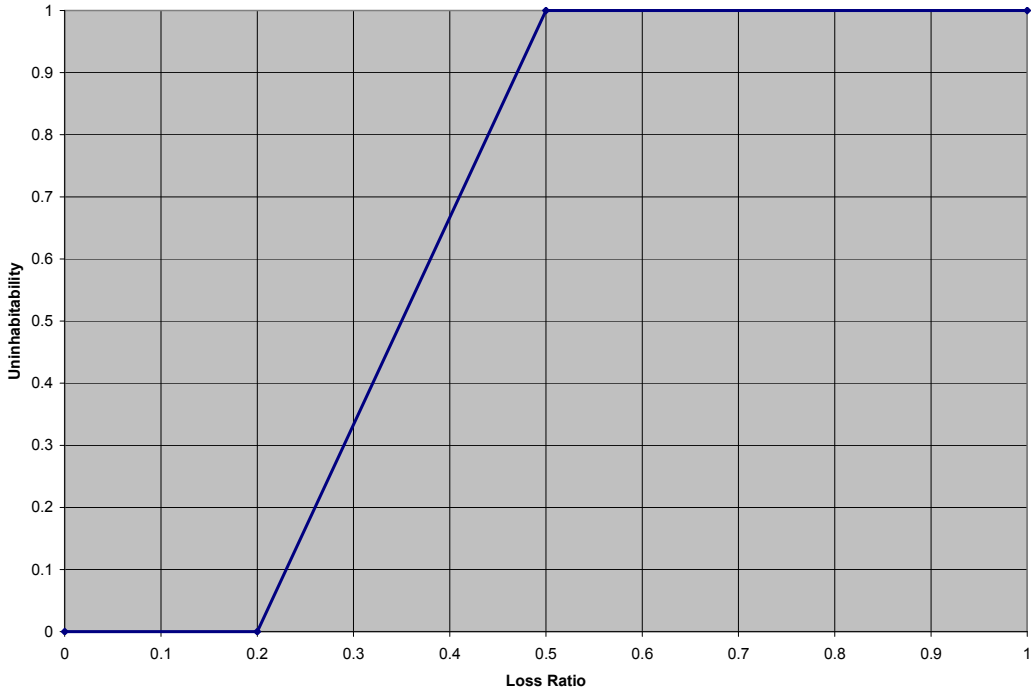

Figure 11.3. Empirical Un-Inhabitability Function for Single-Family Buildings.

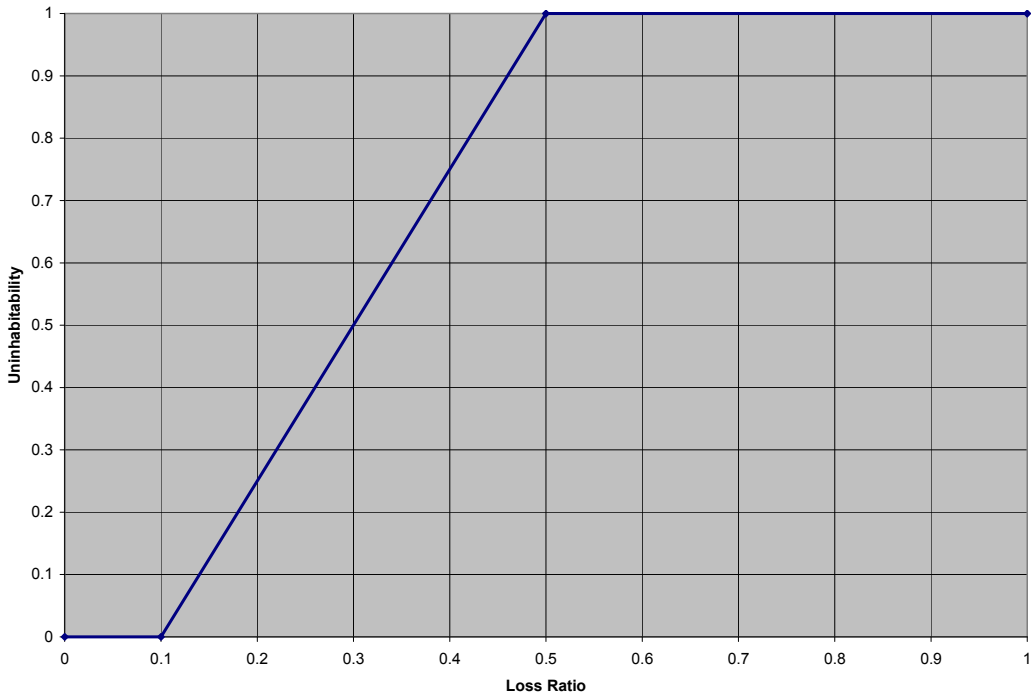

Figure 11.4. Empirical Un-Inhabitability Function for Multi-Family Buildings.

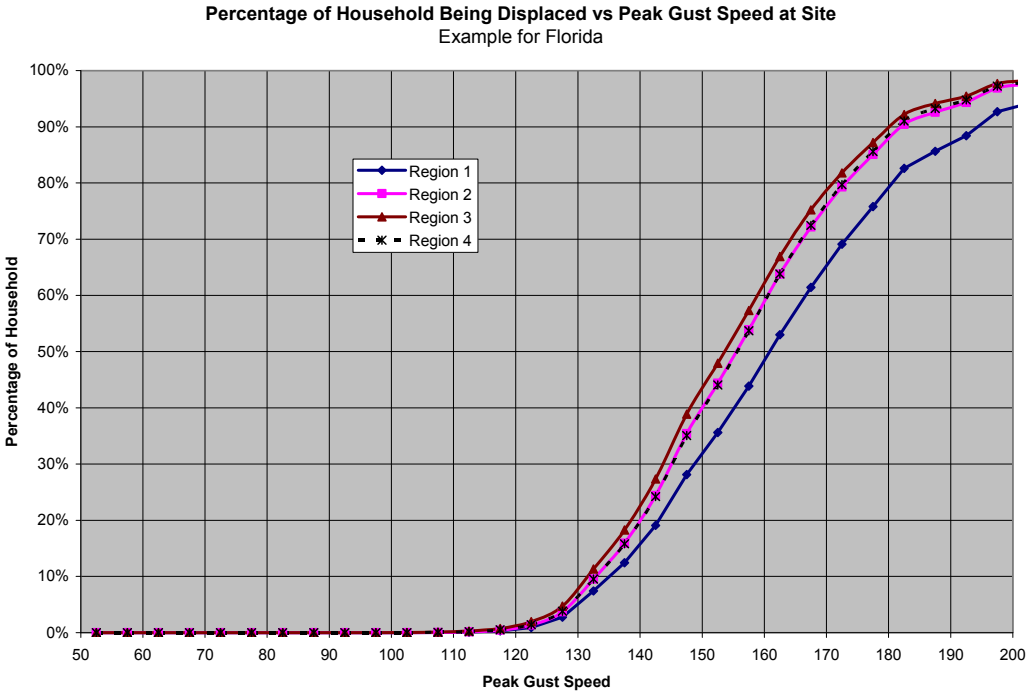

Figure 11.5. Example of Computed Percentage of Household Being Displaced as a Function of Peak Gust Wind Speed at Site.

Table 11.1. Default Weights for Demographic Variables

Symbol	Description	Default Value
w_I	Income Factor Weighting	0.73
w_E	Ethnic Factor Weighting	0.27
w_O	Ownership Factor Weighting	0.00
w_A	Age Factor Weighting	0.00
$(w_I + w_E + w_O + w_A)$	Total	1.00

implification has been developed to estimate the integrated uninhabitability ratio using mean building losses instead of the probability density functions of building loss. Mean building loss is readily available within Hazus.

A study was carried out to examine the relations between the integrated un-inhabitability ratios, which are evaluated by the integrals in Equation 11.2, and the mean building loss ratios. The results are shown in Figures 11.7 and 11.8 for single-family and multi-family buildings respectively. It is found that the scatter is very insignificant; that is, the mean building loss is a good predictor of the un-inhabitability. Fitted mean functions are also shown in Figures 11.7 and 11.8. These functions are used in Hazus in place of Equation 11.8 as follows,

$$U_a = S \cdot F_S(X_S) + M \cdot F_M(X_M), \tag{11.6}$$

where

Table 11.2. Default Fractions of Displaced Households Seeking Public Shelter

Symbol	Description	Default Value
Income		
$(F_I)_1$	Household Income < $10000	0.62
$(F_I)_2$	$10000 < Household Income < $20000	0.42
$(F_I)_3$	$20000 < Household Income < $30000	0.29
$(F_I)_4$	$30000 < Household Income < $40000	0.22
$(F_I)_5$	$40000 < Household Income	0.13
Ethnicity		
$(F_E)_1$	White	0.24
$(F_E)_2$	Black	0.48
$(F_E)_3$	Hispanic	0.47
$(F_E)_4$	Asian	0.26
$(F_E)_5$	Native American	0.26
Ownership		
$(F_O)_1$	Own Dwelling Unit	0.40
$(F_O)_2$	Rent Dwelling Unit	0.40
Age		
$(F_A)_1$	Population Under 16 Years Old	0.40
$(F_A)_2$	Population Between 16 and 65 Years	0.40
$(F_A)_3$	Population Over 65 Years Old	0.40

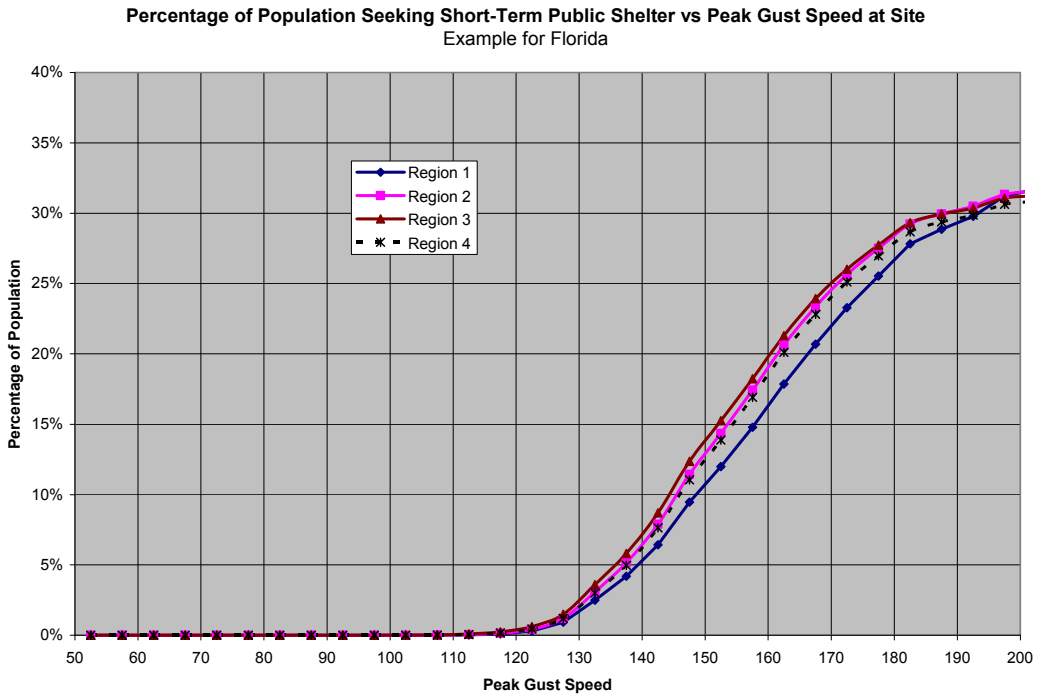

Figure 11.6. Example of Computed Percentage of Population Seeking Short-Term Public Shelter as a Function of Peak Gust Wind Speed at Site.

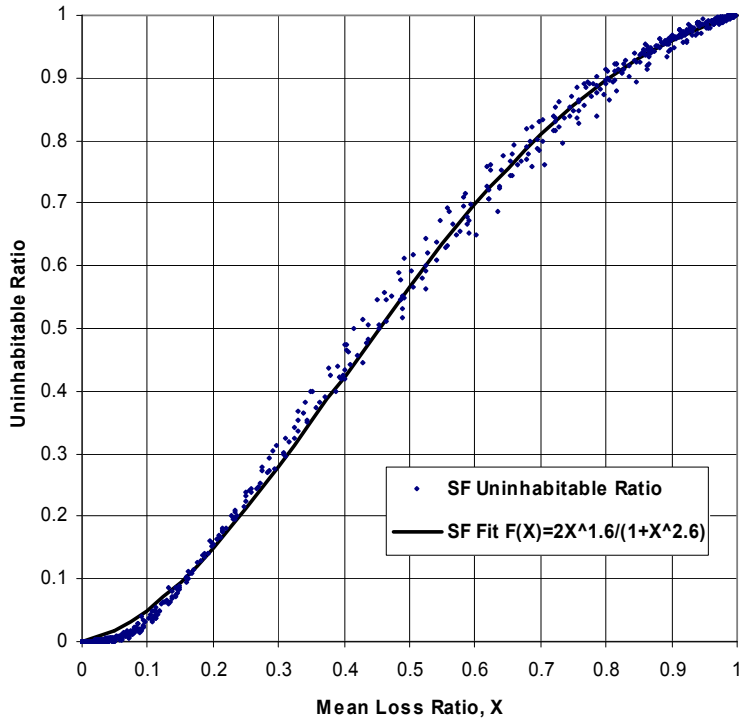

Figure 11.7. Uninhabitability as a Function of Mean Building Loss for Single-Family Buildings.

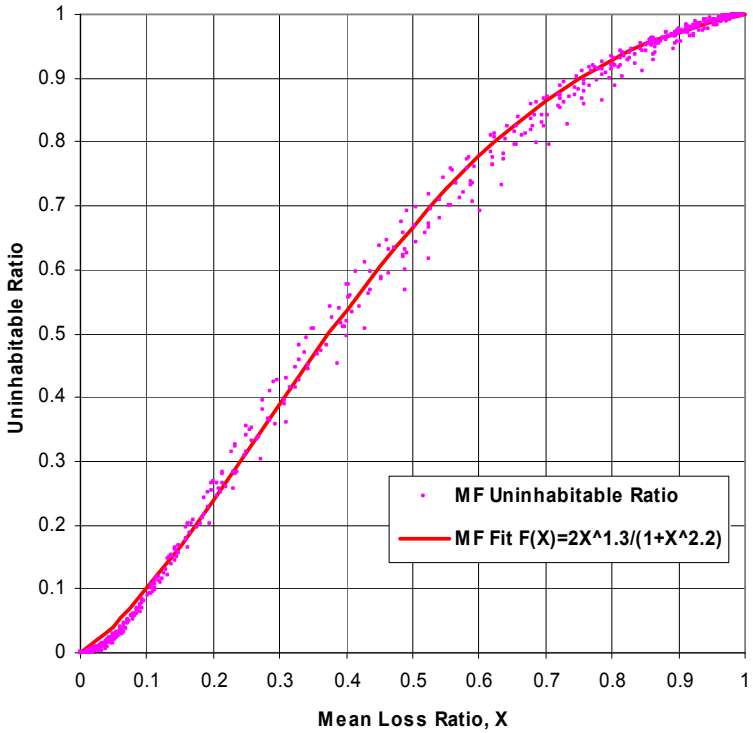

Figure 11.8. Uninhabitability as a Function of Mean Building Loss for Multi-Family Buildings.

$$F_S(X_S) = \frac{2X_S^{1.6}}{1+X_S^{2.6}} \tag{11.7}$$

$$F_M(X_M) = \frac{2X_M^{1.3}}{1+X_M^{2.2}} \tag{11.8}$$

and X_S and X_M denote the mean building loss ratios for single-family and multi-family buildings respectively. Equations 11.6 and 11.7 are plotted in Figures 11.7 and 11.8, respectively.

Because of the small amount of scatter in Figures 11.7 and 11.8, results computed using Equation 11.5 instead of Equation 11.2 are nearly identical to those shown in Figures 11.5 and 11.6. Therefore, the simplified approach is used in the fast-running implementation of the Hazus software to compute displaced households and population seeking short-term public shelters.

Chapter 12. Tree Blowdown

12.1 Introduction and Background

Damage to structures caused by windthrown trees is an ongoing problem in forested areas. In addition, during Hurricane Hugo, for example, most of the damage to the electric power distribution system was caused not by the direct action of wind but by trees falling on the distribution lines and breaking the lines (Cook, 1990). Tree debris produced by Hurricane Hugo also hampered emergency crews and delayed repairs to lifelines (Cook, 1990). At Charleston Naval Base, windthrown trees broke buried water lines, disrupting the water supply (Strehmeyer, 1990).

Extreme winds associated with thunderstorms and extratropical storms also cause extensive tree-induced damage. For example, in May 1990, there were in excess of 300 separate reports of downed trees. Of the 150 reported downed power lines, approximately 30% were caused by trees falling across the lines. Of the 100 reports of damage to structures, approximately 40% were caused by downed trees, with one case producing a fatality.

Trees have both positive and negative effects in the presence of extreme winds. On the positive side, trees provide shelter to structures, reducing the likelihood of damage produced by the direct action of wind. On the negative side, the existence of many trees surrounding a structure increases the likelihood of a tree striking and damaging the structure.

This chapter describes the tree blowdown methodology implemented in Hazus and the two damage/loss models that use the results produced by the tree blowdown methodology. The first estimates the quantity of tree debris after a hurricane. The second estimates the additional economic loss to residential buildings and contents caused by fallen trees.

Figure 12.1 shows a high-level flow chart of the data and the models. The combination of tree data by census tract and a tree blowdown probability model provide the elements needed for estimating debris quantities, while the tree data, blowdown model, hit probability and damage model, along with a cost model, yield the estimation of damage and loss to residential buildings due to tree blowdown, given a defined hurricane climate.

Section 12.2 provides a brief overview of related research. The wind throw model is described in Section 12.3, and the blowdown probability curves produced by the model are presented in Section 12.4. The development of the tree inventory database is presented in Sections 12.5 and 12.6. The tree debris model is described in Section 12.7, and the damage and loss models for residential buildings and contents are presented in Sections 12.8 through 12.10.

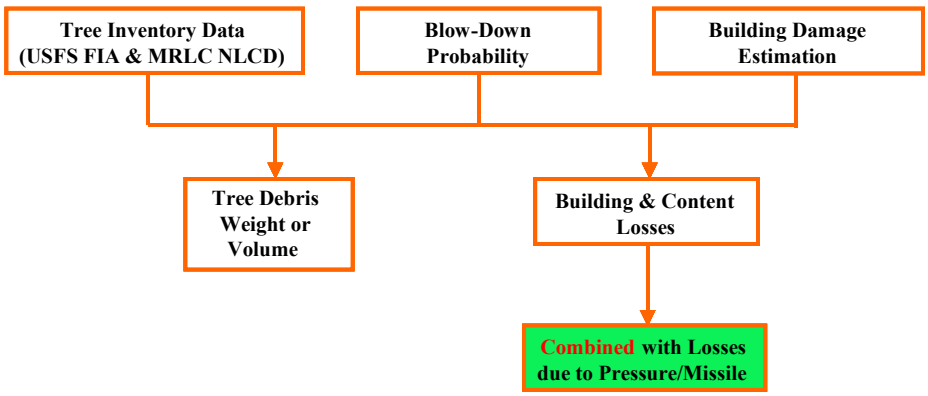

Figure 12.1. Estimation of Tree Blow-Down Debris and Damage to Buildings.

12.2 Related Research

Virtually all the research related to natural blowdown of trees has been performed by the forestry industry. This research is prompted by large annual losses of harvestable wood in many countries. In New Zealand, the average annual losses of softwood trees due to catastrophic wind events ranges between 0.02% and 3.5% (depending on the forest) of the total stock. The extent of attritional damage associated with lesser winds varies between 0% and 1% of the growing stock per annum (Somerville, 1993). Over the period 1981-1990, more than 50% of the total yield in the Czech Republic had to be cut down due to injuries produced by windthrow or snowbreak (Slodicak, 1993).

The research performed by the forestry industry (predominately in the U.K. and Europe) includes full-scale measurement of tree response due to wind action, measurements of windspeeds within canopies, static pull down tests and relatively simple mathematical models to estimate the forest blowdown potential. The model described herein draws on work done by the forestry industry in the U.K. and Europe combined with research performed in the United States. Very little research in the U. S. has been directed toward assessing the risk of forest blowdown produced by natural wind; however, the most relevant research was directed toward assessing tree blowdown probabilities associated with the effects of nuclear weapons (Twisdale, et al., 1984). The ten-year research program produced a computer simulation methodology termed BLOWTRAN (BLOWdown TRANSport) described in the section "Damage to Forests" in the EM-1 Nuclear Effects Manual. The BLOWTRAN model is adapted as described herein to obtain estimates of tree blowdown associated with natural wind.

12.3 Wind Throw Model

12.3.1 Wind Load Response and Breakage Model

The mathematical model used in BLOWTRAN to determine the drag loads acting on a tree is based on the model developed by the United States Forest Service (USFS) during the early 1950s. The drag force, F_D, acting on the tree crown is a function of the dynamic pressure acting on the tree crown combined with the effective surface area and the

effective drag coefficient. Both the drag coefficient and the effective crown area of a tree subject to strong winds decrease due to streamlining of the leaves and branches, with the end result being that the wind force acting on the tree is nearly proportional to velocity.

To determine the effect of streamlining the tree-crown system, and to develop a model to define the wind loads, the USFS conducted full-scale drag tests on 13 coniferous trees (Sauer, et al., 1951) and 18 broadleaf trees (Lai, 1955). More recent full-scale measurements on over 30 coniferous trees (Frank, et al., 1987; Frank, et al., 1989; Frank, et al., 1991) supplement the USFS data. All of the full-scale test data used herein were carried out by mounting full-size trees on the rear of a tractor trailer and driving at a constant velocity. Base overturning moments and shear forces were measured for mean velocities ranging between 6 m/s and 32 m/s in the more recent tests, and 5 m/s to 25 m/s in the USFS tests.

The drag data from these full-scale tests are correlated as functional relationships of two dimensionless parameters that describe the variation in the drag force with the bending moment at the base of the crown, as a function of the wind force, and the tree crown and stem characteristics. The drag force, F_D, in the USFS model is expressed as

$$\frac{F_D}{\frac{1}{2}\rho U^2} = \frac{d_c^3}{h}\frac{1}{W_{dbf}}\Psi_D \tag{12.1}$$

where h *is* the distance between the effective center of pressure and the base of the crown, d_c is the diameter at the base of the crown, W_{dbf} is the ratio of the weight of the dry branches to the weight of the dry foliage, and Ψ_D is a drag function. The wind velocity, U, in Equation 12.1 is the relative velocity (i.e., wind velocity minus the velocity of the tree) and, therefore, aerodynamic damping is inherently included in Equation 12.1. The drag function, Ψ_D, is given as:

$$\Psi_D = \frac{k_2 k_2 \left(\frac{R}{W_{dc}}\right)^{-1.5}}{k_1 + k_2 \left(\frac{R}{W_{dc}}\right)^{-1.5}} \tag{12.2}$$

where k_1 and k_2 are drag function parameters, W_{dc} is the dry crown weight, and R is the restoring force in the stem at the base of the crown. In the static case, the restoring force, R, is equal to the drag force, F_D. In Equation 12.2, the parameter k_1 is directly proportional to the drag coefficient for a perfectly rigid tree, and k_2 is the parameter responsible for reducing the effective drag force with increases in wind speed. Small values of k_2 describe a tree which streamlines readily; conversely, large values of k_2 describe a tree which does not readily streamline. The dry crown weight, W_{dc}, in Equation 12.2 does not need to be determined explicitly for each tree since it has been found to be strongly correlated with the height of the crown, H_c, and the stem diameter, d_c, at the base of the crown. Empirical relationships for the dry crown weight have been developed for a

number of hardwood and coniferous tree species (Storey, Fons, and Sauer, 1955; Lai, 1955; Twisdale, et al., 1989) in the form

$$ln(W_{dc}H_c) = a + b\,ln\,d_c + \varepsilon \tag{12.3}$$

where H_c is the height of the crown, a and b are regression constants, and ε is a normally distributed error term. The r^2 values for these species-dependent empirical relationships exceed 0.93 in all cases. Similar relationships for the parameter W_{dbf} have also been developed.

Because the dry crown weight, W_{dc}, and the ratio of the weight of the dry branches to the weight of the dry foliage, W_{df}, are determined through empirical relationships, the basic inputs required for the drag (or loading) side of the model are:

(i) Tree height, H_{bh};

(ii) Diameter at breast height, d_{bh} (1.3 meters above ground);

(iii) Species;

(iv) Stem form parameters, a_s and c_s, which describe the taper in the stem;

(v) Percent crown;

(vi) Drag parameters k_1 and k_2.

The species-dependent variables, a_s, c_s, k_1, and k_2, are given for a variety of conifers and broadleaf trees in Twisdale, et al. (1989) and Vickery, et al. (1993).

Statistical distributions for the drag parameter, k_1, have been developed for 12 species (three conifers and nine broadleaf trees) and a relationship between the modulus of rupture and k_1 was developed so that the value of k_1 can be estimated for species where direct measurements are not available. Figure 12.2 shows the drag parameters k_1, and k_2 plotted versus the modulus of rupture, σ_r, for broadleaf trees where it is evident that trees having higher drag coefficients (as defined using k_1) are generally stronger. In the case of conifers, no trend of increasing k_1 with increasing σ_r was observed; however a weak positive correlation between σ_r and k_2 was observed. For broadleaf trees, the drag parameter k_1 (as shown in Figure 12.3) is modeled as a lognormal distribution where

$$m_{ln\,k_1} = 7.777 + 0.04198\,\sigma_r \tag{12.4a}$$

$$\sigma_{ln\,k_2} = 0.679 \tag{12.4b}$$

are the logarithmic mean and standard deviation, respectively. The drag parameter k_2 is also lognormally distributed with the logarithmic mean and standard deviation given as

$$m_{ln\,k_1} = 12.98 + 0.0145\,\sigma_r \tag{12.5a}$$

$$\sigma_{ln\,k_2} = 0.679 \tag{12.5b}$$

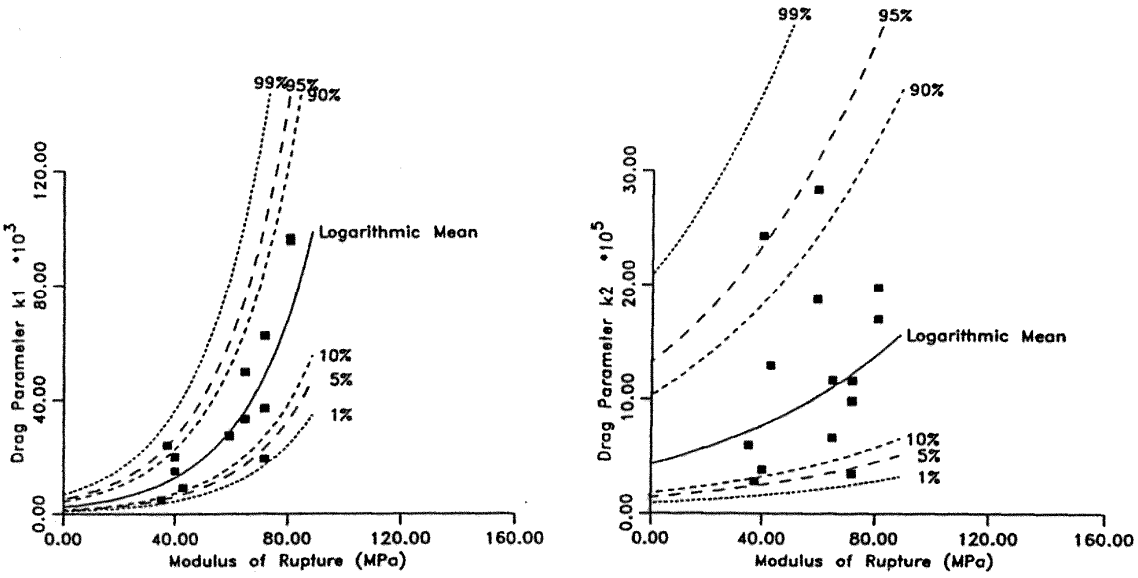

Figure 12.2. Drag Function Parameters k_1 and k_2 versus σ_r for Green Wood (Broadleaf Trees).

Tree response is modeled using a single degree of freedom model given as

$$m_e\ddot{x} + c\ddot{x} + kx = F_D(t) \tag{12.6}$$

where an effective mass, m_e, located at the center of pressure, is used to predict the dynamic response of the tree subjected to either a static or dynamic wind load. The drag force is assumed to act as a point load located at the center of pressure (in the crown at a height, H_{cp} above breast height).

The linear spring stiffness for the tree is derived from small deflection theory as

$$K = \frac{3EI_{bh}}{H_{bh}^3}\overline{K}\psi(c_s, f_1) \tag{12.7}$$

where I_{bh} is the moment of inertia at breast height, H_{bh}, is the height of the tree above breast height, E is the species-dependent Young's modulus, and $\overline{K}$ is a stiffness modulus parameter which accounts for the natural variations in the stiffness from the reference (or theoretical value). Statistical distributions of $\overline{K}$ used herein have been determined from static pull-down tests on both conifers and broadleaf trees (Frank, et al., 1987, 1989; Vickery, et al., 1991). The shape function, $\psi(c_s, f_1)$, accounts for the variable moment of inertia along the tree stem. The shape of the stem of a tree is hyperbolic in nature (Behre, 1927), such that the inside diameter, d, at any point along the stem is defined by

$$d = d_{bh}\frac{f}{a_s(f + c_s)} \tag{12.8}$$

where a_s and c_s are the species-dependent stem form parameters and f is the non-dimensional distance measured from the top of the tree. The $3EI/H^3$ term in Equation 12.7 is the stiffness of a uniform cantilever. The shape function modifies the stiffness to account for the shape of the stem.

The tree period and effective mass of the equivalent single degree of freedom system is determined using species-dependent empirical relationships for the tree period combined with the calculated spring constant, K. The tree period, T, is obtained from

$$T = a_1 + b_1 \frac{H_{bh}^2}{d_{bh}} + \varepsilon \tag{12.9}$$

where a_1 and b_1 are species-dependent regression constants, and ε is a normally distributed error term.

Bending stresses in the extreme fiber of the tree along the length of the stem prior to yielding are given by

$$\sigma = \frac{Md}{2I} \tag{12.10}$$

where $I = I_{bh}\left[\frac{1}{a_s\left(f + c_s\right)}\right]^4$, d is the inside diameter, and M is the bending moment.

The region of maximum stress, and hence the point at which the tree will likely fail, varies with the position of the applied load. In general, trees loaded near the top will tend to break in the crown, and as the effective load point moves closer to the ground, the location of maximum stress moves toward the base of the tree.

In order to determine whether or not failure occurs, a reference deflection, y_r, at the point of application of the load is determined from small deflection theory for a reference strain equal to σ_r/E, where σ_r, the modulus of rupture for green wood. The maximum linear spring resistance, R_m, is given as

$$R_m = \overline{R}_b \, K_r \, y_r \tag{12.11}$$

where $\overline{R}_b$ is a random variable representing the variability in the strength of the tree stem. Statistical distributions for $\overline{R}_b$ have been described in Frank, et al. (1987; 1989) and Vickery, et al. (1993) from the results of static pull-down tests for a number of broadleaf and coniferous trees.

In the case of conifers, $\overline{R}_b$ was found to be negatively correlated with diameter at breast height for both root and stem failures (i. e., larger diameter trees are less likely to be able to develop the theoretical maximum resistance moment). This negative correlation was less pronounced in the case of broadleaf trees.

The breakage defection, y_b, is obtained from

$$y_b = \mu y_r \tag{12.12}$$

where the ductility, μ, is a random variable whose statistical parameters have, again, been determined using the results of static tree pull-down experiments for a wide range of species. Once the breakage deflection has been reached, the tree is assumed to have failed. The height above ground at which a stem failure occurs is determined by sampling uniformly over the region where the stem bending stress exceeds 90% of the maximum calculated value.

Uprooting failures are treated similarly to stem breakage failures by replacing $\overline{R}_b$ and μ. with data derived from pull-down tests, where failure occurred by uprooting. Given tree size and the modulus of rupture, σ_r, the single most important (and uncertain) parameter describing the overall resistance of the tree to blowdown is $\overline{R}_b$. Table 12.1 summarizes the basic parameters (and relationships between parameters) necessary for modeling the response of a tree to wind (or blast) loads. Information on the parameters a_s, c_s, T, μ, $\overline{K}$, $\overline{R}_b$, C_p, W_{dc}, $W_{db/f}$, and k_2 are species-dependent and are derived from experimental studies. The values of these parameters are given in Vickery, Frank, and Twisdale (1993) for a number of tree species. The information given in Vickery, Frank, and Twisdale summarizes data from a wide range of sources. In addition to species-dependent parameters, data is given for generic conifers and broadleaf trees. Information on tree height, H_{bh}, diameter, d_{bh}, and % crown, f_c, varies with species and location; however, information on typical values of H_{bh}, d_{bh}, and f_c is readily available in the forestry literature. Values of σ_r and E are given in the USDA Wood Handbook (USDA, 1974).

12.3.2 Wind Modeling for Simple Terrains

In the case of relatively open terrain, similar to open country or suburban exposures in most building codes, where the variation in windspeed with height can be adequately modeled using logarithmic or power law models, simulating the incident windfield is relatively straightforward. In these basic cases, a windspeed time history is simulated using

$$U(t) = \overline{U} + \sum_{j=1}^{N} a_j \cos\left(2\pi \Delta f_j + \phi_j\right) t \tag{12.13}$$

where $U(t)$ *is* the instantaneous windspeed at time (at the height of the center of pressure) and $\overline{U}$ is the mean windspeed at the height of the estimated center of pressure within the crown of the tree, Δf is a frequency increment, ϕ_j *is* a random phase angle sampled uniformly over the interval $0 \le \phi \le 2\pi$, and a_j i*s* a frequency dependent amplitude. The amplitude term, a_j, is given as

$$a_j = \left[2 S_u\left(f_j\right) \chi^2\left(f_j\right)\right]^{\frac{1}{2}} \Delta f \tag{12.14}$$

Table 12.1. Input Parameters for Modeling of Trees

Number	Variable	Description	Functional Relationship	Distribution
1	d_{bh}	Diameter at breast height	User supplied	Uniform
2	H_{bh}	Height above breast	User supplied	Truncated Normal
3	f_c	% Crown	User supplied	Truncated Normal
4	a_s	Stem form parameter	User supplied	Lognormal
5	c_s	Stem form parameter	$c_s = \frac{a}{a_s} - 1$ (1)	Normal Error Term
6	T	Fundamental period	$T = a + bH_{bh}^2 / d_{bh}$ (1)	Normal Error Term
7	μ (2)	Ductility	User supplied(1)	Lognormal
8	$\overline{K}$ (2)	Stiffness parameter	User supplied(1)	Lognormal
9	$\overline{R}_b$ (2)	Strength parameter	$ln\,\overline{R}_b = a + b\,ln\,d_{bh}$ (1)	Normal Error Term
10	C_p	Center of pressure (tree in uniform flow)	User supplied(1)	Truncated Normal
11	W_{dc}	Weight of dry crown	$ln(w_{dc}\,H_c) = a + b\,ln\,d_{bh}$ (1)	Normal Error Term
12	$W_{db/f}$	Ratio of dry branches weight to dry foliage	$ln(w_{dc/f}) = a + b\,ln\,d_{bh}$ (1)	Normal Error Term
13	K_1, k_2	Drag function parameters	User supplied(1)	Normal Error Term
14	d_c	Diameter of base of crown	$d_c = \frac{d_{bh}\,f_c}{a_s\,(f_c + c_s)}$	NA
15	σ_r	Modulus of rupture for green wood	User supplied	NA(3)
16	E	Modulus of elasticity for green wood	User supplied	NA(4)

(1) Species- (site-) dependent data derived from tests. Data available in Vickery, Frank, and Twisdale (1992).
(2) Separate distributions are given for stem failure and uprooting.
(3) Natural variation in σ_r is accounted for with $\overline{R}_b$ distribution.
(4) Natural variation in E is accounted for with K distribution.

where $S_u(f_j)$ is the value of the spectrum of longitudinal turbulence at frequency f_j and $\chi^2(f_j)$ is the magnitude of the aerodynamic admittance function at frequency f_j.

The velocity spectrum, $S_u(f)$, used in this study is based on the ESDU (1975) formulation:

$$\frac{fS_u(f)}{\sigma_u^2} = \frac{4n}{\left(1 + 70.8n^2\right)^{\frac{5}{6}}} \tag{12.15}$$

where

$$n = {}^{x}L_u f / \overline{U} \tag{12.16}$$

and the integral length scale ${}^{x}L_u$ is given as

$${}^{x}L_u = \frac{25z^{0.35}}{z_0{}^{0.063}} \tag{12.17}$$

where the height above ground, z, is equal to the height to the center of pressure of the crown, and z_0 is the aerodynamic surface roughness.

The aerodynamic admittance function, $\chi^2(f)$, is determined using the coherence function for vertical separations given in Bowen, Flay, and Panofsky (1983), where the square of the coherence function is given as

$$R_{uu}^2(z_1, z_2, f) = exp\left[-\left(12 + \frac{11\Delta z}{z}\right)\frac{f\Delta z}{z}\right] \tag{12.18}$$

and

$$\chi^2(f) = \iint_{H_c} R_{uu}(z_1, z_2, f)\, dz_1, dz_2 \tag{12.19}$$

The integral in Equation 12.19 is solved numerically for various combinations of crown height, H_c, and H_b (height to base of the crown), with the solution approximated as

$$\chi^2(f) = \frac{1.0}{1 + a_1 n + a_x n^2} \tag{12.20}$$

where

$$n = \frac{fH_c}{\overline{U}} \tag{12.21}$$

The coefficients a_1 and a_2 vary with H_c/H_b. They are evaluated for H_c/H_b ranging between 0.1 and 10 and stored for later use. Ignoring the displacement height, d, the mean and turbulence profiles for these "open" cases are given as (ESDU 1982)

$$\frac{\overline{U}(z)}{U_{ref}} = \frac{ln\left(\frac{z}{z_0}\right)}{ln\left(\frac{z_{ref}}{z_0}\right)} \tag{12.22}$$

and

$$\frac{\sigma_u}{\overline{U}(z)} = \frac{7.5\eta\left[0.538 + 0.09\, ln\left(\frac{z}{z_0}\right)\right]^p}{1 + 0.156\, ln\left(\frac{u_*}{f_c\, z_0}\right)} \tag{12.23}$$

where z_{ref} is the reference height, $\overline{U}(z)$ is the windspeed at height z, $\sigma_u(z)$ is the RMS longitudinal windspeed at height z, $\overline{U}_{ref}$ is the mean windspeed at the reference height, u_*, is the friction velocity, f_c is the coriolus parameter, and

$$\eta = 1 - \frac{6 f_c z}{u_*} \text{ and } p = \eta^{16} \tag{12.24}$$

12.3.3 Example Tree Response – Ponderosa Pine

The wind-induced response of a Ponderosa Pine tree characterized in Table 12.2 was examined in some detail, as described here. Figure 12.3 shows the input velocity spectrum at the center of pressure in conjunction with the resulting base bending moment spectrum for mean windspeeds ranging between 10 m/s and 25 m/s. The intensity of turbulence at the center of pressure is about 25%. A resonant peak is seen clearly in Figure 12.3; however, the importance of the resonant response diminishes with increasing windspeed due to increases in the aerodynamic damping. Sensitivity studies performed where the weight of the dry crown *(W_{dc})* was both increased and decreased indicate that the resonant portion of the tree response decreases with increasing crown weight. For very large values of W_{dc} the tree response is nearly quasi-static.

Table 12.2. Characteristics of Key Parameters for Example Ponderosa Pine Tree Response Estimates

Parameter	Value
Height (m)	16.4
Diameter at Breast Height (cm)	18
% Crown	56
Dry Crown Weight (N)	90
Drag Parameter k_1	8,669
Drag Parameter k_2	399,528
Period (seconds)	3.28

Figure 12.4 shows the mean, RMS, and maximum base bending moments plotted versus the mean wind speed 10 m above ground, showing the effect of dry crown weight (W_{dc}) on tree response. The windspeed is increased to the point where the tree fails. The dry crown weight has little effect on the base bending moments at low windspeeds. In this example, for a mean windspeed of 10 m/s, the peak base bending moment is proportional to W_{dc} raised to the power of 0.14, whereas for a mean windspeed of 25 m/s, the peak base bending moment is proportional to W_{dc} raised to the power 0.4. In this example, the effect of crown weight is less important than the model of Mayhead, et al. (1975), where the mass of the crown is included in the drag force model raised to the power of 0.67. It is noteworthy that the drag model proposed by Mayhead, et al. for Sitka Spruce given in the form

$$F_D = A_1 U^2 m_c^{0.67} \exp\{-0.0009779 U_2\} \tag{12.25}$$

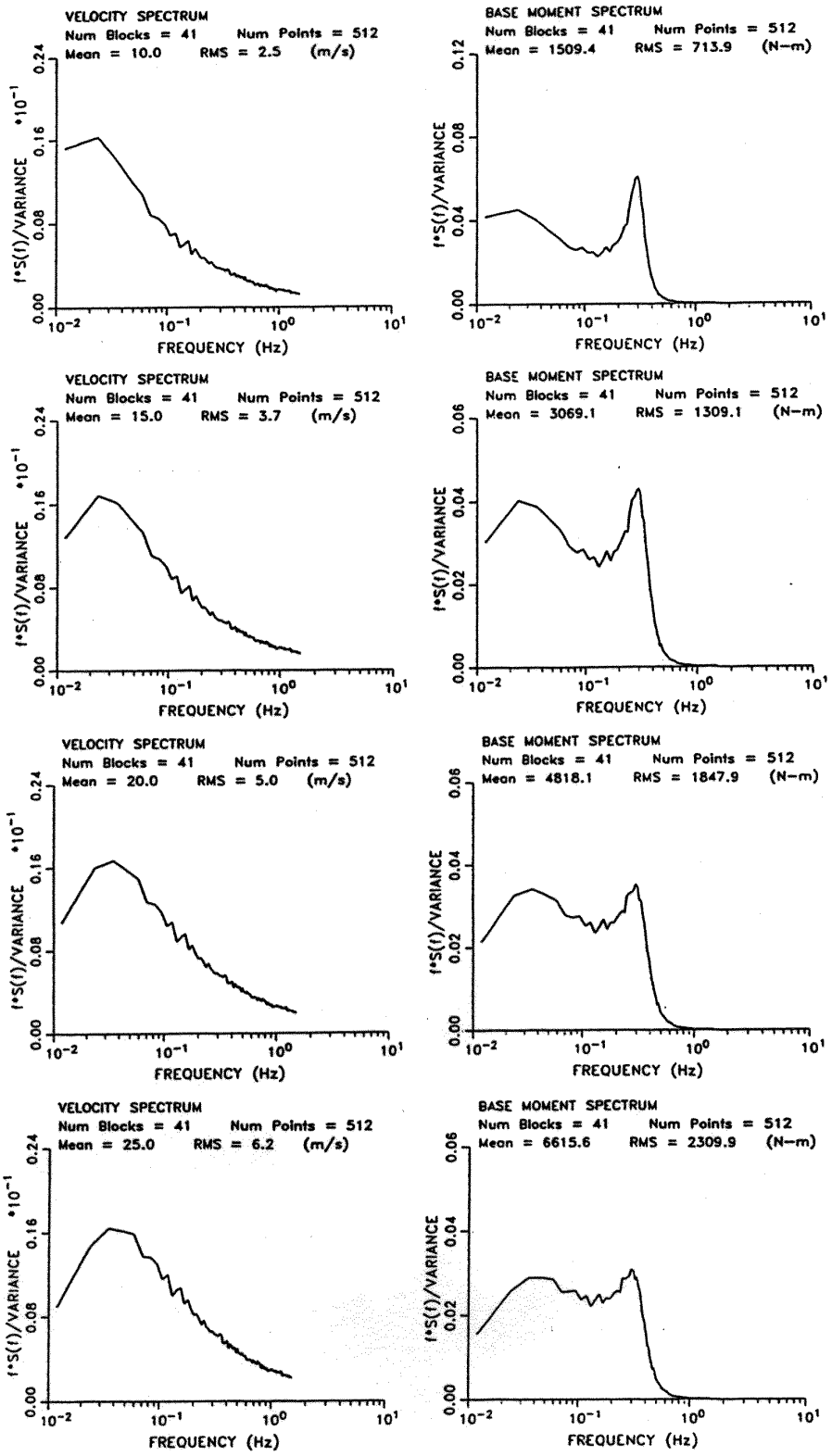

Figure 12.3. Velocity Spectra and Base Moment Spectra for Ponderosa Pine (Suburban Exposure).

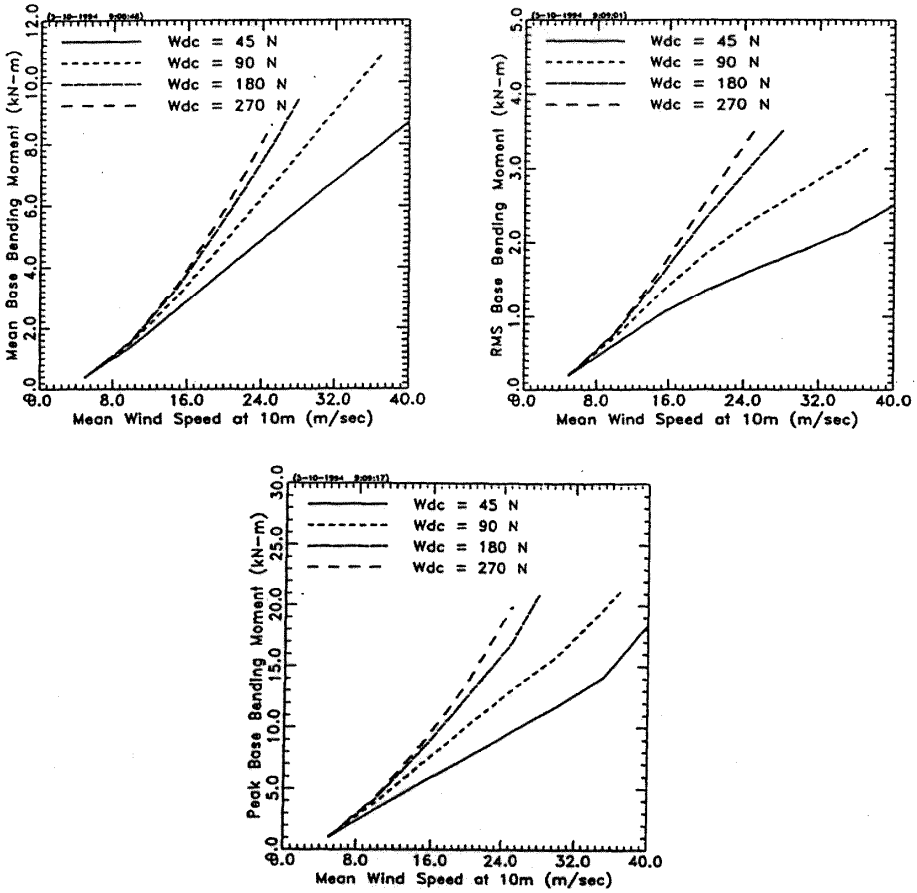

Figure 12.4. Mean, RMS, and Peak Base Bending Moment Versus Windspeed Showing Effect of Crown Weight on Tree Response.

(where m_c is the live branch weight and A_1 is a constant) yields a maximum drag force for a windspeed equal to 32 *m/s.* Higher windspeeds result in a drag force, F_D, which decreases.

Figure 12.5 shows the peak base bending moment for the Ponderosa Pine tree characterized in Table 12.2, plotted versus both the mean windspeed at 10 m and the peak windspeed at the center of the crown for typical open country (z_0 = 0.03 m) and suburban (z_0 = 0.3 m) windfields. The response of this example tree is clearly governed by the peak windspeed, and that the peak base bending moment increases approximately linearly with increases in the peak windspeed.

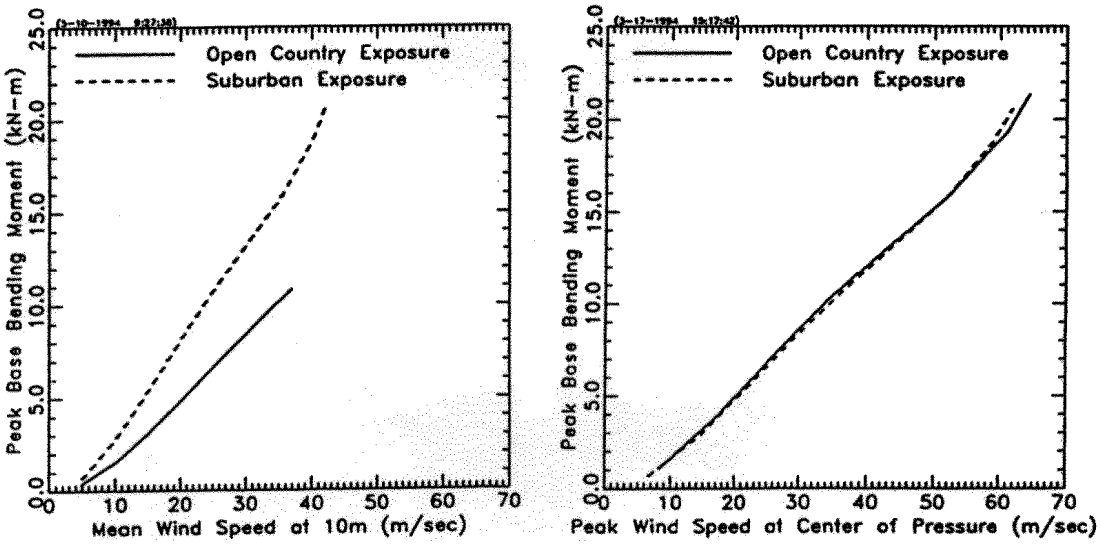

Figure 12.5. Mean and Peak Base Bending Moment Versus Peak Windspeed at Center of Pressure (Open and Suburban Terrains).

12.3.4 Wind Modeling in Forested Areas

Flow within and above plant canopies has been studied by numerous investigators over the past few decades. These studies include full-scale measurements, wind tunnel investigations, and mathematical modeling. In the case of forest flows, examples of full-scale measurements are given in Oliver and Mayhead (1974), Thompson (1979), and Bergstrom and Hogstrom (1989) for pine forests; Amiro and Davis (1988) for a Black Spruce forest; Amiro (1990a) for pine, spruce, and aspen forests; Baldocchi and Meyers (1988) for an Oak-Hickory forest; and Milne (1993) and Gardiner (1994) for a Sitka Spruce forest. Wind tunnel simulations range from very simplistic models using arrays of rigid rods to model the vegetation (Seginer, et al., 1976) to detailed aeroelastic modeling of forests (Stacey, et al., 1994). Mathematical models used to model flow within and above plant canopies include first-order closure models (e.g., Li, et al., 1985), second-order closure models (e.g., Meyers and Paw, 1986), and simplified empirical models (e.g., Cionco, 1972). A reviews of mathematical techniques used to model flow within canopies is given in Massman (1987). All of the full-scale studies noted above were carried out in relatively dense forests, so the results are not directly usable for estimating flow conditions in relatively lightly forested suburban areas, and no published measurements of wind flow conditions in lightly forested regions typical of suburban areas were found.

In the investigation described herein, the first-order closure model described in Li, et al. (1985), Li, et al. (1990), and Miller, et al. (1991) was used to describe the flow structure within and above the "forest" canopy. The computer code was provided by D. R. Miller of the University of Connecticut. The main inputs to the model include a description of the Leaf Area Index (LAI) profile of the plant canopy, defined as the leaf area per unit area of soil, an effective drag coefficient for the vegetation, and two windspeeds. Mean

windspeed and turbulence intensity profiles resulting from the model were compared to full-scale measurements in forests for cases where information on the LAI profile was also available.

Figure 12.6 shows profiles of LAI along with the measured and simulated mean, turbulence intensity, and peak windspeed profiles (peak windspeed is defined as the mean plus three standard deviations) for data given in Gardiner (1994), Stacey, et al. (1994), Baldocchi and Meyers (1988), and Amiro (1990). A drag coefficient of 0.16 (e.g., Meyers and Paw (1986) and Amiro (1990b)) was used in all cases. Figure 12.6 indicates that the first order closure model results reproduce the mean velocity profile reasonably well, through to the underside of the canopy where the secondary maxima produced by the model is greater than the maxima observed in the full-scale measurements. The RMS velocity, at height z, $\sigma_u(z)$, is estimated from

$$\sigma_u(z) = 2u_* = 2l(z)\frac{\partial u}{\partial z} \tag{12.26}$$

where $l(z)$ is the mixing length at height z above the ground surface. Details on the mixing length model are given in Miller, et al. (1991). Equation 12.26 is valid above the displacement height, d, but not beneath $z = d$. Below $z = d$ the turbulence intensity is set equal to the value computed at the lowest level in the grid. As indicated in Figure 12.6, there is no inclination for modeled local turbulence intensities to consistently overestimate or underestimate the measured intensities within the canopy; however, the modeled intensities consistently underestimate the observed intensities beneath the canopy. Within the canopy, the modeled turbulence intensities agree surprisingly well with the measured intensities. The agreement is better than the agreement between observed and modeled intensities in a Maize canopy given in Meyers and Paw (1986) using a second order closure model.

12.3.4.1 Canopy Modeling

The LAI distribution for a forested suburban region is modeled in the form

$$LAI(z) = \frac{B}{\sqrt{2\pi S}}\left[-\frac{1}{2}\left[\frac{\xi - \bar{\xi}_p}{S}\right]^2\right] \tag{12.27}$$

where S = 0.25, $\bar{\xi}_p$ is the nondimensional distance to the center of pressure measured from the base of the crown, and B is a scale factor which is a function of LAI and $\bar{\xi}_p$. A model similar to Equation 12.27 was used by Milne and Brown (1990) to describe the LAI profile in a Sitka Spruce forest. Mean and turbulence intensity profiles were developed for values of C_dLAI ranging from 0.01 and 0.3 for forests having average percentage crowns of 30%, 40%, 50%, and 60%. The mean value, $\bar{\xi}_p$, is taken as being equal to 0.5 (i.e., acting in the center of the crown).

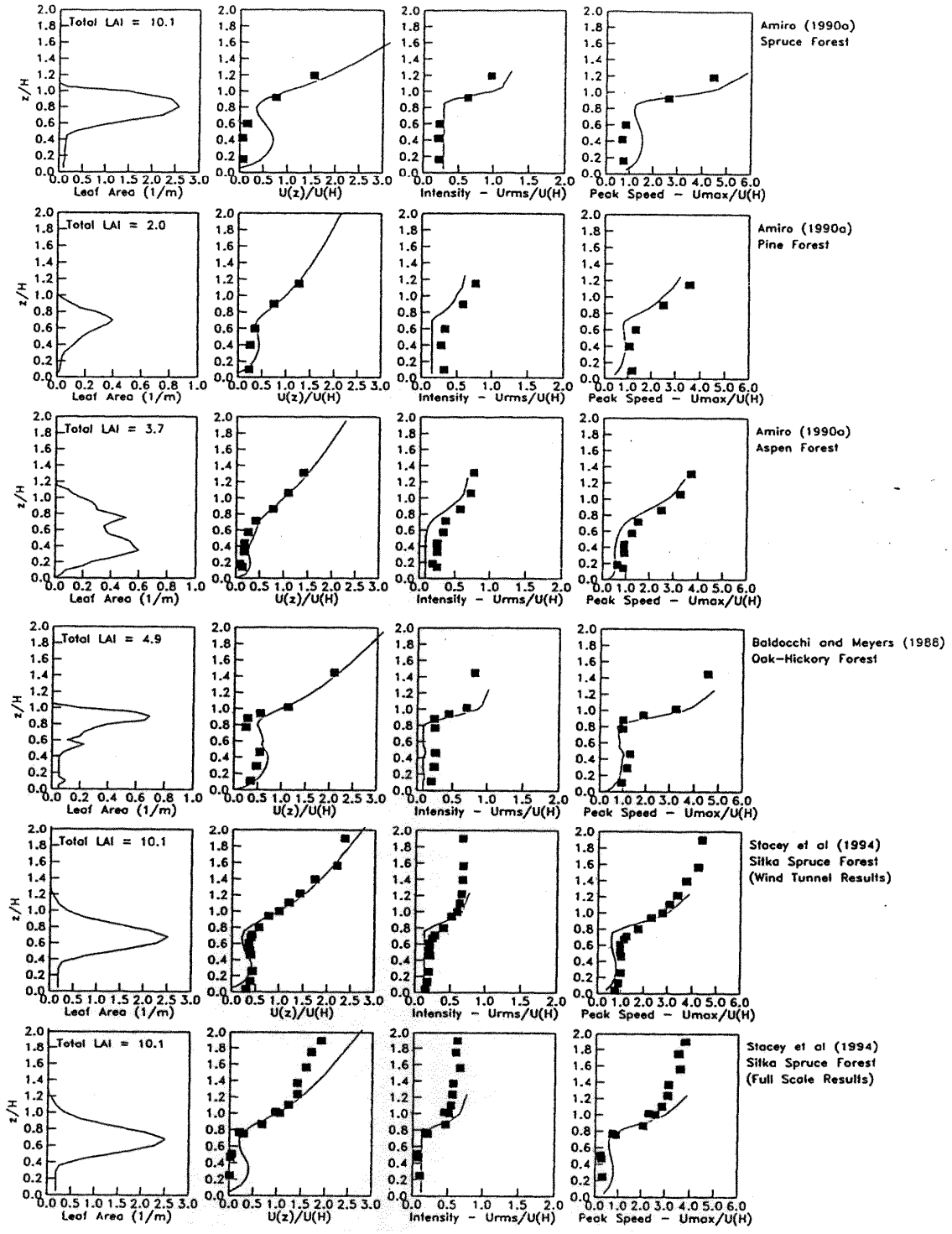

Figure 12.6. Measured Comparison of Modeled Mean and Turbulence Intensity Profiles in Forests.

Figure 12.7 shows the mean velocity and turbulence intensity profiles generated for some example C_dLAI profiles. Profiles are given for mean crown percentages within the forested area of 60%. Also shown in Figure 12.7 are the turbulence intensity and mean velocity profiles generated using the ESDU models for the atmospheric boundary layer. In developing the velocity profiles given in Figure 12.7, the displacement height, d and the surface roughness length, z_o were obtained by plotting the mean wind speed profile in semi-logarithmic space with various assumed values of d/H and selecting the combination of the two values that best fit the wind speed profile resulting from the simulation. The resulting the values of d/H and z_o/H are consistent with the information given in Shaw and Pereira (1982) and Massman (1987). The relationships between d/H and z_0/H are presented in Figure 12.8 as a function of C_dLAI. The comparison of the numerical model results with the ESDU model, show remarkable agreement above the height of the canopy for both the mean velocity and the turbulence intensity.

Given the mean velocity and turbulence intensity profiles generated for the range of C_dLAI described above, the mean wind speed at a height of (2H-d) coupled with the estimate of the local z_o is used to estimate the open terrain wind speed using the methodology given in ESDU (1982). The velocity spectrum at the center of pressure is determined using Equation 12.17, with the height replaced by $z - d$, and is combined with the admittance function defined in Equation 12.20 to develop the effective wind spectrum for use in the response estimates. In the development of the velocity profiles used herein, the influence of buildings and structures on the flow field is ignored.

12.3.4.2 Effective Windspeeds in Forested Areas

Since the tree blowdown model requires the windspeed acting at the effective center of pressure to determine the wind-induced response, effective values of $\overline{U}$ and σ_u acting at the center of pressure must be defined. These effective values are determined by integrating the product of the windspeed at height z and the frontal area at height z (assuming C_d is constant over the tree height) and equating this product with the product of an effective windspeed and the full frontal area of the tree. Effective values of the mean windspeed and turbulence intensity acting at the center of pressure were computing using two different approaches, the first of which assumes that the drag force is linearly proportional to velocity, and a second approach where the drag force is assumed to be related to the local velocity squared.

Drag Force Proportional to Velocity. Effective values of the mean velocities acting at the center of pressure of a tree in a forested area are computed as

$$\overline{U}_{eff} = U_H \frac{\int_0^H \xi(z) LAI(z) dz}{\int_0^H LAI(z) dz} \tag{12.28}$$

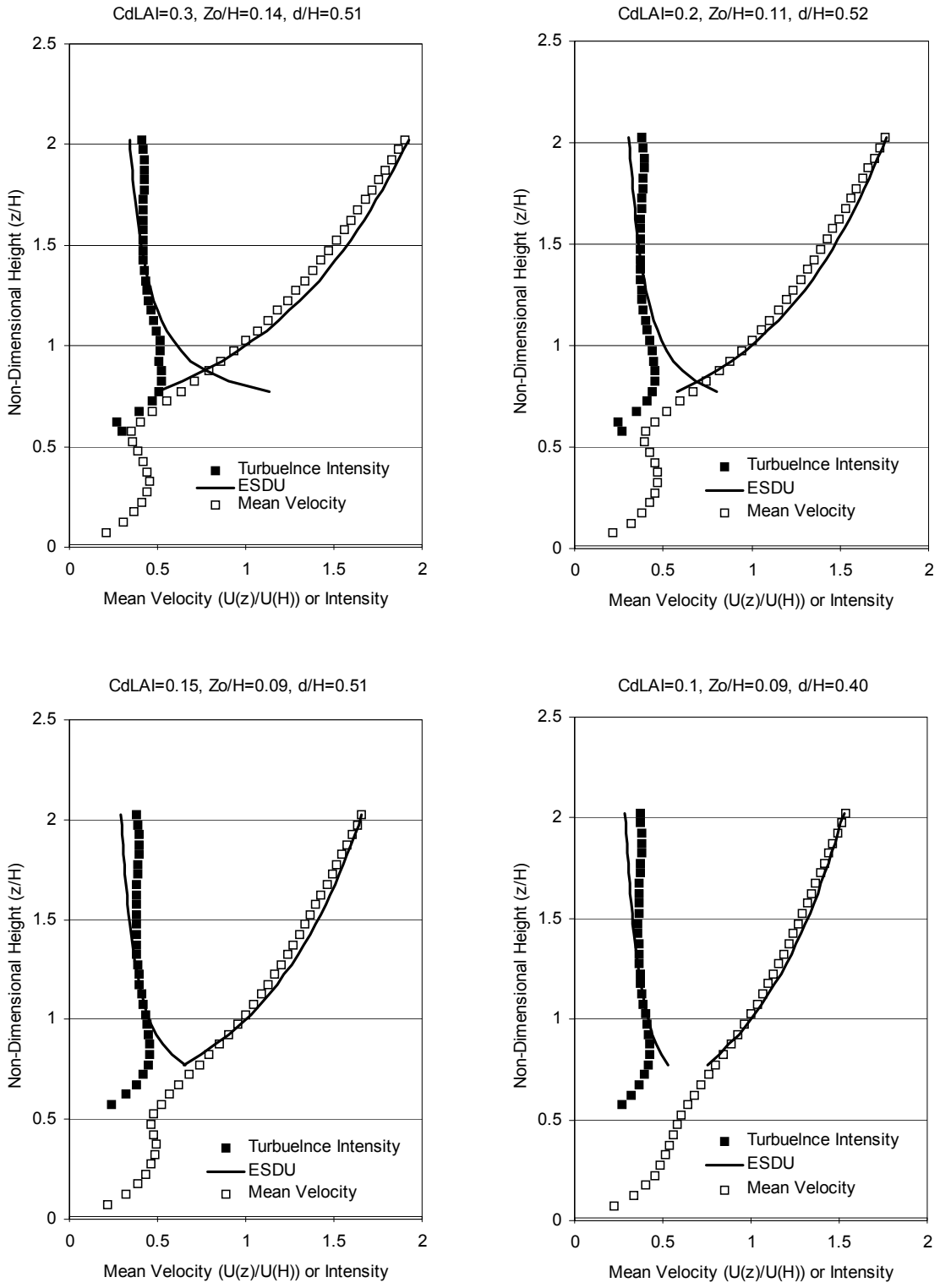

Figure 12.7. Mean and Turbulence Intensity Profiles for Various Values of C_dLAI.

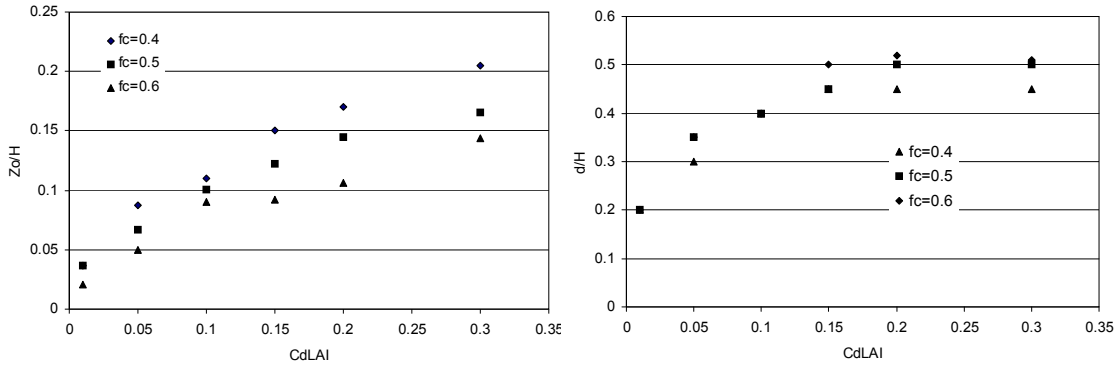

Figure 12.8. z_o/H and d/H Plotted vs. C_dLAI for Three Different Values of Crown Fraction.

where $\xi(z) = U(z)/U_H$ *is* obtained from the first order closure model and LAI(z) is the distribution of the leaf density over the height of the tree. The effective RMS velocity is computed from

$$\overline{U}_{eff}\left(1+g\frac{\sigma_{u_{eff}}}{\overline{U}_{eff}}\right)=U_H\int LAI(z)\xi(z)(1+gI_u(z))dz \tag{12.29}$$

where the peak factor, g, is taken as 3.0, and $I_u(z)$ is the turbulence intensity profile obtained from the first order closure model.

As noted earlier, the response of the tree is governed by the peak windspeed, not the mean windspeed, and as a result the effective location of the center of pressure is derived using the estimated peak wind profile.

The effective center of pressure is determined from

$$H_{cp_{eff}}=\frac{U_H\int_0^H \xi(z)(1+gI_u(z))LAI(z)zdz}{\hat{U}_{eff}\int_0^H LAI(z)dz} \tag{12.30}$$

where $\hat{U}_{eff}$ is the effective peak velocity given as

$$\hat{U}_{eff}=\overline{U}_{eff}\left(1+g\sigma_{u_{eff}}\right) \tag{12.31}$$

Drag Force Proportional to Velocity Squared. The effective value of the mean velocity, $\overline{U}_{eff}$, acting at the center of pressure is derived from

$$\overline{U}_{eff}^2 = U_H^2 \frac{\int_0^H \xi^2(z) LAI(z) dz}{\int_0^H LAI(z) dz} \tag{12.32}$$

The effective turbulence intensity, defined as

$$I_{u_{eff}} = \frac{\sigma_{u_{eff}}}{\overline{U}_{eff}} \tag{12.33}$$

is derived from

$$\overline{U}_{eff}^2 = \frac{U_H \int_0^H LAI(z) \xi^2(z) \left[1 + 2gI_u(z) + g^2 I_u^2(z)\right] dz}{\int_0^H LAI(z) dz} \tag{12.34}$$

the effective peak velocity $\overline{U}_{eff}^2$ is given as

$$\overline{U}_{eff}^2 = \overline{U}_{eff}^2 \left[1 + 2gI_{u_{eff}} + g^2 I_{u_{eff}}^2\right] \tag{12.35}$$

where again the peak factor, *g,* is set equal to 3. The effective height at the center of pressure is determined from

$$H_{cp_{eff}} = \frac{U_H^2 \int_0^H \xi^2(z)(1 + 2gi_u(z))^2}{\hat{U}_{eff}^2 \int_0^H LAI(z) dz} \tag{12.36}$$

The effective values, $\overline{U}_{eff}$, $\sigma_{u_{eff}}$, and $H_{cp_{eff}}$ determined using the linear and quadratic dependencies on windspeed typically vary by less than 10%, with the average of the two approaches being used to compute the tree response.

12.3.5 Simulation Methodology

In the simulation process, values of the key tree parameters given in Table 12.1 are obtained from sampling from the appropriate distributions. Using the sampled value of the center of pressure, the crown shape parameters *B* and $\overline{\xi}_p$ are determined, after which the values of U_{eff}/U_H and σ_u/U_H and effective value of center of pressure taking into account the velocity profile are calculated as described in Section 12.3.4.1. Given the new value of the center of pressure, combined with the sampled values of $\overline{R}_b$, for root and

stem failure, the failure mode (root failure or stem breakage) is determined. Given this information, time series of windspeeds (ten minutes in length) are generated, having a mean windspeed, U_H, and turbulence intensity, σ_r/U_H, and the response of the tree is calculated. Using an iterative interval halving technique, the minimum mean windspeed, U_H, required to fail the tree is determined, after which another tree is sampled and the process is repeated. The simulation process is repeated 100 times with the resulting failure windspeeds (converted to equivalent open country mean values) used to define the probability of failure distribution. Simulations for each tree examined are performed for a range of forest densities. Using the mean values of C_dA calculated for trees in a uniform wind, the average tree density, γ, *(stems/Ha)* necessary to provide the effective C_dLAI corresponding to the velocity and turbulence intensity profiles used can then be determined from

$$\gamma = \frac{10^4 C_d LAI}{C_d A} \text{ stems/}Ha \tag{12.37}$$

The information on failure windspeeds and tree density are used to determine the probabilities of trees failing and striking a typical residential structure as discussed in the following sections.

12.4 Blowdown Results

12.4.1 Tree Blowdown Curves

Simulations were performed for values of C_dLAI of 0.3, 0.2, 0.15, 0.10, 0.05 and 0.01. For each simulation, the forest canopy was approximately uniform in height (COV = 8%) and the tree diameters varied by ±1.25 cm about the mean value. Figure 12.9 shows example cumulative failure probability distribution for both homogenous deciduous and coniferous forests for three different mean values of height-diameter classes. Information on typical height and diameters and relationships between diameter and crown weight was taken from Storey and Pong (1957) for trees in a mixed hardwood forest in North Carolina. As noted in Figure 12.9, gust failure windspeed (in open country terrain) decreases with increasing forest density.

12.4.2 Tree Blowdown Validation

A validation study of the tree blowdown curves presented in Section 12.4.1 was undertaken in eight randomly selected subdivisions in eastern North Carolina immediately following Hurricane Isabel in 2003. In each of the selected residential subdivisions the survey teams counted the number of trees on each lot, counting the number of trees in each of 3 previously defined height ranges (consistent with the height ranges used in Hazus), the tree type (evergreen or deciduous) and the performance of the tree (uproot failure, stem failure or no failure). In one of the surveyed subdivisions (South Mills, NC) each tree height was estimated and the diameter at breast height was measured, and the dimensions of each lot was obtained. In all cases the address of the lot was recorded.

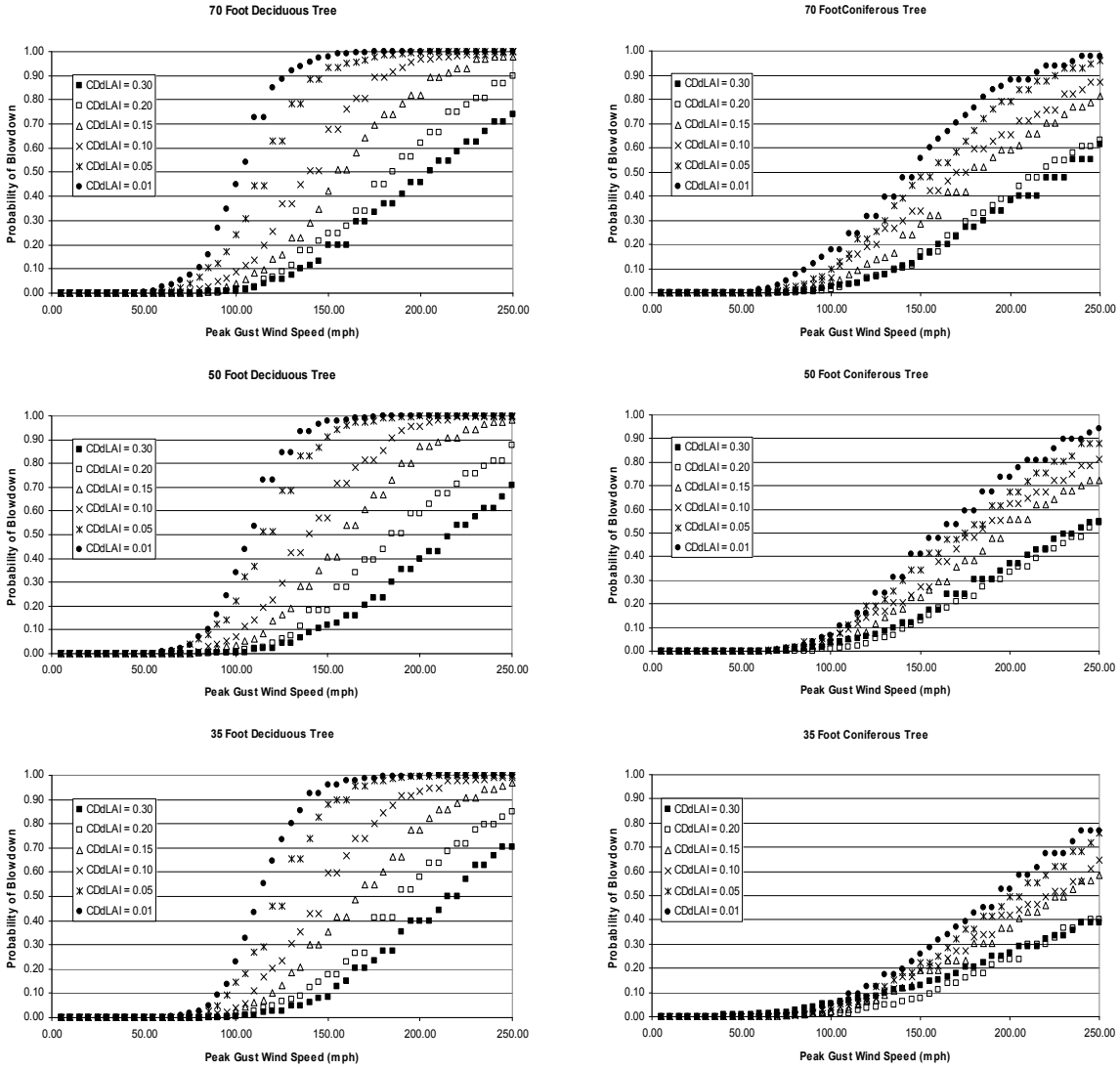

Figure 12.9. Tree Blowdown Curves.

Table 12.3 presents a summary of the data collected at the eight sites, including the estimated peak gust wind speed, the number of lots surveyed, the total number of trees surveyed, the percent of trees blown down, and the total area surveyed. A total of 1158 trees were surveyed, with the sample comprising 628 conifers and 530 deciduous trees.

Table 12.4 presents a more detailed summary presenting the number of trees in each height class as well as indicating the number of trees in each height class that fail by uprooting or through stem failure. Approximately 12% of the conifers were blown down and about 10% of the deciduous trees were blown down. The deciduous trees were more likely to fail from uprooting, whereas in the case of the conifers, stem and uprooting failures were approximately equally likely.

Table 12.3. Summary of Tree Blowdown Data

Location	Peak Gust Wind Speed (mph)	Number of Lots Surveyed	Total Number of Trees	% of Trees Blown Down
Ahoski 1	86	20	54	3.7%
Ahoski 2	86	28	113	5.3%
Elizabeth City 1	95	34	171	5.8%
Elizabeth City 2	95	45	217	8.8%
Manteo 1	92	9	178	18%
Manteo 2	92	32	150	11%
South Mills	92	27	150	19.3%
Windsor	84	28	125	8.8%
Total		223	1158	10.8%

Table 12.4. Summary of Number of Failed Trees by Height Class

		Conifers					Deciduous				
		Height Range (feet)					Height Range (feet)				
Location		<30	30-40	40-60	> 60	All	<30	30-40	40-60	> 60	All
Ahoski 1	# Trees	1	4	11	4	20	9	8	17	0	34
	# Uproot Failures	0	0	0	0	0	1	0	0	0	1
	# Stem Failures	0	1	0	0	1	0	0	0	0	0
	Total # Failures	0	1	0	0	1	1	0	0	0	1
Ahoski 2	# Trees	5	9	9	15	38	23	14	19	19	75
	# Uproot Failures	1	1	0	0	2	1	0	2	0	3
	# Stem Failures	0	0	0	1	1	0	0	0	0	0
	Total # Failures	1	1	0	1	3	1	0	2	0	3
Elizabeth City 1	# Trees	0	10	41	39	90	17	22	38	4	81
	# Uproot Failures	0	0	0	2	2	1	1	4	0	6
	# Stem Failures	0	1	0	0	1	0	0	1	0	1
	Total # Failures	0	1	0	2	3	1	1	5	0	7
Elizabeth City 2	# Trees	3	11	73	61	148	26	23	11	9	69
	# Uproot Failures	1	0	2	0	3	2	2	1	3	8
	# Stem Failures	0	0	2	3	5	2	0	1	0	3
	Total # Failures	1	0	4	3	8	4	2	2	3	11
Manteo 1	# Trees	2	4	91	0	97	26	45	10	0	81
	# Uproot Failures	0	1	6	0	7	4	3	0	0	7
	# Stem Failures	0	2	13	0	15	0	3	0	0	3
	Total # Failures	0	3	19	0	22	4	6	0	0	10
Manteo 2	# Trees	14	24	21	23	82	6	48	14	0	68
	# Uproot Failures	0	0	5	1	6	0	3	0	0	3
	# Stem Failures	0	1	3	2	6	0	1	0	0	1
	Total # Failures	0	1	8	3	12	0	4	0	0	4
Windsor	# Trees	3	6	23	23	55	25	23	12	10	70
	# Uproot Failures	0	0	1	1	2	1	1	0	0	2
	# Stem Failures	0	0	1	1	2	1	1	1	2	5
	Total # Failures	0	0	2	2	4	2	2	1	2	7
South Mills	# Trees	2	47	21	28	98	5	19	17	11	52
	# Uproot Failures	0	7	2	8	17	0	2	1	0	3
	# Stem Failures	0	1	1	1	3	0	2	2	2	6
	Total # Failures	0	8	3	9	20	0	4	3	2	9
Total	# Trees	30	115	290	193	628	137	202	138	53	530
	# Uproot Failures	2	9	16	12	39	10	12	8	3	33
	# Stem Failures	0	6	20	8	34	3	7	5	4	19
	Total # Failures	2	15	36	20	73	13	19	13	7	52

Within the Hazus tree blowdown model, each family of tree blowdown curves (probability of blowdown vs. wind speed) is stored as a function for a range of tree densities (trees/acre) for 3 pre-defined height classes for the coniferous and deciduous tree types. The original tree blowdown curves were developed by computing the probability of blowdown as a function of the effective drag per unit land are within the modeled "forest" canopy, rather than the number of trees per acre. The effective drag per unit land area is defined using a parameter referred to as C_dLAI, where C_d is a drag coefficient and LAI is the Leaf Area Index. The value of C_dLAI for an area is often obtained using satellite imagery to estimate the LAI and multiplying by a typical drag coefficient, but can also be estimated by dividing the effective total drag area in the forested region, C_dA, by the total land area covered by the trees.

The estimated values of C_dLAI at the eight sites range between 0.01 and 0.02. The lowest two values of C_dLAI used in the development of the tree blowdown curves used in Hazus are 0.01 and 0.05, and these curves are given in Figure 12.10 along with the observed blowdown data for each study region. Separate plots are given for each height class and tree type (deciduous or coniferous). The large diamond shaped point on each plot represents the weighted average probability of blowdown for all trees of the class at all sites surveyed.

From the plots, it is seen that the collected data from Hurricane Isabel agree well with the probability of blowdown curves for deciduous trees. However, less agreement is seen when coniferous trees are considered. It appears that for this case, the curves underestimate the actual probability of blowdown. In light of this comparison, the tree blowdown probabilities for coniferous trees were shifted to better agree with the available validation data.

The blowdown functions have been shifted as follows:

- All functions for short (< 40') conifers were shifted by 30 mph
- All functions for medium (40' to 60') conifers were shifted by 15 mph
- All functions for tall (> 60') conifers were shifted by 10 mph.

Figure 12.11 shows the resulting shifted functions for coniferous trees along with the validation data.

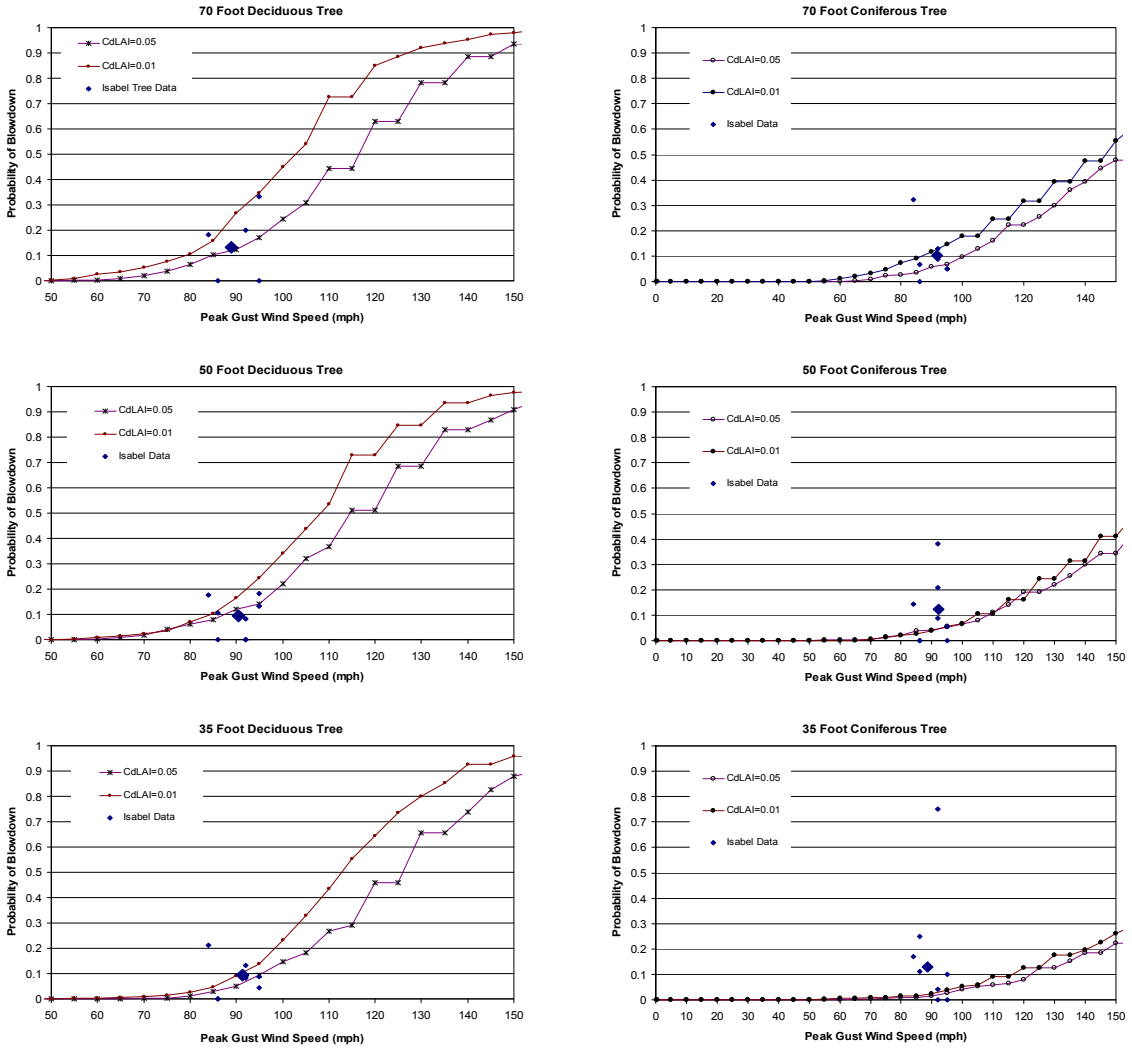

Figure 12.10. Probability of Blowdown Curves with Treefall Data Collected Following Hurricane Isabel.

12.5 Tree Inventory Data by County

12.5.1 Forest Inventory Analysis (FIA) Program and Database

The Forest Inventory Analysis (FIA) Program and Database of US Forest Service (USFS) is a nationwide tree inventory database updated on a 5-year cycle by states/regions. It is derived through a field survey and statistical analysis procedure. The database provides a spatial resolution down to the county level for the final product that is accessible in the public domain. It was initially designed for the use primarily by the lumber industry; however, it contains data such as tree count and tree diameter distribution per species in every county that are useful for the analysis described in this section. It is recognized as an authoritative source of forest/tree data on a nationwide scale. The MRLC uses FIA data to verify the accuracy of satellite imagery analysis on forest cover.

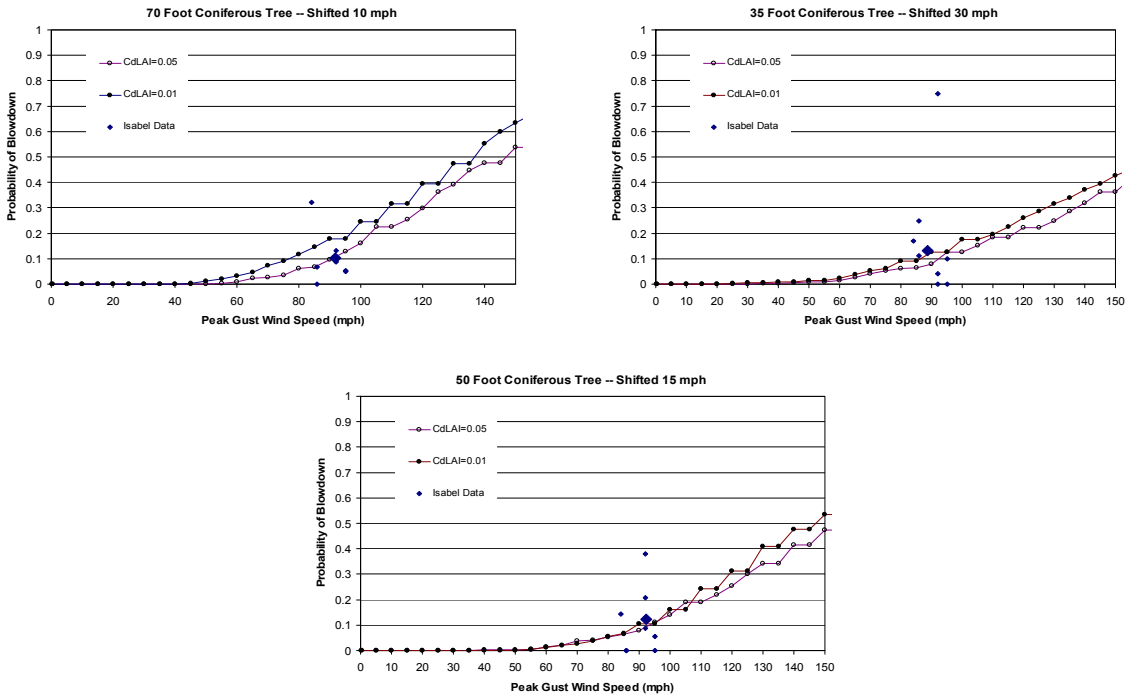

Figure 12.11. Shifted Probability of Blowdown Curves for Coniferous Trees with Treefall Data Collected Following Hurricane Isabel.

12.5.2 Average Tree Density and Tree Height Distribution at County Level

The tree blowdown methodology utilizes FIA's tree count on forest land and tree height per species per county, downloaded from the USFS website. The data incorporated into Hazus 2.0 dates between 2006 and 2010 for all states (except Hawaii which was not available at the time of this writing), with the vast majority being from 2008-2009. Prior versions of Hazus relied upon diameter distributions to determine tree height, but tree height is now readily available for most of the 1279 counties in the 22 hurricane states and the District of Columbia via download from the FIA. For those counties that did not have tree height or tree density distribution information, data from neighboring counties were used. In the case of Hawaii, data from American Samoa were used.

Using tree height information, Tree height distributions were simplified into three groups (30-40 ft, 40-60 ft, and over 60 ft tall) and summarized over all species for each county.

For each county, the average tree density is derived by dividing the tree count on forest land by the total area of forest land of the county. The forest land area used was also downloaded from the FIA database.

It should be noted that the FIA field survey and resulting database includes only contiguous tree covered areas not less than 12 acres in area. For the purpose of the Hazus model, the average tree density and tree height distribution obtained as described above are applied to all tree covered areas in a county, including smaller patches and strips of

tree covered areas embedded in residential subdivisions as identified by the MRLC land cover database.

12.6 Hazus Tree Coverage Database

The procedures carried out to derive a default tree database for Hazus from the MRLC land use database and the FIA tree database are described in this section.

12.6.1 MRLC National Land Cover Data

As described in detail in Chapter 3, the MRLC (Multi-Resolution Land Characteristics consortium) land cover database, presented in 30m resolution grids, provides relatively high spatial resolution of defined land cover types and percent tree canopy. Using the MRLC land cover database, combined with data derived from the FIA database, makes it possible to estimate the number of trees and predominant tree type at higher geographical resolutions than counties, including resolution at the census block level as required for Hazus.

12.6.2 Tree Density, Tree Height, and Predominant Tree Type by Census Tract and Census Block

For the Hazus wind risk software product, a default tree database is developed that contains variables as outlined below for each census tract.

The predominant tree type is defined in the MRLC land cover database as:

- "Coniferous" if 75% or more of the tree covered area is identified as "Evergreen" type in the MRLC land cover database;
- "Deciduous" if 75% or more of the tree covered area is identified as "Deciduous" type in the MRLC land cover database;
- "Mixed" if neither of the above two criteria holds.

Census blocks also hold to the same set of rules, however, if a census block had no forested land according the MRLC, then its predominate type defaults to the tracts predominate type.

To determine tree density at the census block level, the average tree density at the county level is first determined by dividing the tree count on forest land by the total area of forest land of the county. Second, the average canopy percentage in each county over areas determined to be evergreen forest, deciduous forest, mixed forest and woody wetlands was computed. Third, the stems per acre for 100 percent tree canopy for each county was computed assuming tree density and average canopy computed over forested areas are proportional. For example, if a county had 75 stems per acre with an average tree canopy of 50 percent, the stems per acre at 100 percent canopy was assumed to be 150 stems per acre. The maximum stems per acre was capped at 400. Finally, the average tree canopy over forested land of each census block was multiplied by its county's corresponding stems per acre for 100 percent tree canopy.

Stems per acre at the tract level is calculated by weighting the stems per acre at the census block level by area of the census block, and aggregating up to the census tract level as per Equation 12.39

$$S_t = \sum_{i=1}^{n} S_i * \frac{A_{Ci}}{A_T} \quad (12.39)$$

where:

S_t = Stems per acre at the tract level

S_i = Stems per acre at Census block *i*

A_{Ci} = Area of Census block *i*

A_T = Total area of Census tract

n = Number of Census blocks in the tract

Trees less than 30 ft tall and less than 5 inches in diameter are not included in the variable of "Forest Land Tree Density of County" or in the subsequent analysis. Trees less than 30 ft tall normally have trunk diameters less than 5 in and small crown weights. These trees are neglected in the debris volume and building damage models.

The tree height distribution represents the proportions of short (30-40 ft), medium (40-60 ft) and tall (>60 ft) trees. They sum-up to 100%. In general, tree heights rarely exceed 100 ft. which represents the 99.9th percentile height for trees over 30 ft tall in the 22 states covered by the hurricane model. On a nationwide base, the average tree heights within the three bins are 35.0, 49.7 and 74.9 ft, respectively.

The format of the Hazus tree coverage database is summarized in Table 12.5. An example of the Hazus tree data is shown in Figure 12.12 for Wake County, NC at the census tract level. A map of tree density is shown in Figure 12.13. The city of Raleigh, NC is in the lower density area in the center of the county.

Table 12.5. Hazus Tree Data Format

Census Tract	Predominant Tree Type	Stems per Acre of Land	Tree Height Distribution, %		
			30-40 ft	40-60 ft	>60 ft
xxxxxxxxxxx	Coniferous, Deciduous, or Mixed	0-400	0-100	0-100	0-100

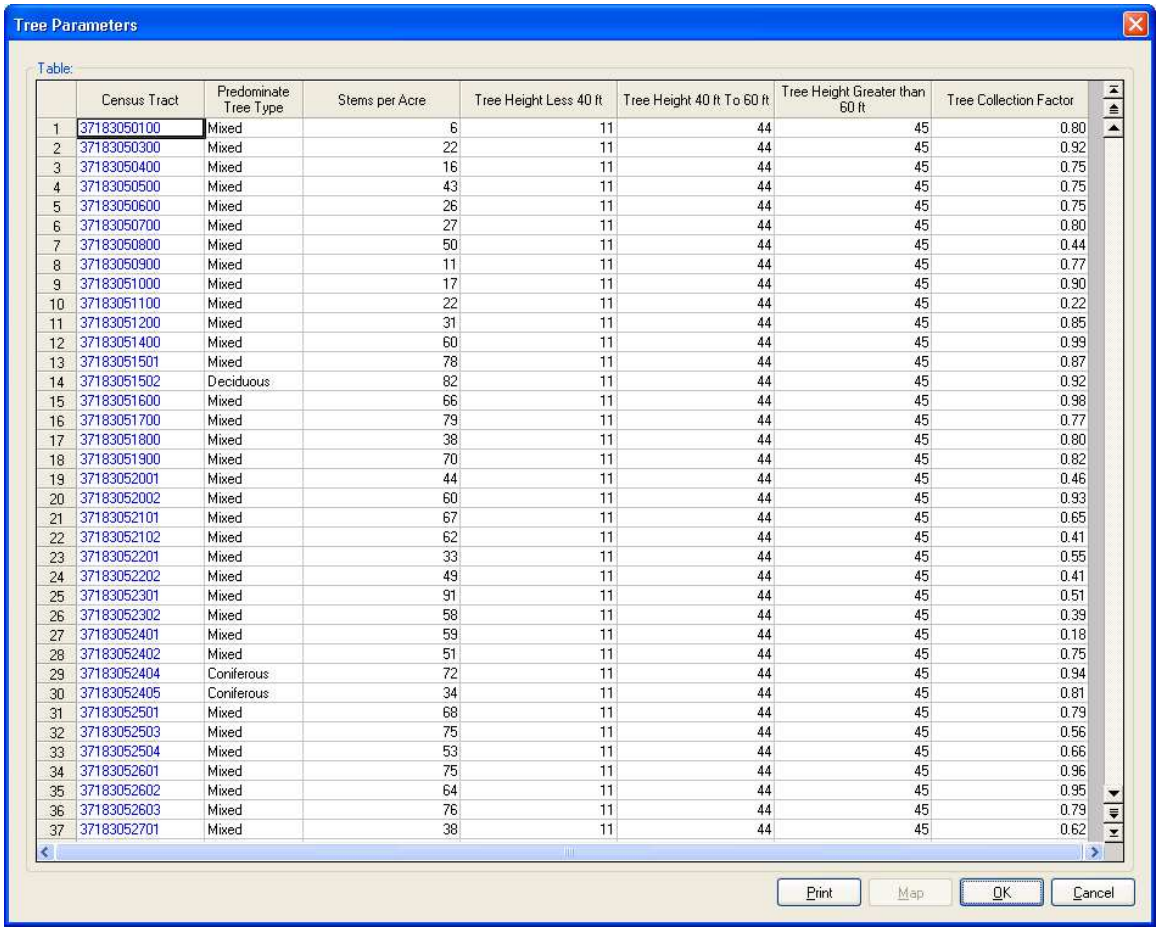

	Census Tract	Predominate Tree Type	Stems per Acre	Tree Height Less 40 ft	Tree Height 40 ft To 60 ft	Tree Height Greater than 60 ft	Tree Collection Factor
1	37183050100	Mixed	6	11	44	45	0.80
2	37183050300	Mixed	22	11	44	45	0.92
3	37183050400	Mixed	16	11	44	45	0.75
4	37183050500	Mixed	43	11	44	45	0.75
5	37183050600	Mixed	26	11	44	45	0.75
6	37183050700	Mixed	27	11	44	45	0.80
7	37183050800	Mixed	50	11	44	45	0.44
8	37183050900	Mixed	11	11	44	45	0.77
9	37183051000	Mixed	17	11	44	45	0.90
10	37183051100	Mixed	22	11	44	45	0.22
11	37183051200	Mixed	31	11	44	45	0.85
12	37183051400	Mixed	60	11	44	45	0.99
13	37183051501	Mixed	78	11	44	45	0.87
14	37183051502	Deciduous	82	11	44	45	0.92
15	37183051600	Mixed	66	11	44	45	0.98
16	37183051700	Mixed	79	11	44	45	0.77
17	37183051800	Mixed	38	11	44	45	0.80
18	37183051900	Mixed	70	11	44	45	0.82
19	37183052001	Mixed	44	11	44	45	0.46
20	37183052002	Mixed	60	11	44	45	0.93
21	37183052101	Mixed	67	11	44	45	0.65
22	37183052102	Mixed	62	11	44	45	0.41
23	37183052201	Mixed	33	11	44	45	0.55
24	37183052202	Mixed	49	11	44	45	0.41
25	37183052301	Mixed	91	11	44	45	0.51
26	37183052302	Mixed	58	11	44	45	0.39
27	37183052401	Mixed	59	11	44	45	0.18
28	37183052402	Mixed	51	11	44	45	0.75
29	37183052404	Coniferous	72	11	44	45	0.94
30	37183052405	Coniferous	34	11	44	45	0.81
31	37183052501	Mixed	68	11	44	45	0.79
32	37183052503	Mixed	75	11	44	45	0.56
33	37183052504	Mixed	53	11	44	45	0.66
34	37183052601	Mixed	75	11	44	45	0.96
35	37183052602	Mixed	64	11	44	45	0.95
36	37183052603	Mixed	76	11	44	45	0.79
37	37183052701	Mixed	38	11	44	45	0.62

Figure 12.12. Hazus Tree Coverage Data for Wake County, NC.

12.7 Debris Generated from Tree Blowdown

Hurricanes generate considerable amounts of debris from tree blowdown. In most cases, local and state governments, with federal assistance, are responsible for collecting and disposing of this debris. Tree debris disposal totals from Hurricane Isabel in North Carolina totaled over 3.2 million cubic yards and cost communities in the state over $31 million to collect and dispose of this debris. Section 12.7.1 discusses how Hazus-MH estimates the total overall tree debris generated by hurricanes. Section 12.7.2 presents the methodology for estimating the amount of tree debris to be collected as the result of hurricanes. Section 12.7.3 presents comparisons of modeled versus actual collected tree debris from several recent hurricanes including Isabel (2003), the four hurricanes that struck Florida in 2004, Wilma (2005), and Rita (2005).

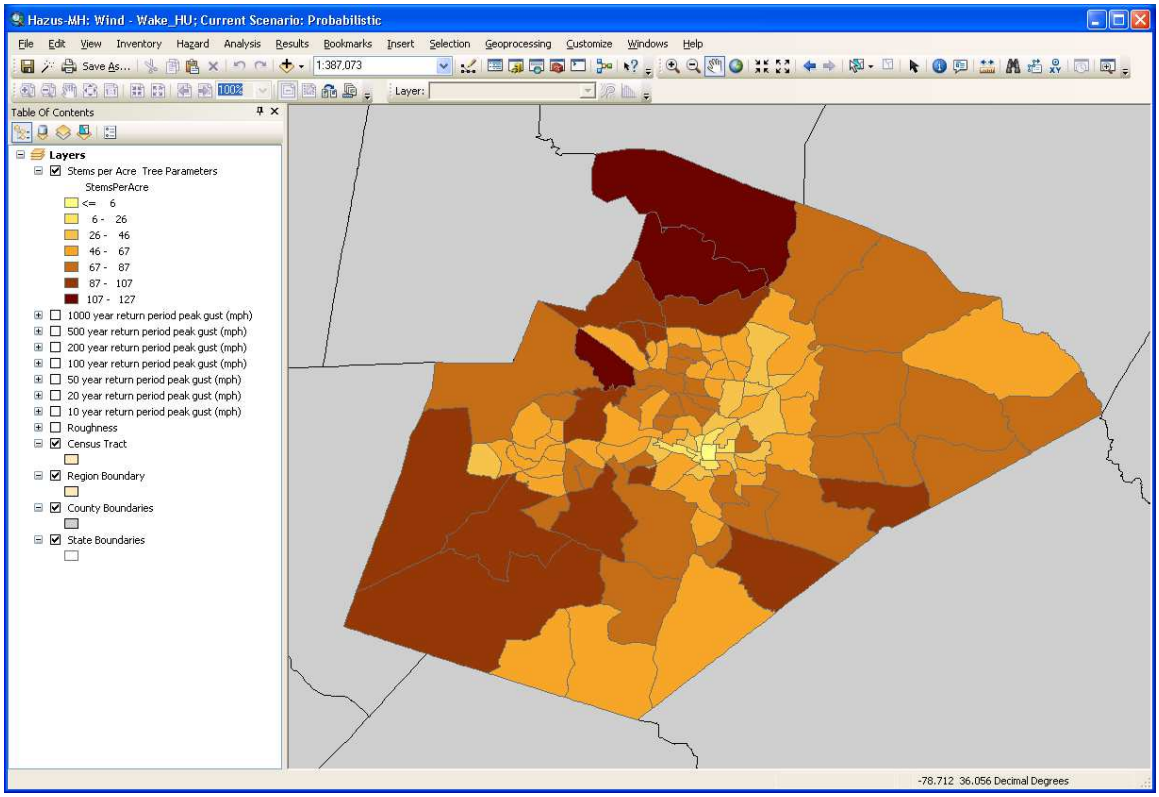

Figure 12.13. Map of Tree Density for Wake County, NC.

12.7.1 Total Weight and Volume of Downed Trees

The tree debris model combines the tree coverage database and the tree blowdown model to produce estimates of tree debris weight by census tract. The tree debris weight reported by Hazus is the expected green weight of trees greater than 30 ft tall that are expected to fail at a given windspeed for a given density of trees. The entire weight is reported as debris, even though tree debris in unpopulated areas may not be collected.

Hazus-MH computes the total weight of tree debris based on the modeled windspeed and the density of trees for the census tract (or block). The tree blowdown functions presented in Section 12.4.1 are converted to debris functions by relating the $C_D LAI$ values to number of trees per acre and multiplying the probability of blowdown values by the total expected weight of trees per acre, for the given type, height, and density of trees. Figure 12.14 shows the tree debris functions implemented in Hazus-MH.

Hazus-MH MR1 estimated the cubic yardage of tree debris using a multiplier of 3.6 cubic yards per ton based on figures reported by Escambia County, Florida after Hurricane Opal (Escambia County, 1996). Further research into appropriate bulking factors to be used to convert weight of tree debris to volume has revealed a wide range of factors used by various sources. Table 12.6 shows bulking factors developed from several different sources as a part of the development of the tree debris model for MR2.

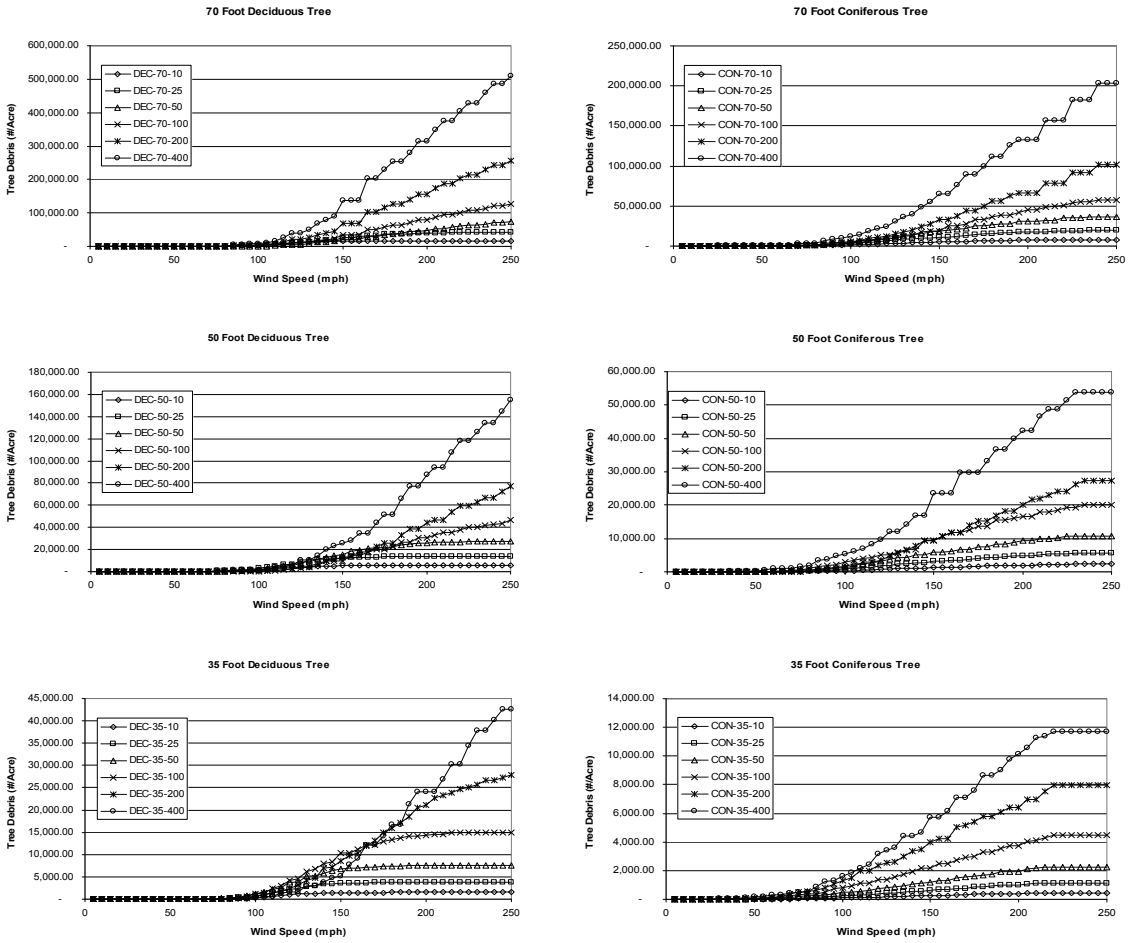

Figure 12.14. Tree Debris Functions in Pounds per Acre.

Based on the data presented in Table 12.6, it appears that the actual bulking factor should be based on a number of different types of debris – from leaves and loose brush to large limbs and stumps. It is also likely that the appropriate bulking factor will be a function of the strength of the hurricane. The majority of tree debris from weaker storms will be the result of failed limbs within the crown and will not include very many entire trees or stumps. On the other hand, stronger storms will cause more complete tree uprooting and devastating crown damage and result in denser tree debris.

A bulking factor of 4 is more appropriate for chipped or compacted tree debris, while a factor of 10 represents bulkier, uncompacted unclipped debris. For the base estimation of tree debris volume, the bulking factor in Hazus-MH is now taken as 10 CY/ton to represent uncompacted and unchipped debris. Users performing level 2 and 3 analyses are encouraged to develop their own local bulking factors based on the relationship between tree debris volume and weight from earlier or current hurricanes affecting their areas, and/or modifying the bulking factor to reflect their local debris chipping/compacting procedures.

Table 12.6. Tree Debris Related Bulking Factors from Various Sources

Source	Description	Bulking Factor (CY/ton)
FEMA 9580.1	Woody Debris	4
SC Dept of Health and Environmental Control	Wood Chips	4
MS Dept of Environmental Quality	Uncompacted Limbs and Leaves	12
CA Integrated Waste Management Board	Large Limbs and Stumps	1.85
	Mixed Yard Trimmings	18.5
	Wood Chips	4
	Prunings, Dry	54
	Prunings, Wet	43
	Prunings, Shredded	3.8
	Leaves, Dry	5.8
	Leaves	24
Solid Waste Authority of Palm Beach County, FL	Vegetative Debris	5.5
Alachua County, FL Public Works Department	Hurricane Debris from Frances and Jeanne	10.5
City of Honolulu, HI Refuse Department	Uncompacted Yard Waste	8
	Compacted Yard Waste	4.6
	Wood Chips	4
	Loose Brush	10

12.7.2 Tree Debris Collection Model

The methodology for estimating tree debris collection quantities is based on building density, length of roads, and census block shapes. This empirical method is based on the concept that trees downed in close proximity to streets, highways, or buildings make up the great majority of trees brought to the curb for collection and disposal.

12.7.2.1 Tree Debris Collection Model Description

The underlying premise of the tree debris collection model is that trees that fall in close proximity to highways, streets, and buildings are going to be collected and brought to the curb for collection. As such, an area reduction factor was developed based on a predetermined collection area around each of the streets and buildings within a study region.

The model applies a reduction factor to the overall estimate of downed trees currently produced as described in Section 12.7.1. The tree debris collection model is expressed in Equation 12.40.

$$D_c = \sum_{i=1}^{n} D_i * \frac{A_{Ci}}{A_{Ti}} \qquad (12.40)$$

where:

D_c = Tree debris collected

D_i = Total tree debris predicted by Hazus for census block i

A_{Ci} = Collection area calculated for census block i

A_{Ti} = Total area of census block i

n = Number of census blocks in the study region

The model was developed by running Hazus-MH at the census block level. The census block level was chosen because the boundaries of census blocks are most often represented by highways, streets, and roads with relatively few streets contained inside. A method for aggregating census block factors to the census tract level for study regions defined at the census tract level is discussed in Section 12.7.2.2.

The collection area (A_{Ci}) for each census block is first calculated based on the density of buildings within the census block (buildings per acre). As a baseline, it is assumed that downed trees will be picked up for an area of a one acre per building in the census block, with a maximum collection area set at the area of the census block. The result is that all tree debris is assumed to be collected in census blocks when the building density is equal to or greater than one building per acre.

For census blocks with building densities lower than one building per acre, the model also determines an alternative collection area along the census block perimeter and any roads within the census block. The depth of this perimeter collection area varies based on the building density of the census block because areas with little or no development will only have enough trees cleared to keep the roads safe for travel. The depth of the perimeter collection area varies from 25 to 200 feet linearly as building density varies from 0 to 1 building per acre.

25 feet was chosen as the minimum depth for the perimeter collection area to account for trees that fall into roadways and rights of way in undeveloped areas. 200 feet was chosen as the upper bound to be consistent with building-based collection area described above because a 200 foot by 200 foot square is approximately one acre in area.

The perimeter collection area is calculated in the following manner:

- The perimeter and area of each census block are calculated.
- The ratio of the square root of the area to the perimeter is then used to approximate the aspect ratio of each census block. This ratio is 0.25 for square blocks and approaches 0.0 for long slender blocks.
- From the aspect ratio and total area of each block, the width and length of an equivalent rectangle are determined.
- Perimeter collection areas are calculated for each block using the approximate length and width with the perimeter collection area depth, as shown in Figure 12.15.
- For census blocks that contain roads within their boundaries, an interior road collection area is calculated using the length of the interior roads and the depth of the perimeter collection area determined above. This area is added to the perimeter collection area.

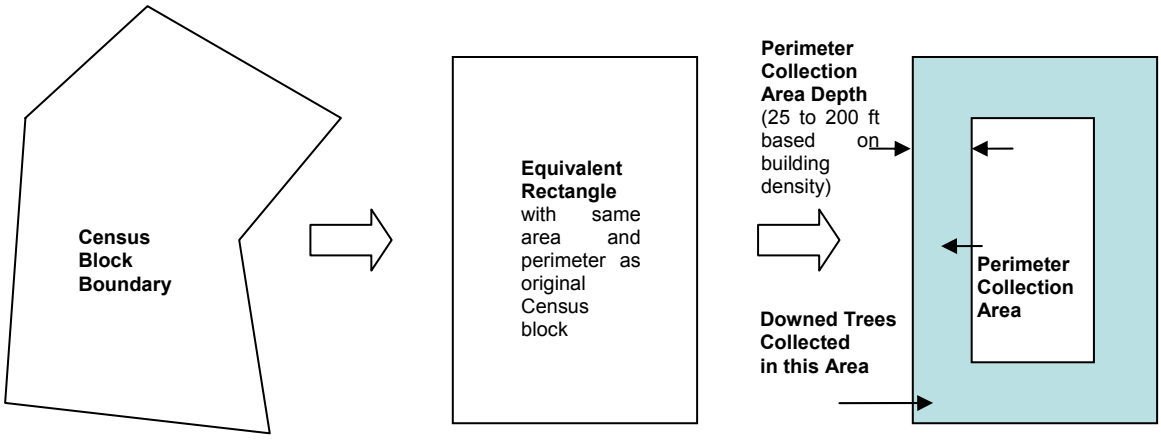

Figure 12.15. Calculation of Perimeter Collection Area for a Census Block with No Interior Roads.

- The perimeter collection area is then compared to the building based collection area (number of buildings times one acre). The larger of the two areas is retained as the total collection area (A_{Ci}), provided that the area is less than the overall census block area.

The presence and length of interior roads present inside each census block was determined by overlaying ESRI Streetmap USA data on the Hazus census blocks.

Figure 12.16 shows the relationship between equivalent census block width and building density for each census block analyzed in the Hampton Roads region of Virginia. The equivalent census block width is defined as the smaller dimension of the equivalent rectangular area calculated for each census block. The different series in the graph represent different ranges of the calculated tree debris collection factors (A_{Ci}/A_{Ti}). The collection factors are:

- Less than 0.5 for census blocks that are substantially wider than four times the perimeter collection area depth and/or that have less than 0.5 buildings per acre,
- Equal to 1.0 for census blocks with widths less than or equal to twice the perimeter collection area depth and/or with more than one building per acre, and
- Between 0.5 and 1.0 for census blocks that have widths between two and four times the perimeter collection area depth and/or building densities between 0.5 and 1.0 buildings per acre.

Thus, in Figure 12.16, we see that only wide census blocks with low building densities are assigned collection factors less than 0.5.

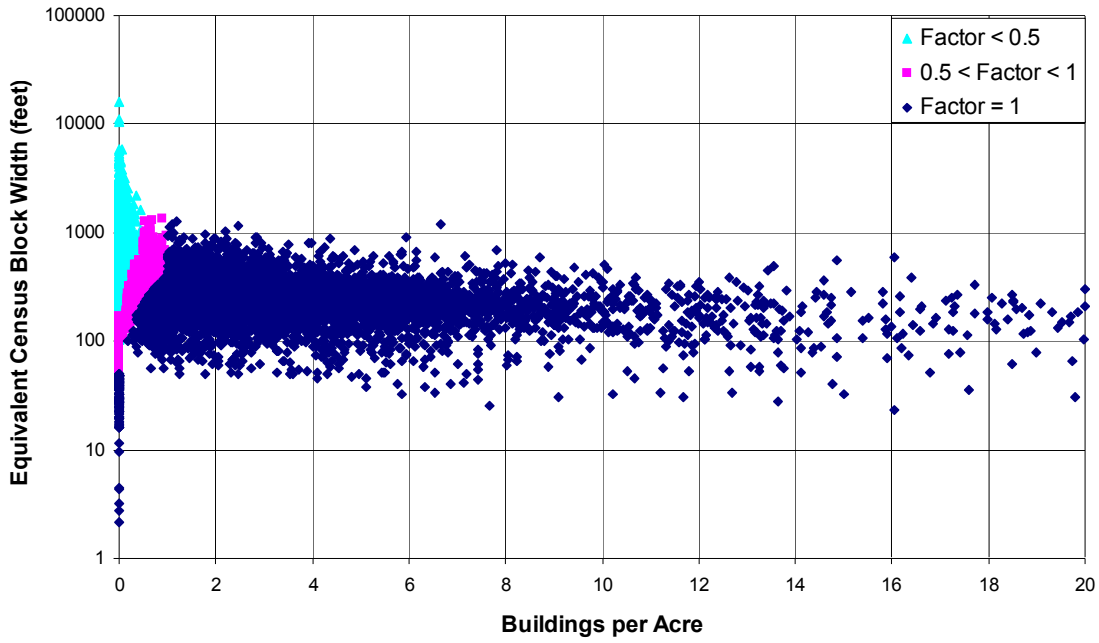

Figure 12.16. Equivalent Census Block Width versus Buildings per Acre for Hampton Roads Region of Virginia.

The resulting factors are then applied to the Hazus-MH results for tree debris quantities for each census block.

While Hazus 2.0 does not use Census 2010 blocks, collection factors were updated with 2010 Census blocks in mind. In particular, only those blocks that had less than one building per acre, did not have a collection factor of one already, or were divided into smaller portions according to the Census 2010 were updated.

Divided blocks in the 2010 Census pertain to those Census 2000 blocks that were divided into smaller portions. It was assumed that new roads were put in areas that previously did not have any. The area of these smaller portions is known, and was assumed to be square. Assuming the same building density of the Census 2000 block from which they originated, a new collection factor was determined for each of these smaller portions. These smaller portions were then area weighted and aggregating up to their original Census block to come up with a new collection factor for the original Census 2000 block (not to exceed a value of one). Figure 12.17 shows a schematic mapping of a single Census 2000 block that was divided into smaller portions and made into two Census 2010 blocks.

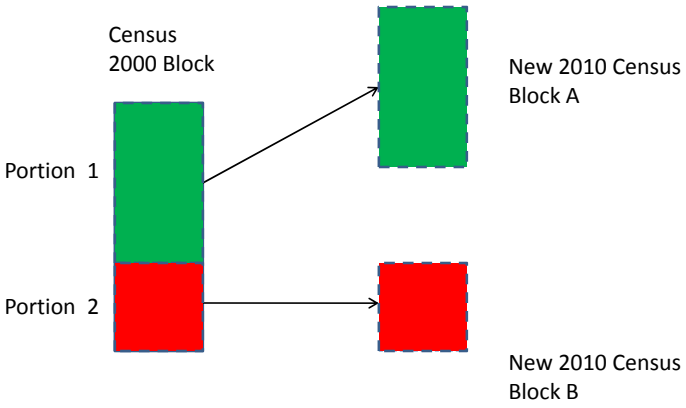

Figure 12.17. Schematic Mapping of a Census 2000 Block Partitioned into Smaller Census 2010 Blocks.

12.7.2.2 Implementing into Hazus-MH

Factors for all census blocks are pre-calculated for inclusion in Hazus-MH. These reduction values are stored in the "Tree Parameters" table in the "Tree Debris Collection Factor" column, as shown in Figure 12.18. Like the other tree parameter data, this field could also be modified by the user if more detailed information is available for individual areas at the local level.

Hazus-MH multiplies both the weight and volume of tree debris estimates in the debris analysis results table by the collection factors and presents two columns of output, as indicated in Figure 12.19.

Requiring that this analysis be completed at the census block level greatly increases the time it takes to run Hazus. In order to accommodate analyses run at the census tract level, the factors developed for individual census blocks are aggregated to the census tract level using the following equation:

$$F_{CT} = \sum_{i=1}^{n} \frac{A_{CBi} * F_{CBi}}{\sum_{i=1}^{n} A_{CBi}} \qquad (12.41)$$

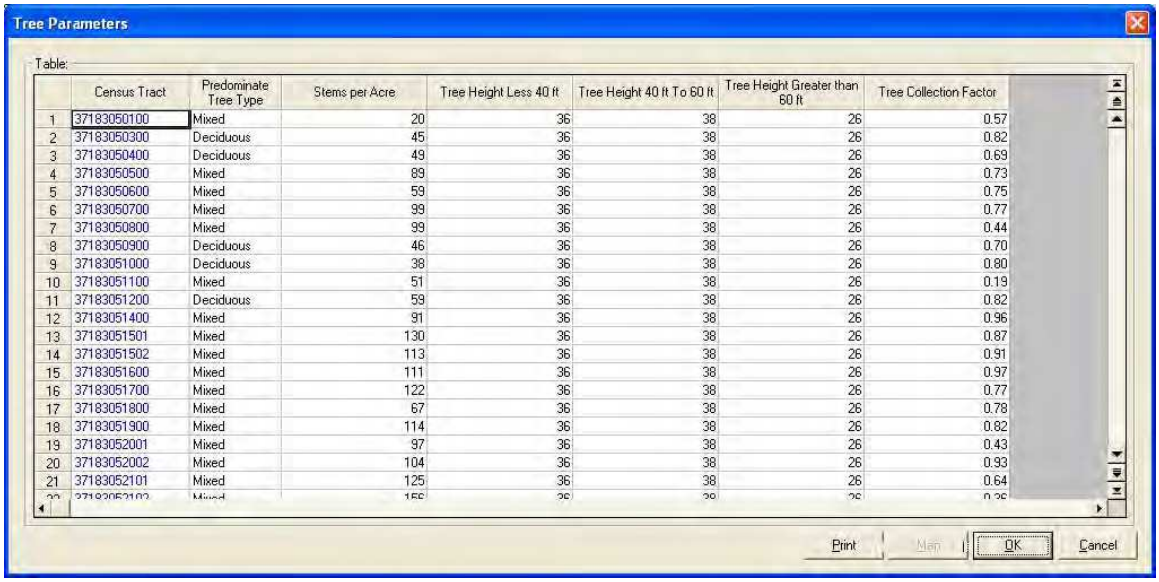

Figure 12.18. Addition of Tree Collection Factor to Tree Parameter Table in Hazus-MH

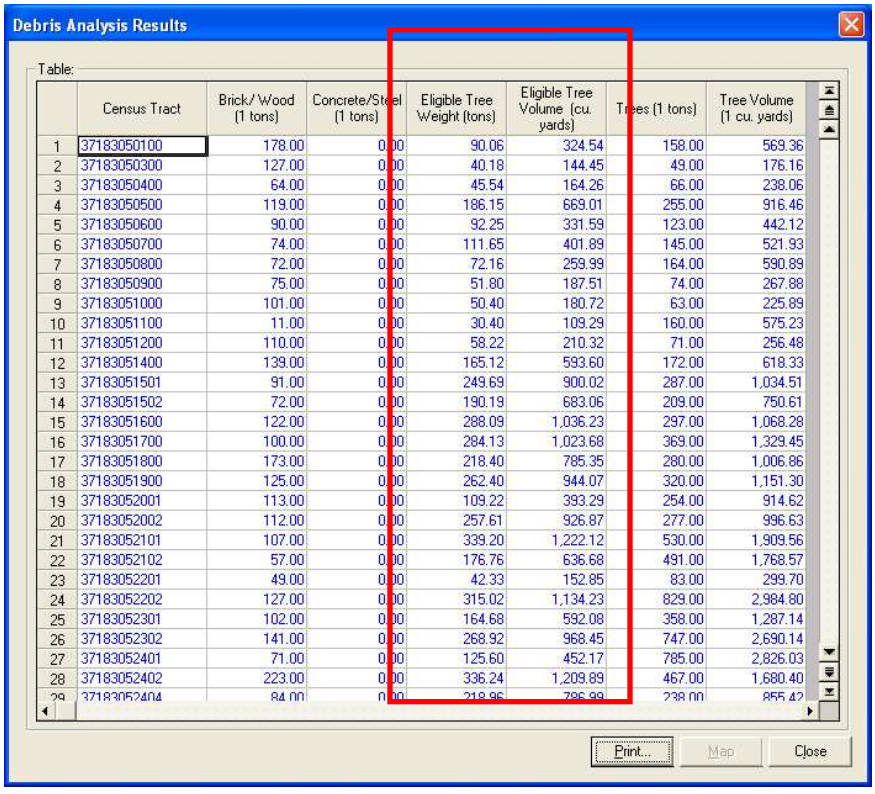

Figure 12.19. Hazus-MH Debris Results Table

where:

F_{CT} = Tree debris collection factor for a given census tract

A_{CBi} = Area of census block *i*

F_{CBi} = Tree debris collection factor for census block *i* (A_{Ci}/A_{Ti})

A_{CT} = Area of corresponding census tract

n = Number of census blocks in the current census tract

If Hazus-MH is run using uniform tree characteristics within each census tract (as is the case with the default data provided in Hazus-MH), identical estimates of tree debris generation and collection will be produced regardless of whether the analysis is run at the census tract or census block level. However, if the tree parameter data is changed such that the data vary by census block within a census tract, then results will differ and Hazus-MH must be run at the census block level for the desired results. This issue is discussed further in the next section.

12.7.2.3 Other Considerations for Hazus 2.0

While the collection factors can be aggregated to the census tract level as discussed in the previous section, the tree debris generation and collection results are sensitive to whether tree parameters are tabulated at the block or the tract level.

Prior to Hazus 2.0, the tree parameter data were assumed to be the same for every census block within a given census tract. This situation can introduce substantial biases in the tree debris generation and collection estimates for rural counties where census tracts are very large geographically and there may be only one or two census tracts for an entire county. One such area is Camden County, NC.

Tree fall frequencies surveyed in Camden County following Hurricane Isabel in 2003 demonstrated that tree coverage was scattered throughout the county with large areas of open land and smaller areas of clustered trees. Since Camden County has only one census tract, Hazus-MH considered the county to have uniform tree coverage prior to the release of Hazus 2.0.

In order to investigate further, the MRLC (Multi-Resolution Land Characteristics) land use, land cover data was revisited for a rural, four-county study region in North Carolina. Tree density statistics were re-calculated at the census block level for Camden, Chowan, Gates and Perquimans counties. The revised tree parameters were input into Hazus and the Hurricane Isabel scenario was re-run. Table 12.7 summarizes the results of this re-analysis for these four counties.

The large reductions in debris generated and collected indicate that the tree debris estimation is sensitive to the tree parameter data that is input to the tree blowdown and debris collection models. This indicates that when running level 2 or 3 analyses with refined local data, it is desirable to re-classify the land use, land cover data by census

block when using Hazus to predict tree debris generation and collection quantities. This is especially true for rural counties with large census tracts.

Table 12.7. Comparison of Modeled Tree Debris Generation and Collection Weight with Tree Parameters Compiled at the Census Tract and Census Block Levels.

	Tree Debris Generated (tons)			Tree Debris Collected (tons)		
County Name	Standard Tree Parameters	Revised Tree Parameters	Percent Reduction	Standard Tree Parameters	Revised Tree Parameters	Percent Reduction
Camden	338,711	199,911	41.0%	9,453	6,199	34.4%
Chowan	311,757	264,208	15.3%	17,539	11,276	35.7%
Gates	1,130,284	889,938	21.3%	36,609	27,493	24.9%
Perquimans	540,251	314,369	41.8%	23,386	12,631	46.0%

12.7.3 Comparison of Modeled and Reported Tree Debris

This section describes the methodology and presents a comparison of a prototype implementation of the methodology with tree debris statistics received from the North Carolina (NCDEM, 2004) and Virginia (Roarty, 2004) Departments of Emergency Management following Hurricane Isabel in 2003 (NC Department of Emergency Management, 2004; and Roarty, 2004).

12.7.3.1 Example Tree Collection Data – Hurricane Isabel, North Carolina

Tree debris collection data were obtained from the North Carolina Department of Emergency Management to assess how the methodology performs on an actual storm. Data were available for all counties in North Carolina that filed for federal assistance for debris cleanup. The data for the counties analyzed in this study are presented in Table 12.8.

These data were compiled by the North Carolina Department of Emergency Management using tree debris quantities from project worksheets completed by local governments following Hurricane Isabel. The numbers represent a combination of actual and estimated tree debris quantities by county based on their availability on the project worksheets. It is also important to note that there is a separate line noted for “State Agencies”. The debris quantity reported for this entry is likely to result from additional debris collected from several of the affected counties studied. Because of this, the tree debris volumes reported by county are likely to be slightly lower than actual. However, this volume is less than 2% of the total tree debris volume reported.

Hazus-MH was run using a Hurricane Isabel scenario for the 20 North Carolina counties listed in Table 12.8. Figure 12.20 compares modeled tree debris weight (total and collected) to the actual weight of tree debris reported collected by county in North Carolina for Hurricane Isabel (reported weights calculated from reported cubic yards with an assumed bulking factor of 10 cubic yards per ton). The series labeled “All Downed Trees” represents the total tree debris estimated by Hazus before applying the collection factors.

The county names along the abscissa are ordered by increasing average census block building density. In other words, the most rural counties appear on the left and least rural

Table 12.8. North Carolina Tree Debris Collection Data for Hurricane Isabel (2003)

County	Tree Debris Volume (CY)	Collection/Disposal Cost ($)	Unit Cost ($/Cubic Yard)
Beaufort	436,323	10,781,089	24.71
Bertie	82,222	932,359	11.34
Camden	706	28,765	40.74
Carteret	135,434	802,920	5.93
Chowan	476,768	3,704,690	7.77
Craven	52,729	453,677	8.60
Currituck	60,400	402,098	6.66
Dare	220,113	1,973,850	8.97
Gates	4,094*	45,688	11.16
Hertford	58,194	400,399	6.88
Hyde	48,503	384,263	7.92
Jones	3,414	44,924	13.16
Martin	69,951	283,732	4.06
Northampton	37,747	228,001	6.04
Onslow	8,881	260,441	29.33
Pamlico	4,697	159,095	33.87
Pasquotank	773,216	3,039,044	3.93
Perquimans	33,600	239,320	7.12
Tyrrell	3,700	43,424	11.74
Washington	152,404	361,538	2.37
State Agencies	53,121	974,307	18.34
Region Total	**2,716,217**	**25,543,624**	**9.40**

* Volume estimated from cost of removal

(most urban/suburban) appear on the right. There appears to be a trend of greater over prediction of tree debris for the more rural counties. It is not possible to determine whether this trend is due to an overestimate of the number trees blown down, an overestimate of the collection factors in rural areas, an underreporting of tree debris collection in some rural counties, or some combination of the three.

The overall estimate of tree debris collected for the 20 North Carolina counties considered is about 41 percent lower than the actual totals collected by the Department of Emergency Management.

12.7.3.2 Example Tree Collection Data – Hurricane Isabel, Virginia

Data from the Virginia Department of Emergency Management were available for the 16 counties and communities that make up the Hampton Roads area. These data were compiled by the Hampton Roads Planning District for the Virginia Department of Emergency Management. The debris data for Virginia are shown in Table 12.9.

The debris data received from the Virginia Department of Emergency Management included the following caveats:

- Debris quantities from military facilities in the region are not included.

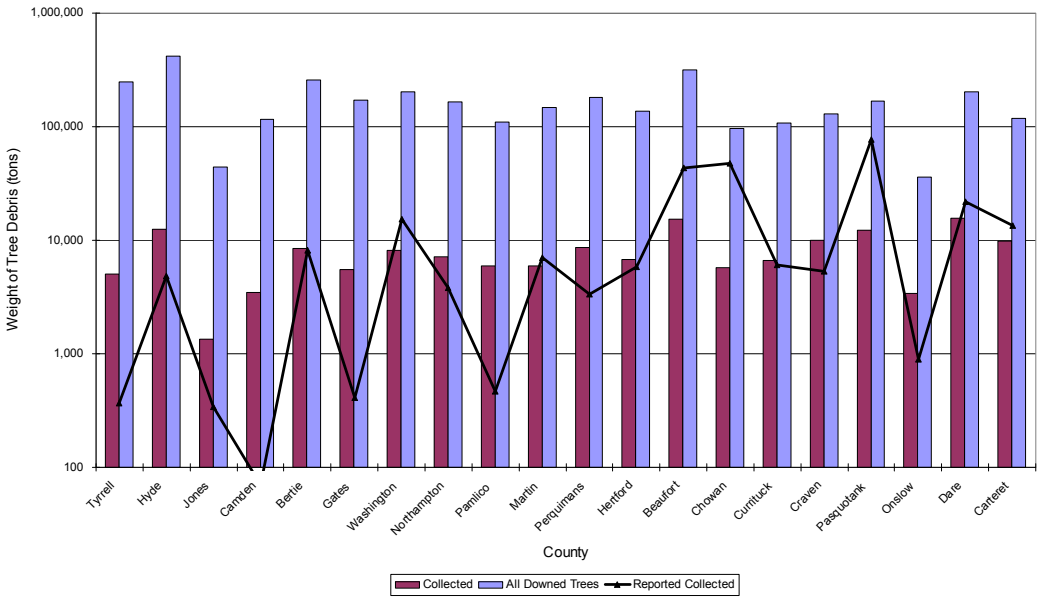

Figure 12.20. Comparison of Modeled Total and Collected Tree Debris Weight with Collection Totals Reported by NC DEM by County in North Carolina for Hurricane Isabel.

- The data shown above is for all debris, not just trees/vegetative debris. However, conversations with Virginia DEM and the Hampton Roads Planning District confirmed that over 95% of the debris reported was from vegetative sources.
- Approximately 25% of the debris was reported by the Hampton Roads District of the Virginia Department of Transportation (VDOT). This debris was collected from the study area, but the proportion belonging to each county or community is unknown and is not included in the analysis.
- VDOT is responsible for collection of vegetative debris from federal highways in the entire Hampton Roads region, as well as for the collection of debris along state roads in the counties not labeled "(city)". Debris collection from state roads in counties labeled "(city)" is the responsibility of the city government.

The modeled tree debris weight was compared directly to the data provided by the Virginia DEM without modifications for the caveats listed above, assuming a bulking factor of 10 cubic yards per ton. The counties appear in order of increasing average census block building density.

Figure 12.21 shows that for twelve of the sixteen counties, the total weight of tree debris generated by all downed trees is less than that reported by the Virginia Department of Emergency Management, indicating either that the default tree densities and/or the calculated tree blowdown rates are too low in these counties or that there are other sources of debris that are not being modeled in Hazus.

Table 12.9. Virginia Debris Collection Data for Hurricane Isabel (2003).

County	Debris Volume (CY)
Chesapeake (city)	915,101
Franklin (city)	119,000
Gloucester	190,000
Hampton (city)	749,503
Isle of Wight	152,953
James City	411,848
Newport News (city)	577,045
Norfolk (city)	1,014,000
Poquoson (city)	175,795
Portsmouth (city)	430,000
Southampton	185,200
Suffolk (city)	400,000
Surry	59,514
Virginia Beach (city)	922,000
Williamsburg (city)	79,000
York	602,830
VDOT HR District	2,365,860
Total Debris:	**9,349,649**

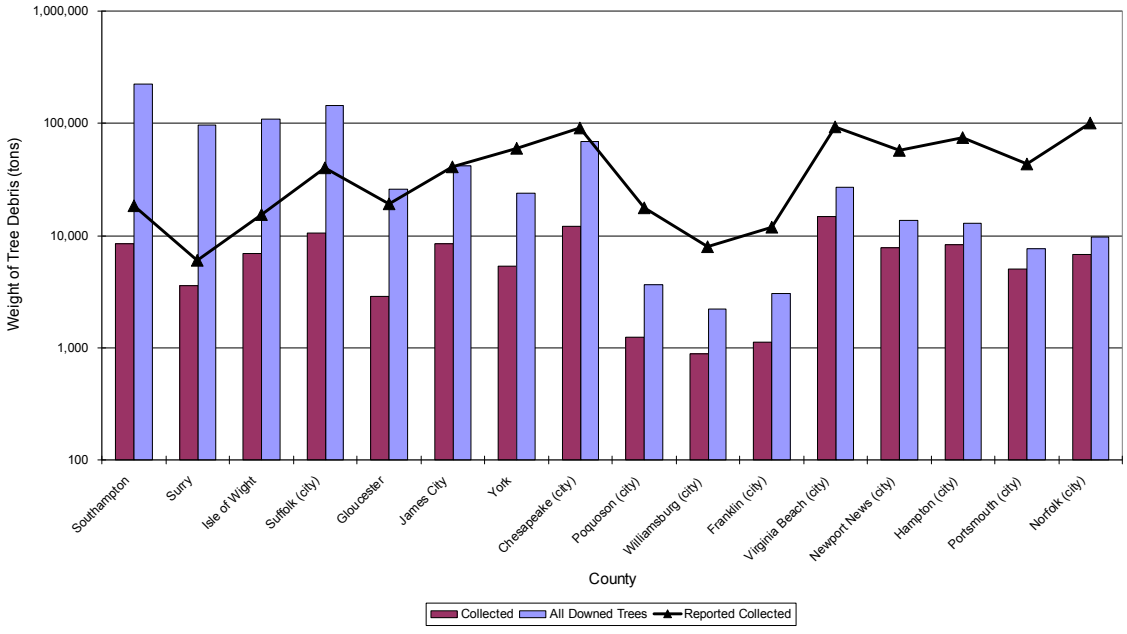

Figure 12.21. Ratio of Modeled Tree Debris to Actual Debris Collected by County in Virginia for Hurricane Isabel.

Aggregating the data over all 16 Hampton Roads communities, we find that the debris collection model underestimates the total debris collected (excluding the VDOT contribution) by about 90%. However, given that the tree blowdown model is apparently under predicting the quantity of downed trees and the various limitations of the raw data set discussed above, it is difficult to conclude that the Virginia example indicates any serious flaws in the model. The model appears to capture the proper trends and produce reasonable estimates of tree debris collection rates in rural, suburban and urban areas. Additional validation and refinement of the model is recommended as similar data sets become available for future hurricanes of varying intensities and geographic locations.

It is important to note that, in general, the Virginia Counties considered have substantially higher building densities (areas are more urban/suburban) than the counties analyzed in North Carolina. Table 12.10 lists the building densities for each of the 36 counties investigated with the average modeled tree debris collection rates. Building densities are calculated as the total number of buildings in the Hazus general building stock model divided by the land area of the county or region. Likewise, average modeled tree debris collection rates are determined by dividing the total collected tree debris volume by the total blown down tree volume modeled by Hazus for the county and region levels.

Table 12.10. Building Density and Average Tree Debris Collection Rate by County for North Carolina and Virginia.

North Carolina			Virginia		
County	Buildings per Acre	Average Tree Collection Rate (%)	County	Buildings per Acre	Average Tree Collection Rate (%)
Beaufort	0.039	4.93	Chesapeake (city)	0.308	17.88
Bertie	0.019	3.24	Franklin (city)	0.502	37.11
Camden	0.019	3.00	Gloucester	0.099	10.91
Carteret	0.113	8.33	Hampton (city)	1.325	64.92
Chowan	0.053	5.95	Isle of Wight	0.058	6.45
Craven	0.076	7.80	James City	0.220	19.99
Currituck	0.067	6.18	Newport News (city)	1.132	57.63
Dare	0.106	7.77	Norfolk (city)	1.717	69.96
Gates	0.020	3.23	Poquoson (city)	0.446	33.96
Hertford	0.039	4.92	Portsmouth (city)	1.451	66.52
Hyde	0.008	3.00	Southampton	0.017	3.79
Jones	0.015	3.00	Suffolk (city)	0.085	7.43
Martin	0.034	4.01	Surry	0.017	3.74
Northampton	0.028	4.32	Virginia Beach (city)	0.865	54.10
Onslow	0.103	9.52	Williamsburg (city)	0.496	39.54
Pamlico	0.031	5.41	York	0.306	22.12
Pasquotank	0.084	7.17			
Perquimans	0.034	4.79			
Tyrrell	0.008	2.00			
Washington	0.025	3.98			
20 NC Counties	**0.047**	**4.68**	**16 VA Counties**	**0.231**	**12.87**

For the Virginia counties considered, the tree debris collection model estimates 12.9% of the total tree debris being collected versus only about 4.7% for the much more rural counties of North Carolina. Note that although the average building density exceeds 1.0 buildings per acre for several Virginia counties, the average tress collection ratios are still

less than 100% because some of the census blocks in those counties have building densities lower than 1.0 buildings per acre.

The trend of decreased over-prediction of tree debris as building density increases may also be due in part to different disposal means used in rural versus urban areas. In rural areas, it is common to see residents and farmers burning tree debris from their property immediately following the storm, or chopping and storing the wood for use to heat their homes for the winter. This behavior reduces the amount of debris that will actually be brought to the curb for collection by local and state governments.

By contrast, residents of urban and suburban areas tend to not only bring the tree debris that falls to the curb, but actually create additional debris by removing any part of the broken trees that remained standing. These residents may also take advantage of the opportunity to dispose of other vegetative debris stored on their property. This behavior may lead to increased tree debris generated and collected in urban and suburban areas.

A potential example of this trend was discovered in the data received from the North Carolina Department of Emergency Management. One largely urban and suburban county reported over 65,000 cubic yards of vegetative debris at a removal cost of over $1.5M while Hazus-MH did not predict any downed trees for this county because the windspeeds in Hurricane Isabel did not exceed 50 mph (3 second gust).

Another observation that may lead to underestimating tree blowdown in urban/suburban areas is that the tree database and tree blowdown model only consider trees greater than 30 feet tall. The percentage of tree weight or volume coming from trees less than 30 feet tall is likely to be larger in urban/suburban areas than rural areas.

12.7.3.3 Comparison to Other Collection Data

In addition to the county data compared for Hurricane Isabel in NC and VA, tree debris estimates were also available from the following storms. Table 12.11 presents a list of areas for which estimates of tree debris collected are available for the corresponding storms.

Figure 12.22 presents a comparison of modeled tree debris collected to actual quantities reported for the hurricanes and locations mentioned above. This comparison considers the weight of tree debris in tons, however, most hurricane tree debris reports are volume (cubic yards). The vertical line for each storm-location combination represents a range of weights based on bulking factors ranging from 4 to 10 cubic yards per ton. The small horizontal line represents either the actual tonnage reported (if no vertical line is present) or tonnage estimated assuming a bulking factor of 6 cubic yards per ton.

Table 12.11. Locations of Collected Tree Debris Estimates by Hurricane Name and Year

Storm – Year	Locations with Data
Rita – 2005	State of Texas
Wilma – 2005	Palm Beach, Broward, & Miami-Dade Counties, FL
Charley + Frances + Jeanne + Ivan – 2004	State of Florida, Alachua & Orange Counties, FL
Isabel – 2003	States of North Carolina & Virginia
Erin + Opal – 1995	Escambia County, FL

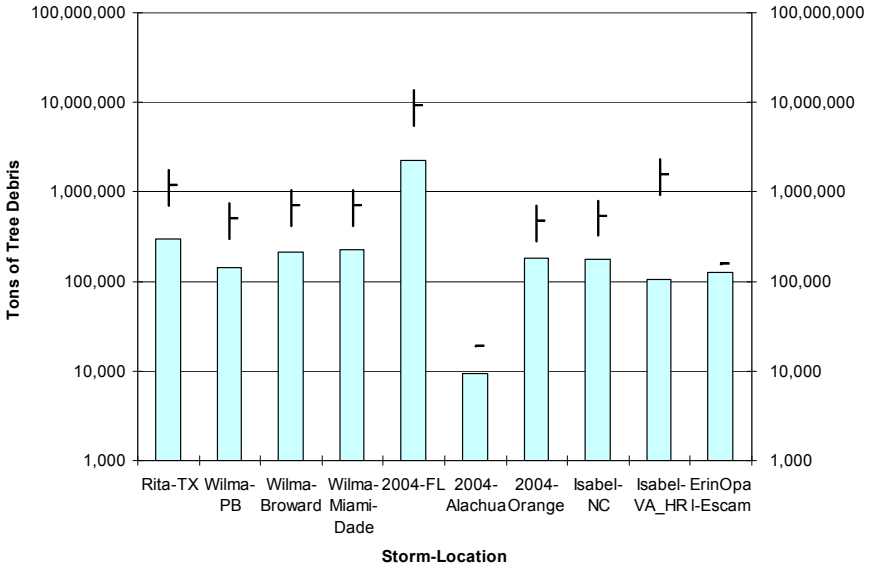

Figure 12.22. Comparison of Modeled Tree Debris Collected to Reported Amounts for Various Locations and Various Hurricanes.

12.8 Tree Blowdown Damage to Buildings

12.8.1 Overview

The building damage-to-loss model estimates expected loss as function of wind speed for 2 tree types, 3 tree height groups, 6 tree densities, 4 building geometries, and 2 wall construction types. These result in 288 normalized loss curves for tree blowdown damage to buildings, for building loss and contents loss respectively. The tree blowdown loss curves are combined with the fast-running normalized loss curves presented in Chapter 7 to form loss curves in each census tract that model wind, missile, and tree damage effects.

A Monte Carlo simulation approach is employed to derive the blowdown loss functions. A total of 10,000 simulations are performed to derive each function, which is taken to be the mean of the 10,000 simulated losses. Figure 12.23 illustrates the process for one simulation. The following sections describe the elements not presented in the previous sections.

12.8.2 Tree Drop Tests

The severity of tree damage to buildings is dependent on the tree impact energy and the structure's impact resistance. In an effort to investigate tree impact damage on residential structures, the Wind Load Test Facility at Clemson University conducted tree drop tests on modeled partial house structures. To simulate the tree trunk, the Clemson tests used two steel pipes of different weights, namely 450 lb and 950 lb, both at a length of 20 ft. The pipes were released from standing position on a rig about 18 ft from the modeled structure and free-fell to the modeled house structure. The lighter pipe hits the eave with impact energy of 3600 lb-ft, and the larger pipe hits with an impact energy of 7600 lb-ft.

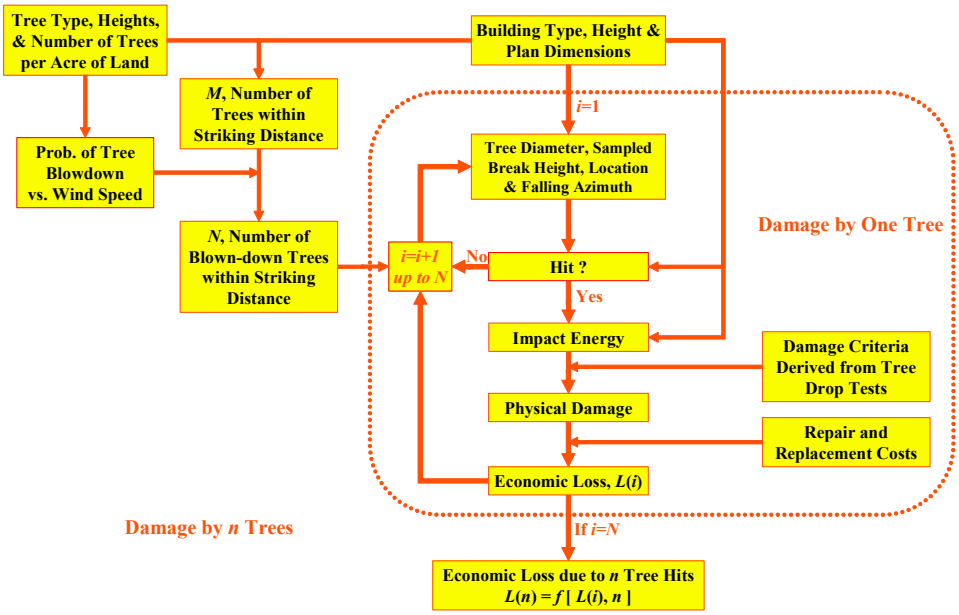

Figure 12.23. Simulation Scheme for Tree Blow-Down Damage to Building.

Video recordings were taken during the fall and impact, and still pictures were also taken of the damage after impact. Figure 12.24 to Figure 12.27 show examples of the impact damage recorded from the tests on several modeled structures with different impact resistance capacities.

12.8.3 Relationship between Damage Severity and Impact Energy

A quantitative relationship between physical damage state and the tree impact energy is essential to estimate tree blowdown damage, and ensuing economic losses, to buildings. The Clemson University tree drop test data aided in developing this relationship. The assumptions involved in establishing the damage state severity model include:

A. A tree falls solely under the action of gravity. The actions of blowing wind and the remaining resistance from root-soil interaction (for uprooting) or the

remaining resistance from wood fibers at breakpoint (for above ground breakage) are neglected.

B. A tree trunk impact is required to cause damage.

C. The tree trunk does not bounce after it hits the building.

D. If it exceeds the impact resistance of the structure, an impacting tree trunk cuts into the building until all of its kinetic energy dissipates into the structure.

E. A tree hit does not cause the complete collapse of a building.

Different building components will present different resistances to a tree trunk as it cuts through the structure. The resistance associated with a specific component of the building, such as the roof deck, top plate or bond-beam, wall sheathing, or an elevated

Figure 12.24. Small Pipe Impacting Wall Without Plywood Sheathing, 3600 lb-ft at Impact, Breaking Top Plates and Half-Way Cutting Into Wall.

Figure 12.25. Small Pipe Impacting Wall with Plywood Sheathing, 3600 lb-ft at Impact, Breaking Top Plates and 1/4 Cutting Into Wall.

Figure 12.26. Large Pipe Impacting Roof and Wall Without Plywood Sheathing, 7600 lb-ft at Impact, Breaking Roof, Top Plates and Entire Wall with Apparent Residual Energy Hitting Ground.

Figure 12.27. Large Pipe Impacting Roof and Wall With Plywood Sheathing, 7600 lb-ft at Impact, Breaking Roof, Top Plates and 1/8 Wall.

floor, is assumed to be constant. Based on the limited number of tree drop damage states recorded by Clemson University and additional engineering inferences, an extended number of damage states are defined for the subsequent estimation of direct economic losses, in relation to impact energy, as shown in Table 12.12. Tree heights that will potentially produce the indicated impact energy and corresponding damage states are also presented for given stand-off distance, breaking point, and fall azimuth, etc. using pine trees as an example.

12.9 Estimation of Direct Economic Loss from Physical Damage States

Cost Estimation Assumptions and Data. The cost estimates were prepared with data from RSMeans 2002 Repair and Remodeling Cost Data and the Means CostWorks 2002 software. The cost estimates have prices adjusted locally for Miami, which is consistent with the costing data of the original loss curves.

In preparing these cost estimates, the following assumptions about the construction were made:

- Roof covering is shingles
- ½" plywood roof deck
- Wood truss roof structure
- The average room size is 200 SF

Table 12.12. Damage States in Relation to Impact Energy

Damage State #		1	2	3	4	5	6	7	8
1-Story Wood	Impact Energy (lb-ft)[1]	250	2000	5600	6400	8800			
	Example Tree Height[2] (ft)	30.0	46.9	57.5	59.0	62.6			
	Damage State Description	Surface damage	Roof deck crack	Top-plates rupture	¼ Cut into wall	Cut through wall			
2-Story Wood	Impact Energy (lb-ft)	250	2000	5600	6400	8800	14400	15200	17600
	Example Tree Height (ft)	32.0	50.2	61.3	62.8	66.6	72.5	73.3	75.2
	Damage State Description	Surface damage	Roof deck crack	Top-plates rupture	¼ Cut into upper wall	Cut through upper wall	Floor-plates rupture	¼ Cut into lower wall	Cut through lower wall
1-Story Masonry	Impact Energy (lb-ft)	250	2000	11000	13000	19000			
	Example Tree Height (ft)	30.0	46.9	65.2	67.2	72.0			
	Damage State	Surface damage	Roof deck crack	Bond-beam rupture	¼ Cut into wall	Cut through wall			
2-Story Masonry	Impact Energy (lb-ft)	250	2000	11000	13000	19000	30000	32000	38000
	Example Tree Height (ft)	32.0	50.2	69.3	71.4	76.2	82.1	83.0	85.3
	Damage State Description	Surface damage	Roof deck crack	Bond-beam rupture	¼ Cut into upper wall	Cut through upper wall	Floor-plates rupture	¼ Cut into lower wall	Cut through lower wall

Notes: 1. Impact Energy is defined as the energy derived from the normal component of impact velocity with respect to the eave line.
2. Assume a pine tree with stand-off distance of 30ft, breaking at ground level and hitting eave perpendicularly.

- There are 7 rooms on average in a one-story building, and 14 rooms in a two-story building
- There is 1 bathroom in a one-story building, and 2 in a two-story building
- Contents value per square foot are 50% of the building value
- Value of building is 80 dollars per SF.

The general approach consisted of estimating the size of the opening that was created for each of the damage states, then estimating the extent of damage to various components of the building such as roof covering, roof structure, walls, flooring, contents, and electrical, etc. The extent of the area damaged accounted for the replacement of "units" of a component – for example, an even number of 4x8 sheets of plywood on the roof, etc. Table 12.13 and Table 12.14 list the assumed damage areas used in the one-story and two-story cost estimates, respectively. Content damage is estimated using the areas in Table 12.13 and Table 12.14 and a simple cost per square foot valued at 50% of the assumed building value (i.e., $\$40/ft^2$).

Table 12.13. Assumed Damage Areas Used in One-Story Cost Estimates

	Damage State #			
	1	3	4	5
	Surface Damage	Roof Only	Roof and 1/4 Wall	Roof and Wall
Component				
Window (sf)	0	0	1.75 or 0	7
Roof Structure (SF)	0	200	200	200
Roof Covering(SF)	100	210	210	210
Walls(SF)	32	32	32 or 10	64
Electrical (l.f)	0	0	10	50
Flooring(SF)	0	75	200	200
Floor Structure(SF)	0	0	0	0
Contents(SF)	0	100	150	150
Partitions(SF wall)	0	200	320	400
Plumbing(each)	0	0.07	0.11	0.14
Heating(SF area)	0	100	160	200
Kitchen and Appliances(each)	0	0.07	0.12	0.14
Assumed Opening Size				
Roof (SF)	0	16	40	48
Wall (SF)	0	0	12	48

Table 12.14. Assumed Damage Areas Used in Two-Story Cost Estimates

	Damage State #			
	1	3	4	5
	Surface Damage	Roof Only	Roof and 1/4 Wall	Roof and Wall
Component				
Window (sf)	0	0	3 or 0	14
Roof Structure (SF)	0	200	200	200
Roof Covering(SF)	100	210	210	210
Walls(SF)	64	64	32 or 10	128
Electrical (l.f)	0	0	30	100
Flooring(SF)	0	300	300	400
Floor Structure(SF)	0	0	0	64
Contents(SF)	0	150	200	300
Partitions(SF wall)	0	210	420	600
Plumbing(each)	0	0.05	0.1	0.28
Heating(SF area)	0	105	210	300
Kitchen and Appliances(each)	0	0.025	0.05	0.14
Assumed Opening Size				
Roof (SF)	0	16	40	48
Wall (SF)	0	0	12	96

Additional Assumptions for One-Story. The cost estimates for Damage State 5 (roof and wall) includes 50% of a 3'x5' typical window assuming that there is a 50% chance that a window will be involved in the damaged area. The assumption is that the amount of glazing on a home is approximately 20% of the wall area, which translates to about a 50% chance that any vertical slice will involve a window. For damage state 4 (roof and 1/4 wall) the area of window was reduced further still to reflect the likelihood that the damage is only to the wall above the window, and repair to the window may be less likely. For masonry homes, it was assumed that the windows would not be affected for this damage state.

One seventh of the cost of a set of kitchen appliances and cabinets was included to reflect the fact that 1 in 7 rooms is a kitchen which is likely involved in the damaged area. Similarly for plumbing, 1/7 of a package of plumbing cost is included (which is dominated by bathroom fixtures), based on the assumption that 1 in 7 rooms is a bathroom.

The extent of required wall repair in damage state 4 for masonry walls is assumed to be less than for wood frame walls, because the CMU units are smaller, and therefore the area to be repaired can be more localized.

Additional Assumptions for Two-Story. Damage state 8 includes one full window in the cost estimate. In the same manner as the one-story building, it is assumed that there is a 50% chance that a window will be damaged on each story, or the equivalent of one full window.

For kitchens and plumbing (bathrooms) the likelihood of impacting 1 of 7 rooms on any floor was accounted for in the estimate by costing in 1/7 of the cost of a complete set of kitchen appliances/cabinets or plumbing fixtures.

The area of flooring affected in each damage state accounts for the dripping of water from one story to another.

The completed cost estimates are presented in Table 12.15. The estimates are also illustrated in Figure 12.28 to Figure 12.30 for building, contents, and combined costs as functions of impact energy. For damage states whose costs were not estimated item-by-item, overall costs were estimated based on incremental costs by comparing to the costs estimated item-by-item. Maximum potential losses resulting from *one* tree hit are also estimated to be approximately $10,000 of structure and $8,000 of contents for one-story, and $17,000 and $13,000 for two-story, all assumed to be reached at impact energy of 100,000 lb-ft.

Table 12.15. Estimated Building Repair Costs by Damage State

Damage State #		1	2	3	4	5	6	7	8
12-Story Wood	Impact Energy (lb-ft)[1]	250	2000	5600	6400	8800			
	Damage State	Surface damage	Roof deck crack	Top-plates rupture	¼ Cut into wall	Cut through wall			
	Building Cost ($)	125	800	3789	5752	6212			
	Contents Cost ($)	0	200	4000	6000	7000			
	Combined Cost ($)	125	1000	7789	11752	13212			
2-Story Wood	Impact Energy (lb-ft)	250	2000	5600	6400	8800	14400	15200	17600
	Damage State	Surface damage	Roof deck crack	Top-plates rupture	¼ Cut into upper wall	Cut through upper wall	Floor-plates rupture	¼ Cut into lower wall	Cut through lower wall
	Building Cost ($)	162	1000	3937	5923	7000	7800	9600	10283
	Contents Cost ($)	0	200	5500	8000	9000	10200	11400	12000
	Combined Cost ($)	162	1200	9437	13923	16000	18000	21000	22283
12-Story Masonry	Impact Energy (lb-ft)	250	2000	11000	13000	19000			
	Damage State	Surface damage	Roof deck crack	Bond-beam rupture	¼ Cut into wall	Cut through wall			
	Building Cost ($)	101	600	3765	5539	6692			
	Contents Cost ($)	0	200	4000	6000	7000			
	Combined Cost ($)	101	800	7765	11539	13692			
2-Story Masonry	Impact Energy (lb-ft)	250	2000	11000	13000	19000	30000	32000	38000
	Damage State	Surface damage	Roof deck crack	Bond-beam rupture	¼ Cut into upper wall	Cut through upper wall	Floor-plates rupture	¼ Cut into lower wall	Cut through lower wall
	Building Cost ($)	114	700	3888	5708	7000	7800	9600	11243
	Contents Cost ($)	0	200	5500	8000	9000	10200	11400	12000
	Combined Cost ($)	114	900	9388	13708	16000	18000	21000	23243

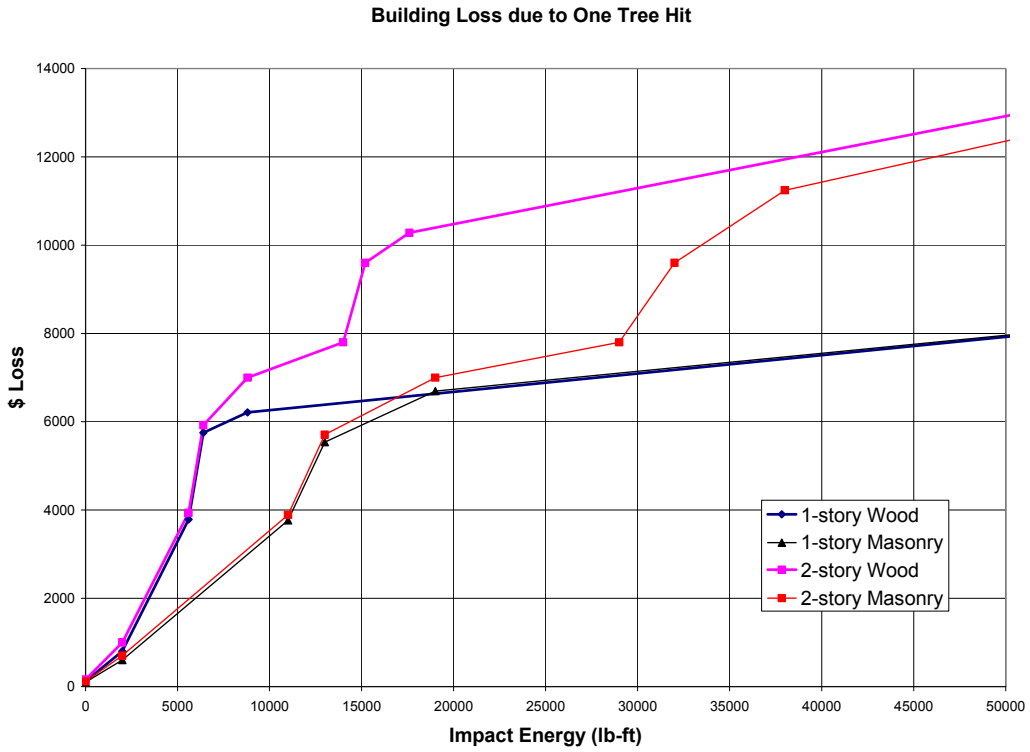

Figure 12.28. Building Repair Cost Estimates as Functions of Impact Energy.

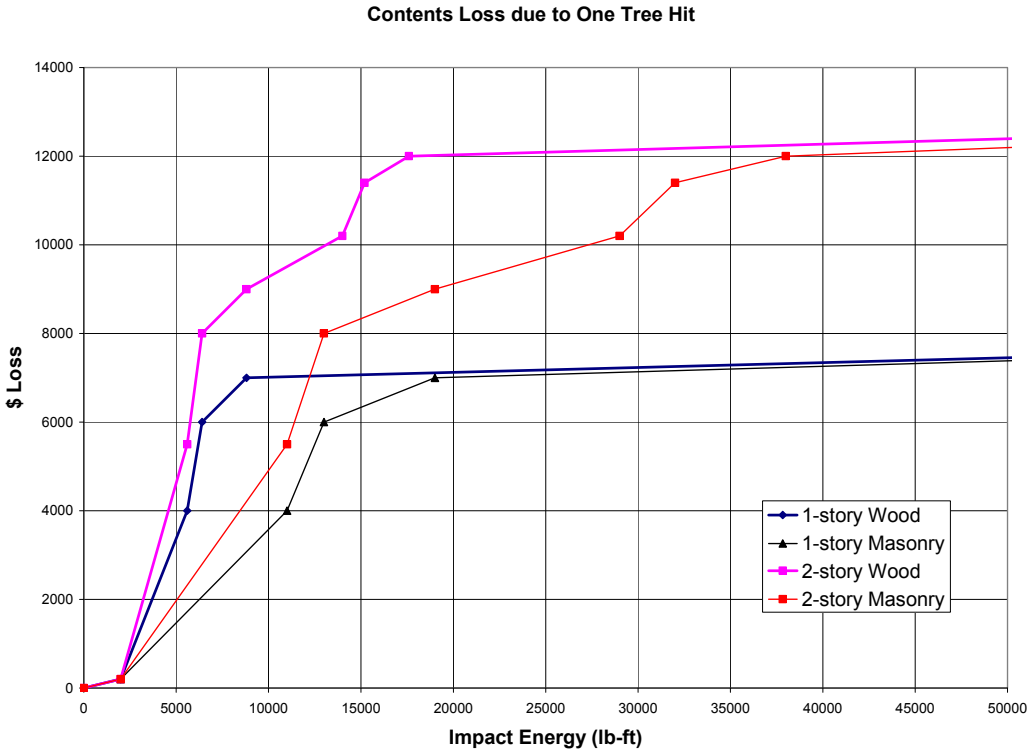

Figure 12.29. Contents Repair Cost Estimates as Functions of Impact Energy.

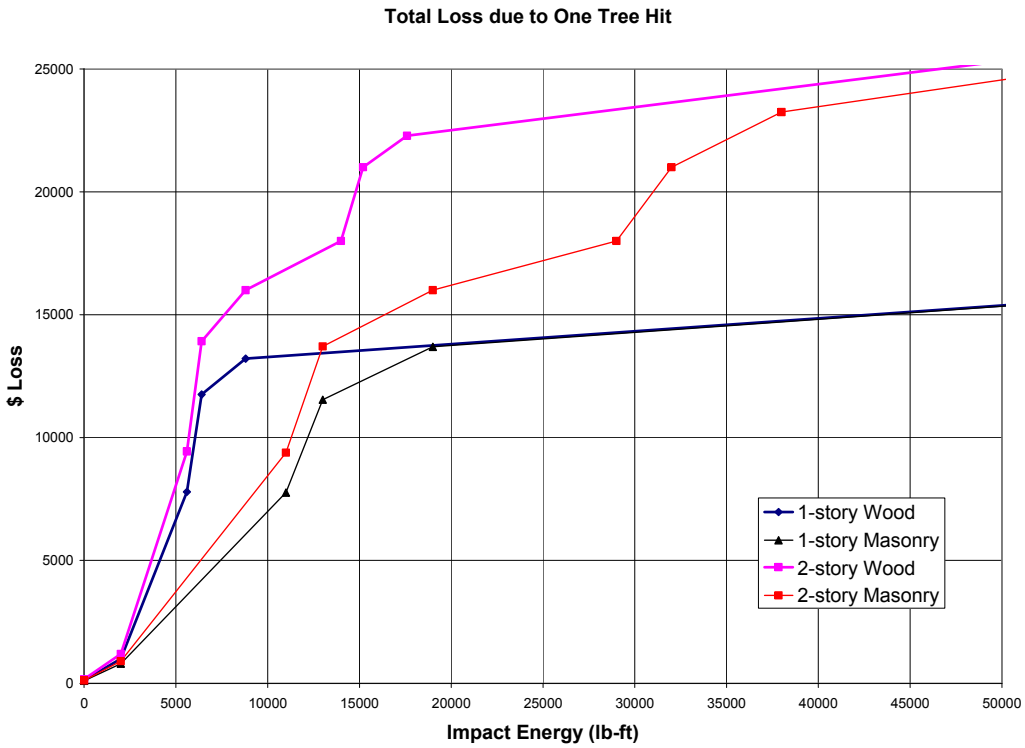

Figure 12.30. Total Repair Cost Estimates as Functions of Impact Energy.

12.10 Mean Loss as a Function of Wind Speed

12.10.1 Losses Due to Tree Blowdown

Using the methodology illustrated in Figure 12.23 and the assumptions and results discussed in the previous sections, mean building and contents losses are derived as functions of peak gust speed based on 10,000 simulations for each of the 288 cases summarized in Table 12.16. In the simulations, trees are assumed to be distributed uniformly random over areas not occupied by the building, with a 10 ft clearance from the building perimeter. The fall azimuth is also assumed to uniformly random.

Table 12.16. Parameter Matrix for the 288 Cases Studied

Parameter	Wall Type	Dimension (Value $)	Tree Type	Tree Height	Tree Density
Number of Values	2	4	2	3	6
Values	Wood	50x24x 9 (96k)	Evergreen	312-40ft	10
	Masonry	60x30x 9 (144k)	Deciduous	412-60ft	25
		40x30x17 (192k)		≥60ft	50
		50x30x17 (240k)			100
					200
		(all hip roofs)			400

For multiple impacts, each impact is assumed to damage a previously undamaged portion of the structure.

Examples of building and contents loss functions are presented in Figure 12.31 through Figure 12.35, each of which demonstrates the dependence of loss functions on one of the parameters listed in Table 12.16. Figure 12.36 compares the building and content losses for one specific combination of input parameters.

12.10.2 Loss Function for a Specific Building Type in Given Census Tract

The basic normalized loss functions and the tree inventory data are used in Hazus as follows to derive a normalized loss function for a specific building type in a specific census tract:

Input: Census tract tree inventory data: dominant tree type, tree density, and tree height distribution

For Evergreen: Census tract loss function = height group *proportion weighted average* of loss functions for the *3 height groups*, for the census tract tree type and density, and for the specific building mapped

For Deciduous: Census tract loss function = height group *proportion weighted average* of loss functions for the *3 height groups*, for the census tract tree type and density, and for the specific building mapped

For Mixed: Census tract loss function = **sum** of height group proportion weighted averages of loss functions for the 3 height groups for the *two base tree types* **divided by 2**, for the census tract tree density, and for the specific building mapped

12.10.3 Combining Tree Blowdown Normalized Loss Functions with the Basic Fast-Running Building and Contents Loss Functions

The following simplified method is used to combine the tree blowdown normalized loss with the basic fast-running loss functions described in Section 7.7 for single-family residential building and content losses:

$$\text{Total Loss} = \text{Basic Loss Ratio} + \text{Tree Damage Loss Ratio} - (\text{Basic Loss Ratio} * \text{Tree Damage Loss Ratio}) \quad (12.42)$$

The only assumption associated with deriving this equation is that the damage areas on a structure resulting from the two damage mechanisms are mutually independent.

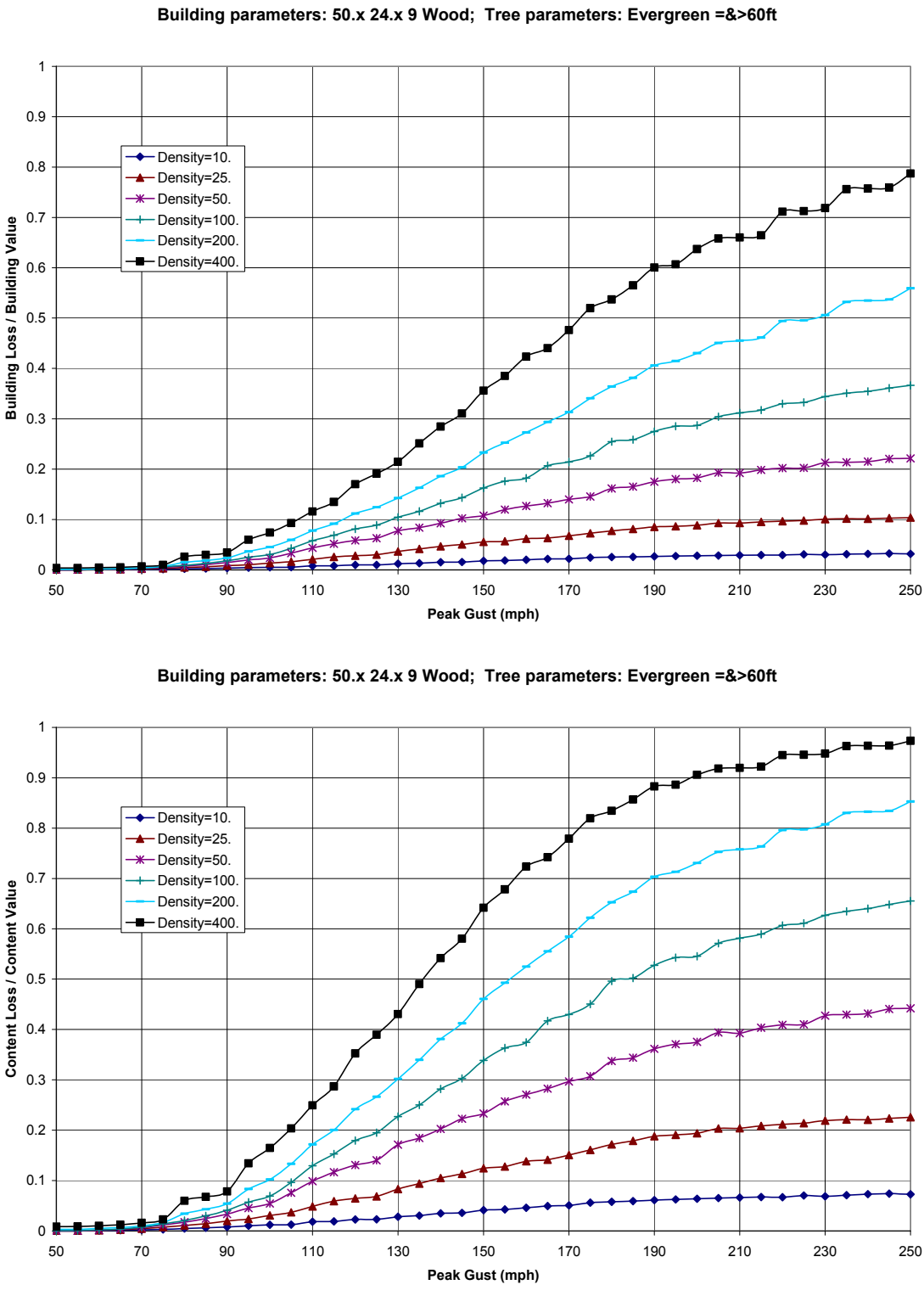

Figure 12.31. Dependence on Tree Density of Building (Upper) and Contents (Lower) Loss Functions.

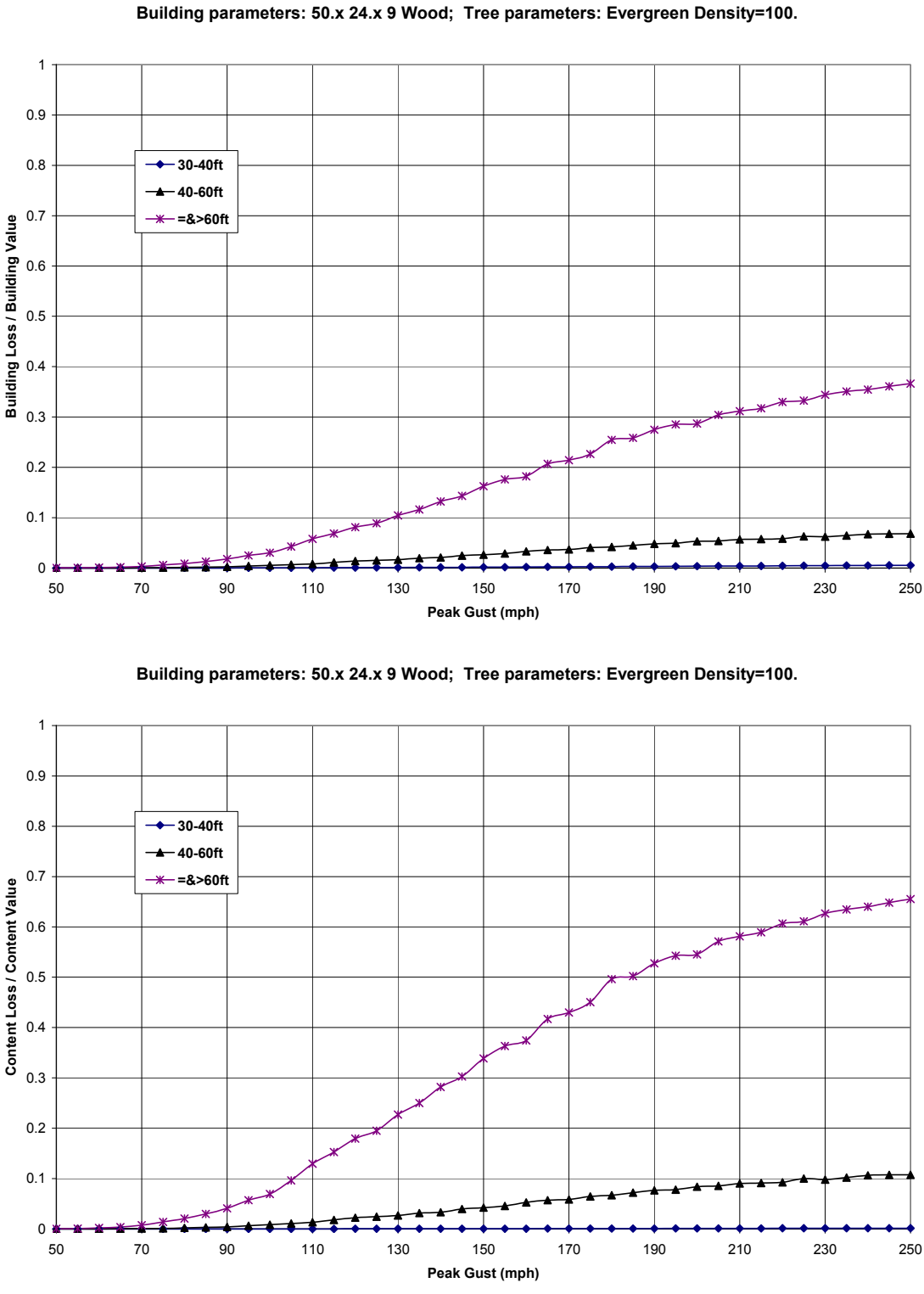

Figure 12.32. Dependence on Tree Height of Building (Upper) and Contents (Lower) Loss Functions.

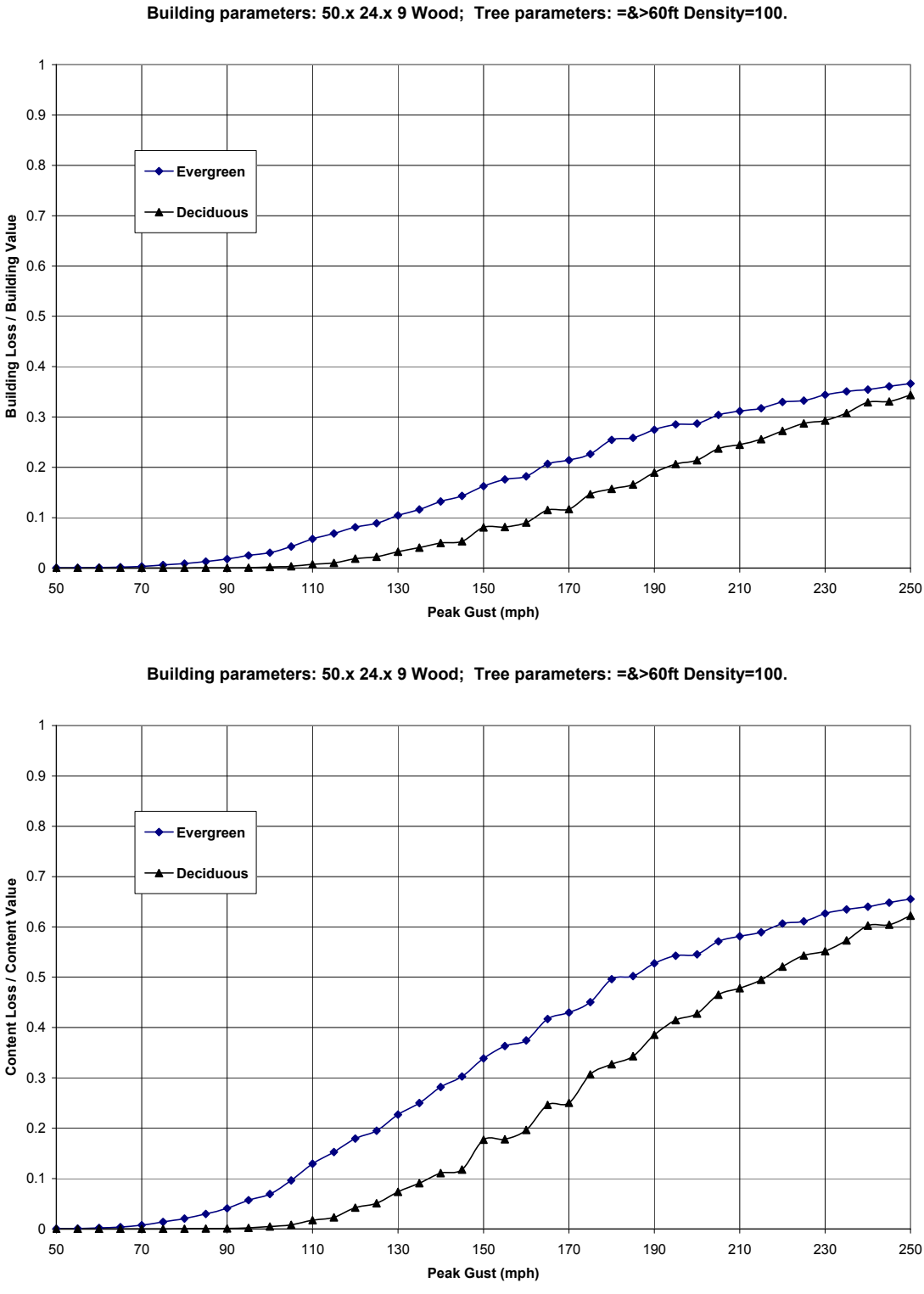

Figure 12.33. Dependence on Tree Type of Building (Upper) and Contents (Lower) Loss Functions.

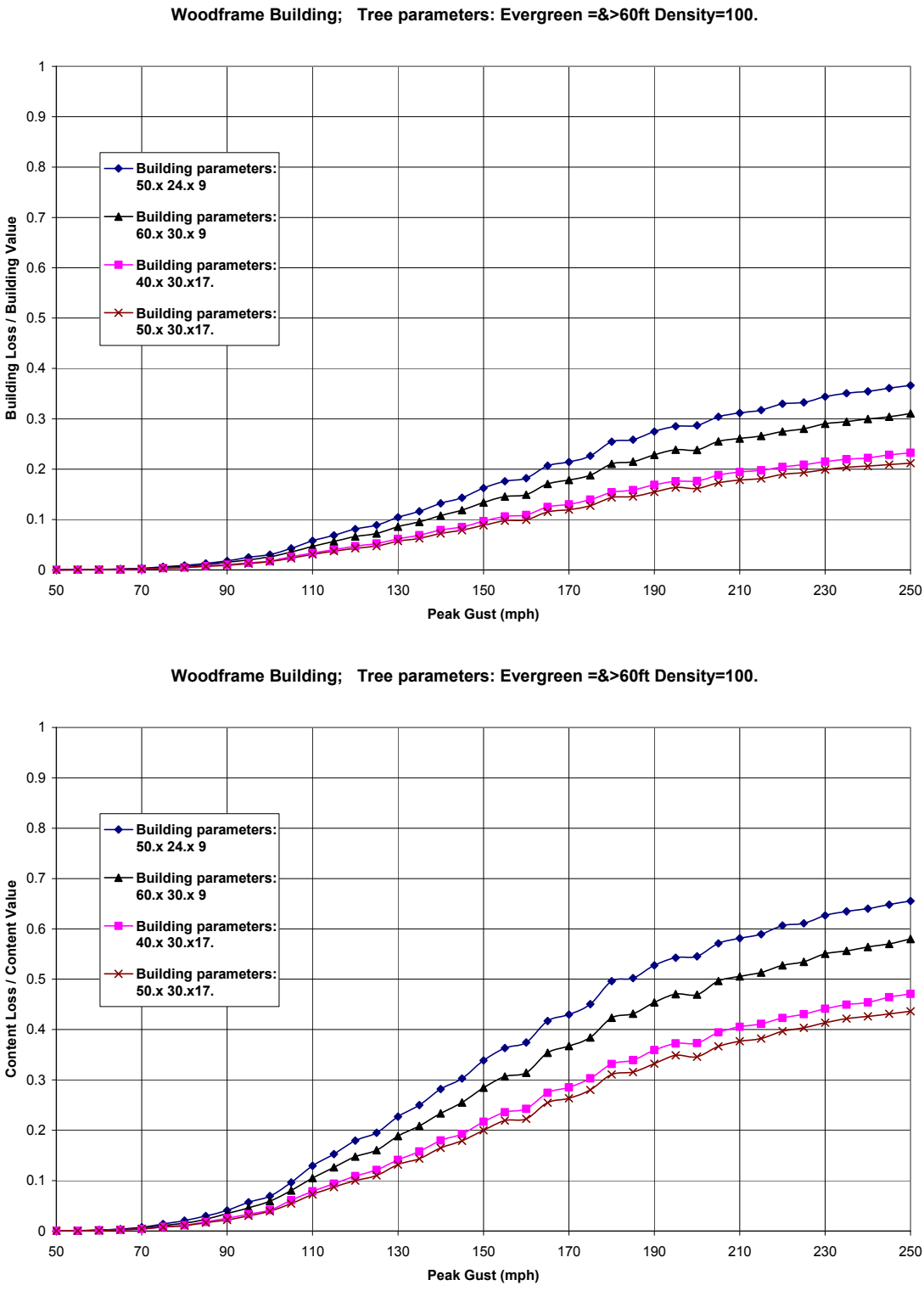

Figure 12.34. Dependence on Building Dimensions (ft) of Building (Upper) and Contents (Lower) Loss Functions.

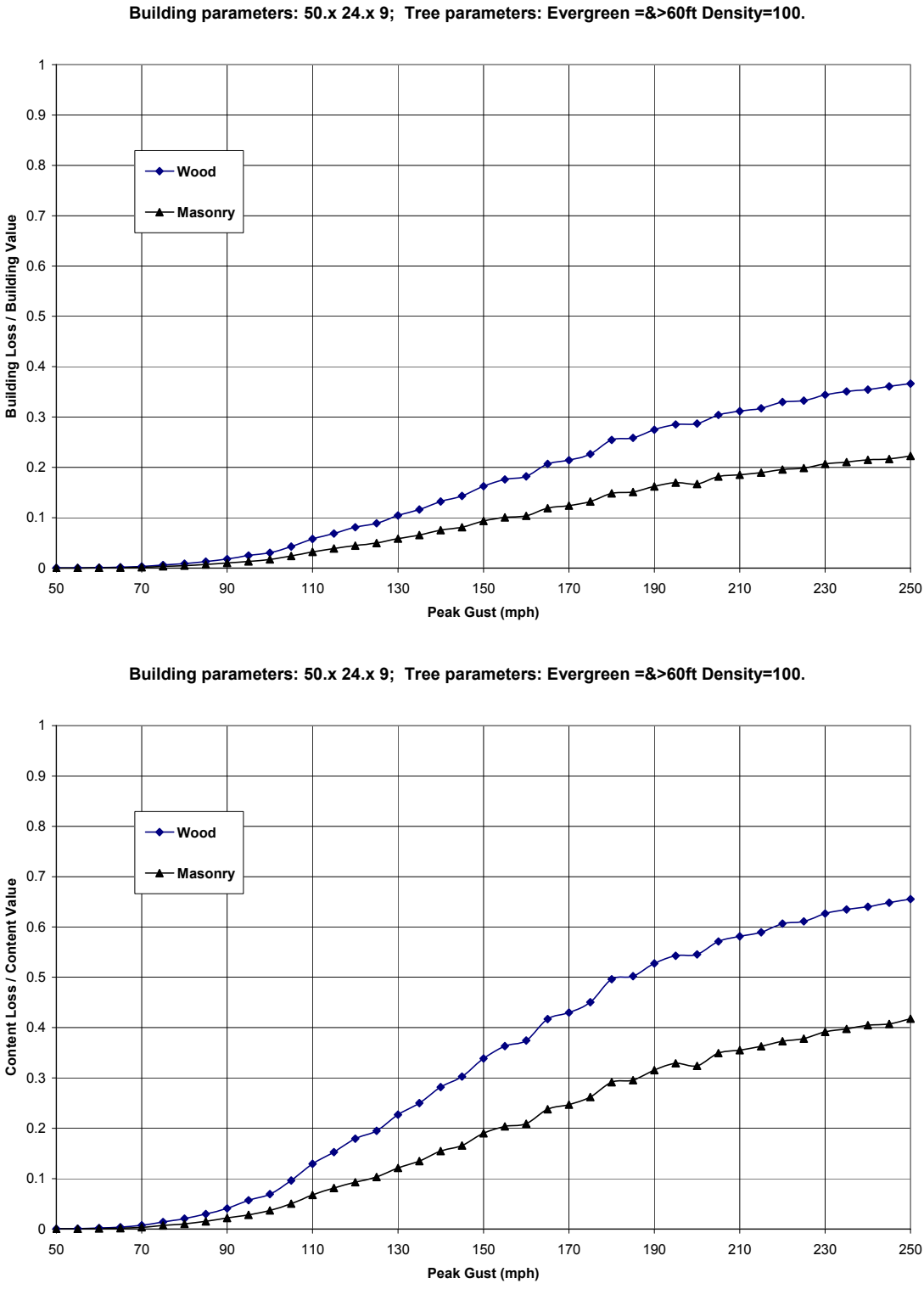

Figure 12.35. Dependence on Wall Type of Building (Upper) and Contents (Lower) Loss Functions.

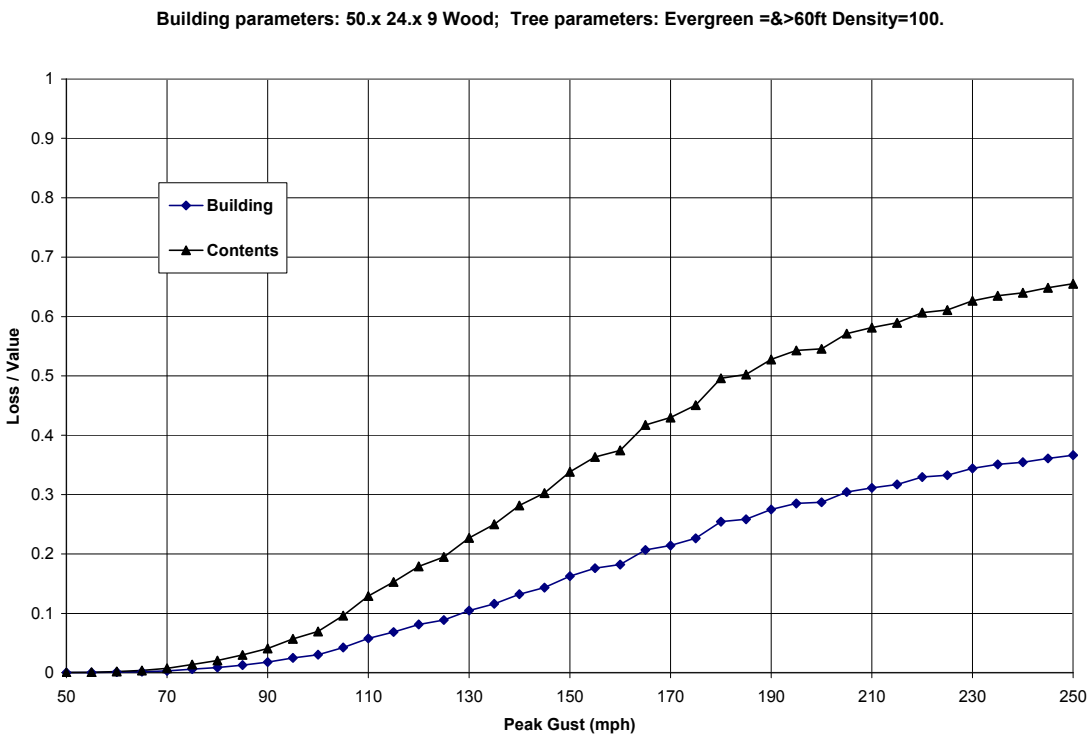

Figure 12.36. Building and Contents Loss Comparison.

Chapter 13. Coastal Storm Surge

13.1 Introduction

This chapter describes the development and validation of a hurricane storm surge and wave hazard and building loss modeling capability for Hazus-MH. The coastal surge model couples existing, publicly available hazard models estimate the storm tide and coastal wave heights produced by a single hurricane event. The storm tide model is the SLOSH (Sea, Lake, and Overland Surges from Hurricanes) methodology described in NOAA Technical Report NWS 48 (Jelesnianski et al. 1992). The wave model is the SWAN (Simulating WAves Nearshore) model developed and distributed by Delft University of Technology.

The coupled surge and wave models have been modified to use the hurricane wind field model in HAZUS-MH developed by Applied Research Associates (ARA). The primary motivation for this decision is to use the same validated and peer reviewed wind field model for predicting both direct wind damage and coastal surge damage. In addition, the storm tide estimates obtained from SLOSH using the ARA hurricane wind field model are more accurate, on average, than the storm tide estimated obtained from SLOSH using the default SLOSH wind field model.

A methodology for combining wind and flood losses to buildings at the building sub-assembly level is presented in Section 13.3. The methodology is designed to avoid "double counting" of damage to building component due to wind and flood; however, the methodology does not attempt to determine the fraction of the combined loss that is attributable to wind or flood.

Six recent hurricane events are used to throughout the report validate the wind field, storm tide, and wave models. The coastal storm surge hazard and combined wind and flood loss methodologies have been implemented in Hazus to estimate direct, building-related economic losses to the general building stock due to a user-specified hurricane scenario.

13.2 Coastal Storm Surge and Wave Hazard Models

This section describes the implementation and validation of a hurricane storm surge and wave hazard modeling capability for HAZUS-MH. The coastal surge model couples existing, publicly available hazard models to estimate the storm tide and coastal wave heights produced by a single hurricane event. The specific component models are:

1. SLOSH (Sea, Lake, and Overland Surges from Hurricanes) – FORTRAN and C source code for version 3.94 (2009) provided by National Weather Service's Meteorological Development Laboratory (NWS/MDL). The SLOSH methodology is described in NOAA Technical Report NWS 48 (Jelesnianski et al. 1992).

2. SWAN (Simulating WAves Nearshore) – Developed and distributed by Delft University of Technology. This software can be used freely under the terms of the GNU General Public License. See http://130.161.13.149/swan/support/copyright _and_ liability.htm. A listing of SWAN publications is available at http://vlm089.citg.tudelft.nl/ swan/index.htm.
3. ARA Hurricane Wind Field Model – Executable code distributed with HAZUS-MH; source code developed and owned by Applied Research Associates, Inc. The hurricane wind field model is described in Section 2 of the HAZUS-MH Hurricane Model Technical Manual (FEMA 2009a). Additional details and updates are provided in Vickery et al. (2000 and 2009).

For use in HAZUS, both SLOSH and SWAN have been modified to use the ARA hurricane wind field model. The primary motivation for this decision is to use the same validated and peer reviewed wind field model for predicting both direct wind damage and coastal surge damage.

The following recent hurricane events have been selected to validate the coastal surge models:

1. Andrew (1992) – Southeast Florida
2. Isabel (2003) – North Carolina
3. Ivan (2004) – Northwest Florida
4. Katrina (2005) – Mississippi
5. Gustav (2008) – Louisiana and Texas
6. Ike (2008) – Texas

These events are used to validate the wind field, storm tide, and wave models. The validation comparisons for Hurricane Andrew are for storm tide only.

13.2.1 Wind Speed, Wind Direction, and Atmospheric Pressure Validation

Comparisons of modeled 10-minute mean wind speeds, wind directions, and atmospheric pressures to observations from the validation events are summarized in this section. The modeled values are from the SLOSH wind field model (Jelesnianski et al. 1992) and the ARA wind field model (Vickery et al. 2000, 2009; FEMA 2009a). The modeled estimates are compared to data measured at sites located both over land and over water during the validation events.

Simulated hurricane wind speeds, wind directions, and atmospheric pressures are compared to 64 surface level records obtained from ASOS towers, C-MAN stations, buoy stations, and Florida Coastal Monitoring Program (FCMP) sites located along the hurricane tracks. Approximately 80 percent of the land based stations are located at distances of 20 km or less from the coast. Both the land based measurements of wind

speeds and the marine measurements of wind speeds have been adjusted to be representative of a height of 10 m above the local ground level or sea surface.

Summary comparisons of the observed and modeled maximum wind speeds and minimum atmospheric pressures are presented in Figure 13.1. The observed wind speeds and atmospheric pressures are compared to the simulated results obtained either from model runs using the ARA storm track and the ARA wind field model (open red circles) or from model runs using the ARA storm track and the SLOSH wind field model (filled black squares).

The comparisons indicate that the simulated wind speeds produced by the ARA wind field model are about 2% higher than the observed data, while the simulated wind speeds produced by the SLOSH wind field model are about 5% higher than the observed data. The R2 statistic for the ARA wind field model results is 73% compared to 57% for the SLOSH wind field results. The ARA and SLOSH modeled minimum atmospheric pressures are both very similar to the observed data.

Table 13.1 shows the average and root mean square (RMS) errors of the modeled wind speed, wind direction, and pressure time histories for the five hurricanes. The comparisons indicate that the ARA model provides better overall RMS estimates of wind speed and atmospheric pressure for all five hurricanes.

Appendices O through S present the modeled and observed time histories of the 10-min mean wind speeds, wind directions, and atmospheric pressures produced by Hurricane Isabel (2003), Hurricane Ivan (2004), Hurricane Katrina (2005), Hurricane Gustav (2008), and Hurricane Ike (2008), respectively. Also given in Appendices O through S are the modeled maximum 10-min mean wind speeds, as well as the landfall wind fields obtained from model runs using the ARA wind field model or the SLOSH wind field model.

In summary, the wind field validation comparisons suggest that the modeled wind speeds and atmospheric pressures produced by the ARA wind field model are generally in better agreement with the observed data than those produced by the SLOSH wind field model.

13.2.2 Storm Tide Implementation and Validation

Storm tide estimates produced by SLOSH model for the six selected validation events are compared to measurements from NOAA tide gauge stations and FEMA or USGS high water marks (HWM). Comparisons are performed for Hurricane Andrew (1992) in the Biscayne Bay area, Hurricane Isabel (2003) along the Atlantic Coast of North Carolina, Hurricane Ivan (2004) along the north central Gulf of Mexico Coast, Hurricane Katrina (2005) along the Mississippi Gulf Coast, Hurricane Gustav (2008) along the north central Gulf of Mexico Coast, and Hurricane Ike (2008) along the Texas Gulf Coast.

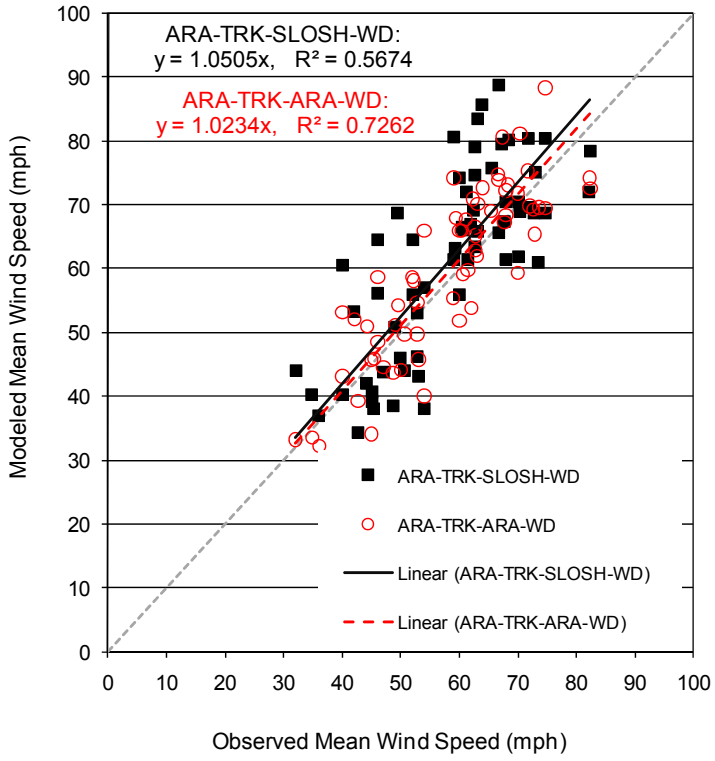

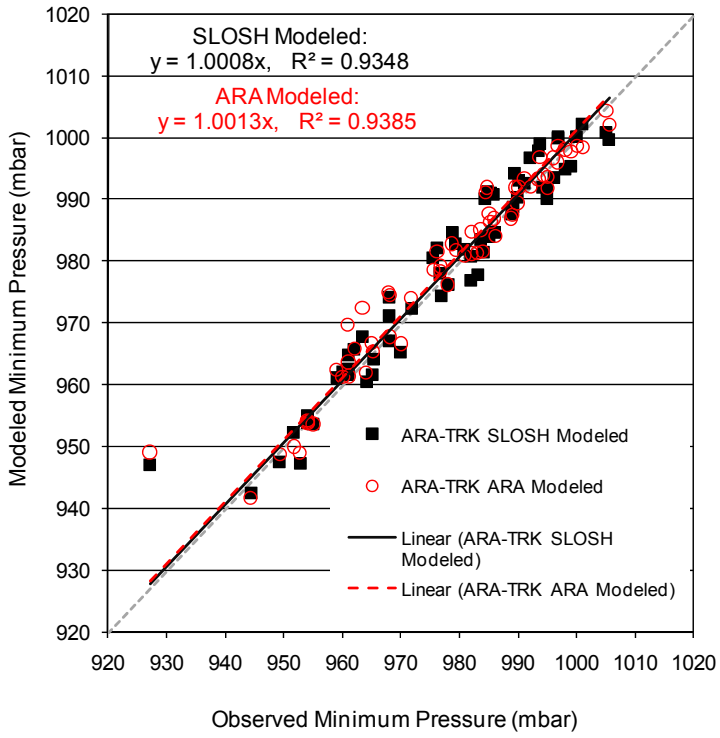

Figure 13.1. Summary Comparisons of Modeled and Observed Wind Speeds and Minimum Atmospheric Pressures.

Table 13.1. Error Analysis of Modeled Wind Speed, Wind Direction, and Atmospheric Pressure Time Histories

Hurricane	Range		Number of Data	Obs		SLOSH-Obs		ARA-Obs	
				Mean	Std	mean	RMS	mean	RMS
Isabel	Wind Speed (mph)	0-20	195	14.7	4.6	1.1	9.5	11.6	14.7
		20-40	1103	31.0	5.5	-2.6	9.8	3.5	7.5
		40-60	512	48.0	5.6	-2.3	9.0	1.3	7.6
		60-80	58	63.3	2.2	-3.3	5.5	-0.5	7.6
		all	1868	35.0	12.4	-2.2	9.4	3.6	8.6
	Wind Direction (deg)	0-45	447	27.1	12.3	16.3	19.4	41.6	43.7
		45-90	293	62.5	12.8	9.3	18.8	23.6	30.2
		90-135	214	113.3	14.1	6.9	17.6	10.8	17.7
		135-180	335	160.7	12.0	8.6	21.1	3.9	10.6
		180-225	261	198.4	12.3	-10.4	18.6	-24.9	27.7
		225-270	171	241.2	11.6	-28.4	37.2	-24.9	35.6
		270-315	65	293.2	13.3	14.5	17.6	27.0	28.6
		315-360	79	342.2	12.7	14.5	15.3	30.4	31.1
		all	1865	133.3	91.2	4.8	21.4	12.1	30.9
	Pressure (mbar)	945-965	7	963.6	0.8	0.1	1.0	5.3	5.6
		965-980	41	973.0	4.5	-2.7	3.5	3.3	4.3
		980-989	60	985.0	2.4	-5.4	6.0	0.4	2.5
		989-1030	756	1004.0	7.7	-7.4	8.2	-3.5	5.1
		all	864	1000.9	11.3	-7.0	7.8	-2.9	4.9
Ivan	Wind Speed (mph)	0-20	104	17.4	1.5	7.7	9.6	6.5	8.2
		20-40	909	32.4	5.3	1.2	9.2	2.6	7.6
		40-60	429	47.5	5.7	5.8	11.6	2.1	7.9
		60-80	88	65.8	4.1	7.2	14.8	2.0	11.8
		all	1530	37.6	12.0	3.3	10.3	2.7	8.0
	Wind Direction (deg)	0-45	228	26.0	12.7	2.8	13.7	23.5	26.9
		45-90	281	61.2	10.4	1.9	14.0	22.1	28.1
		90-135	225	109.9	12.0	9.2	21.6	21.4	29.1
		135-180	170	155.6	13.7	15.8	21.0	18.7	21.9
		180-225	109	192.2	14.1	15.1	22.1	17.7	20.5
		225-270	188	252.4	10.7	6.8	14.1	14.4	17.9
		270-315	193	285.3	12.5	2.3	13.4	11.3	26.2
		315-360	116	342.0	12.3	-6.9	15.0	11.3	17.2
		all	1510	159.9	105.5	5.6	16.8	18.3	24.8
	Pressure (mbar)	920-945	11	935.7	6.3	15.5	15.8	18.2	18.5
		945-965	21	956.3	5.0	13.2	15.3	17.5	19.5
		965-980	76	972.2	4.1	4.5	9.7	8.0	11.1
		980-989	53	984.9	2.6	-0.4	3.4	3.0	4.5
		989-1030	544	1001.6	5.6	-3.6	4.4	-0.7	2.3
		all	705	994.8	15.0	-1.7	6.1	1.3	6.0
Katrina	Wind Speed (mph)	0-20	49	15.6	3.3	13.7	13.8	10.8	11.1
		20-40	236	32.4	5.7	7.3	10.8	6.6	8.7
		40-60	402	49.2	5.9	8.5	14.7	5.4	9.1
		60-80	139	66.1	3.8	8.8	16.6	6.6	10.3
		80-100	1	81.7	0.0	6.0	6.0	12.6	12.6
		all	827	45.3	14.5	8.5	14.0	6.3	9.3
	Wind Direction (deg)	0-45	195	30.9	8.4	6.5	11.7	21.6	24.2
		45-90	222	71.3	11.2	2.0	11.5	16.7	21.5
		90-135	197	108.7	13.5	-1.5	12.5	7.6	14.1
		135-180	83	154.3	11.3	-5.9	20.2	-1.7	18.5
		180-225	60	204.8	10.8	-6.3	21.4	-6.3	18.4
		225-270	37	247.6	10.2	-8.5	21.5	5.1	27.0
		270-315	18	290.4	12.5	0.0	10.8	24.8	27.0
		315-360	14	336.7	13.6	15.0	24.5	32.9	38.4
		all	826	105.9	72.6	0.5	14.6	12.1	21.0

Table 13.1. Error Analysis of Modeled Wind Speed, Wind Direction, and Atmospheric Pressure Time Histories (Continued)

Hurricane	Range		Number of Data	Obs		SLOSH-Obs		ARA-Obs	
				Mean	Std	mean	RMS	mean	RMS
Katrina	Pressure (mbar)	920-945	4	938.1	8.0	26.0	30.7	25.5	30.6
		945-965	34	958.0	5.1	1.1	4.8	0.8	3.8
		965-980	70	974.5	4.5	0.6	3.4	0.0	2.9
		980-989	114	984.9	2.4	-0.7	2.1	-0.9	2.1
		989-1030	275	996.1	4.1	-2.1	2.6	-1.0	2.0
		all	497	987.4	12.7	-0.9	4.0	-0.5	3.6
Gustav	Wind Speed (mph)	0-20	1081	13.8	4.7	16.5	17.5	16.1	17.0
		20-40	2197	29.6	5.4	16.9	20.8	12.1	14.8
		40-60	933	47.1	4.9	11.1	16.7	5.5	12.2
		60-80	56	67.3	6.6	4.7	7.6	-1.0	7.6
		80-100	5	81.0	1.2	-2.9	3.1	-8.9	8.9
		all	4272	30.0	13.3	15.3	19.0	11.5	14.8
	Wind Direction (deg)	0-45	1811	22.8	11.9	0.3	12.9	17.4	20.7
		45-90	703	62.4	12.8	-0.7	23.3	11.4	23.0
		90-135	708	112.9	14.7	6.0	18.2	14.1	20.0
		135-180	797	158.3	14.3	-1.4	10.6	11.3	13.8
		180-225	418	195.9	15.6	-20.4	23.8	-4.3	13.6
		225-270	235	240.5	12.5	-18.1	25.2	-8.7	19.1
		270-315	67	293.1	13.4	-6.4	9.8	-9.7	17.0
		315-360	381	346.1	10.8	17.9	19.6	35.2	38.1
		all	5120	116.1	100.1	-0.5	17.4	13.4	21.5
	Pressure (mbar)	945-965	37	963.4	0.6	2.8	2.9	3.6	3.8
		965-980	523	973.2	4.1	-1.6	3.7	-0.5	3.3
		980-989	542	984.6	2.5	-1.0	3.3	-0.6	2.5
		989-1030	3725	998.6	5.4	0.1	1.8	-1.2	2.0
		all	4827	994.0	10.3	-0.2	2.3	-1.0	2.3
Ike	Wind Speed (mph)	0-20	295	12.1	4.0	13.5	16.9	5.2	7.7
		20-40	1971	32.4	5.1	18.8	21.0	15.2	17.8
		40-60	2110	48.7	5.7	8.8	13.1	7.6	12.2
		60-80	827	67.9	5.5	-4.3	8.6	-2.2	7.9
		80-100	12	81.0	0.6	-14.5	14.9	-9.6	11.6
		all	5215	43.6	15.5	10.7	16.2	8.7	13.9
	Wind Direction (deg)	0-45	1981	19.5	10.4	6.8	13.2	13.8	17.3
		45-90	524	62.8	11.3	-1.3	10.5	6.2	12.4
		90-135	338	111.3	12.5	-1.1	22.9	13.7	24.1
		135-180	454	161.1	11.6	15.5	32.8	24.1	28.9
		180-225	1005	199.7	11.8	19.3	21.9	27.8	30.0
		225-270	425	241.0	10.2	22.0	30.6	20.8	25.7
		270-315	171	292.1	13.5	21.9	27.3	30.7	33.3
		315-360	279	344.8	12.6	17.3	21.9	27.5	31.1
		all	5177	126.2	106.8	11.0	20.6	18.5	23.6
	Pressure (mbar)	945-965	982	958.1	3.3	0.2	1.4	0.4	1.6
		965-980	1346	972.1	4.5	-3.0	3.4	0.0	1.3
		980-989	1466	984.5	2.5	-4.8	5.0	-0.3	1.2
		989-1030	1474	992.5	2.9	-3.6	3.8	0.7	1.5
		all	5268	978.7	12.8	-3.1	3.8	0.2	1.4

Three sets of comparisons of the observed and modeled storm tide are performed for Hurricane Andrew and Hurricane Isabel. The first comparison uses the ARA storm track and the SLOSH wind field model (denoted as ARA-TRK-SLOSH-WD). The second comparison uses the ARA storm track and the ARA wind field model (denoted as ARA-TRK-ARA-WD). The third comparison uses the NOAA storm track and the SLOSH wind field model (denoted as NOAA-TRK-SLOSH-WD). For the remaining validation events, only the first two sets of comparisons are performed.

Detailed results for each event are provided in Appendices T through Y. The main conclusions can be summarized as follows:

- For Hurricane Andrew (Appendix T), the summary comparisons indicate that the ARA-TRK-ARA-WD model and the NOAA-TRK-SLOSH-WD model produce storm tide estimates that are 6% and 3% higher, on average, than the observations, while the values of the simulated storm tide produced by the ARA-TRK-SLOSH-WD model average about 14% higher than the observed data. In all three cases, the models tend to overestimate the smaller HWM observations (i.e., observations between 5 and 10 feet) and underestimate the larger HWM observations (i.e., observations above 12 feet).
- For Hurricane Isabel (Appendix U), the comparisons of the observed and simulated storm tide show that the ARA-TRK-ARA-WD model produces underestimates of about 11% on average, while both the ARA-TRK-SLOSH-WD model and the NOAA-TRK-SLOSH-WD model significantly underestimate the storm tide by 42% to 45%, respectively, on average. For this event, none of the three models does very well at explaining the scatter in the observed data.
- For Hurricane Ivan (Appendix V), the comparisons indicate that the values of the simulated storm tides produced by the ARA wind field model and the SLOSH wind field model both compare well to the observed data. The storm tide time series analysis for this event indicates that the ARA wind field model tends to produce lower mean and root mean square (RMS) errors than the SLOSH wind field model.
- For Hurricane Katrina (Appendix W), the comparisons indicate that the values of the simulated storm tide, for both the ARA wind field model and the SLOSH wind field model, are comparable to the observed data on average, but both models tended to over predict at the low end and under predict at the high end.
- For Hurricane Gustav (Appendix X), the SLOSH wind model and ARA wind model produce average underestimates of the observed storm tides of 24% and 20%, respectively. The underestimates are largest at the six locations with observed storm tides in excess of 10 feet. For this event, the model runs with ARA wind field model generally produce lower mean time history errors and lower RMS time history errors than the model runs using the SLOSH wind model.

- For Hurricane Ike (Appendix Y), the SLOSH wind model and ARA wind model produce average underestimates of the observed storm tides of 5% and 10%, respectively; however, the standard deviation of the errors from the ARA wind model results are smaller than the standard deviations of the errors from the SLOSH wind model results. The model runs with ARA wind field model generally produce slightly smaller mean time history errors and slightly smaller RMS time history errors than the model runs using the SLOSH wind model.

Table 13.2 summarizes the mean and RMS errors of modeled storm tide time histories for the five most recent validation events. The results show that the model run with ARA wind field model results in lower overall mean and RMS errors for four of the five hurricanes. The only exception is Hurricane Katrina, which has by a wide margin the fewest storm tide time history observation points of the five hurricanes.

In summary, comparisons suggest that the values of the model computed storm tide produced by the ARA wind field model tend to match the observed data better than those produced by the SLOSH wind field model.

13.2.3 Wave Model Implementation and Validation

For use in HAZUS, the primary purpose of the wave hazard model is to predict hurricane-induced wave heights in developed areas inundated by hurricane storm surge. A secondary purpose is to estimate wave setup stresses for coupling back into SLOSH, which will result in higher still water elevation predictions. In this section, we review the wave models considered for use in the HAZUS coastal surge methodology, discuss the computational grids used in the wave modeling methodology, show validation results for the SWAN near shore wave model, describe how the coastal surge wave model will be coupled with the storm surge model (SLOSH), and discuss how the modeled waves will ultimately be propagated into inundated areas using the transect-based approach documented in the HAZUS-MH Flood Model Technical Manual (FEMA 2009b).

13.2.3.1 Wave Models Considered

Three public-domain wave models were considered for use in the HAZUS coastal surge methodology. These models are briefly described in the following paragraphs:

13.2.3.1.1 WAVEWATCH-III

WAVEWATCH-III is a third generation deep water wave model developed by the National Centers for Environmental Predictions of the National Weather Service. This model is a product of continued development of WAVEWATCH-I developed at Delft University of Technology and WAVEWATCH-II developed at National Aeronautics and Space Administration. The model accounts for wave growth and decay due to surface wind stress, bottom friction, nonlinear wave-wave interactions and wave dissipation. Although efficient in computation in the deep water, it is not suitable for computations of wave characteristics in shallow water.

Table 13.2. Error Analysis of Modeled Storm Tides vs. Observed Time Histories

Hurricane	Unit	Surge Range	Numer Data	Obs		SLOSH-Obs		ARA-Obs	
				Mean	Std	mean	RMS	mean	RMS
Isabel 2003	(ft NAVD)	0-3	3338	1.3	0.8	0.2	0.8	0.4	1.0
		3-6	1575	4.3	0.9	-1.3	1.8	0.0	1.1
		6-9	500	6.7	0.7	-3.3	3.8	-1.0	1.8
		all	5413	2.7	2.0	-0.6	**1.6**	0.1	**1.1**
Ivan 2004	(ft NGVD)	0-3	544	2.1	0.9	-0.4	1.9	0.1	1.5
		3-6	1083	4.0	0.7	-0.9	1.2	-0.3	0.8
		6-9	52	6.5	0.2	0.8	1.1	0.2	0.6
		all	1679	3.5	1.3	-0.7	**1.4**	-0.2	**1.1**
Katrina 2005	(ft NAVD)	0-3	65	2.8	0.1	1.1	1.1	1.3	1.4
		3-6	357	4.2	0.7	0.5	1.0	0.8	1.3
		6-9	30	7.0	0.8	-0.9	1.3	0.5	0.6
		all	452	4.2	1.1	0.5	**1.0**	0.9	**1.2**
Gustav 2008	(ft NGVD)	0-3	7085	1.7	0.7	0.6	1.6	0.9	1.8
		3-6	5436	4.2	0.8	-0.7	1.8	-0.1	1.2
		6-9	2366	7.3	0.9	-2.2	3.1	-1.9	2.3
		9-12	993	10.5	0.9	-5.3	5.4	-4.0	4.0
		12-15	560	13.3	0.8	-6.4	6.5	-5.2	5.2
		all	16440	4.3	3.1	-0.8	**2.6**	-0.3	**2.1**
Ike 2008	(ft NAVD)	0-3	963	2.0	0.8	2.9	4.4	3.2	4.4
		3-6	5429	4.9	0.8	-1.5	3.1	-1.2	3.1
		6-9	11235	7.4	0.8	-1.3	3.0	-0.8	2.6
		9-12	7871	10.3	0.8	-0.2	3.3	-0.5	3.1
		12-15	3147	13.2	0.9	0.6	2.0	-0.4	1.7
		15-18	766	15.6	0.5	0.1	2.2	-1.0	2.1
		18-21	4	18.3	0.6	-6.3	6.3	-6.8	6.8
		all	29415	8.4	3.1	-0.7	**3.0**	-0.6	**2.8**

13.2.3.1.2 STWAVE

STWAVE (Steady State Spectral Wave) is a nearshore wave model developed and supported by the Coastal and Hydraulics Laboratory at the US Army Corps of Engineers Engineer Research and Development Center. The model simulates depth-induced refraction, shoaling, breaking, and diffraction. The full-plane version of STWAVE (allowing propagation and generation from all directions) is comparable to SWAN in terms of run-time and memory requirements.

13.2.3.1.3 SWAN

Simulating WAves Nearshore (SWAN) is a third-generation spectral wave model capable of generating two-dimensional wave energy spectra under specified conditions of winds, currents and bathymetry. It accounts for nearshore wave behavior such as wave breaking and wave setup and thus is suitable for shallow water computations of wave characteristics.

13.2.3.2 Computational Grids Used in the Coastal Wave Modeling Methodology

Due to time and resource limitations, it was not feasible to evaluate, implement and validate two different nearshore wave modeling options. Given the project team's previous experience with SWAN and the ability to use a SWAN to model both deep water and shallow water waves on both structured and unstructured grids, SWAN has been selected for use as the wave model in the HAZUS coastal surge methodology.

13.2.3.2.1 Implementation of SLOSH Grids and ARA Hurricane Wind Field in SWAN

For computational efficiency, SLOSH uses continuously varying grid cell sizes within each basin. It uses large grid cells near the deep water boundary and progressively smaller grid cells near the coast. In addition SLOSH uses different types of grid formats (polar, elliptical, hyperbolic, etc.) to represent a basin. To eliminate the need for duplicate and potentially conflicting bathymetry data for the storm surge and wave models, we have elected to directly use the SLOSH grids in SWAN by enabling the curvilinear grid option in the SWAN command file. The center of each SLOSH grid cell becomes a grid point in SWAN, with the average depth of the SLOSH cells used as the depth or elevation at that point. This approach is taken for two reasons: (i) to keep an identical computational grid as the input grid so that no additional interpolations are needed by SWAN, and (ii) to compute the wave parameters at the same locations in where surge is calculated in SLOSH.

The ARA hurricane wind field model is implemented in SWAN by using a nonstationary input of wind vectors at the computational grid points. These nonstationary wind vectors are computed for the duration of each SWAN run at fixed time intervals using ARA hurricane wind field model.

13.2.3.2.2 Wave Boundary Conditions for SWAN Runs on SLOSH Grids

Nonstationary wave conditions at the open ocean boundaries of a SLOSH basin are imposed in terms of wave spectra obtained through a SWAN (or WAVEWATCH III) run on a relatively large coarse grid with cells that are 20 km × 20 km in size. This grid is denoted as the Northwest Atlantic grid. The outline of this large grid is shown in red in Figure 13.2 along with the New Orleans SLOSH basin outline in blue. At first, a SWAN (or WAVEWATCH-III) run on this large grid is carried out using the nonstationary wind inputs at the coarse grid points for a given storm duration. The wave spectra obtained at the open boundary of a SLOSH basin from this run are then used as a boundary condition in the SWAN run in the SLOSH basin for the same storm duration.

13.2.3.3 Wave Model Validation Comparisons

Validation results for Hurricanes Isabel, Ivan, Katrina, Gustav and Ike are provided below. Significant wave heights, and in some cases the mean wave directions, are compared with the data obtained from the National Data Buoy Center (NDBC) and the United States Geological Survey (USGS).

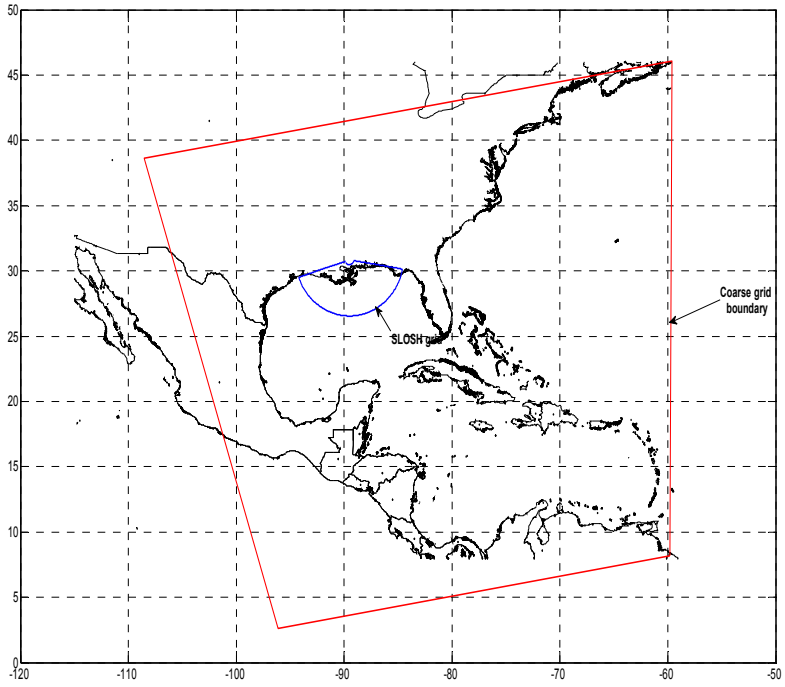

Figure 13.2. Northwest Atlantic Grid Domain.

13.2.3.3.1 Hurricane Isabel (2003)

Hurricane Isabel made landfall near Drum Inlet, North Carolina at approximately 1700 UTC on 18 September 2003 as a Category 2 hurricane.

Observed Data

One NDBC buoy (41025) is selected for validating wave heights in Hurricane Isabel, and the Pamlico Sound Hatteras basin is used in the simulation. The location of the buoy and the basin outline are shown in Figure 13.3.

Comparisons to Observed Data

Observed significant wave heights during Hurricane Isabel at buoy 42025 are compared with those obtained using SWAN. In the comparison, two cases of simulation results are shown. In the first case, the wave spectra obtained from a separate SWAN run in the Northwest Atlantic 20 km grid are used in the simulation. In the second case, the simulation is carried out without any boundary conditions.

The results are shown in Figure 13.4 where it can be seen that the boundary conditions have a substantial effect on the modeled significant wave height. Including wave boundary conditions in the simulation increases the modeled significant wave height by about 4 m. Due to the lack of a complete record at this buoy, a full comparison is not possible.

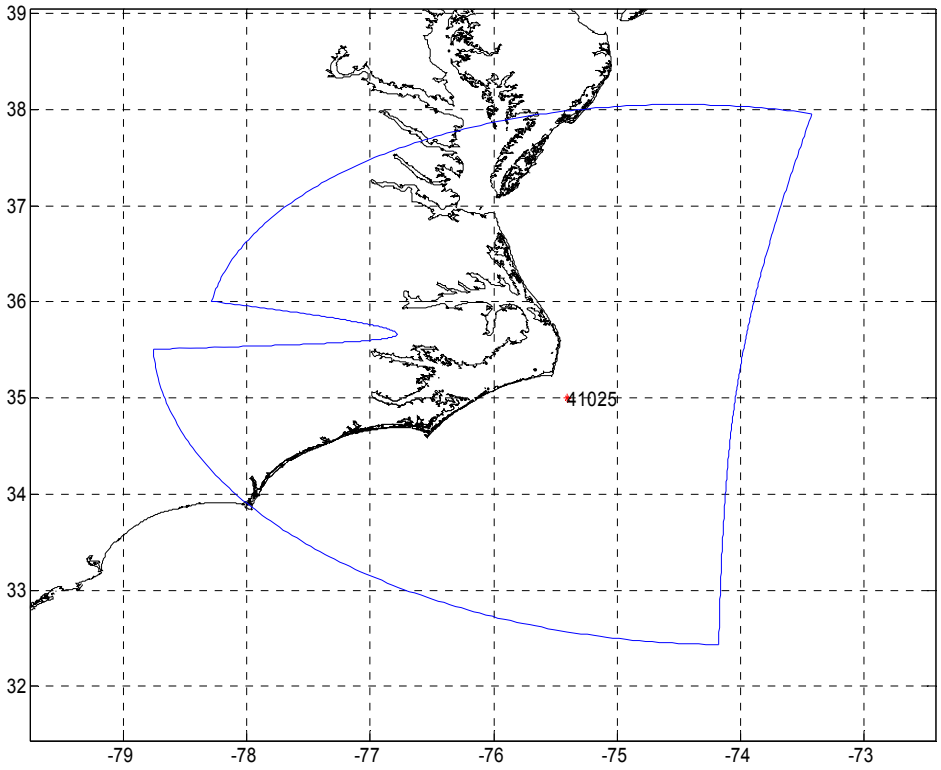

Figure 13.3. Location of NDBC Buoy in Pamlico Sound Hatteras SLOSH Basin.

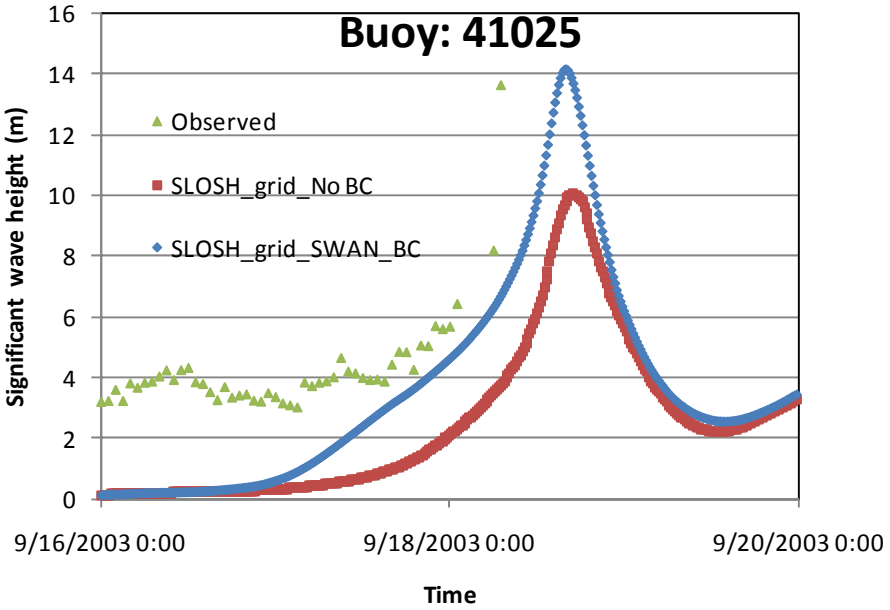

Figure 13.4. Comparison of Significant Wave Heights – Hurricane Isabel, Buoy 41025.

13.2.3.3.2 Hurricane Ivan (2004)

Hurricane Ivan made landfall as a Category 3 hurricane near Gulf Shores, Alabama at about 0650 UTC September, 2004.

Observed Data

Three NDBC buoys (42039, 42040, and 42007) are selected for validating wave heights in Hurricane Ivan, and the New Orleans SLOSH basin is used for the simulation. The location of the buoys and the basin outline are shown in Figure 13.5.

Comparisons to Observed Data

Observed significant wave heights and mean wave directions during Hurricane Ivan at NDBC buoys 42039, 42040 and 42007 are compared with those obtained from SWAN. In the comparison, two cases of simulation results are shown. In the first case, the wave spectra obtained from a separate SWAN run in the Northwest Atlantic 20 km grid are used in the simulation. In the second case, the simulation is carried out without any boundary conditions.

The comparison results are shown in Figure 13.6 and Figure 13.7. The boundary conditions have a substantial effect on the significant wave heights at the locations of the deep water buoys 42039 and 42040, whereas at the location of relatively shallow water buoy 42007, the boundary conditions do not play a significant role in the peak value of the modeled significant wave height. Including wave boundary conditions in the simulation increases the significant wave height at 42039 by about 1.5 m.

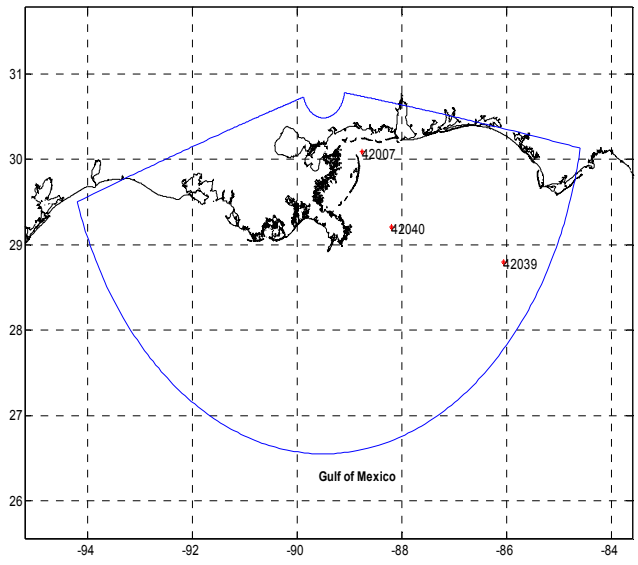

Figure 13.5. Locations of NDBC Buoys in the New Orleans SLOSH Basin.

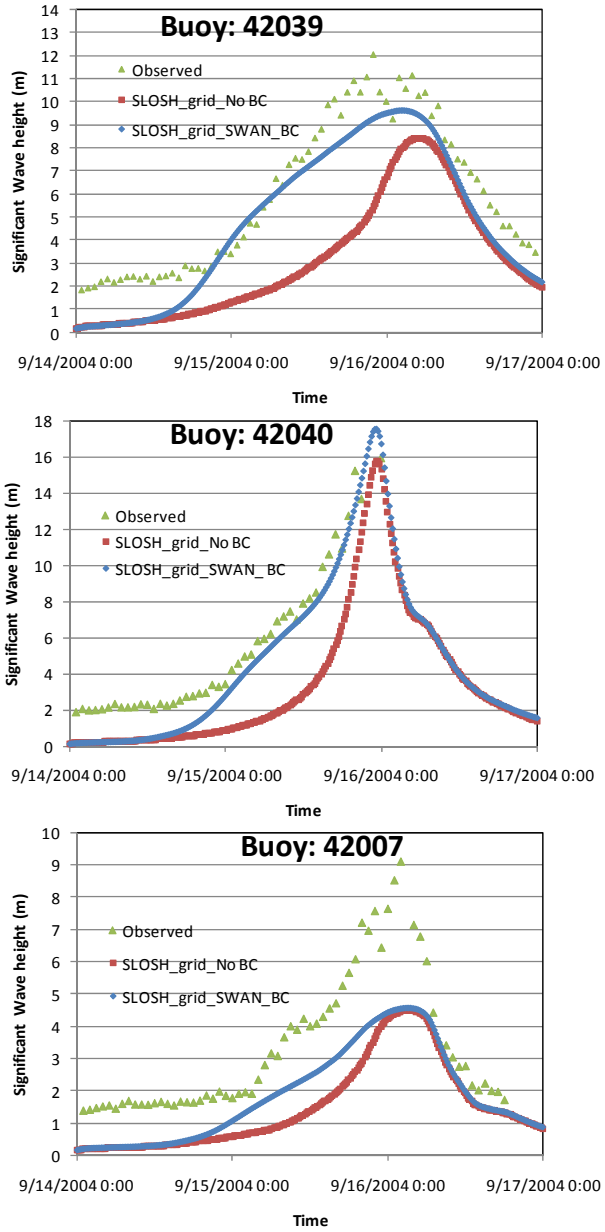

Figure 13.6. Comparison of Significant Wave Heights – Hurricane Ivan, New Orleans SLOSH Basin.

The significant wave height simulated with boundary conditions included shows reasonably good agreement with the observed data for buoys 42039 and 42040. However, there is a significant difference at buoy 42007. Possible causes include: (1) neglecting the pre-storm tide anomaly and storm surge in the simulation, (2) inaccurate bathymetry, and/or (3) insufficient grid resolution at this location.

The simulated mean wave directions at all three buoy locations shown in Figure 13.7 are in good agreement with the observations.

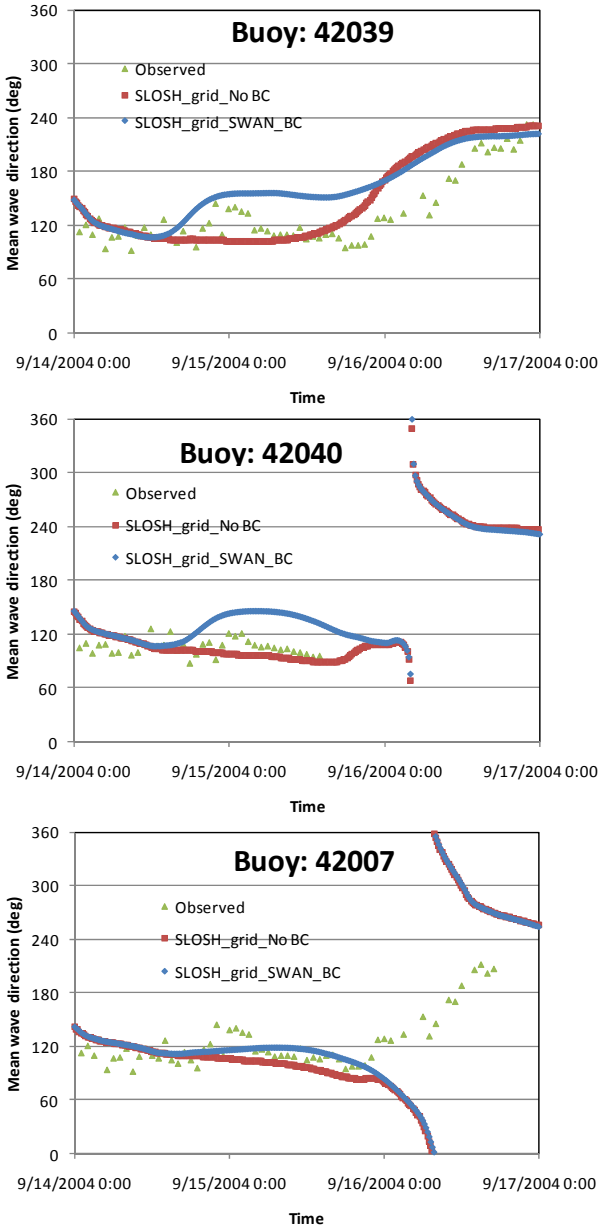

Figure 13.7. Comparison of Mean Wave Directions – Hurricane Ivan, New Orleans SLOSH Basin.

13.2.3.3.3 Hurricane Katrina (2005)

Hurricane Katrina made landfall as a Category 3 hurricane near Buras, Louisiana at 1110 UTC 29 August, 2005.

Observed Data

Three NDBC buoys (42039, 42040, and 42007) are selected for validating wave heights in Hurricane Katrina. The New Orleans, Mississippi Gulf Coast and Mobile Bay SLOSH basins are used in different SWAN runs. The locations of the three buoys relative to the three basins are shown in Figure 13.8, Figure 13.9, and Figure 13.10, respectively.

Comparisons to Observed Data

Observed significant wave heights during Hurricane Katrina at NDBC buoys 42039, 42040, and 42007 are compared with modeled results obtained from SWAN. In the comparison, two cases of simulation results are shown. In the first case, the wave spectra obtained from a separate SWAN run in the Northwest Atlantic 20 km grid are used in the simulation. In the second case, the simulation is carried out without any boundary conditions.

The comparison results are shown in Figure 13.8 through Figure 13.10. Including wave boundary conditions obtained using either SWAN or WAVEWATCH III on the Northwest Atlantic grid significantly improves the estimates at the deep water buoy locations (i.e., 42039 and 42040), with the boundary conditions obtained from the SWAN run providing better estimates than those obtained from the WAVEWATCH III run.

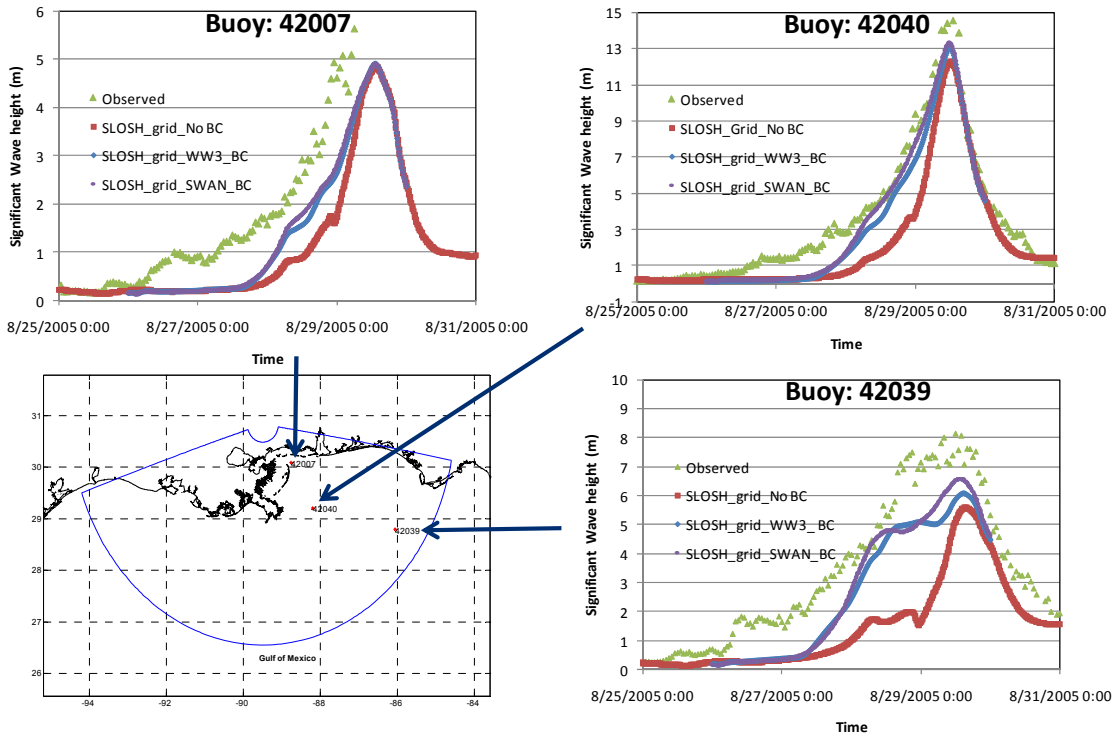

Figure 13.8. Comparison of Significant Wave Heights – Hurricane Katrina, New Orleans SLOSH Basin

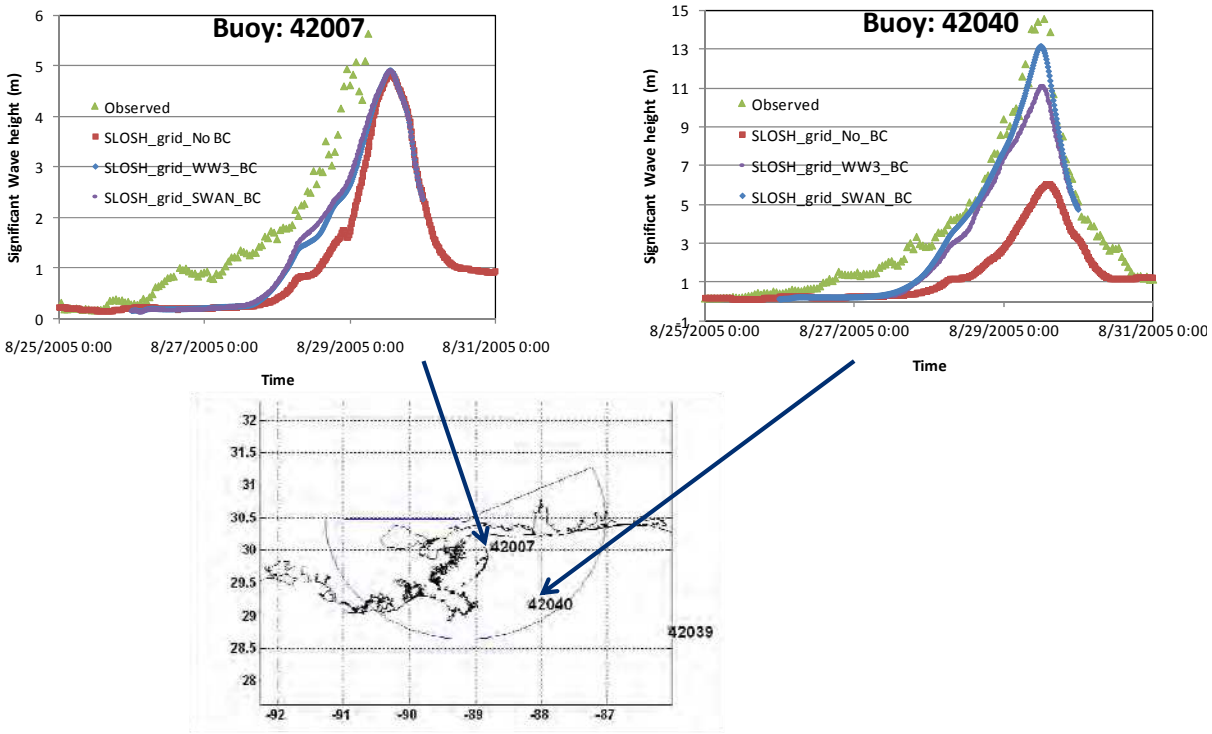

Figure 13.9. Comparison of Significant Wave Heights – Hurricane Katrina, Mississippi Gulf Coast SLOSH Basin.

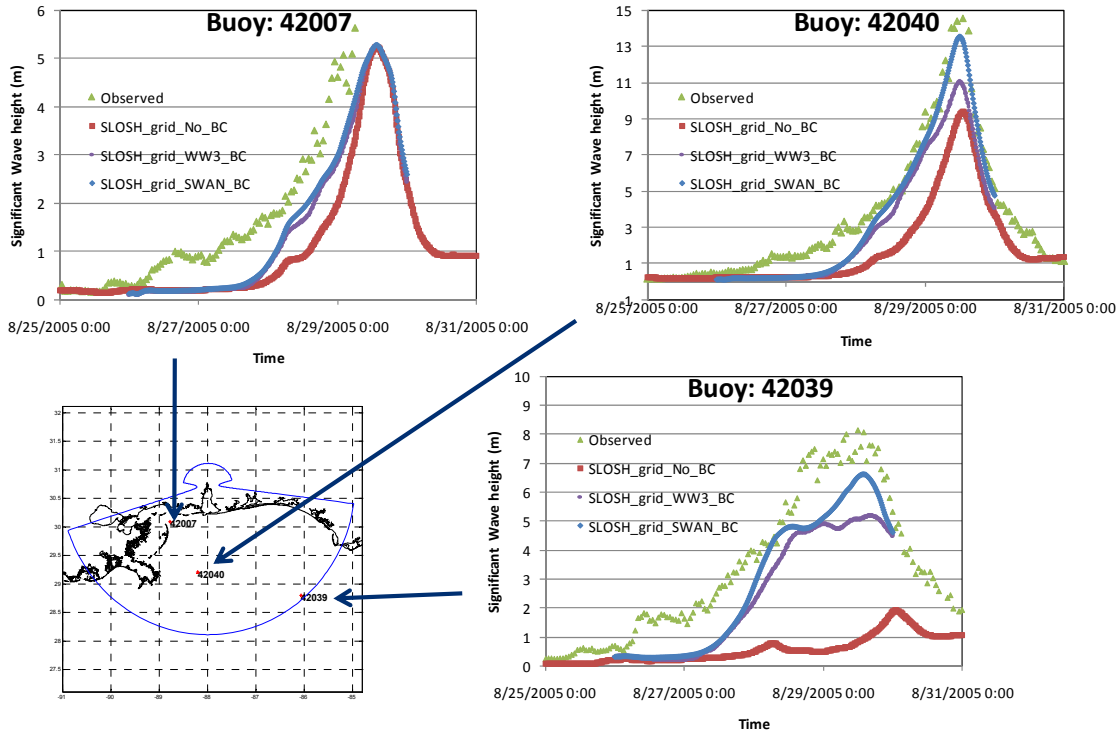

Figure 13.10. Comparison of Significant Wave Heights – Hurricane Katrina, Mobile Bay SLOSH Basin.